Peripheral factors affecting human colour perception

Lauren Elizabeth Welbourne

Doctor of Philosophy

University of York

Psychology

June 2016

Abstract

Human colour perception is mediated by multiple factors. These include: the external environment, physiological structures within the eye, and the neuronal pathways that originate in the eye. The aim of this thesis was to further investigate the impact of three main factors on both the perception and cortical representation of colour. These factors were: the external, changing seasonal environment, genetically determined differences in the number of photoreceptor types, and spatial filters inherent to cortical and pre-cortical luminance and chromatic pathways.

Novel findings and methods were demonstrated in this thesis:

1) For the first time, it was found that natural seasonal changes in the chromatic environment (in York, UK) affect the perception of unique yellow; this finding supports the existence of a slow normalisation mechanism, which is governed by changes in the average chromatic environment.
2) Genetically atypical individuals, who have fewer photoreceptor types (dichromats), demonstrated no differences in achromatic contrast discrimination thresholds compared to colour-normal trichromats. Therefore, for this particular measure, dichromats do not appear to benefit from increased neuronal resources from 'unused' chromatic pathway populations. A multi-channel LED system was developed to allow the isolation of photoreceptor responses in individuals with an additional photoreceptor type (tetrachromats). Modelling of this system indicated that precision in the cone spectra used to generate the stimulus, relative to the observer's actual cone sensitivities (i.e. peak wavelength sensitivities), is crucial for successful isolation of the cones.
3) fMRI-based population receptive field (pRF) mapping was used to measure pRF sizes in the pre-cortical channels. Between the pathways, no differences in pRF sizes were found, however, differences in fMRI measures of spatial frequency sensitivity were observed. These data indicate that spatial frequency tuning in early visual cortex may be decoupled from population receptive field sizes.

Table of Contents

List of Figures

List of Tables

Table 4.7 Mean spatial sensitivity index (with standard error) for each visual area in each condition, for foveal and peripheral eccentricities in Trichromats and the Dichromat. For the trichromats the means are across subjects for each visual, for the dichromat the mean value at each visual area is given (excluding the L-M condition). 209

List of Equations

Acknowledgements

This thesis would not have been possible without the support, guidance, and friendship of my primary supervisor, Professor Alex Wade. Alex provided unwavering optimism, generosity with his time, and Game of Thrones discussions, which have made the entire PhD process interesting and enjoyable. I would also like to thank my co-supervisor Professor Antony Morland, for his thoughtful insights, support, and for letting me take over his lab space for the past few years. Further thanks go to Professor Peter Thompson for his helpful discussions and input during my TAP meetings.

I would like to thank the staff at YNiC for their help getting my fMRI projects up and running, particularly Dr Andre Gouws, who provided invaluable programming and technical assistance. My thanks also go to Marc Green and Garry Turner, who were instrumental to the development of the LED system, and were always happy to help when we needed modifications or repairs.

My family have been a constant source of motivation and support – special thanks to my Mum who agreed to help with proof reading, and to my Dad, Nic and Bob for helping me de-stress with a beer (or two). Thank you to my fellow PhD students and numerous office mates over the years for making the experience so much fun, and providing much needed reassurance during the tougher times of the process. To my friends outside of the Department, thanks for the encouragement and reminding me to take a break occasionally.

Finally, I would like to dedicate this thesis to my awesome husband, Tom. Your love, friendship, pep talks, humour, intelligent feedback, and complete support, have helped motivate me throughout. Thank you for everything.

Declaration

I declare that the work presented in this thesis is original and my own, and was carried out under the supervision of Professor Alex Wade and Professor Antony Morland. This work has not been submitted to this or any other University for a degree.

Some of the data collection was carried out by MSc and 3rd year undergraduate project students, who I co-supervised on projects: data from Experiment 1 in Chapter 3 was collected by Victoria Wilkinson and Johanna Gledhill; data from Experiment 1 in Chapter 4 was collected by Freya Lygo, Fraser Aitken, and Su Zhao; and data from Experiment 1 in Chapter 5 was collected by Hannah Clawson, Isabelle Coleman, and Nikola Grujic. Dr Gabriele Jordan at Newcastle University carried out the diagnosis of three dichromatic subjects for Experiment 2 in Chapter 3. Marc Green and Garry Turner provided technical assistance in the build of the LED system described in Chapter 5. All of the reported data analyses, experimental design, creation of the stimuli, and all other data collection were performed by myself, under supervision.

Data presented in Chapter 2 were published in:

Welbourne, L.E., Morland, A.B. & Wade, A.R (2015). Human color perception changes between seasons, *Current Biology*, *25*(15), 646-647

The data were also presented in a talk at the following conference:

OSA Fall Vision Meeting, Philadelphia, USA (October, 2014)

Welbourne, L.E., Morland, A.B. & Wade, A.R. (2014), The impact of seasonal adaptation on unique hues, *Journal of Vision*, *14*(15), 28

Data from Chapter 3 were presented in a preliminary, incomplete form in a poster presentation at the following conference:

ECVP, Liverpool, UK (August, 2015)

Welbourne, L.E., Gledhill, J., Wilkinson, V. & Wade, A.R. (2015), Contrast detection differences between dichromats and trichromats, *Perception*, *44*(S1), 302

Data from Chapter 4 were presented in poster format at the following conferences:

ECVP, Barcelona, Spain (August, 2016)

Welbourne, L.E., Lygo, F., Zhao, S., Aitken, F. & Wade, A.R., Investigating the relationship between population receptive field (pRF) sizes and spatial resolution using chromatic stimuli

OSA Fall Vision Meeting, San Jose, USA (October, 2015)

Welbourne, L.E., Lygo, F., Zhao, S., Aitken, F. & Wade, A.R. (2015), Population Receptive Field (pRF) Mapping Using Chromatic and Achromatic Stimuli, *Journal of Vision*, *16*(4), 41-42

AVA Christmas Meeting, London, UK (December, 2015)

Welbourne, L.E., Lygo, F., Zhao, S., Aitken, F. & Wade, A.R., Population receptive field (pRF) mapping of chromatic channels

Chapter 1 Introduction

1.1 Overview

The human experience of colour is mediated by factors peripheral to the cortex, which affect both the light that reaches the retina as well as the capacity to transmit the information to the cortex. These pre-cortical factors exist both within the physiology of the eye as well as in the external environment. This thesis asks three questions relating to these factors:

- How does adaptation to natural changes in the external environmental impact on unique hue settings?
- How do variations in the number of photoreceptor types impact visual processing?
- How are spatial properties of the three pre-cortical pathways represented in early visual cortex?

A combination of psychophysical techniques, functional magnetic resonance imaging (fMRI), and optical design of a multi-channel LED system were used to answer these questions.

This chapter has two aims: to provide an overview of human visual processing from retina to cortex, and to introduce the pre-cortical factors that are explored in this thesis. These aims will be addressed in parallel, as there is an inherent relationship between the two. First, a description of visual processing from retina to cortex will be given, with an introduction to the three pre-cortical pathways. Second, the processes involved in normal human

colour vision will be described, along with a description of colour-vision abnormalities (dichromacy and tetrachromacy). Finally, an introduction to the unique hues will be provided. Each of these sections will be accompanied by an outline of what will be explored in the associated empirical chapters.

1.2 Visual processing and pre-cortical pathways

Light entering the eye triggers a cascade of neuronal responses and computations that end, ultimately, in conscious perception.

To reach the photoreceptors, light passes through a number of structures that filter out harmful radiation (e.g. ultraviolet (UV) light) from the electromagnetic spectrum, including the cornea, lens, and the aqueous and vitreous humour (see Figure 1.1). The transmittance properties of each of these features determine which wavelengths of light are able to pass through and reach the retina. These were measured by Boettner and Wolter (1962) in surgically removed human eyes, at points after the cornea, aqueous humour, lens, and vitreous humour. There is a cumulative effect on transmittance as light passes through each of these structures, which can be seen in Figure 1.2. Changes in the transmittance properties of any of these structures can therefore have implications on the light reaching the retina.

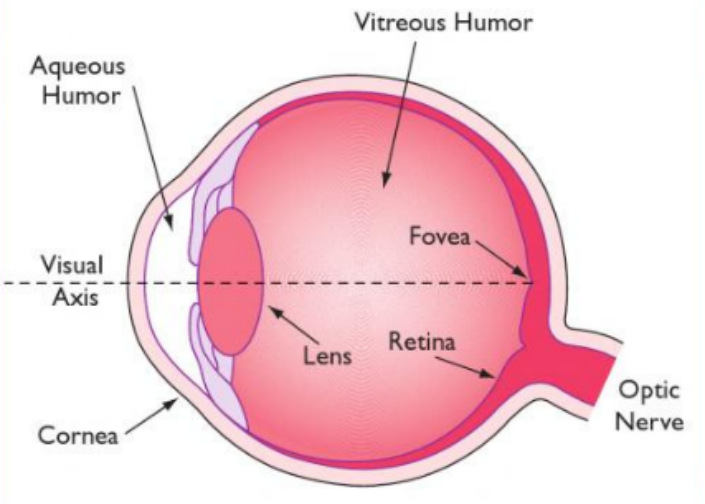

Figure 1.1 A schematic cross-section through the human eye, taken from Figure 2.3 of Packer and Williams (2003).

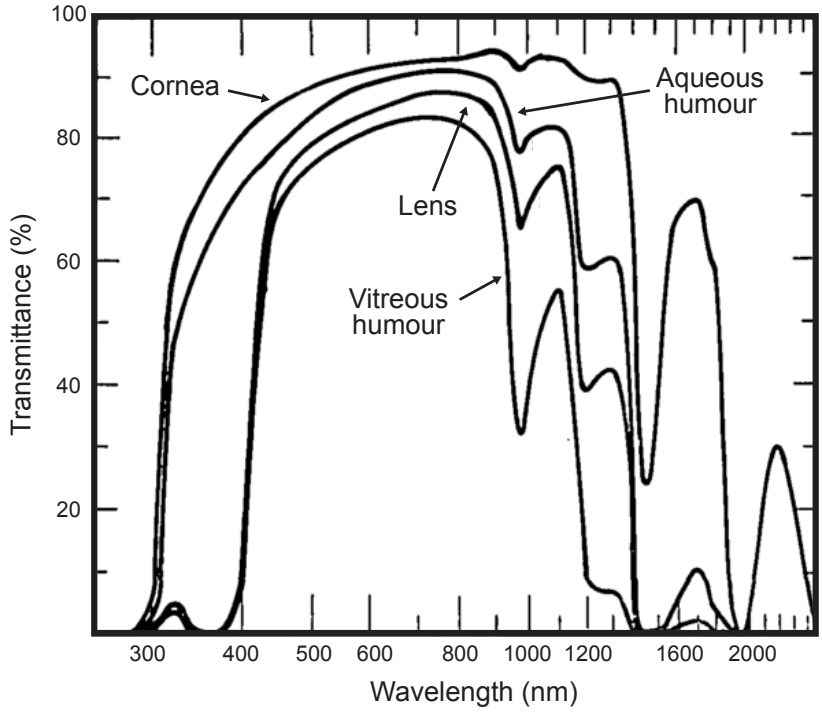

Figure 1.2 Proportion of light passing through different structures as a function of wavelength. Each curve represents measurements taken after passing through each structure, and therefore shows the cumulative transmittance at different points in the eye (with vitreous humour being the last point before the retina). Figure adapted from Boettner and Wolter (1962).

When light reaches the retina, light sensitive cells – the photoreceptors – are stimulated by the different intensities and wavelengths of the light source; these responses ultimately give rise to the perception of colour, which will be

discussed further in the following section. Responses generated within the photoreceptors are carried to cells in the retinal layers (e.g. bipolar and ganglion cells) and down the optic nerve of each eye. The left and right hemispheres of the brain receive input from the opposite visual field, and as such the responses from the nasal retina (towards the nose) and temporal retina (towards the side of the head) in each eye, which view different halves of the visual field, are separated. Nasal inputs cross over to the opposite hemisphere at the optic chiasm, where the two optic nerves meet (Andrews, Halpern, & Purves, 1997). From the optic chiasm the structures are then mirrored in each hemisphere, with each processing the input for the contralateral (opposite) visual field. The inputs pass down the optic tract from the optic chiasm to the lateral geniculate nucleus (LGN). This structure is composed of distinctive layers, which correspond to inputs from the various cell types within the retina. The LGN responses are projected via the optic radiation to the primary visual cortex (V1), where this layered structure is somewhat preserved. This projection path from retina to cortex is neatly illustrated by Solomon and Lennie (2007), shown in Figure 1.3.

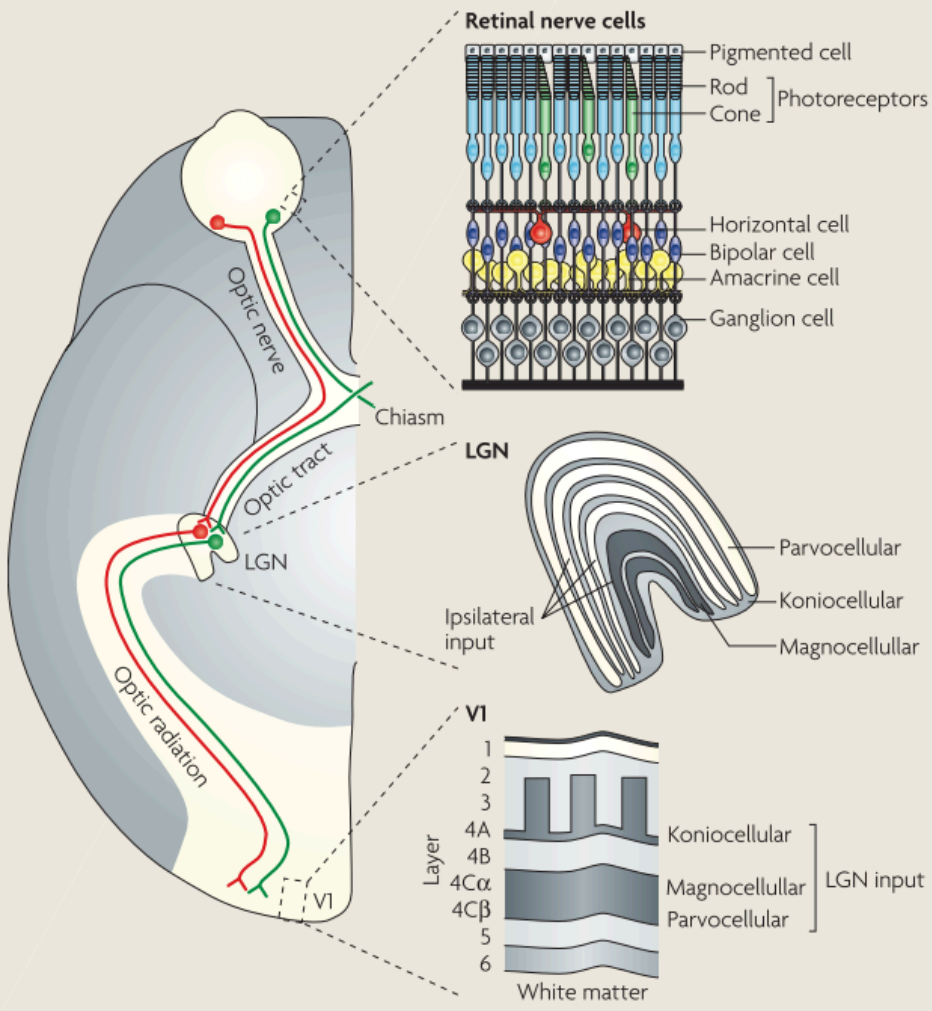

Figure 1.3 Illustration of the visual pathway route, taken from Box 1 of Solomon and Lennie (2007). The green line represents nasal retina projections passing to the contralateral (opposite) hemisphere, and the red line represents the temporal retina projections, which pass to the ipsilateral (same) hemisphere.

The layers within the LGN have been well studied in both human and non-human primates, such as macaques – which generally represent a good model of the human visual system (van Essen, 2004). The characteristic striping of the LGN (which can be seen in Figure 1.3) primarily represents cells in the parvocellular and magnocellular pathways, with separate layers of each corresponding to contralateral and ipsilateral input from the retina. These pathways originate from different classes of retinal ganglion cell (RGCs) in the retina. The input into the magnocellular pathway is mostly from parasol

RGCs, and input into the parvocellular pathway is mostly from midget RGCs (Callaway, 2005; Dacey, 2000; Lee, Martin, & Valberg, 1988). Furthermore, the LGN also contains cells from the koniocellular pathway, which receive input from small bistratified ganglion cells (Dacey & Lee, 1994).

Different types of ganglion cells receive input (indirectly) from different numbers of photoreceptors, with midget cells receiving input from far fewer photoreceptors – in a smaller area of the retina – than parasol cells. The size of the area of retina that provides input into a cell corresponds to the size of the area in visual space that the cell responds to – this is the receptive field (RF) of the cell. At the retinal level, RF sizes are very small, and this allows for high spatial resolution; midget cells have both a small RF as well as a large population, and are therefore capable of resolving spatial frequencies of up to 60 cycles per degree. The larger parasol cell RF sizes enable a spatial resolution of up to 20 cycles per degree (Wandell, 1995). As the projections move up through visual processing, inputs from multiple ganglion cells are combined within the LGN, and, in turn, inputs from multiple cells in the LGN are combined within primary visual cortex. With each progression through the visual system hierarchy, the size of the RFs increase, as a result of combining increasing numbers of cell RFs (Hubel & Wiesel, 1962).

The magnocellular (MC), parvocellular (PC) and koniocellular (KC) pathways draw their inputs from different weighted combinations of cone photoreceptors. The magnocellular pathway is driven, predominantly, by the summed outputs of L and M cones via parasol retinal ganglion cells. As such, the MC pathway responds strongly to achromatic luminance contrast. The PC

pathway is driven by cells responding to both L-M (opponent red/green) and luminance contrast, and is characterised by its higher spatial resolution and relatively slow temporal response profile. Finally, the koniocellular pathway carries opponent S-cone signals (S-(L+M)) driven largely by S-cone on-bipolar cells. Because of the different cell classes contributing to the PC, MC and KC pathways, stimuli with particular chromatic properties can be used to isolate each pathway. Specifically, the PC pathway is driven strongly by isoluminant red/green stimuli and the KC pathway can be driven almost exclusively with S-cone isolating patterns. Achromatic stimuli can drive all three pathways to some extent but isolation of the MC pathway can be improved with low spatial and high temporal frequency patterns.

The primary difference between these pathways, in terms of human visual perception, is the type of chromatic/achromatic perception elicited. However, there are other notable differences between these pathways, which can be measured behaviourally with psychophysical experiments, at a neuronal level with single-cell recordings, or at a broader cortical level with techniques such as fMRI.

One such difference is spatial resolution. Behavioural experiments in humans have shown that contrast sensitivity peaks at low spatial frequencies in both of the chromatic pathways, but the luminance pathway shows peak sensitivity at higher spatial frequencies (Webster, De Valois, & Switkes, 1990). Measurements of cells in magnocellular and parvocellular layers of the macaque LGN reflect these behavioural measurements, showing that the magnocellular cells respond best to higher spatial frequencies when presented

with luminance stimuli, whereas parvocellular cells show optimum responses to low spatial frequencies when presented with chromatic stimuli (Derrington, Krauskopf, & Lennie, 1984; Derrington & Lennie, 1984).

As described above, the distinct magnocellular and parvocellular pathway layers in the LGN are mostly preserved in the primary visual cortex (V1). However, it is unclear how well defined these pathways are through other areas in early visual cortex (V2-V4), and whether they are associated with distinct differences in average receptive field sizes. Chapter 4 outlines an fMRI technique that produces estimates of cortical population receptive field (pRF) sizes, and further describes literature relevant to spatial frequency tuning and receptive field sizes in relation to the luminance and chromatic pathways. The experiments described in Chapter 4 used pRF mapping to identify whether pRF size differences were observed between the pathways within early visual cortex, and if these were coupled with either behavioural measurements, or cortical fMRI measurements, of spatial frequency tuning.

1.3 Human colour vision

The three pre-cortical pathways define the three-dimensional colour vision of trichromats. However, these pathways, and the ability to interpret broadband wavelengths of light as colour, starts with the stimulation of the photoreceptors; 'rods' and 'cones' are both types of photoreceptor. The density of cones is at its peak in the central fovea, and it rapidly decreases with eccentricity up to approximately 15° visual angle, where it stabilises at very low-density levels. Conversely, rod photoreceptors are completely absent in the central fovea and gradually increase in density up to their maximum at

approximately 20°, before the density starts to decrease again (see Figure 1.4). The rods are highly sensitive to light so are utilised in dim light conditions, but they provide poor visual acuity, whereas the cones are less sensitive to light but enable colour vision and good visual acuity in central vision (Purves *et al.*, 2001).

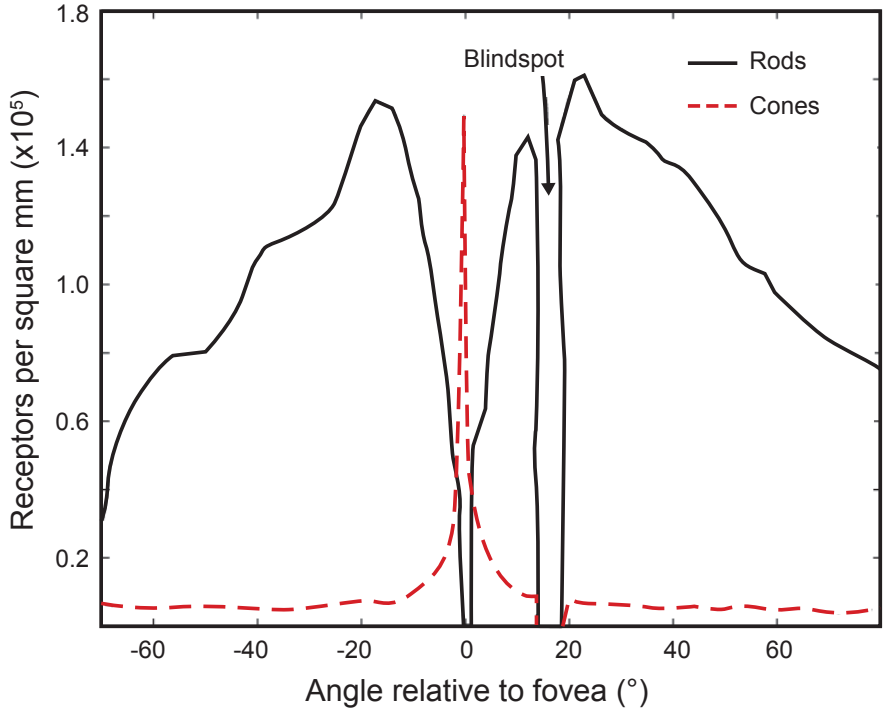

Figure 1.4 Distribution of rods and cones across the retina. The blindspot marks the location of the optic nerve, where there are no rods or cones. Adapted from Wandell (1995).

In "colour-normal" trichromatic individuals there are three types of cone photoreceptor, which are commonly referred to by their optimal wavelength sensitivities: L (long), M (middle), and S (short) cones. Various psychophysical measurements of the L, M, and S cone sensitivities have been recorded in recent decades, with slight variation in the tails of the sensitivity distributions of the cones, but they typically show similar peaks in sensitivity (at approximately 570nm, 545nm and 440nm, for L, M, and S cones,

respectively) – see Figure 1.5 for the sensitivities of each of the cones across wavelengths, as reported by Stockman and Sharpe (2000).

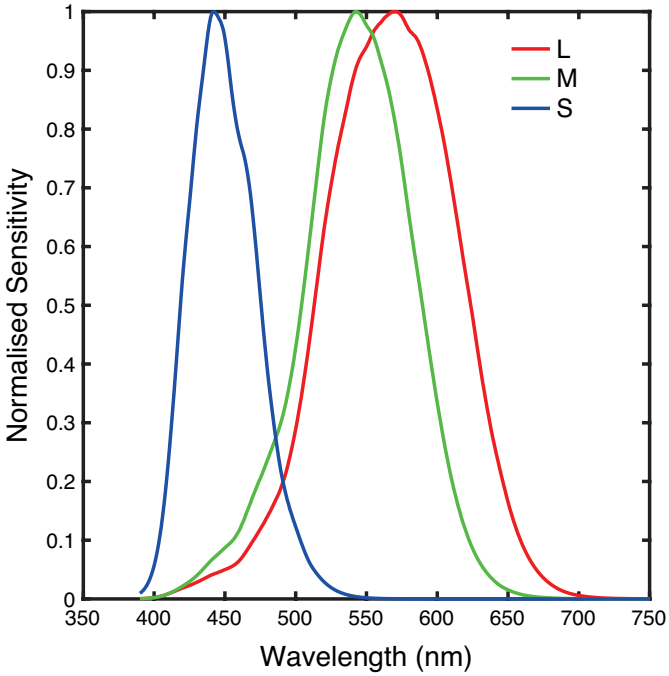

Figure 1.5 L, M, and S cone sensitivities ('cone fundamentals') plotted as a function of wavelength, from Stockman and Sharpe (2000) (downloaded from www.cvrl.org), plotted with normalised sensitivity values.

In the retina of a trichromat the L and M cones make up the majority of all cones, with S cones contributing as few as 4% of the total number (Roorda & Williams, 1999). L and M cones are highly clustered in the central fovea, whereas S cones are spread sparsely and regularly across the fovea, avoiding the central 0.2° or so entirely. This distribution of cones across the retina is referred to as a cone mosaic, and can be imaged using an ophthalmoscope after selectively bleaching the cones with 470nm and 650nm light (Hofer, Carroll, Neitz, Neitz, & Williams, 2005); Figure 1.6 shows an example of how the cones are distributed in a single trichromatic observer using a false coloured image. The ratio of L to M cones varies considerably between individuals, with values reported by Carroll, Neitz and Neitz (2002) ranging

between L:M ratios of 0.4 and 13, with the majority of subjects falling within a ratio range of 1 to 4.

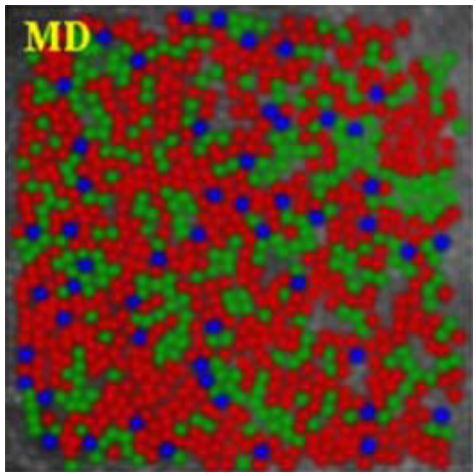

Figure 1.6 False colour image showing the distribution of L (red), M (green) and S (blue) cones in a single subject, 'MD' (taken from Hofer *et al*, 2005).

The responses of each of these photoreceptor types into the subsequent layers of the retina produce the basis of opponent mechanisms. Each cone has synaptic connections either directly or indirectly with a number of bipolar and horizontal cells, which ultimately synapse with ganglion cells (Wandell, 1995). A single bipolar cell will receive direct or indirect (via horizontal cells) input from a number of cones in a small section of the retina, which represent input from a small specific part of the visual field – this is the cell's 'receptive field' (Lennie, 2003). The receptive field is generally organised into a centre and surround, with the central input received directly from the cones, and the surround input received via the horizontal cells. These inputs have opposing signal responses – either 'on' centres with 'off' surround, or vice versa – that enables a comparison of the cone activation between the centre and surround regions. This organisation also exists within the ganglion cells, with different bipolar (and amacrine) cells contributing to either centre or surround inputs,

which ultimately determines the opponency of the cell – one of the three opponent pathways: luminance (L+M), red-green (L-M), and blue-yellow (S-(L+M)).

1.3.1 Dichromacy

Humans are predominately trichromatic, however, some individuals have abnormal or absent cone types which result in colour vision deficiencies – primarily characterised by poorer colour discrimination ability. 'Red-green colour blindness' is the most common type of colour vision deficiency, implicating either the L or M cones, and affecting approximately 8% of males and 0.42% of females (Morgan, Adam, & Mollon, 1992; Sharpe, Stockman, Jägle, & Nathans, 1999). The genes associated with the L and M cones are found on the X-chromosome, i.e. they are sex-linked genes, which accounts for the higher prevalence in males. Males have a single X chromosome, whereas females have two, and so abnormalities in either the L or M cone genes are inherited as dominant traits in males, but must be present on both X chromosomes in females to produce the equivalent deficiency (Sharpe et al., 1999). These deficiencies can be split into 'anomalous trichromacy' and 'dichromacy', and further split into protan and deutan forms, which refers to the particular cone type that is affected (L and M cones, respectively).

Anomalous trichromats have three types of cone, like trichromats, however one of those cones (typically L or M) is abnormal – the peak sensitivity of the anomalous cone is shifted in comparison to its non-anomalous counterpart. This results in the wavelength sensitivity spacing of the L and M cones being much smaller, such that these individuals have a reduced ability to distinguish

between colours that vary in this region of the spectrum. Anomalous trichromacy contributes to the largest percentage of colour vision deficiencies, affecting approximately 6% of males and 0.39% of females (Sharpe et al., 1999). The degree of deficiency varies between individuals, and depends on the peak sensitivity of the anomalous cone, i.e. whether the anomalous cone has a peak sensitivity that is very close to the healthy L or M cone (Jordan, Deeb, Bosten, & Mollon, 2010; Regan, Reffin, & Mollon, 1994; Shevell, He, Kainz, Neitz, & Neitz, 1998). As will be described in section 1.3.2, genetic carriers of anomalous trichromacy have the potential for tetrachromatic colour vision when all of the four cone types (three normal, and one anomalous) are expressed in the retina.

In comparison to anomalous trichromacy, dichromacy tends to produce similar levels of deficiency in all individuals with this condition. Dichromats have one totally absent cone type, which results in a more severe inability to distinguish between particular colours. The prevalence is lower than for anomalous trichromacy, with approximately 2% of males being affected (Morgan et al., 1992; Sharpe et al., 1999), but this is nevertheless considered a substantial percentage of the population.

The effect of an absent cone type on the dichromat cone mosaic is typically consistent with a 'replacement' model: the total number of cones is the same between dichromats and trichromats, with the missing cone type being replaced by the remaining L or M class of cone (Berendschot, van de Kraats, & van Norren, 1996). However, it has been observed that some dichromats do not demonstrate a replacement of cones, and instead have non-functional

patches of cones corresponding to the affected cone type, see Figure 1.7 for a comparison between patchy and non-patchy dichromatic cone mosaics (Carroll, Neitz, Hofer, Neitz, & Williams, 2004). As a patchy mosaic is not considered to be common in dichromats, and since the appropriate equipment necessary to determine dichromatic cone mosaics is not available here, the replacement model is assumed in dichromatic subjects recruited for the research in this thesis.

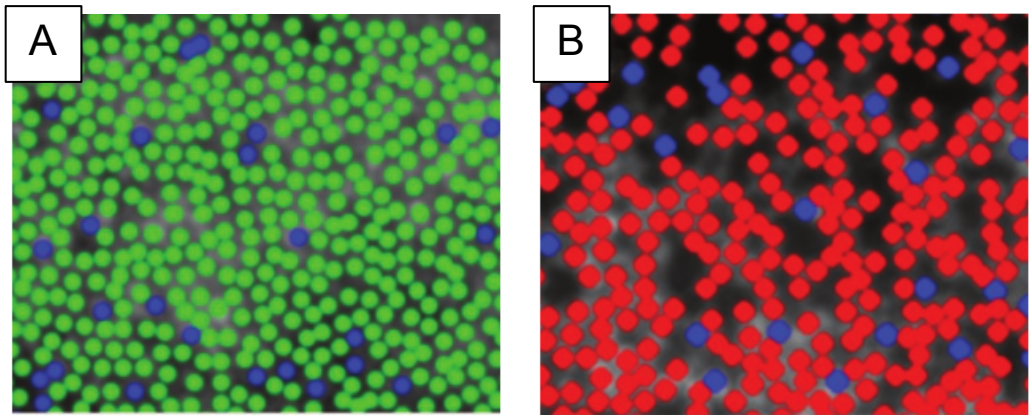

Figure 1.7 False coloured images of a dichromat with (A) a non-patchy cone mosaic, where absent L cones are replaced with M cones, and (B) a patchy cone mosaic, where absent M cones have *not* been replaced by L cones. Blue, green, and red colours correspond to S, M and L cones, respectively. Images taken from Carroll *et al* (2004).

A fundamental consequence of dichromacy is two-dimensional, rather than three-dimensional, colour vision; dichromats lack an L-M opponent pathway and have poorer colour discrimination ability compared to trichromats (Sharpe, de Luca, Hansen, Jägle, & Gegenfurtner, 2006). However, the prevalence of dichromacy in humans has motivated investigations into the potential advantages to dichromatic vision – animal models are useful in this line of research, as they perhaps represent more evolutionary valid behavioural consequences of different colour vision types.

Polymorphic colour vision (a roughly equal split of trichromats and dichromats within a species) is common amongst a number of non-human primates, such as marmosets, macaques, capuchin and spider monkeys (Jacobs, 2007). The dichromats and trichromats within these species are thought to benefit from different hunting and foraging strategies. For instance, it has been found that dichromatic male and female capuchin monkeys spend more time hunting camouflaged surface-dwelling insects than trichromatic females who are more efficient at detecting embedded and non-camouflaged insects (Melin, Fedigan, Hiramatsu, Sendall, & Kawamura, 2007). Saito *et al* (2005) carried out a lab-based camouflage task with dichromatic and trichromatic macaques, capuchins monkeys, and chimpanzees. The animals were trained to identify textured shapes from a textured background – both were the same colour, but were composed of elements with different shapes/sizes/orientations. Once trained, the same tasks were carried out under a red-green camouflage condition, in which both shape and background were coloured with red and green patches (patterned much like camouflage army clothing). For all species, the dichromatic individuals performed better than chance in the camouflage condition, whereas the trichromats all performed at chance level.

This dichromatic advantage in performing camouflage tasks has also been tested in humans using a camouflage paradigm (Morgan et al., 1992). Subjects were required to perform a 4-alternative-forced-choice (4AFC) task, indicating in which quadrant they identified the camouflaged 'texture'; the target texture was composed of a number of elements that all differed from the surrounding elements by one feature, either in size or orientation. This

stimulus was then presented in both a camouflage condition (each element randomly coloured red or green), and control conditions (all elements were the same colour, either red or green). It was found that dichromats performed comparably well in both camouflaged and control conditions, and were significantly better (in % correct responses) than trichromats on the red-green camouflage tasks. Suggesting that dichromats were less affected by colour interference than trichromats.

However, in both human and non-human primates there are also reports that dichromats do not show any advantages on these types of task. Caine, Surridge and Mundy (2003) mimicked a naturalistic setting of foraging using coloured cereal balls on coloured backgrounds, and tested dichromatic and trichromatic marmosets. They found that the dichromats did perform equally well on camouflage and non-camouflage conditions (whereas trichromats performed worse in the camouflage condition), however there was no significant difference in performance between dichromats and trichromats on the camouflage task, suggesting no behavioural advantage of dichromacy on this type of task. Hiramatsu *et al* (2008) performed field observations to measure foraging efficiency in dichromatic and trichromatic spider monkeys, and found no differences between the groups. They did show that luminance contrast (between foliage and fruit) was the most important factor in foraging efficiency, but this was true in both dichromats and trichromats. Finally, a human study was carried out by Bompas, Kendall and Sumner (2013), which simulated a naturalistic foraging task by getting subjects to identify fruit pieces on a bush from various distances (1, 4, 8, and 12 metres). On average the trichromats made faster responses and fewer errors than dichromats, and

the advantage of the trichromats increased with distance. This indicates that *trichromatic* advantages in foraging are primarily in spotting fruit from a distance rather than at close range.

If there *are* any behavioural advantages of dichromacy in foraging and camouflage breaking, they may reflect underlying low-level visual processing differences between dichromats and trichromats. Dichromats lack a functional/behavioural L-M pathway (not necessarily anatomically), and so if there were any visual enhancements in dichromats they would likely be reflected in specific properties of either the luminance or S-cone pathways, which may benefit from an increased input. Sharpe *et al* (2006) found that dichromats had higher sensitivity (lower thresholds) than trichromats for high temporal frequency stimuli that targeted individual cone types (cone isolation), but lower sensitivity than trichromats for low temporal frequencies. The L-M pathway is associated with high sensitivity at low frequencies, whereas the luminance pathway is associated with high sensitivity at higher frequencies. The authors suggest that the luminance pathway in dichromats benefits from an increased input into luminance-tuned cells, as demonstrated by the higher sensitivity at high frequencies, and that the findings support a lack of the L-M pathway (the functional pathway, rather than an anatomical pathway), because of the decreased sensitivity at low frequencies.

It is unclear whether enhanced contrast sensitivity for *temporal* frequencies could be related to the reported dichromatic advantages in foraging/camouflage breaking. However, enhanced contrast sensitivity for other parameters may be important. While the study by Hiramatsu *et al*

(2008) observed no performance differences between dichromatic and trichromatic spider monkeys, it did find that luminance contrast contributed to foraging efficiency. These findings therefore indicate that luminance contrast discrimination may be important in camouflage breaking.

Contrast discrimination in the luminance domain was explored in this thesis as a potential site of enhancement in dichromats. Chapter 3 discusses key contrast detection and discrimination literature, with a focus on the luminance pathway. Experiments described in Chapter 3 tested a hypothesis that dichromats and trichromats may differ in their sensitivity in this domain at a neuronal population level.

1.3.2 Tetrachromacy

In a mid-20th century paper, de Vries (1948) described the cone sensitivity response curves of individuals with normal and deficient colour vision, acquired via various methods (e.g. colour mixing, colour adaptation, flicker photometry). Within this paper, two women, who were the daughters of a deuteranomalous (anomalous trichromat) man, were also tested. The responses of these women were, for some methods, analogous to anomalous responses, and in others represented responses in between those expected for trichromatic and anomalous individuals. de Vries concluded that, in line with heredity predictions, the women should possess all three normal cone types (L, M, and S) as well as the additional anomalous cone, and therefore "…these daughters must be tetrachromatic…" (p380, 1948). This was the first report of 'tetrachromacy' – identified as the result of being a genetic carrier for anomalous trichromacy. In the years following this study evidence of weak

tetrachromacy has emerged, however the only case of strong tetrachromacy was reported by Jordan, Deeb, Bosten and Mollon (2010), where a single carrier of deuteranomally (cDa29) performed as would be expected by a tetrachromat, with demonstrations of colour discrimination that are not possible by trichromats. Conversely, it was also found that a number of genetic carriers for anomalous trichromacy showed no evidence of performing any differently to a trichromat – these were 'non-behavioural' tetrachromats.

Tetrachromatic women are carriers of genes that cause the colour vision deficiency anomalous trichromacy (specifically affecting either the L or M cones); as described previously, this deficiency affects the peak sensitivity of a cone type, and results in varying degrees of colour discrimination difficulties depending on the degree of shift in the cone peak. Tetrachromacy can only occur in females due to the X chromosome location (Xq28) of the genes coding for the L and M cone photopigments. For example, because women have two X chromosomes they have the capacity to possess genes for normal L cones on one X chromosome, and genes for anomalous L cones on the other (Neitz & Neitz, 2011).

A process known as random X chromosome inactivation determines which of a female's X chromosomes will be expressed for any given photoreceptor cell, i.e. paternal or maternal genes for L and M cones, resulting in the expression of all four cone types that are carried by tetrachromats (Jordan et al., 2010; Lyon, 1961, 2002).

X chromosome inactivation is the first of two processes that determine the type of cone that is expressed in each photoreceptor cell. The second determinant is the binding process between the locus control region (LCR) and the opsin genes for the L and M cones. The L cone genes are located upstream of the M cone genes, and therefore have a higher probability (p=0.66) of binding with the LCR because it is, in turn, upstream of the L cone genes (Jordan et al., 2010). Therefore random X chromosome inactivation first determines whether the maternal or paternal X chromosome is activated, and then the cone type expressed from that chromosome is determined by whether the LCR binds with the first (L) or second (M) opsin gene. In the case of the tetrachromats, when the X chromosome carrying the anomalous gene is activated the LCR would either bind with the normal (e.g. L) or the anomalous (e.g. M) cone genes.

There are vast individual differences in whether the LCR binds with the first or second opsin gene, as demonstrated by the large variation in L:M cone ratios observed between individuals (Carroll *et al.*, 2002). Therefore in tetrachromats, where there are three cone types reliant on this process, a potentially vast range of cone ratios are possible – some may have relatively equal numbers of each cone type, while others may have much closer ratios to an anomalous trichromat (for example, mainly normal L and anomalous M, with few normal M), or to a trichromat (for example, mainly normal L and normal M, with few anomalous M). Therefore these cone ratios may be a key factor affecting whether these women are behavioural or just genetic tetrachromats.

A number of tasks were utilised by Jordan *et al* (2010) to probe the abilities of the carriers of anomalous trichromacy. The first task was a Rayleigh Match procedure performed on an Oculus Anomaloscope; the subject was required to adjust the brightness of a monochromatic field to match a red/green mixture, which was set at different ratios of Red:Green by the experimenter. In addition, the subject provided a rating on the quality of the chromatic match (where 5 indicated a perfect colour match) – only the Red:Green ratios scoring 5 were used to calculate that subject's matching range. There were no significant correlations for the match mid-points or ranges between carriers and their sons. However, it was found that one carrier, cDa29, did not accept any match for any of the Red:Green ratios presented.

To further investigate this, a temporal 3-alternative-forced-choice (3AFC) task was utilised to determine whether the potential tetrachromat could successfully discriminate between stimuli in a performance version of the Rayleigh Match. Three stimuli were presented in rapid succession, one of which was composed of a mixture of Red and Green lights, and the other 2 were monochromatic orange lights (see Figure 1.8A) – the subject's task was to indicate which of the 3 stimuli was the 'odd one out', i.e. the red and green mixture. Multiple trials were completed for a range of combinations of Red:Green ratios for the mixture stimulus and luminance for the monochromatic field. The lower graph in Figure 1.8B shows that subject cDa29 (open circles) makes no errors in identifying the red and green mixture across all Red:Green ratios – consistent with her performance on the Rayleigh Match task where she was unable to accept any matches. Conversely, the

other carriers ('cDa' and 'cPa') and controls ('mCo' and 'fCo'), made the most errors in the 3AFC task for the red/green ratios that had they previously accepted as a match to the monochromatic orange field, i.e. they were unable to differentiate the mixture from the monochromatic fields, as expected.

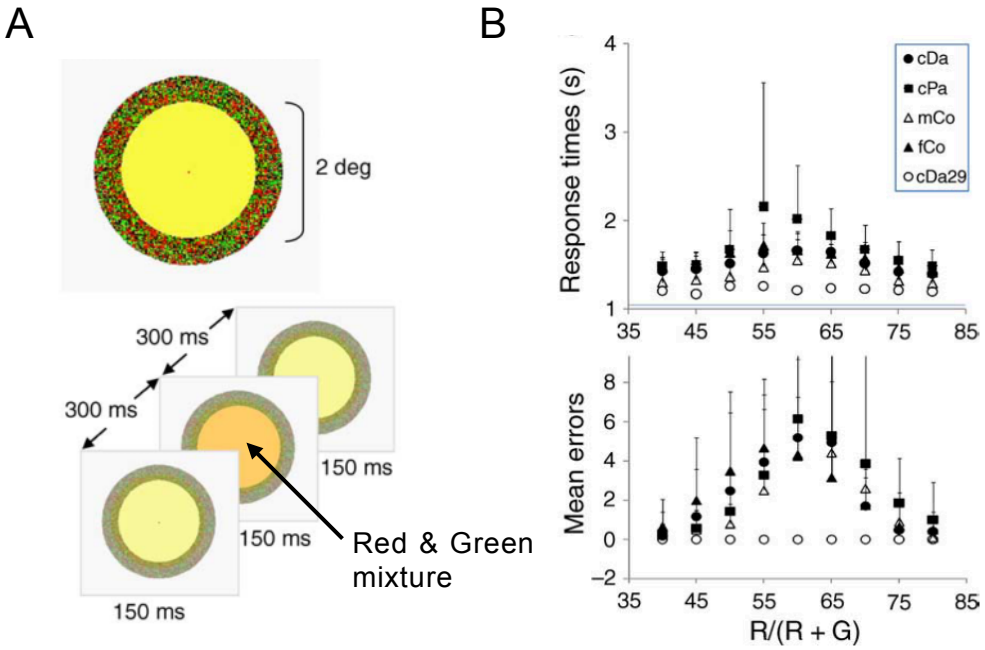

Figure 1.8 (A) Example stimuli and presentation of stimuli in the temporal 3AFC task. Each stimulus is surrounded by an annulus of colour noise. (B) Response times (upper graph) and mean errors (lower graph) at each red/green ratio (R/(R+G)). Figures taken from Jordan *et al* (2010).

In addition to these tasks, multidimensional scaling was used to further probe the colour discrimination abilities of the subjects. The stimuli were composed of custom-designed pigment mixtures, which, in particular combinations, produced stimuli that were only distinguishable to the tetrachromatic observer, and indistinguishable to others.

Jordan *et al* (2010) ran genetic sequencing of all the carriers and their sons, to establish with certainty the genes that were carried, and the spectral peak of each of the photopigment genes they carried. Interestingly, individuals with similar spectral spacing of the L, L-prime (anomalous) and M cones compared

to cDa29, did not perform as well as cDa29, suggesting that the spectral spacing of the additional pigment may be necessary but not sufficient in demonstrating behavioural tetrachromacy.

At present, the authors and the methods described above are the only ones currently measuring responses from tetrachromats. While these methods are useful diagnostic tools, they do not enable any further probing of the cone responses, or investigation into the possible opponent pathways that may result from the presence of four cone types. Chapter 5 explores the use of a silent substitution and cone isolation method, using a multi-channel LED system, for isolating the anomalous 4th cone ('L-prime') in a tetrachromat. A demonstration of the system with trichromats and dichromats was described, and modelling was provided to simulate the possible difficulties associated with isolating responses from this 4th cone in a tetrachromat.

1.4 Unique hues

From the late 19th century, the observation that particular hues could be reliably set to fit the criteria of a "unique hue" has been investigated. A hue that does not appear to contain a mixture of any other colour, for instance a green that does not appear yellowish nor bluish, can be considered unique; the four recognised unique hues are red, green, yellow and blue (Dimmick & Hubbard, 1939).

These four unique hues are interesting in that they reflect perceptual properties of the opponent channels. For unique green or unique red to appear neither yellowish nor bluish, it has to elicit a null response in the

yellow-blue (S-(L+M)) channel. Conversely, for unique yellow or unique blue to appear neither greenish nor reddish, it has to elicit a null response in the red-green (L-M) channel (Jameson & Hurvich, 1955).

However, despite these perceptual associations with the opponent systems, the actual input from the L, M, and S cones into these systems need to be transformed in order to reflect the observed psychophysical unique hue settings. Early modelling demonstrated that a linear transformation of the L, M, *and* S inputs into a red-green system produced good estimates of unique yellow and unique blue, but into a yellow-blue system the estimates of unique green and unique red were not as good, and instead the inputs required some non-linear transformation into this system (Jameson & Hurvich, 1968; Werner & Wooten, 1979).

Subsequent models of unique yellow discussed by Neitz, Carroll, Yamauchi, Neitz and Williams (2002) illustrate that unique yellow settings can be matched by a gain adjustment of the L and M cone inputs into an opponent red-green system. However, in line with the more complicated non-linear relationship previously observed between unique green and the yellow-blue channel, there is increasing evidence than the determinants of unique green are numerous. For instance, it has been shown that longer wavelength settings of unique green are selected in individuals with a higher density of macular pigment, which affects the absorption of light prior to reaching the photoreceptors (Welbourne, Thompson, Wade, & Morland, 2013). Furthermore, a study by Schmidt, Touch, Neitz and Neitz (2014, 2016) has demonstrated that while, in agreement with other studies, the ratio of L:M

cones in the retina does not affect unique yellow settings between individuals (Neitz et al., 2002), there is evidence that this ratio affects unique green settings.

In general, unique green settings show much more variance between individuals than any of the other unique hues, whereas unique yellow demonstrates a remarkable stability (Kuehni, 2004). The variability in unique green settings may strengthen a hypothesis that the settings are determined by numerous factors (as indicated above). However, the stability of the unique yellow settings hints at an equally interesting situation, whereby the settings are somehow *not* affected by individual differences in cone ratios, and therefore demonstrates that these settings are perhaps normalised based on the external input into the cones (Neitz et al., 2002).

Chapter 2 explores the potential impact of normalisation to the natural external environment on unique yellow and unique green settings. Literature regarding how chromatic adaptation affects unique hues is discussed, along with studies that observe how the average chromaticity of the environment changes between seasons at different locations. A longitudinal experiment was carried out to measure differences in unique yellow and unique green settings between winter and summer – these seasons experience a large change in the amount of green vegetation in the environment.

1.5 Outline of the thesis

Each empirical Chapter contributes to the thesis objective – to explore peripheral factors that contribute to human colour perception. Further

literature relevant to each peripheral factor is discussed in the context of the experiments that were carried out, within each Chapter.

The organisation of these factors within the thesis is as follows: Chapter 2 addresses the impact of changes in the external environment on unique hues; Chapter 3 investigates the performance of dichromatic and trichromatic individuals on a contrast discrimination task; Chapter 4 utilises pRF mapping techniques to measure pRF sizes within each of the pre-cortical pathways; and Chapter 5 reports the development of a multi-channel LED system and models the implications of using such a system for testing tetrachromatic women. Chapter 6 summarises the conclusions and novel contributions made by each of these experiments, and discusses other peripheral factors that are not explored here, as well as future directions for some of the experiments that were carried out.

Chapter 2 Longitudinal Measurements of Unique Hues

2.1 Overview

Neurophysiological explanations for the unique hues have been persistently inconclusive. Multiple factors have been shown to correlate with the large individual variation in unique green settings (Schmidt, Neitz, & Neitz, 2014; Welbourne et al., 2013), yet it remains a largely unexplained percept. Explanations for unique yellow settings have in recent years focused on studies showing that adaptation to artificially altered chromatic environments affects unique yellow settings – thereby implicating a plastic neuronal mechanism. To date, however, there are no reports measuring whether adaptation to natural changes in the chromatic environment, i.e. between seasons, causes a similar shift in these settings.

Chapter 2 will first outline previous research on unique hue shifts following adaptation, as well as studies that have measured the chromatic changes that occur between seasons, and then describe a longitudinal experiment that investigates whether unique hue settings shift following adaptation to natural, environmental changes that occur between winter and summer in York (UK).

2.2 Background

2.2.1 Adaptation

Unique yellow settings are considered to be relatively stable between individuals, despite large individual variability in L and M cone ratios (Carroll

et al., 2002; Neitz *et al.*, 2002). One explanation for this stability might be that unique yellow is set by the environment rather than retinal physiology. Some support for this idea has come from studies showing that long-term, artificial manipulation of environmental light conditions can alter subjects' unique yellow settings.

Neitz *et al* (2002) investigated whether unique yellow is determined by an experience-based mechanism, by measuring unique yellow settings after long-term chromatic adaptation. Unique yellow is considered to be the equilibrium point of the L-M colour opponent channel, however, for this to be the case the cone inputs from each cone type need to be reweighted, such that an additional weighting is applied to the M cone inputs prior to applying any L-M opponency. Neitz *et al* hypothesised that adaptation to an extreme chromatic environment would cause a shift in the relative weightings of the L and M cone inputs, to compensate for a change in the average chromatic environment, and as such cause a shift in unique yellow settings. To investigate this, four participants were used in an adaptation experiment, which contained two periods of adaptation: one to red and one to green chromatic environments, using either tinted contact lenses/goggles or a light-filtered room. Unique yellow measurements were first obtained for several days prior to each adaptation period (on a Maxwellian-view apparatus using an adjustment method) in order to collect baseline measurements of unique yellow. Subjects were then exposed to altered chromatic environments for periods of between 4 to 12 hours a day (the rest of the day and night was spent in a normal visual environment), for a minimum of 10 days. Unique yellow measurements were taken at the start of each day, before being exposed to the

altered chromatic environment. Over the period of adaptation to the red chromatic environment, the settings gradually shifted to longer wavelengths, with a gradual decrease back towards the baseline after several weeks without any periods of altered chromatic environment. Similarly, the settings shifted to shorter wavelengths after adaptation to the green chromatic environment, followed by a gradual return to baseline after the adaptation period (see Figure 2.1 for an example from one subject).

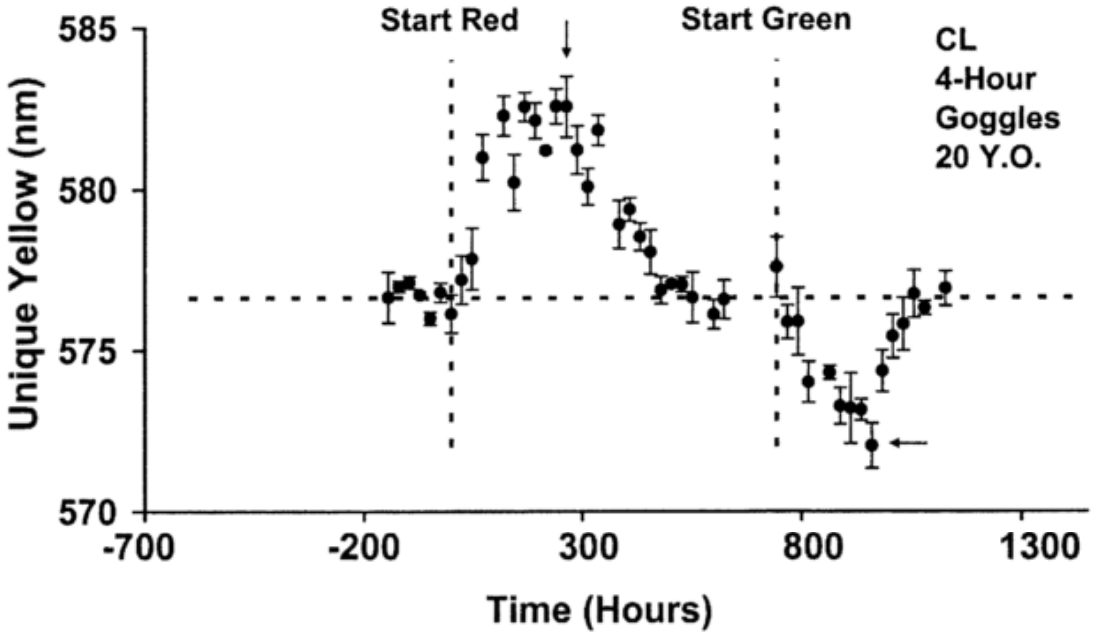

Figure 2.1 Unique yellow wavelengths (nm) for one participant, taken from Neitz *et al* (2002). Settings are shown over the days of the experiment. The dotted lines indicate the start of the adaptation periods to red and green (as labelled), with arrows indicating the last day of each adaptation type.

The same pattern of unique yellow shift was also found for a subject who had one eye occluded during the adaptation procedures, and was tested with only the occluded eye – this indicates that the adaptation effect occurs beyond the retinal level. The authors concluded that the long-lasting (but reversible) effect of visual environment on unique yellow wavelength settings suggest that this percept is mediated by a plastic normalisation process. Specifically, the equilibrium point of the L-M opponent channel, as determined by the

weighting of the L and M cone inputs, is dependent on the average chromaticity of the environment. It was also apparent that it takes several weeks to both adjust to the altered environment, as well as return back to the baseline following a period of adaptation, demonstrating the normalisation process twice for each adaptation condition (i.e. also re-adapting to the normal chromatic environment).

A study by Belmore and Shevell (2008) replicated the findings of the red chromatic environment found by Neitz *et al* (2002) using an alternative paradigm whereby two subjects adapted to a display on a CRT monitor for one hour per day (rather than filtering their chromatic environment) – one of the subjects also performed the experiment again with adaptation to a light-filtered room (for four hours a day) to mimic one of the adaptation conditions used by Neitz *et al.* The adaptation stimulus on the CRT monitor consisted of a red grating pattern (Judd chromaticity coordinates: x=0.6, y=0.35) – the orientation and location of the grating lines updated every five seconds. Baseline unique yellow settings were made over six days prior to the start of the adaptation experiment; unique yellow settings were made by adjusting the relative radiance of a red primary in a mixture of red and green lights (660nm and 540nm, respectively) until the mix appeared unique yellow (neither reddish nor greenish). Multiple unique yellow settings were made across different light levels by adjusting the radiance of the 540nm light. Following adaptation, the authors observed an increase in the intensity of red light used for creating unique yellow (in the red and green mixture) for all light levels, and for both the CRT and light-filtered room adaptation methods. These

findings correspond to the longer wavelength settings seen by Neitz *et al* after adaptation to the red chromatic environment.

A further study by Belmore and Shevell (2011) measured the effect of long-term and short-term adaptation on unique yellow settings. They used chromatic adaptation paradigms to identify how each type of adaptation affects unique yellow settings, and what the combined effect of both types is. The same methods were used as in the previously described study by the same authors, with the addition of short-term adaptation effects on unique yellow, which were measured before and during the implementation of long-term adaptation. Two subjects first carried out a week of measurements using only short-term adaptation and dark-adaptation conditions. The short-term (three minutes) chromatic adaptation was to a red light (660nm) on a Maxwellian-view optical system. The week of baseline measurements was followed by a two week cycle of testing which involved taking unique yellow settings after short-term adaptation, and further measurements after long-term adaptation of one hour to the red-lined grating pattern. Following both short and long-term adaptation, there was found to be an increase in the levels of red light required in the red/green mixture to reach the perceptually unique yellow point, compared to settings taken after dark-adaptation. There was a further increase in the level of red light used in the unique yellow setting when both short- and long-term adaptation conditions were combined, indicating a cumulative impact of short- and long-term adaptation, and that long-term adaptation effects were not disguised by the short term effects.

Literature investigating the impact of chromatic adaptation on unique green settings is remarkably sparse. No reports have been identified that measure how unique green settings would shift following the same adaptation conditions presented in the studies above. However, there is evidence that unique green settings can be affected by other adaptation conditions. For example, a long-running debate concerned whether unique green settings were distributed bimodally within the population. Initial studies offered some evidence for bimodality (Cobb, 1975; Rubin, 1961), however a unimodal distribution is now predominately supported (Hurvich, Jameson, & Cohen, 1968; Jordan & Mollon, 1995; Welbourne et al., 2013). Hurvich *et al* (1968) proposed that the bimodal distribution observed by Rubin (1961) was a result of non-neutral adaptation in the observers; a neutral state of adaptation was not ensured in all his subjects because they performed unique yellow settings prior to unique green settings, and therefore the bimodal unique green measurements may actually represent effects caused by this adaptation.

Hurvich *et al* (1968) measured unique green settings in observers following three adaptation conditions (dark, bright light, and bright light following unique yellow settings), to investigate how much the settings shifted between the conditions. On average there was a smaller shift in settings between dark and bright adaptation (~5nm), than between dark and bright following unique yellow adaptation (~10nm). For the latter pair of conditions, there was a particularly large variability in the amount of shift, with some subjects showing small differences (<5nm) and others showing large difference (>15nm). These findings help explain Rubin's (1961) bimodality finding: they demonstrate that there is large variability in the effect of adaptation to yellow

prior to carrying out a unique green task, and therefore show that large numbers of subjects could potentially generate a bimodal spread of unique green settings. However, these findings also demonstrate that unique green settings can be shifted following adaptation to unique yellow, at least in the short term.

To date there are no reports of whether unique hue settings shift as a result of natural changes in the environment, i.e. between seasons. Subjectively, the most obvious change between winter and summer is an increase in the amount of greenery in the environment. If these natural changes were large enough, then in summer they may mimic the effect of a green-adaptation paradigm. Since adaptation to green chromatic environments has been shown to have an impact on unique yellow, but not specifically on unique green, it may be expected that only unique yellow would be likely to show any impact of seasonal adaptation.

However, it is first important to establish whether measurable differences in the average chromatic environment do occur between seasons, to indicate whether a shift in unique yellow settings is feasible as a result of changing seasonal environments. Measurements of this kind are discussed in the following section.

2.2.2 Chromatic changes between seasons

A popular model of the average chromatic environment, referred to as the "Grey World" hypothesis, assumes that the average reflectance of the environment is grey and that on average the chromatic world humans are

exposed to does not vary across time or space (Buchsbaum, 1980; Granzier, Smeets, & Brenner, 2006). However, it has since been shown that this is not the case, and that differences in the mean spectra of natural scenes can be observed between both different locations as well as between seasons at the same locations.

Webster and Mollon (1997) sampled a number of scenes using a spectroradiometer and digital photographs, to measure the variability in the colour statistics of the images – image properties were converted into LMS cone excitation levels, and contrasts across opponent axes were calculated (i.e. L+M, L-M and S-(L+M)). Large variability was observed across the scenes, however, the variability was primarily restricted across a blue to green/yellow axis, i.e. in-between the S-(L+M) and L-M axes, which represented changes between, for example, dry arid scenes and lush green scenes. Further to this work, Webster, Mizokami and Webster (2007) took photographs of the natural scenes (avoiding obvious manmade structures) in two different seasons, for two locations: Western Ghats in India, and Sierra Nevada in the USA, to measure differences in RGB values of each pixel between seasons. They estimated LMS cone excitations, as well as chromatic and luminance contrasts, from the RGB values of the images. Between seasons they found that the changes originated largely from systematic variation in the average surface *reflectance* spectra, rather than the *illuminant*. The dominant change found in the environments they measured was a shift between greenish and yellowish colours, depending on the season, with the greenish shift occurring due to an increase in foliage.

2.3 Aims & hypotheses

The northerly latitude of the local environment in York (a semi-rural English city) results in profound seasonal changes in the natural environment. In winter there is very little green vegetation compared to the summer months. There is no record of how given scenes in York vary in their reflectance properties between the seasons, however, the studies described above predict a shift to, on average, a greener chromatic environment in summer compared winter.

It has been shown that a shift in unique yellow settings can be observed following adaptation to extreme changes in the chromatic environment, which includes adaptation to artificially 'green' environments. Shifts in unique green settings have only been clearly shown following adaptation to yellow environments.

The experiment described in this Chapter investigated whether natural changes in the chromatic environment can cause a shift in unique hue settings. Longitudinal testing was performed on the same set of subjects following adaptation to winter and summer environments. Based on the research described above, it was hypothesised that unique yellow settings are determined by the weighting of L and M cone inputs, and that these weightings change following long-term adaptation to a change in the chromatic environment. Specifically, unique yellow wavelengths were predicted to shift to shorter wavelengths in the summer (following adaptation to a greener environment) compared to winter, in line with the direction of

shift observed by Neitz *et al* (2002). Conversely, other measures that are not thought to be affected by the weighting of L and M cone inputs, or by adaptation to a greener environment, would remain stable, namely, unique green settings and Rayleigh matches. Rayleigh matches require a match to be made between a two-primary mixture (red and green) and a monochromatic light (yellow/orange); this is a metameric match that represents the same stimulation of cones for both stimuli, and it is therefore determined by photoreceptor sensitivities. To analyse the reflectance properties of typical scenes from the University of York campus between seasons, two sets of photospectrometer measurements – one in each season – were taken at several fixed locations, to provide an example of how the average chromatic environment changes between seasons. It was hypothesised that a seasonal shift would be observed in the average chromaticity, with greener scenes dominating the summer months.

2.4 Methods

2.4.1 Subjects

Seventy-two participants were tested in both winter (January-February) and summer (June-July). Participants were only eligible for the study if, prior to each testing session, they had not been out of the UK for more than one week in the previous 3 months, and they must also have been in the UK continuously for a full month prior to the date of testing. These criteria ensured a minimum period of one month for environmental adaptation prior to each testing session.

The winter and summer testing sessions were separated by at least four months; the average number of days between testing sessions was 133 (± 11 days). Green foliage from deciduous trees had been absent for ~3 months prior to the winter session, and the regrowth of this foliage had been stable for ~2 months prior to the summer session.

Five participants (two female) were excluded from the data analysis, as they made Rayleigh matches that indicated inherited colour vision deficiencies. Therefore, 67 subjects (22 males, 45 females), with a mean age of 21.7 years (± 2.7), were included in the data analysis. All of these participants were confirmed as colour-normal observers using Rayleigh matches.

The departmental Ethics Committee at The University of York granted approval for this study.

2.4.2 Equipment

A three channel colorimeter (Wright, 1928, 1939), originally built at Imperial College London in the 1930's, was used for making Rayleigh matches as well as central (foveal) and peripheral settings of unique yellow and unique green. The colorimeter contains a single monocular eyepiece which is fitted with a doublet to counteract chromatic aberration, the colorimeter also has two 'arms': the 'matching arm' holds three primary stimuli (which can be set at a range of wavelengths for red, green and blue) and the intensity of each can by adjusted using three 'primary dials', which move neutral photometer wedges over each of the primary stimuli (providing a continuous variation of the

intensity); it also has a 'test arm' that holds a single stimulus, the wavelength of this stimulus can be adjusted using the 'test dial' (see Figure 2.2).

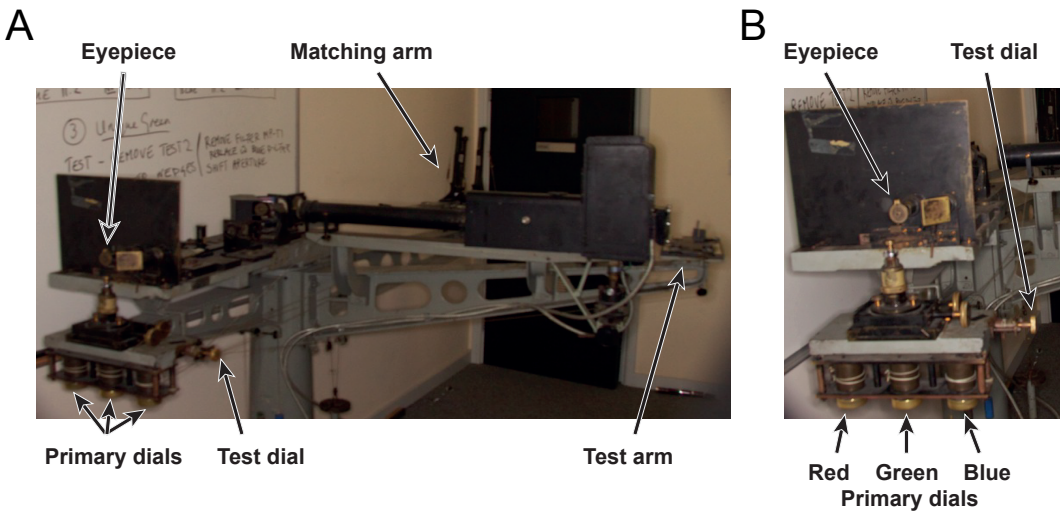

Figure 2.2 Photographs of the colorimeter equipment, with key components labelled. (A) Full view of the colorimeter, (B) close-up of the observer's view of the colorimeter.

Depending on the measurement being taken, the participant either viewed a square, bipartite field (1.33° × 1.33°), or a single rectangular field (the bottom half of the bipartite field, resulting in a 0.67° × 1.33° viewing angle). The top half of the field contains a "mixing light," which can contain a selection of the primaries from the matching arm (blue, green, and red set at 460nm, 555nm, and 666nm, respectively). The observer can adjust the intensity of each of these primaries independently. The bottom half of the field contains a monochromatic light from the test arm, which can either be set to a specific wavelength for use as a "reference light", to be matched by the mixture in the top half of the field, or alternatively, this half of the field can be used as a "test light", and be adjusted in isolation (with the top half of the field occluded) until a particular wavelength value was obtained (e.g. perception of unique yellow).

For the peripheral unique hue measurements, a small dim LED was added to the right of the field; when the observer was fixating on the LED it placed the centre of the stimulus 6.5° into the periphery. To prevent the stimulus from fading in the periphery (Toxler's fading (Simons *et al.*, 2006; Troxler, 1804)), a 4Hz square-wave flicker was applied to the stimulus using a metal disc (composed of alternating 90° sectors and gaps) which was powered by a small motor.

The colorimeter was calibrated for each season of testing with a fibre-optic photospectrometer ("Jaz", Ocean Optics, FL) operating at 2nm resolution and using 3 scans to average for taking the wavelength measurements. This device was, itself, calibrated against a National Institute of Standards Technology-traceable standard light source. Several measurements were taken at each of the colorimeter levels used to confirm the peak wavelength value for each level (consistent values were obtained for all levels in both seasons). Calibration allowed the fit and correction of slight nonlinearities in the colorimeter scale, which were modelled with a second order polynomial (see Figure 2.3); the colorimeter values recorded for all unique green and unique yellow settings were converted into wavelength values using the polynomial formula acquired from the calibration taken within the same season.

The same photospectrometer was also used to obtain measurements of the spectral environment at three fixed outdoor scenes, using a 30° spatial integrating lens.

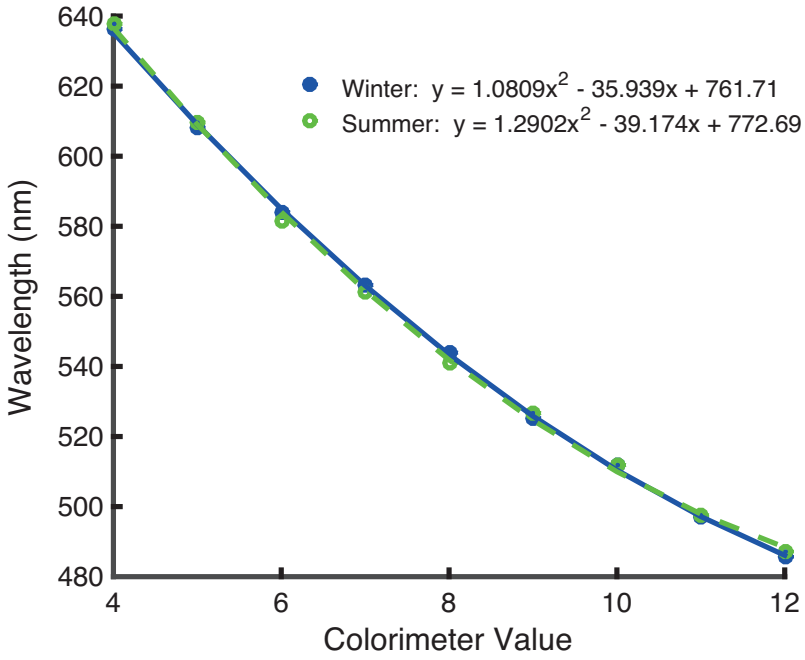

Figure 2.3 Calibration data and polynomial curve for winter and summer calibrations of the colorimeter test arm. Polynomial formulas for each season are shown in the legend.

For the Rayleigh matches, log(R/G) values were calculated for each match using the radiance of the red and green primaries; the colorimeter readings, from the positions of each of the neutral photometer wedges on each primary (red, *r*, and green, *g*), were converted using the known gradients of the wedges (R_g=0.2, G_g=0.1943) in the following formula: (r*R_g)-(g*G_g). This conversion was done for each match prior to assessing mean values and matching ranges for each subject.

Optical devices, such as colorimeters, may be sensitive to seasonal temperature changes (Jordan & Mollon, 1993). To account for this, the temperature of the lab was monitored throughout each season of testing using a digital thermometer, accurate to +/- 1°C (1.8°F). The temperature was

comparable between seasons (winter: M=24.08 (°C), SD=1.70; summer: M=24.07, SD=1.63).

2.4.3 Design

All subjects performed all conditions of the experiment in both seasons of testing to allow for within-subject comparisons of the measures taken within each season.

2.4.4 Procedure

The same order of testing was used in both seasons of testing. Participants would first dark-adapt for approximately five minutes, followed by carrying out Rayleigh matches. There would be a short break (lights remained off) while the aperture of the stimulus was adjusted, then unique green matches would be made (centrally then peripherally), and finally unique yellow matches would be made (centrally then peripherally). All readings from the colorimeter were made using a small torch; the light was shielded by hand in the direction of the observer to limit the observer's exposure to further light sources throughout the testing procedure. Small breaks were taken between each set of measurements, usually lasting for the time it took to switch on/off the fixation LED and motor (to apply the flicker) in the peripheral task, although longer breaks were encouraged if required by the observer.

2.4.4.1 Colour matching and unique hues

For the Rayleigh matches, participants viewed the bipartite field through the eyepiece of the colorimeter while resting on a chin support. The bottom half of the field was set to a reference wavelength of 585nm, and the top half of the field was composed of red and green primaries (set at 666nm and 555nm,

respectively). The participant was instructed to adjust the intensity of each primary in the top half of the field, making as many adjustments as necessary, until it appeared to perfectly match the bottom half of the field in both colour and brightness. Following this initial match, a further six matches were made, giving a total of seven Rayleigh matches made by each subject; three matches were made by adjusting the green primary while the red primary remained at the value of the initial match, and the final three matches were made by adjusting the red primary, while the green primary was set to its average value (obtained from the previous matches). Between each match, the primary due to be adjusted was reset to a randomised starting value. Rayleigh matches were converted to log(R/G) prior to analysis, where R and G are the relative radiance of the red and green primaries, respectively (as described previously). The means and variances of the matches were used to identify whether any participants showed evidence of inherited colour-vision deficiencies – by having large matching ranges and/or means that fell outside the standard deviation of the mean for all subjects. As stated, this resulted in the exclusion of five participants.

For the unique hue settings, the top half of the bipartite field was occluded, and participants were required to adjust the wavelength of the bottom half of the field until they perceived it to be the specified unique hue. Unique green was described as the point at which the stimulus appears neither yellowish nor bluish, and unique yellow was described as the point at which the stimulus appears neither reddish nor greenish. Prior to making the adjustments for each unique hue, the subjects were instructed to spend time exploring the range of colour either side of the specified unique hue (i.e. from yellow, to

green, to blue, for unique green, and from red, to yellow, to green, for unique yellow). Subjects were also advised to make very small adjustments of the dial in order to best achieve the required unique hue. Both central and peripheral measurements of the unique hues were obtained; the peripheral measurements (at 6.5° eccentricity) were taken outside the fovea to remove any effect of macular pigment on the measurements (which is only present in the fovea).

Beginning with central unique green, the subject fixated on the stimulus and carried out six repeats of the adjustment, with the experimenter randomising the starting value between each adjustment. Six peripheral unique green measurements were then obtained using the same method, while the participant fixated on the LED and the flicker was applied to the stimulus (as described in 2.4.2). Subjects were instructed to maintain fixation on the LED at all times. The process of obtaining central and peripheral measurements was then repeated for unique yellow.

A final concern was that despite a five minute period of dark adaptation at the beginning of the session, observers might maintain weak photoreceptor-level adaptation to either the previous experimental stimuli or the recent outside environment (Hurvich et al., 1968). To test for stimulus 'history', the data were analysed to identify any effect of trial order. For most of the measurements, there was a correlation between trial number and the wavelength settings, but when the first trial was excluded no correlations were observed (see section 2.5.1 for results of these tests). Therefore the first trial was excluded prior to averaging and analysing (although it should be noted

that no difference in the overall findings was observed with these first trials included).

2.4.4.2 Spectral measurements

Three locations were selected from outside scenes situated around the Department of Psychology at the University of York. The positions at which these measurements were taken were marked to ensure the repeat measurements taken within and between seasons were always at the same precise position and angle. The locations were examples of the environment regularly experienced by the subjects (students at the University of York), and contained a combination of man-made objects (cars, buildings, pavements, etc.) and natural surfaces (trees, grass, shrubbery, etc.). Measurements were all taken at approximately 2pm using three different integration times (25ms, 35ms and 50ms), to account for day-by-day differences in light levels and to help avoid sensor saturation. The intensity measurements were recorded as photon counts over the range of 339.6 to 1029.8nm in steps of approximately 0.3nm; these were reduced and resampled to match a scale of 400-700nm (in steps of 1nm) prior to analysis, to represent the visible spectrum better. Finally, measurements were adjusted to absolute intensities by dividing all values by the integration time for that measurement.

2.5 Results

2.5.1 Unique hues

To avoid performing multiple comparisons of the unique hue measurements, a repeated measures ANOVA was first carried out to look for any main effects

of season (winter vs. summer) and eccentricity (central vs. peripheral) on wavelength settings, for the measures of unique yellow and unique green.

A significant effect of season was observed for unique yellow wavelengths settings ($F(1,66)=19.278$, $p<.001$), whilst no effect of season was found for unique green ($F(1,66)=0.360$, $p=.551$). For the eccentricity factor, a significant effect was found for both unique yellow ($F(1,66)=9.493$, $p=.003$) and unique green ($F(1,66)=11.641$, $p=.001$). There was no interaction between season and eccentricity for either unique yellow ($F(1,66)=0.781$, $p=.380$) or unique green ($F(1,66)=0.019$, $p=.891$).

As described in the Methods (2.4.4.1), the first trial was excluded prior to averaging the settings, due to significant correlations between trial number and wavelength settings for a number of the measurements, as shown in Table 2.1; these correlations were no longer significant once the first trial was removed, see Table 2.2. It should be noted that the same significant main effects were observed in the ANOVA even when the first trials were included.

Table 2.1 Pearson correlations between trial number (all trials) and wavelength settings for each unique hue in each season and eccentricity: 'Cent.' is central eccentricity and 'Periph.' is peripheral eccentricity. N=402 for each measurement. Significant correlations ($p<.05$) are highlighted in bold italics.

	Unique Yellow				Unique Green			
	Winter		Summer		Winter		Summer	
	Cent.	Periph.	Cent.	Periph.	Cent.	Periph.	Cent.	Periph.
Pearson Correlation	.140	-.033	.055	-.039	.217	-.124	.105	-.115
Sig. (2-tailed)	***.005***	.508	.272	.436	***<.001***	***.013***	***.035***	***.021***

Table 2.2 Pearson correlations between trial number – with the first trial excluded from each measurement – and wavelength settings for each unique hue in each season and eccentricity: 'Cent.' is central eccentricity and 'Periph.' is peripheral eccentricity. N=335 for each measurement.

	Unique Yellow				Unique Green			
	Winter		Summer		Winter		Summer	
	Cent.	Periph.	Cent.	Periph.	Cent.	Periph.	Cent.	Periph.
Pearson Correlation	.075	.052	.049	.040	.085	.008	.064	-.042
Sig. (2-tailed)	.168	.343	.369	.468	.119	.887	.243	.438

Post-hoc paired *t*-tests were carried out to identify the direction of the main effects highlighted in the ANOVA, specifically, the effect of season on unique yellow for each eccentricity, and the effect of eccentricity on both unique yellow and unique green in each season. Bonferroni correction was applied to the significance values to account for the multiple comparisons. Table 2.3 shows the results of the paired t-tests. Unique yellow wavelengths settings shift to shorter wavelengths between winter and summer, and to shorter wavelengths between central and peripheral eccentricities. Unique green wavelength settings shift to longer wavelengths between central and peripheral eccentricities. After Bonferroni correction, almost all paired comparisons remained statistically significant with the exception of the winter eccentricity comparisons for both unique yellow and unique green (see Table 2.3). Means and standard deviations for each unique hue measurement are shown in Table 2.4.

Table 2.3 Paired t-tests for factors showing a significant effect in the ANOVA (described in text). Significant results (p<.05) are highlighted in bold italics.

Factor	Measurement	Mean difference (nm)	95% Confidence Intervals of the difference		*t* value (df=66)	*p* values (2-tailed, Bonferroni corrected)
			Lower	Upper		
Effect of Season (Winter vs. Summer)	Central Unique Yellow	1.549	0.543	2.555	3.073	***.018***
	Peripheral Unique Yellow	2.011	1.093	2.928	4.374	***<.001***
Effect of Eccentricity (Central vs. Peripheral)	Winter Unique Yellow	1.047	0.116	1.977	2.246	.168
	Summer Unique Yellow	1.509	0.484	2.534	2.939	***.03***
	Winter Unique Green	-3.048	-5.349	-0.747	-2.644	.060
	Summer Unique Green	-3.208	-5.231	-1.185	-3.166	***.012***

Table 2.4 Descriptive statistics for each unique hue measure (for each season and eccentricity).

Unique Hue	Season	Eccentricity	Mean (nm)	Standard Deviation
Unique Yellow	Winter	Central	571.81	4.81
		Peripheral	570.76	3.94
	Summer	Central	570.26	4.99
		Peripheral	568.75	4.95
Unique Green	Winter	Central	519.97	7.84
		Peripheral	523.02	11.40
	Summer	Central	520.47	9.08
		Peripheral	523.68	12.22

The mean differences between seasons (calculated on a subject-by-subject basis prior to averaging) for both eccentricities of unique yellow and unique green are plotted in Figure 2.4.

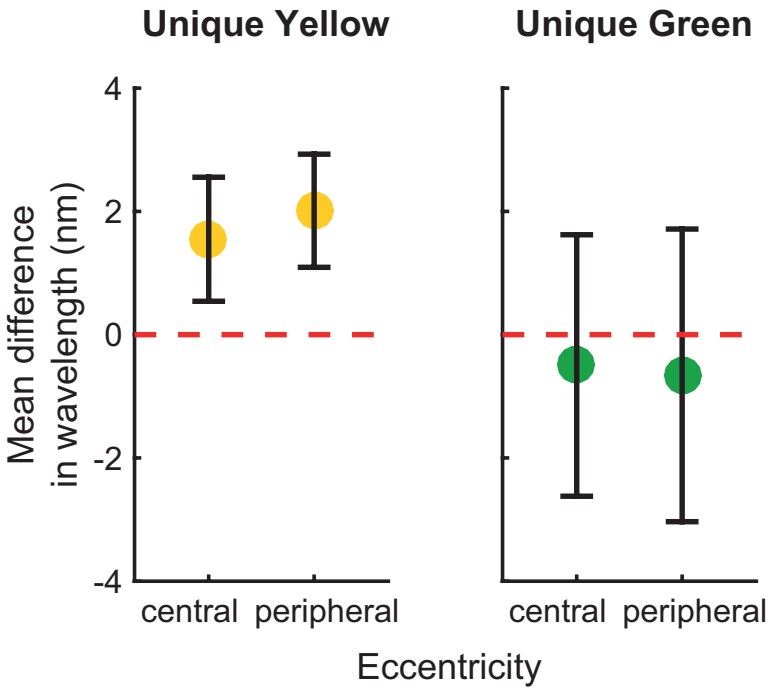

Figure 2.4 Mean difference between winter and summer measurements for each eccentricity and unique hue. With error bars showing the 95% confidence intervals of the mean.

2.5.2 Rayleigh matches

Rayleigh matches were recorded at a central eccentricity in each season. A paired t-test between the values taken in winter compared to summer showed no significant difference between the means ($t(66)=0.054$, $p=.957$). Mean Rayleigh match values (given in log(R/G)) with standard deviations for each season were as follows: winter = -0.140 (± 0.09), summer = -0.141 (± 0.08). The mean difference between winter and summer is plotted in Figure 2.5, with 95% CI error bars.

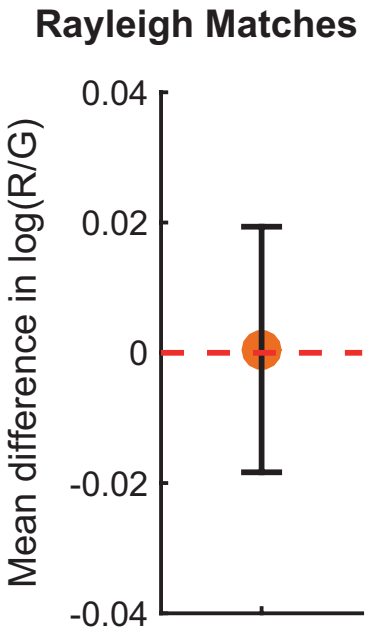

Figure 2.5 Mean difference in Rayleigh matches (in log(R/G)) between winter and summer (measurements taken centrally). Error bars show the 95% confidence intervals of the mean.

2.5.3 Spectral measurements

For each of the three locations where spectral measurements were taken, averages were first calculated for each of the five measurement days; three measurements were taken on each day using different integration times, which were normalised before averaging. For a couple of the days (for different locations), measurements were saturated at all integration levels and were therefore excluded. Averages for each season and each location were then made in order to calculate the difference between seasons. Figure 2.6A illustrates the mean differences between seasons (summer-winter) for the log(intensity) values of the average spectra at each location, with an additional dashed reference line indicating a typical peak reflectance for green vegetation (as estimated in NASA Reference Publication 1139 (Bowker, Davis, Myrick, Stacy, & Jones, 1985)). The peak difference for all the measured locations occurs around the average peak reflectance of vegetation (~550-560nm). For

the locations measured, this indicates that the largest change between seasons was an increase of 'green' in the environment in summer compared to winter.

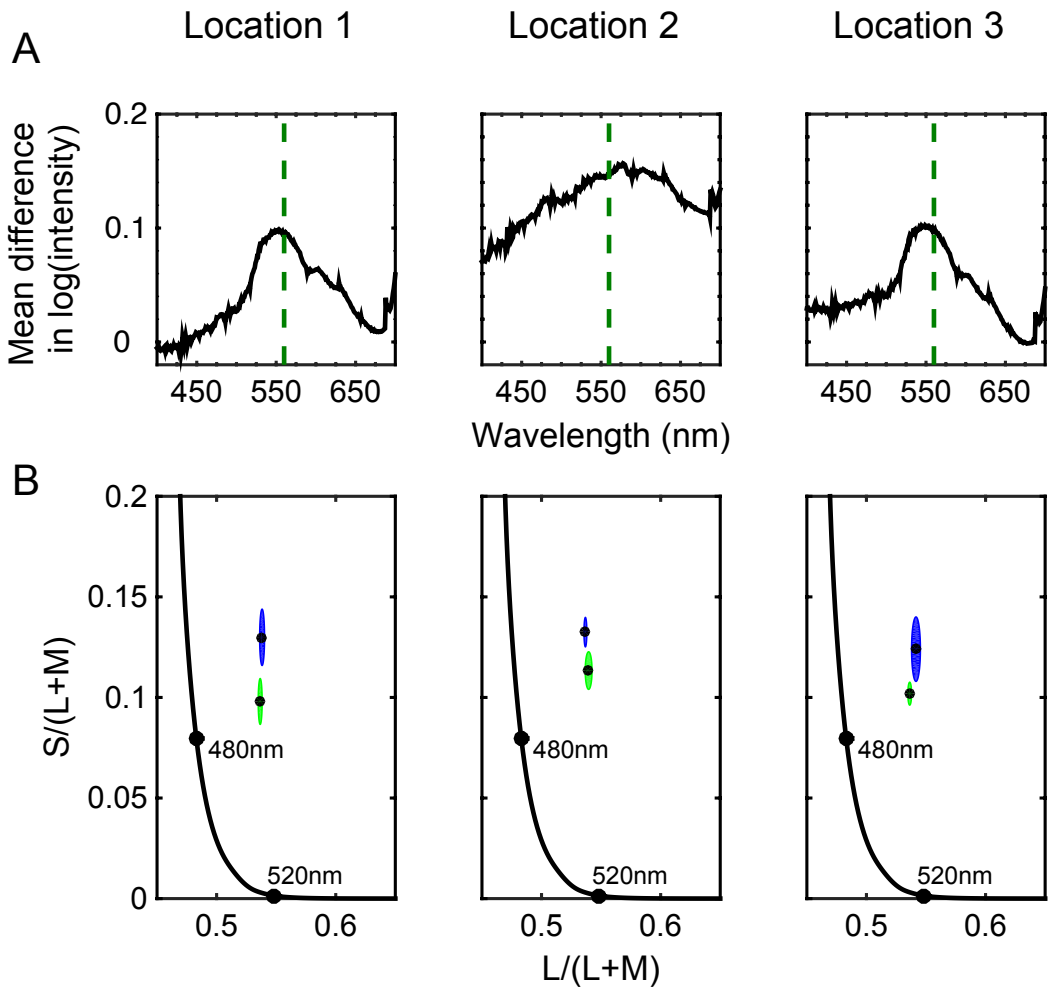

Figure 2.6 A) Mean difference in logged spectra, for summer minus winter, in each location. Green dashed line indicates typical peak reflectance of green vegetation at 560nm (NASA Reference Publication 1139 (Bowker et al., 1985)). B) Plots of mean spectra for each location in MacLeod and Boynton (1979) cone space. The black dots show the means for each location with standard deviations indicated by the green and blue ovals, for summer and winter, respectively.

To better estimate the change between seasons, the mean spectra for each measurement day from each season were converted into LMS cone excitation levels using 2° cone fundamentals (Stockman & Sharpe, 2000) downloaded from the Colour and Vision Research Laboratory online database (www.cvrl.org), and then plotted in MacLeod and Boynton (1979) cone space; Figure 2.6B shows the means and standard deviations of the spectra in the S/(L+M) vs. L/(L+M) cone space for each location.

In order to run an ANOVA on the data using all measurement days, missing values (i.e. where all measurements for a location saturated on a particular day) were replaced with the average value across all other measurement days for that particular location. A repeated measures ANOVA was carried out using S/(L+M) and L/(L+M) as separate measures of the dependent variable, which was the value of the cone space directions, and using factors of location and season. Mauchly's test of Sphericity was violated for the L/(L+M) measure of the location factor ($\chi^2(2)=6.655$, $p=.036$), but not for the S/(L+M) measure or either of the location and season interactions, therefore a Greenhouse-Geisser correction was applied only to the location factor for the L/(L+M) measure.

There was a significant main effect of season on both the L/(L+M) ($F(1,4)=75.779$, $p=.001$) and S/(L+M) ($F(1,4)=13.212$, $p=.022$) dimensions. There was also a significant effect of location on S/(L+M) ($F(2,8)=8.018$, $p=.012$), but not on L/(L+M) ($F(1.058,4.230)=5.850$, $p=.069$, Greenhouse-Geisser corrected), indicating that in general there was more variability on the S/(L+M) dimension than on the L/(L+M) dimension. However, there was an interaction between season and location for L/(L+M) values ($F(2,8)=12.623$, $p=.003$), which likely represents the opposite direction of shift observed for Location 2 for these values between winter and summer, compared to the other two locations. No interaction was found between season and location for S/(L+M) ($F(2,8)=2.619$, $p=.133$). Descriptive statistics showing the means and standard deviations of the values used in the ANOVA (i.e. including the

replacement of missing values with means for that location and season) are presented in Table 2.5.

Table 2.5 Means and standard deviations of the cone space dimensions (S/(L+M) and L/(L+M)) for each location and season.

Dimension	Location	Season	Mean	Standard Deviation
S/(L+M)	1	Winter	0.130	0.012
		Summer	0.098	0.011
	2	Winter	0.132	0.006
		Summer	0.112	0.006
	3	Winter	0.125	0.015
		Summer	0.101	0.006
L/(L+M)	1	Winter	0.538	0.002
		Summer	0.537	0.002
	2	Winter	0.537	0.001
		Summer	0.539	0.002
	3	Winter	0.542	0.003
		Summer	0.536	0.002

Finally, the LMS cone excitation values were used to calculate an estimate of L:M cone absorption ratios. As with the previous analysis, missing values for certain measurement days were replaced with the average for that location and season to allow an ANOVA analysis. A repeated-measures ANOVA was carried out to identify any main effects of the location and season factors on the L:M absorption ratios. Mauchly's test of Sphericity was violated for the location factor ($\chi^2(2)=6.757$, $p=.034$), therefore a Greenhouse-Geisser correction was applied to this factor. There was a significant main effect of season ($F(1,4)=71.815$, $p=.001$) on L:M absorption ratios; on average (across locations) L:M ratios decreased between winter (1.170±0.004 (mean ± standard error)) and summer (1.162±0.003). There was no main effect of location on the L:M ratios ($F(1.055,4.222)=5.898$, $p=.068$, Greenhouse-Geisser corrected), however there was an interaction between location and season ($F(2,8)=12.664$, $p=.003$), which may be driven by the opposite direction of effect of season seen in Location 2 (see Table 2.6).

Table 2.6 Means and standard deviations of the L:M absorption ratios for each location and season.

Location	Season	Mean	Standard Deviation
1	Winter	1.166	.008
	Summer	1.158	.007
2	Winter	1.160	.004
	Summer	1.171	.010
3	Winter	1.184	.016
	Summer	1.157	.007

2.6 Discussion

2.6.1 Summary of Results

A shift in unique yellow wavelength settings occurred between winter and summer, with wavelengths shifting to shorter wavelengths in the summer for both central and peripheral eccentricity measurements. This shift was small (~1.55nm for central, and ~2.01nm for peripheral eccentricity measurements) but highly significant, as tested by both repeated measures ANOVA and paired t-tests (which were Bonferroni corrected). No changes in Rayleigh matches or unique green settings were observed between seasons.

Spectral measurements taken in each season indicated that the largest difference between seasons in the reflectance of the environment occurred at wavelengths of ~550-560nm, which corresponds to the typical peak reflectance of vegetation. Conversion of these spectral measurements into LMS cone excitations showed an overall effect of season on L:M cone absorption ratios, and on cone space dimensions S/(L+M) and L/(L+M). However, there were some inconsistencies between the locations measured, which limit the extent to which conclusions can be drawn regarding the degree of environmental changes in York (UK).

2.6.2 Controls and considerations

An important control for this experiment was testing additional measurements alongside the unique yellow settings. Rayleigh matches are considered to be stable because they depend on the genetically-determined peak sensitivities of the cones present in the retina of the observer (Thomas & Mollon, 2004). Therefore, any changes observed in these matches would indicate equipment related changes between the seasons, rather than an observer-based change. It should be noted that during the mid-20th century, Richter (1948, 1951 - as cited in Jordan & Mollon, 1993) reported seasonal variations in Rayleigh matches, with subjects requiring more red in a red-green mixture to match a monochromatic yellow light during the summer months compared to winter. Jordan and Mollon (1993) were able to replicate Richter's finding, however, they determined that the observed changes found over the period of a year were likely due to ambient temperature fluctuations affecting the prism housing of the anomaloscope used for testing. They supported this conclusion by stabilising room temperature (to within 1°C) to keep the temperature conditions constant for the observers, and locally heating or cooling only the temperature of the prism housing of two Nagel anomaloscopes. It was found that Rayleigh matches shifted to require more red in the red-green mixture when the temperature of the prism housings were increased, and it was therefore concluded that the variations found by Richter may have been an artefact of variants in ambient temperature impacting on the anomaloscope, rather than due to changes in the observer. In the experiment described in this chapter, the laboratory temperature (measured from near the prism housing of the colorimeter) was monitored in

each season, and no change in temperature was observed. This coincides with the finding that Rayleigh matches remained stable between seasons.

A potential confound for the settings made, as outlined in the Methods section (2.4.4.1), was that observers might maintain weak photoreceptor-level adaptation, to either the previously presented experimental stimuli, or the recent outside environment. The effect of short-term adaptation on unique green settings has previously been measured by Hurvich *et al* (1968). It was found that unique green settings taken after dark adaptation differed to settings made after performing unique yellow measurements; wavelengths were longer (by ~10nm) following unique yellow measurements. However, more recent chromatic adaptation experiments conducted by Rinner and Gegenfurtner (2000) assessed the time course of slow phase adaptation using two different testing methods: either asking observers to make a judgement on the appearance of a single stimulus, or to perform a 4-alternative-forced-choice (4AFC) discrimination task – the task occurred every five seconds following an adaptation period of 120 seconds. On average the half-life of the adaptation effect lasted between 15 and 25 seconds, for both versions of the experiment (judgement of appearance and 4AFC). These studies demonstrated short-term adaptation effects on colour judgement tasks, but also indicated that the effects are reduced after a short period of time and therefore have very little long-term impact on colour perception. In the present experiment, the effect of any short-term adaptation was accounted for by removing the first measurement made from the set of six performed by the subjects for each measure prior to averaging and analysing. It was shown that for a number of the measures across eccentricities and seasons (primarily

unique green) a significant correlation could be observed between trial number and wavelength settings, which was subsequently non-significant following the removal of the first trial (as detailed in section 2.5.1). This indicated that the first trial out of the six repeats might have been affected by any lingering short-term photoreceptor-level adaptation.

Further to this, the Belmore and Shevell (2011) work, described previously, indicated that very-long-term adaptation effects were not disguised by any short-term adaptation effect. Specifically, they found larger adaptation effects (shifts in unique yellow settings) when a short-term adaptation condition was used in addition to a very-long-term adaptation condition – compared to when either condition was carried out alone – indicating a cumulative impact of both adaptation types. Therefore it is not expected that any photoreceptor-level adaptation caused by short-term environmental adaptation immediately before the experiment or from previous experimental settings would impinge on very-long-term adaptation effects caused by seasonal environment (in addition to the acknowledged difference between the first measurements made, that were excluded from the average settings). Incidentally, it is noted that the same main effect of season on unique yellow is observed even when the first measurements *are* included, which supports the suggestion that known short-term adaptation effects do not disguise very-long-term adaptation effects.

2.6.3 Modelling the shift in unique yellow settings

Neitz *et al* (2002) found that unique yellow settings shifted in opposing directions following adaptation to red or green filtered chromatic

environments; settings shifted to longer wavelengths following red adaptation, and to shorter wavelengths following green adaptation. The shift from baseline increased gradually over a period of approximately 10 days, up until the intervention was stopped. The shift following the adaptation to the green filtered chromatic environment ranged between approximately 1.3 and 4.6nm, this range encompasses the shift observed between winter and summer for the present experiment, with shifts (to shorter wavelengths) of 1.549nm for central measurements and 2.011nm for peripheral measurements. These shifts fall within the lower end of the range seen by Neitz *et al*; this smaller degree of shift may be expected given that the adaptation is to a less extreme chromatic environment than that produced by coloured filters/contact lenses, despite a longer period of adaptation (minimum one month) to the seasonal environment. A proposed mechanism for unique yellow settings, modelled below, illustrates the mechanistic changes that could generate a shift of the size and polarity observed in both this experiment and that of Neitz *et al.*

Unique yellow is considered to be the neutral point of a red/green (L-M) opponent system. Whilst this is supported by the perceptual definition of unique yellow (neither greenish nor reddish), it does not reflect the actual neutral point of L-M opponent channel curves derived from cone fundamentals, which would predict unique yellow settings far shorter (by ~30nm) than average observed measurements. Neitz *et al* (2002) considered the hypothesis that for the neutral point of this channel to reflect average unique yellow wavelength settings, the relative gain of the L and M cones needs to be adjusted until the weighting of the M cone input is higher than the

L cone input, which shifts the neutral point of this channel to a longer wavelength and therefore better reflects actual unique yellow settings. If this gain control mechanism is plastic – that is, it can adapt to the mean of the environment – it would have the effect of altering the L-M neutral point and, as a consequence, shifting unique yellow settings. Adopting this model, the shifts observed by Neitz *et al* could be explained by a change of 10% in the relative weightings of L and M cone inputs into this hypothetical unique yellow system. The same logic was applied to the data gathered here, and the environmentally driven changes in L and M cone inputs into an opponent L-M unique yellow mechanism were modelled. Figure 2.7A shows a change in this L-M opponent channel output as a result of altering the gain of the M cones across a 10% range. The neutral point of each of these curves is highlighted in the detail view in Figure 2.7B. These curves were calculated using the Stockman and Sharpe (2000) 2° cone fundamentals, and, for simplicity, only changes in the M cone gain were considered. In this model, the shortening of the unique yellow wavelength settings represents a reduction in M gain. A decrease of approximately 3.2% in the relative M cone weighting would be necessary to result in the mean shift that was observed for foveal/central unique yellow settings between winter and summer (1.549nm). This decrease in weighting corresponds to a scenario in which the average relative excitation of the M cones is *increased* in summer (for instance, in response to adapting to a greener chromatic environment), and as a result the weighting of the M cone input would need to be decreased in order to maintain the previous equilibrium of the L and M cone inputs.

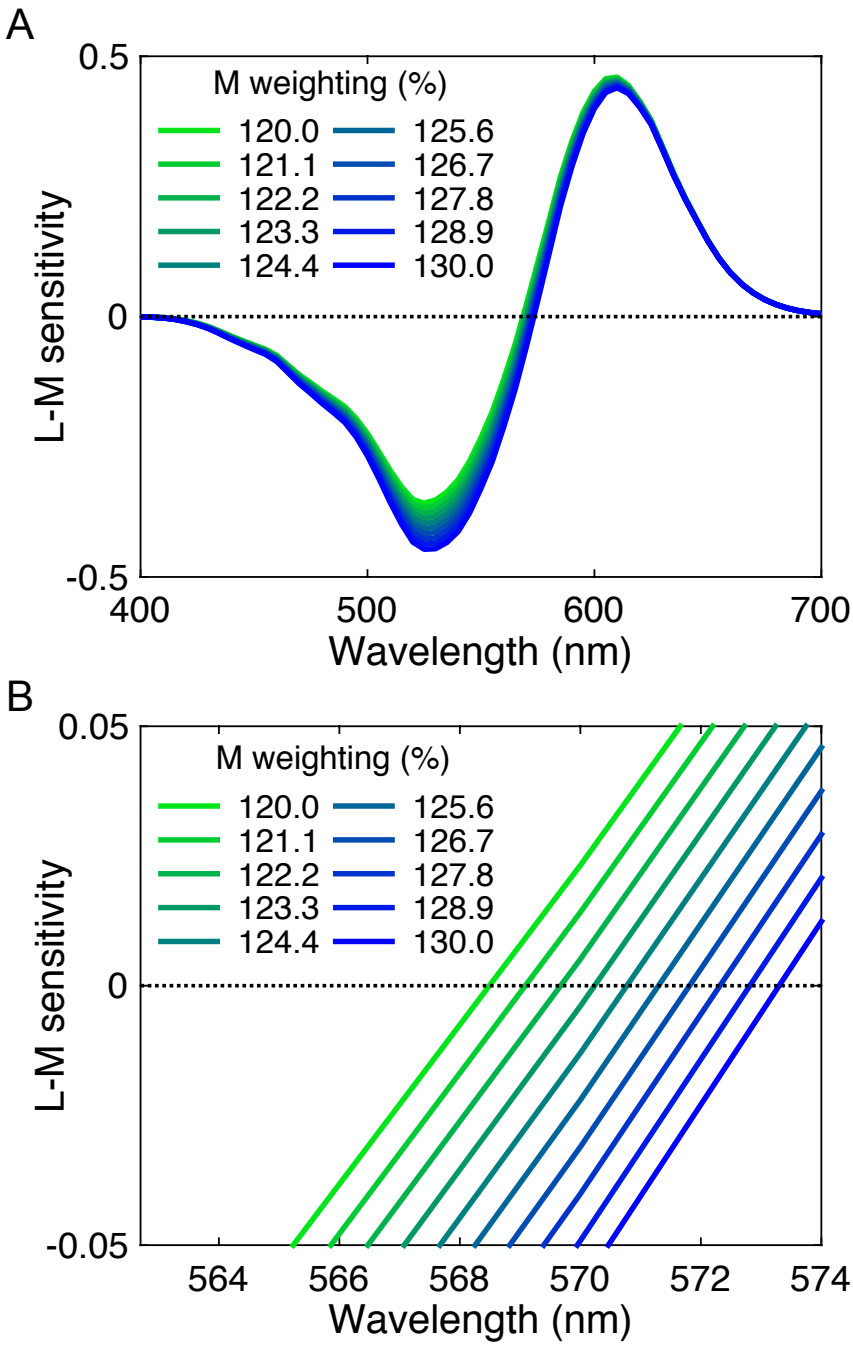

Figure 2.7 Plot of L-M opponent curves, calculated using different M cone weightings (line colours change from blue to green with decreasing weighting of M cone). Curves are shown in (A). Detail view of the zero crossings ('neutral point') of the curves is shown in (B).

Contrary to the proposed mechanism for determining unique yellow, there is to date no clear mechanism that sets unique green, and as noted in the review of unique hue literature, a number of factors have been shown to affect unique green settings. Therefore if a similar model is applied to predict shifts in

unique green values – i.e. S-(L+M) – the extent to which this model can actually predict changes in unique green is limited. Incidentally, if the same change in M cone weightings that was observed for the unique yellow shift (3.2%) is used in this comparable opponent model for unique green, the estimated shift in settings is ~0.14nm to *longer* wavelengths between winter and summer. This prediction is in the same direction as that observed here in the non-significant unique green differences between seasons, i.e. wavelength settings are longer in the summer than the winter for unique green. However, the validity of this proposed model for unique green is dubious because such a system must re-weight the S cone responses by a large amount (by a factor of 55) to make the neutral point of the S and L+M responses correspond to unique green settings. Other models of unique green have since been suggested by Schmidt *et al* (2014), including a system that compares L to M+S signals. However, to best assess the relationship of any of these models to the current experiment, a carefully controlled artificial adaptation experiment measuring unique green settings – equivalent to the Neitz *et al* (2002) study – would produce the clearest indication of whether such a mechanism would be expected to cause a shift (and by what degree) in unique green settings following natural adaptation.

2.6.4 Discussion of the spectral measurements

The spectral measurements that were taken in each season were limited in both quantity and range. Only a small number of locations was assessed, and whilst averaging across locations demonstrated the expected differences in L/(L+M) values (higher in the winter), which are consistent with findings reported by Webster *et al* (2007), one of the locations (a car park) actually

showed the opposite direction of change for this value (as well as for the estimates of L:M absorption ratios).

If the averages across locations are merely used as a potential indicator as to the change in chromatic environment, then the average decrease in L/(L+M) and L:M absorption ratios between winter and summer are consistent with an average *increase* of 'green' in the environment, and also fit with the suggested model for re-weighting the M cone input. The model indicated that a decrease of approximately 3.2% in the M cone weighting would be required to explain the observed shift in unique yellow settings. The mean decrease in M cone weightings, estimated here from the average L:M absorption ratios across locations between seasons, is approximately 0.7%; however, the location showing the largest change in L:M ratios between seasons demonstrated a decrease of approximately 2.3% in the M cone weighting. It should be emphasised that these values are just estimates based on the limited spectral measurements available; more would be required to improved the accuracy of these estimates.

In order to acquire an accurate representation of the average chromatic environment experienced by individuals between seasons, one method would be to take regular photospectrometer samples of the environment from a head mounted position of several observers. This would allow for many samples across the course of a number of 'average' (e.g. working) days to be taken in each season, to compare average environmental exposure for similar daily routines (e.g. commute to and from work, environment experienced throughout day). It would be expected that internal man-made environments

would be unlikely to change between seasons, whilst representative examples of outdoor scenes that are normally experienced would show a marked change in the average chromaticity, as a result of increased green vegetation in the summer. However, there would be practical limitations to gathering such a dataset, such as the setup of the photospectrometer on a transportable (head mounted) medium as well as requiring subjects to wear the equipment for extended periods. Alternative data collection devices based on wearable microcontrollers could help accomplish this goal.

2.6.5 Possible sites for the mechanism

The site of the mechanism that computes unique yellow is still unknown. To identify whether the site was pre-cortical, Neitz *et al* (2002) carried out an additional experiment in which one eye was exposed to chromatic adaptation (first red, then green, via goggles) while the other eye was occluded, for four hours a day over eight days. Only the occluded eye was used to measure unique yellow. They found the same directions of shift in unique yellow as was observed in the binocular adaptation experiments, however the size of the shifts were smaller. These findings indicate that at least some adaptation was occurring at a cortical locus.

This cortical hypothesis was supported by Wuerger, Atkinson and Cropper (2005) who carried out modeling based on the LMS cone excitations elicited by unique hue stimuli, which were gathered for a range of luminance and saturation levels. They aimed to identify how the cone excitations contributed to the unique hue mechanisms, which silence chromatic mechanisms, e.g. the L-M system is silenced to perceive unique yellow or unique blue. For unique

yellow, they showed that a single mechanism would be capable of silencing the L-M system using a large amount of input from the L and M cones, and a small input from the S cones. This mechanism would sum the responses of an L-M input with S cone input ((L-M)+S). The authors propose that this places the site of the mechanism within the cortex, since this is not one of the cone-opponent mechanisms (L-M, and S-(L+M)) that are found pre-cortically within the LGN neurons.

However, Tailby, Solomon and Lennie (2008) have since identified neurons in the macaque LGN that receive an atypical chromatic input, in which the S and M cones are combined and opposed by the L cones. Unlike the more conventional L-M opponent neurons identified by Derrington, Krauskopf and Lennie (1984), these neurons have a preferred colour direction that maps closely to the percept of 'yellow'. If these cells are the source of the unique yellow signal, then plastic changes to their L and M cone input weights may be occurring at the retina.

2.7 Conclusion

A shift in unique yellow settings was observed between winter and summer, while unique green and Rayleigh match settings remained stable. The photospectrometer measurements from the University campus indicated a measureable change in the chromatic environment between seasons; the environment was greener in summer. This was consistent with previous measurements of chromatic shifts between seasons reported by Webster *et al* (2007). It is concluded that the shift in unique yellow is likely to be the result of adaptation to the changes in chromatic environment in each season, which

causes a shift in the weighting of L and M cone inputs into an opponent channel that differences L and M cone inputs.

While it is noted that the samples taken to measure changes in the environment are not thorough representations of total environmental changes experienced by observers, it is reasonable to suggest that the primary environmental difference experienced between seasons relates to natural changes, such as the level of vegetation, which would cause a change in the average environment that the participants were exposed to.

The experiments described in this chapter demonstrate environmental adaptation effects on a particular percept of colour – unique yellow. This is the first reported evidence of unique yellow settings shifting as a result of adaptation to *natural* environmental changes between seasons. This finding supports the hypothesis that unique yellow settings are determined by the neutral point of the L-M opponent channel, following a neural adjustment to the weighting of the L and M cone inputs; this mechanism reweights L and M cone inputs in response to changes in the average chromatic environment. Whilst this type of shift in unique yellow has previously been observed in artificial adaptation experiments, this experiment provides evidence for regular, plastic normalisation, in response to the natural seasonal changes in the environment.

Chapter 3 Visual Processing in Dichromats

3.1 Overview

Dichromats lack a single class of photoreceptor and therefore lack an axis of opponent colour space. However, they do not usually have fewer photoreceptors overall. Might human dichromats therefore have a visual advantage over trichromats in some tasks that depend on the remaining channels? In this Chapter, contrast discrimination in the luminance domain is explored as a potential site of enhancement in dichromats.

Chapter 3 first outlines the key contrast detection and discrimination literature, describing the contrast sensitivity and contrast response functions of the luminance pathway; this literature includes human behavioural and fMRI experiments, as well as animal models that use single-cell recordings. Studies are then discussed that measure anatomical differences between dichromats and trichromats in non-human primates. This literature is used to inform a hypothesis for how neuronal population tuning may differ between dichromats and trichromats, and how this might affect contrast discrimination thresholds between these groups.

Two experiments were performed which both measured contrast discrimination thresholds of luminance gratings across a range of contrast pedestals using a 4-alternative-forced-choice task; Experiment 2 made small improvements on the design from Experiment 1, and recruited a larger sample of subjects to test the hypotheses more completely. It was found that

dichromats and trichromats do not differ in their thresholds for the parameters measured: dichromatic subjects have neither an advantage, nor disadvantage, in their ability to distinguish contrasts in the luminance domain compared to trichromats, at the particular spatial frequency and eccentricity that were measured in these experiments.

3.2 Background

3.2.1 Contrast detection and discrimination of the luminance pathway

The ability to detect variations in luminance levels within the visual world – or within an experimental stimulus – is known as contrast sensitivity. It can be measured psychophysically by adjusting the contrast of a stimulus to determine the contrast detection 'threshold' level, i.e. the contrast level where the observer starts to be able to detect the stimulus above chance levels. When contrast detection thresholds are acquired for stimuli with different spatial frequencies, a contrast sensitivity function (CSF) can be produced, with contrast sensitivity (typically, 1/contrast threshold) plotted as a function of spatial frequency (Enroth-Cugell & Robson, 1966; Schade, 1956). For luminance pathways these functions show the peak sensitivity (where *high* sensitivity is equivalent to a *low* detection threshold) at mid- to low- spatial frequencies, producing a roughly bell-shaped function (see Figure 3.1).

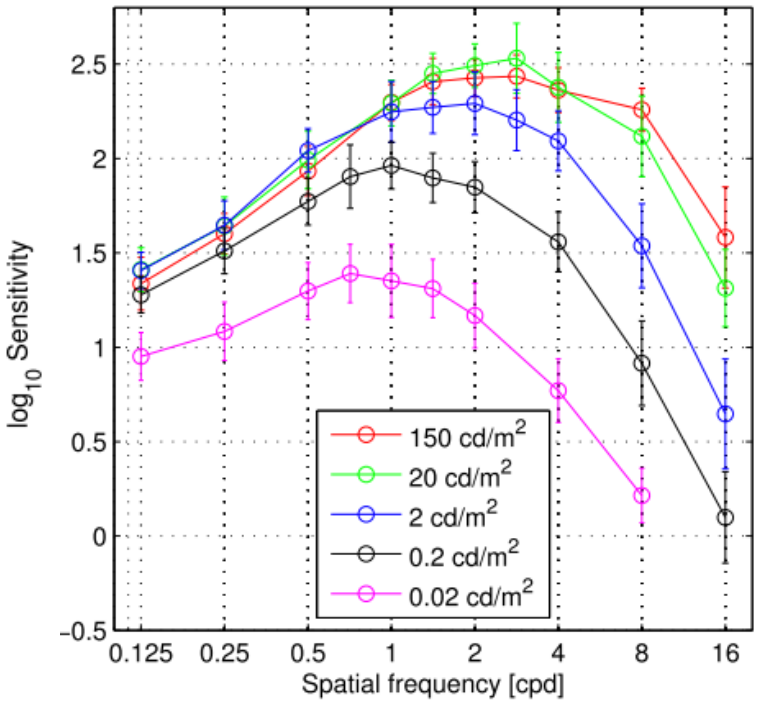

Figure 3.1 Contrast sensitivity functions (sensitivity plotted against spatial frequency) for different levels of background luminance, as illustrate by the legend. These functions represent the mean of seven observers. Taken from Kim, Mantiuk and Lee (2013).

However, whilst CSFs are based on the detection of the stimuli across spatial frequencies, contrast response functions (CRFs) describe the responses to different contrast levels (of a fixed spatial frequency, or other stimulus type). These functions are determined by the nonlinear change in average neuronal response to contrast – responses accelerate at low contrasts and saturate at high contrasts (Baker, 2013). For example, measurements in single-cell animal studies show a nonlinear S-shaped increase in neuronal responses as a function of contrast (Geisler & Albrecht, 1997). The nonlinearity of the neuronal CRF can be probed psychophysically using contrast discrimination experiments that measure a subject's ability to detect or discriminate contrast modulations across a range of contrast 'pedestal' levels. A zero contrast pedestal is a measure of contrast sensitivity (or the 'absolute threshold'). If a pedestal that matches the stimulus (e.g. a grating) is presented in all the

possible target locations, the task now measures the contrast discrimination ability between the contrast of the pedestal and the contrast of the target *plus* the pedestal. This version of the task therefore indicates how large the target modulation needs to be for it to be distinguished from the pedestal contrast. The amount of change in neuronal response due to a unit change in contrast at any pedestal is the slope of the CRF at that point. If discrimination is limited by a constant, relatively late noise source then discrimination thresholds should be proportional to the inverse of the slope (the first derivative) of the CRF function. Figure 3.2 shows an example of a contrast discrimination task that uses a 10% contrast pedestal. If the visual system had a linear response to contrast (constant slope), then the contrast detection threshold across a range of pedestal contrasts would be identical. In reality, the acceleration of neuronal responses at low contrasts results in lower detection thresholds when the pedestal contrast is low (and the slope is steep) compared to when the pedestal contrast is high (and the slope is saturating).

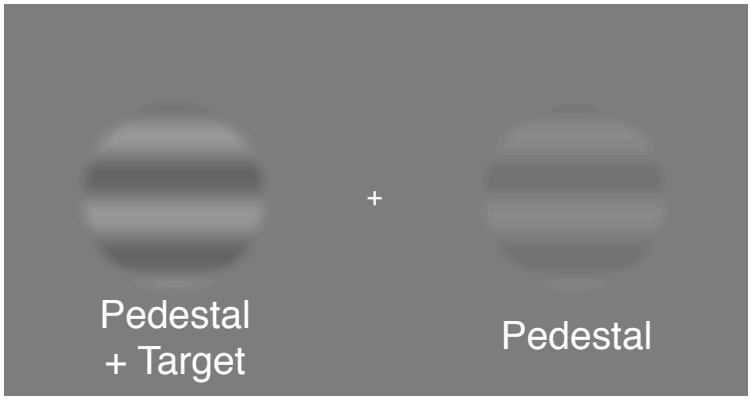

Figure 3.2 Example of stimuli in a 2AFC contrast detection task, with a 10% contrast pedestal. The target has a 10% contrast in this example, so the 'pedestal + target' contrast shown here is 20%.

Contrast discrimination experiments can be performed across a number of pedestal levels to produce a threshold versus contrast (TvC) function. Over

much of the range, contrast thresholds increase with increasing pedestal contrast. However, Nachmias and Sansbury (1974) noted that a different relationship between threshold and pedestal is found at very low levels of pedestal contrast, such that the data indicate a dip at low contrast pedestal levels – this effect is commonly referred to as 'facilitation', and the resultant function known as a 'dipper' function, which can be seen in Figure 3.3 (Legge & Foley, 1980). Typically, the most facilitation – at the lowest point of the dip – occurs when the pedestal contrast level is equal to the absolute threshold value (at a 0% pedestal contrast) (Baldwin, Baker, & Hess, 2016).

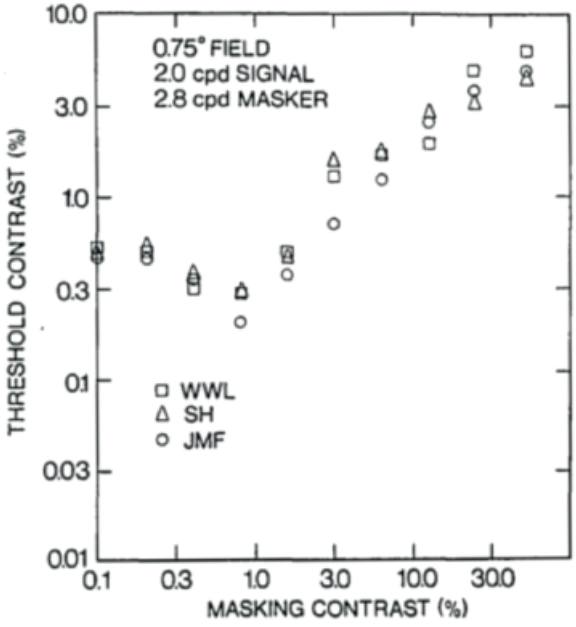

Figure 3.3 Example of dipper functions for three observers ('WWL', 'SH', and 'JMF'), taken from Legge and Foley (1980). Contrast thresholds are plotted as a function of the contrast pedestal (masking contrast).

Human fMRI studies have been used to compare V1 amplitude responses for different contrast levels with psychophysical TvC functions (Boynton, Demb, Glover, & Heeger, 1999). fMRI response amplitudes were found to increase as

a function of contrast, and the response function approximately predicted the contrast thresholds measured in the same subjects outside the scanner.

Signal detection is dependent on noise. If external and/or internal noise is minimised it is expected that thresholds would be improved relative to a system with more noise (Wickens, 2001). Noise in the visual system can arise at many points, but at least one way that noise can be reduced is by averaging responses from uncorrelated neurons. In this case, noise levels are determined by the number of neurons responding to a particular stimulus. Studies by Chirimuuta and Tolhurst have modelled the effect that the number of neurons can have on the accuracy of contrast identification (Chirimuuta & Tolhurst, 2005; Clatworthy, Chirimuuta, Lauritzen, & Tolhurst, 2003). The effect of increasing the number of neurons was equivalent to increasing the mean maximum neuronal response – both improved the accuracy of contrast identification. While this relationship is not entirely straightforward, and does not account for the influence of neurons with a lower, non-optimal response to the stimulus (May & Solomon, 2015), it does contribute to the idea that increasing the number of neurons within a specific tuning population may increase the precision with which the signal is detected, and therefore reduce the threshold of discrimination at that level.

Geisler and Albrecht (1997) measured responses from populations of single cells in the primary visual cortex of macaque monkeys and domestic cats. These measurements were taken for a variety of stimulus dimensions (e.g. contrast, spatial frequency, orientation). To estimate the detection and discrimination performance of each neuron to the various dimensions, 2-

interval-forced-choice (2IFC) 'tasks' were used to model the point at which the responses to two stimuli could be distinguished 75% of the time. This was measured by correctly predicting which interval the target stimulus was presented in for a range of contrast target levels. For the contrast dimension, contrast discrimination thresholds increased when the base-level (pedestal) contrast increased, in line with typical psychophysical TvC functions. However, further to this, the authors present a histogram of the threshold levels that each neuron optimally responded to (i.e. across all the pedestal levels presented). In this instance, the inverse of the TvC function was seen – there was a positively skewed distribution of neurons across contrasts, so the largest percentage of neurons (>70%) responded optimally to lower thresholds (<25% contrast) (associated with low contrast pedestals), and a much lower percentage (<5%) of neurons responded optimally to high thresholds (>75% contrast) (associated with high contrast pedestals).

Combining the modelled predication that larger numbers of neurons should produce better accuracy in contrast discrimination (Chirimuuta & Tolhurst, 2005; Clatworthy et al., 2003), with the observation that fewer neurons contribute to discrimination at high contrast pedestals (Geisler & Albrecht, 1997), can lead to the following prediction: if more neurons were 'introduced' and evenly distributed across the populations that optimally respond to different thresholds, then the *relative* increase in neurons would be greater for those small populations most sensitive to high contrast thresholds, than for the large populations most sensitive to lower contrast thresholds. Therefore, any potential benefits of increased numbers of neurons would be most likely to present for the higher contrast pedestal stimuli.

Trichromats have three types of cone photoreceptor in the retina, which allows for three opponent pathways – luminance (L+M), L-M and S-cone isolating. 'Red-green colour-blind' dichromats lack either the L (protanope) or the M (deuteranope) cone type in the retina. Because of this, these dichromats do not possess a behavioural L-M pathway, and as such no neurons would be tuned to such a pathway within the typical anatomical L-M pathway structure; instead, this anatomical pathway may behave differently. If these 'would-be' L-M tuned neurons were instead allocated to processing luminance or S-cone isolating pathways, there would be an effective increase in the population size of neurons tuned to these pathways in dichromats compared to trichromats. Of course, a re-distribution such as this could have a potential impact on any number of stimulus dimensions within these pathways, and as it is unknown exactly how large the relative increase in neurons would have to be to cause an effect on psychophysical threshold measurements, the resulting hypotheses that can be made are inevitably tentative.

In order to make predictions about the likely consequences of dichromacy on aspects of visual processing, it is first important to understand the current literature investigating possible anatomical differences between the dichromat and trichromat visual systems. The following section discusses this literature, and identifies a number of behavioural studies that have investigated different aspects of visual processing in dichromats, and how this can inform the hypotheses made for the experiments in this Chapter.

3.2.2 Dichromat Vs. Trichromat: anatomy and visual processing

Studies of anatomical visual system differences between human dichromatic and trichromatic individuals have not been carried out, however, these differences have been extensively investigated with non-human primates. An advantage of non-human primate studies is that detailed anatomical measures of visual systems can be performed that would not be possible in human subjects.

Solomon (2002) looked specifically at the koniocellular (KC) pathway 'blobs' found in the V1 of marmosets, and assessed the input from the LGN into the blobs. No differences between dichromatic and trichromatic individuals were observed in the number of KC cells projecting from the LGN to V1, or in the overall density of the blobs in V1. However, as noted by Solomon, work by Lennie, Krauskopf and Sclar (1990) and Leventhal, Thompson, Liu, Zhou and Ault (1995) have both shown evidence of colour-responsive cells within both the blob and interblob regions, and therefore effects of dichromacy (versus trichromacy) would not necessarily be expected to be seen only within the blobs. In order to make a more comprehensive comparison of the marmoset LGN between dichromats and trichromats, and account for the fact that any potential differences may not just be located in KC pathway projections, FitzGibbon *et al* (2015) measured overall LGN volume, with separate measurements for parvocellular (PC), magnocellular (MC), and KC layers. They observed no differences between the dichromats and trichromats for any of the layers in the LGN. Similarly, Goodchild and Martin (1998) used marmosets to measure the projections of the PC, MC and KC layers from the

LGN into V1 and V2. This study used markers for proteins found in each of these layers, and compared the size and distribution of the responses from each protein marker between dichromatic and trichromatic groups. No differences were observed between the groups for any of the layers.

These studies indicate that in non-human primates there are no structural differences in the LGN and visual cortex for pathways associated with processing colour – despite differences in the number of photoreceptor types (and subsequent chromatic pathways) present in each group. Observations made from non-human primate visual systems are useful models of the human visual system. Findings from studies like those described above can lead to a reasonable prediction that *human* dichromatic and trichromatic individuals would not show significant differences in the anatomical structure of their visual systems. If dichromats maintain the same number of post-receptoral neurons, one possibility is that cells in the 'would-be' L-M pathway are re-purposed for processing properties inherent in the other pathways. The remaining question, if this does occur, is whether it would result in any advantage for tasks using those pathways.

A number of studies have identified the possibility that dichromatic individuals show some advantages in visual processing within the luminance domain. For instance, Sharpe *et al* (2006) found evidence of dichromats acquiring lower thresholds than trichromats for a high temporal frequency (16Hz) cone isolating stimuli in a 4AFC contrast detection task. However, they also found that dichromats had higher thresholds for a low temporal frequency (1Hz) stimulus. It was suggested that the disadvantage at low

temporal frequencies could be explained by the lack of an L-M pathway (and subsequent loss of sensitivity for low temporal frequencies, in line with the known temporal resolution of the chromatic channels). Conversely, the advantage at high temporal frequencies indicated a benefit to the luminance-processing pathway, perhaps from an increased input from larger populations of luminance-tuned cells. Further to this, the same authors found that dichromats showed improved visual acuity over trichromats, although interestingly, this was only true for 'multi-gene' dichromats (Jägle, de Luca, Serey, Bach, & Sharpe, 2006); 'single-gene' dichromats only carry one gene to encode one of either the L and M cones, unlike 'multi-gene' dichromats that carry two or more genes for encoding the same cone type (e.g. all encoding for L cones). This distinction between dichromats is outside the scope of the experiments presented here, and therefore the implications will not be considered in the Experiment discussions.

Other studies have failed to observe a difference between these colour-vision groups. For instance, a study by Lutze, Pokorny and Smith (2006) used a 4AFC pedestal paradigm to measure contrast detection thresholds across different luminance level pedestals in dichromats and trichromats, and observed no significant differences in thresholds between the groups. The method used allowed for a comparison of parvocellular versus magnocellular pathway activation, by using a pulsed-pedestal procedure for the parvocellular pathway, and a steady-pedestal procedure for the magnocellular pathway. In both procedure conditions a target square was briefly pulsed; in the pulse-pedestal condition the non-target squares were presented only at the same time as the target, whereas in the steady-pedestal condition all squares were

constantly displayed (all containing the non-target pedestal luminance) and the target luminance replaces one of the squares when pulsed. There are some possible limitations in this experiment, which may have accounted for the results. Firstly, only a small number of dichromats and trichromats were used (four of each); some individual differences in the thresholds *within* the groups would be anticipated, and so having four subjects in each group may not be enough to rule out population differences in the measures. Secondly, the range of luminance pedestal levels used did not cover very high contrast pedestals. The pedestals ranged up to a maximum of 2.26 log td (181.97 trolands), with the surround set at 115 trolands. Using the Michelson formula of $Contrast = (L_{max} - L_{min})/(L_{max} + L_{min})$, where L refers to the luminance level (in this case in trolands), the maximum contrast pedestal tested equates to a Michelson contrast of approximately 0.23 (23% contrast). If dichromats do have additional cells tuned to the luminance pathway, and, as discussed previously, if the small populations of neurons tuned to high contrast pedestals are the most likely to benefit from additional cells, then it is possible that the contrast pedestal levels tested in this study were just not high enough to observe any differences between the groups.

Contrast discrimination within the luminance domain is a reasonable dimension to focus the investigation for a potential dichromatic advantage. The luminance pathway has been implicated by some of the studies described above as a benefactor in the absence of an L-M pathway. Small neuronal populations tuned to high contrast pedestal levels may be most likely to benefit from an increased number of neurons (as measured with contrast discrimination tasks). Other studies measuring differences between

dichromats and trichromats tended to focus on identifying any foraging differences between the two groups (for instance, the literature discussed in Chapter 1). However, these types of foraging tasks, and even camouflage tasks showing a behavioural advantage for dichromats, necessarily implicate the L-M pathway for the trichromatic subjects because the stimuli are red and green. This makes it difficult to assess whether dichromats have any advantages over trichromats in tasks that use *only* the luminance (or S-cone isolating) pathway. Therefore, an advantage of focusing on the luminance pathway in the experiments described in this Chapter is that only one pathway could be implicated in the interpretation of the findings.

3.3 Aims and Hypotheses

The literature discussed has demonstrated that non-human primates show no observable anatomical differences in the LGN or V1 between dichromatic and trichromatic individuals, and it is plausible that the same could be true of humans. If dichromats, who lack a behavioural L-M pathway, do not lose the neurons that would otherwise process such a pathway, and therefore do not show any anatomical differences in their visual systems, it is possible that these 'would-be' L-M tuned neurons are instead utilised in luminance or S-cone isolating pathways. Studies have modelled the effect of increasing the number of neurons on the signal strength of a stimulus, finding that more neurons improve the accuracy of such signals. If 'would-be' L-M tuned neurons in dichromats are evenly distributed across neuronal populations tuned to the remaining pathways, the largest relative increase in neurons would be seen for small populations of neurons, such as those most sensitive to high contrasts.

The ultimate aim of this Chapter was to further investigate if dichromats show any advantages in visual processing compared to trichromats. It is suggested that any advantages found in dichromats may be the result of having a relative increase in the number of neurons tuned to the luminance pathway compared to trichromats. The experiments described here assess this question by measuring contrast discrimination thresholds across a range of contrast pedestals, in the luminance domain. It was hypothesised that dichromats would have lower contrast detection thresholds than trichromats, specifically at high contrast pedestal levels.

3.4 Methodology

3.4.1 Equipment

The experiments described in this chapter were designed and presented using *Psykinematix* (version 1.5) software (KyberVision, Montreal, Canada, psykinematix.com) on an Apple Mac computer (Apple computers, USA), and was viewed on a NEC MultiSync 200 CRT monitor, running at 100Hz. The monitor was calibrated within the Psykinematix software; the geometry of the screen was set by measuring and recording a square patch of a given pixel dimension, and the gamma and colour properties of each gun (red, green and blue) were measured using a 'Spyder4' (Datacolor, NJ, USA) display calibrator. These measurements allowed for the stimulus appearance to be set in LMS space, with the relevant transformation into RGB values carried out automatically by the Psykinematix software, using Stockman and Sharpe (2000) 2° cone fundamentals. In addition, the observer distance from the

monitor was set for the experiment, and the geometry calibration was used to present the stimuli at the requested size and location (in degrees of visual angle).

Participants were screened for colour-vision deficiencies using the 24-plate version of the Ishihara test for colour blindness from 1966 (Kanehara Shuppan Co. Ltd, Tokyo, Japan). The Wright colorimeter (described in section 2.4.2) was used to run Rayleigh matches and a 'red-to-green' match, which are described in the following section.

3.4.2 Design & Stimulus

A 4-alternative-forced-choice (4AFC) design was used to measure contrast detection thresholds at eight different contrast pedestal levels. The stimulus was composed of four horizontal gratings with a 3° diameter (with a spatial frequency of 1 cycle per degree (cpd), and using a Gaussian envelope with a sigma of 0.1), which were each placed at 7° eccentricity (to the centre of the grating) from the central fixation point, as illustrated in Figure 3.4. The phase of the gratings was randomised between each trial. A thin white circle, which appeared for the same time interval as the stimuli, surrounded each grating; the circle removed any spatial uncertainty regarding the location of the stimuli, which was particularly important for conditions with a low, or zero, contrast pedestal. The fixation mark changed between '+', during the presentation of the stimulus (200ms), to 'X' while waiting for the subject to respond. The response time was limited to 2 seconds – the next trial would either begin after the subject's response, or after the 2-second time limit.

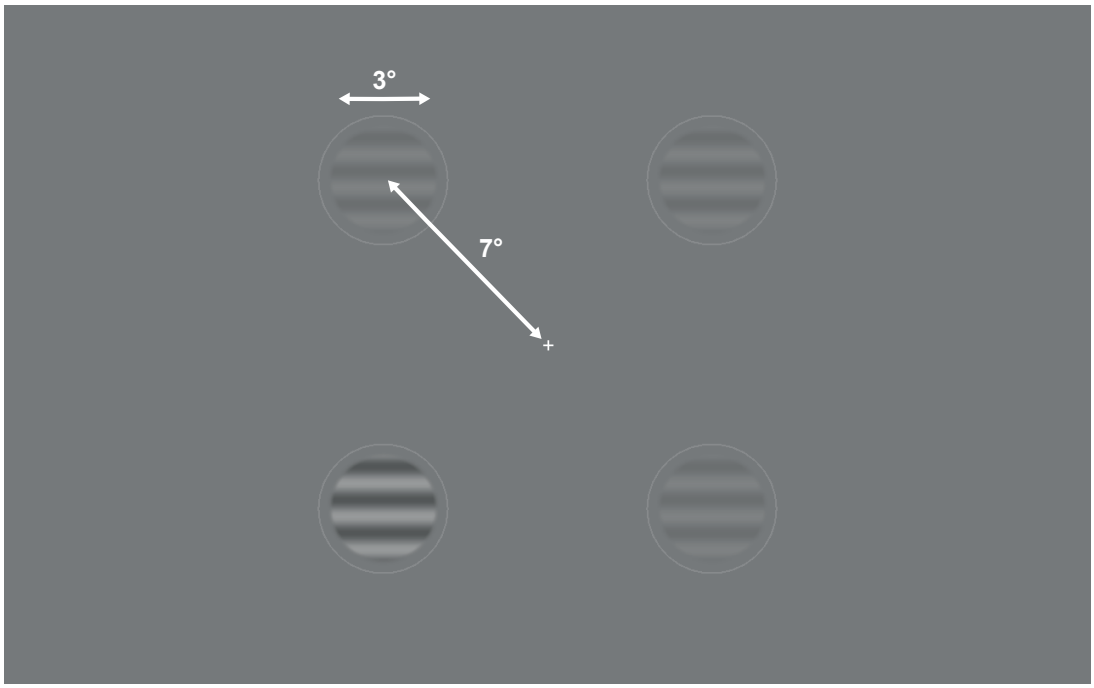

Figure 3.4 Example of a stimulus trial with an 8% contrast pedestal. The target is shown here in the bottom left location.

The contrast pedestals used were selected on a log scale between 0 and 64%, specifically: 0, 1, 2, 4, 8, 16, 32, and 64 (see Figure 3.5). The target grating location was randomised on each trial, and the contrast of the target grating was set using the contrast pedestal plus a target contrast – the target contrast level was adjusted using a Bayesian staircase method. Further specific details of the stimuli and design are described in the method section for each Experiment. Subjects used the keys Q, P, A, and L to indicate the location of the target contrast, which corresponded to top left, top right, bottom left and bottom right, respectively.

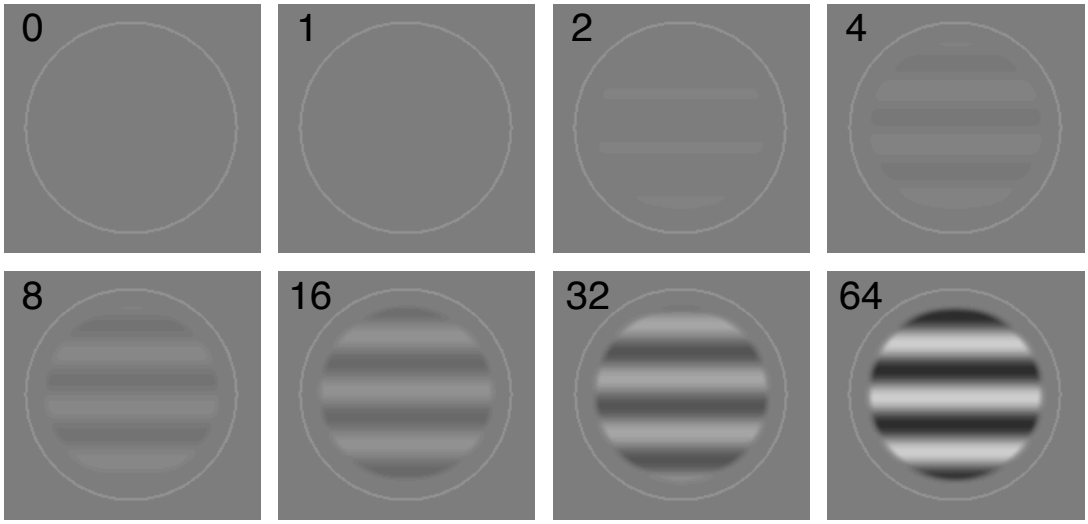

Figure 3.5 Contrast pedestals used in Experiment 1 and 2, with the contrast (%) shown in the top left corner of each image. Gratings are shown with the circle surround that was present during the trials.

The inter-stimulus-interval (ISI), between the response of the subject (or end of the time limit) to the start of the next trial was randomly selected from four time periods ranging between 500ms and 1000ms.

Trials were presented over several blocks, as specified in the Experiments' method sections, which lasted ~11-14 minutes per block depending on overall response times. Fifty test trials of each condition were presented in a block, with an additional 10 practice trials included for each condition in each block (these trials were removed before any data processing). The conditions were randomly interleaved throughout each block to avoid any adaptation to particular conditions. All trials for each condition were then collated to enable psychometric functions to be fitted to the combined trials for each condition.

Colour vision tests were used to determine the colour vision type of the observers (trichromat, anomalous trichromat, or dichromat). An initial screening was done for all participants using the Ishihara plates, which is used

to identify the presence of a red/green colour vision deficiency. Subjects are instructed to look at each plate and read out any digits they can see – some of the plates are perceived as not containing any digits (this is true for both colour-normal and colour-deficient observers, for different plates), while other plates will appear to show different numbers depending on the colour-vision type of the observer. The Wright colorimeter was used to run the Rayleigh Match test and the 'red-to-green' match. For the Rayleigh match, participants adjusted the relative luminance of red (666nm) and green (555nm) primaries in the test field to match a monochromatic 'yellow' light (590nm) in the reference field (see illustration in Figure 3.6A). The red-to-green matching task was performed to better distinguish dichromat from anomalous trichromat observers; subjects adjusted the luminance of a single red primary (666nm) until it was perceived to match in both colour and brightness with a green reference light (555nm) (Figure 3.6B). Trichromat and anomalous trichromat observers would not be able to make a match on this task. Dichromatic observers are able to match at a particular level of red luminance; six repeat measurements were taken if a match could be made.

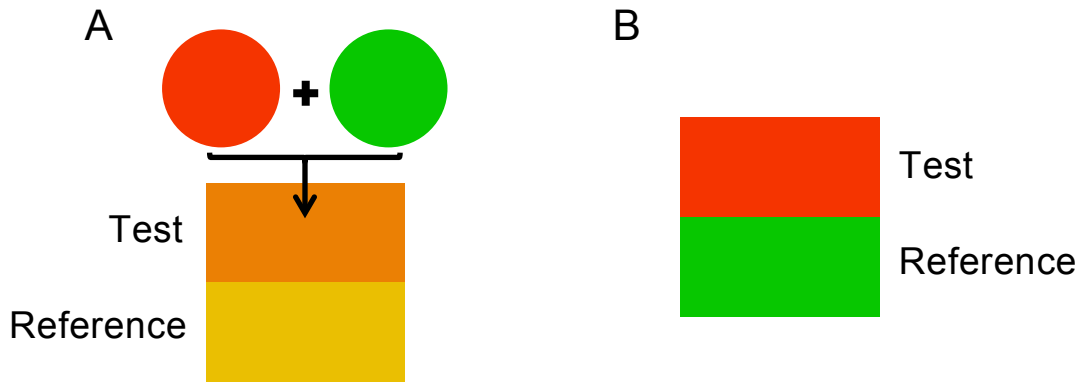

Figure 3.6 Illustration of (A) the Rayleigh match stimulus, showing the two primaries contained within the test field, and (B) the red-to-green match stimulus (each containing a monochromatic primary).

3.4.3 Procedure

Colour vision tests were performed at the start of each session – Ishihara plates were carried out first followed by Rayleigh matches (monocularly on each eye) and the additional red-to-green match (monocularly on one eye). Both matching tasks were performed with the colorimeter.

In total seven Rayleigh matches were made for each eye: an initial match was made by the subject, followed by three matches adjusting only the green primary dial (while the red primary remained fixed at its match position), the green primary was then set to the average of the previous four matches and the procedure repeated with red primary dial adjustments (while the green primary was fixed). This process was carried out for each eye in turn.

The red-to-green match was carried out with whichever eye the subject felt most comfortable using. The subject was asked to adjust the red primary dial across the whole range possible, and identify whether or not they could make a match at any point between the top and bottom of the stimulus field. If no match was possible, the task would end, however if the subjects could make a match they were required to make five further matches (total six including first match), with the position of the dial randomised between each repeat.

Subjects performed a practice run of the contrast detection task (a shortened version lasting ~1-2 minutes) to familiarise themselves with the stimulus and the rate of the trials. If necessary the practice run could be repeated until the subject was confident in the task at hand and how to respond to the stimuli.

Breaks were encouraged between each block of the experiment to ensure subjects remained alert for the task.

The diagnostic criteria for the colour vision groups were as follows: trichromatic subjects were required to have no more than two errors on the Ishihara plates, the Rayleigh match (for both eyes) should have a mean value that is in line with an existing database of colour-normal subjects that were tested in the unique hue experiment described in Chapter 2, as well as a small matching range which was subjectively representative of the average range seen in the same database of subjects (fixed criteria cut-offs were not established), and they should also be *unable* to make a match in the red-to-green match; anomalous trichromatic subjects should produce at least six errors on the Ishihara plates, have mean Rayleigh match values (for one or both eyes) that fall outside the 'normal' range, though the matching range for these subjects can vary, and they should also *not* be able to make a match on the red-to-green match; dichromatic subjects should produce at least 6 errors on the Ishihara plates, have mean Rayleigh match values that fall outside the 'normal' range (for one or both eyes) with larger than normal matching ranges, and, critically, these subjects should be able to make a match on the red-to-green task (this was the deciding factor for a dichromat diagnosis).
Results of the Ishihara plates, Rayleigh matches and the red-to-green match were assessed in parallel to determine the colour vision type of each subject.

The departmental Ethics Committee at The University of York granted approval for these experiments.

3.5 Experiment 1

3.5.1 Introduction

Contrast detection thresholds were measured across a range of pedestal contrasts using achromatic luminance gratings, for dichromatic, trichromatic and anomalous trichromatic individuals. Anomalous trichromats that were identified via the colour-vision tests were tested despite not being a group of focus for this experiment; the data for this group will not be presented and discussed in this chapter, since the hypotheses are based on a dichromat model, though the data are plotted in Appendices A 1 for reference.

A 4AFC design was used, with a Bayesian staircase procedure to adjust the contrast of the target for eight different pedestal levels. Mean thresholds obtained for each pedestal level were compared between the colour vision groups in order to test the hypotheses that dichromatic individuals would show an advantage on this task. Specifically, it was hypothesised that dichromats would have lower contrast thresholds for the highest contrast pedestal condition compared to trichromats.

3.5.2 Methods

3.5.2.1 Subjects

This experiment used 23 male subjects (mean age = 21.4 years (± 3.0)); six were dichromats (mean age = 22.8 years (± 5.5)), seven were anomalous trichromats (mean age = 21.1 years (± 1.6)), and 10 were trichromats (mean age = 20.8 years (± 1.3)). All subjects were recruited from the student population at the University of York. Aside from presenting the colour-vision

data of the anomalous trichromats, to indicate the group criteria, no further data for this group will be presented in the results, but are provided in Appendices A 1.

3.5.2.2 Design & Stimulus

In addition to the details outlined in the Methodology (section 3.4), the Bayesian staircase method used in Experiment 1 comprised 20 levels of target contrast, which were sampled on a log scale between 0 and 20 – in this Experiment these minimum and maximum values were the same for each condition. The Bayesian method selects the target contrast level for a trial based on previous responses, such that the majority of trials should be clustered around the point of the thresholds, i.e. rather than over-testing at contrast levels that produce a ceiling or guess-rate response.

A total of 150 trials were carried out per condition (excluding practice trials), and these were split across three testing blocks – each block consisted of the same number of trials for each condition, i.e. 50 test trials and 10 practice trials.

3.5.3 Results

3.5.3.1 Diagnosis of colour vision deficiency

The results of the Rayleigh match are shown in Figure 3.7, with subjects grouped by colour vision type (as determined by the criteria in section 3.4.3). All the dichromatic subjects produced consistent matches on the red-to-green matching task. None of the trichromatic subjects produced any errors on the Ishihara plates.

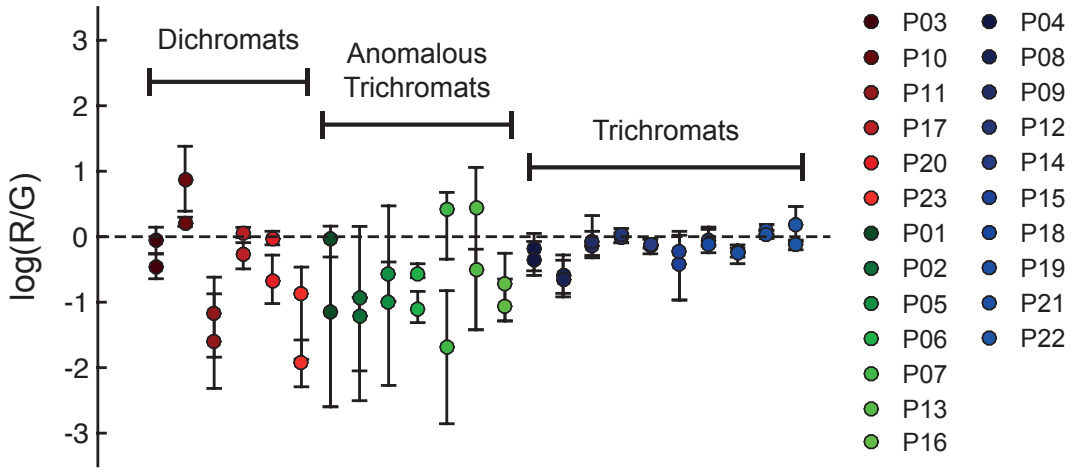

Figure 3.7 Average Rayleigh matches (log(R/G)) with matching ranges, for all subjects, grouped by colour vision type. Each subject, shown on the legend, has two data points showing Rayleigh matches for each eye.

It should be noted that whilst some of the dichromatic subjects appear to have matching ranges and mean Rayleigh match values that are similar to anomalous trichromats (and even some of the less consistent trichromats), criteria for the Ishihara plates and red-to-green match was met to confirm a dichromat diagnosis. These small matching ranges may have been a result of the rigid procedure used for the Rayleigh matches, which did not allow for identifying true minimum and maximum matching points for the dichromatic subjects – subjects were *not* asked to stop the adjustment *as soon as* they could make a match, which meant for some subjects they would adjust across a range and then stop in the middle of the minimum and maximum boundaries.

3.5.3.2 Contrast response 'dipper' functions

The trials from each block were collated together in order for a psychometric function to be fitted for each condition (for each subject) and produce an estimate of the contrast threshold. As a 4AFC method was used, with a guess rate of 25%, the probability correct level used for the threshold was 62%.

Prior to fitting the functions, the target contrast levels were log transformed ($\log_{10}$(Contrast)), to ensure that the functions were appropriately fitted in line with the log sampling of the target contrast levels. The Palamedes Matlab toolbox (Prins & Kingdom, 2009) was used to fit a logistic psychometric function to the data (using 'PAL_PFML_Fit'). The input variables required for fitting the function included: the trial data information (target levels used (after log transform), number of hits and number of trials for each level); estimated ranges for the threshold and slope values, which were free parameters (the threshold could vary up to the maximum value used for the target contrast levels, and the slope could vary up to a maximum beta level of 10 (which was the cap used in the Bayesian staircase)); and information on the guess rate and lapse rate – the guess-rate was fixed to 0.25 (25% chance of correct response) and the lapse rate estimated and fixed at 0.01 (i.e. 1% lapse rate). Bootstrapping of 100 simulations of the data was done to estimate the standard error of the outputted threshold, this was done using the Palamedes 'PAL_PFML_BootstrapParametric' function, which required the same parameters described above, as well as the output from the fit of the data.

Poor fits of the trial data with the psychometric functions – as indicated by the size of the standard error of the threshold estimate – can result in potentially unreliable estimates of thresholds. A rejection criterion was set prior to the extraction of the data to account for any such scenarios. In similar contrast detection studies a standard error of 3dB was used as the cut-off (Wallis, Baker, Meese, & Georgeson, 2013), which equates to approximately 1.4% contrast. However, as none of the subjects were experienced psychophysical observers, a more relaxed rejection criterion of 1.8% contrast (approximately

5dB) was used to allow for more flexibility in the error of the fit. Therefore, any thresholds with a standard error exceeding 1.8% contrast (which was also log transformed along with the target contrast levels) would be replaced with the average threshold for the subject's colour-vision group for that particular pedestal level, in order for the TvC functions to be plotted and for that subject's data to be included in the analysis. However, for the 64% and 0% pedestal conditions, if the criteria was not met the subjects would be removed from the entire data set rather than setting the threshold to the group mean. This was primarily put in place because the highest contrast pedestal was of particular interest in the hypothesis, and it was not appropriate to have these critical values set to the group average as they would bias the data and potentially lead to unrepresentative conclusions.

Across all subjects in the dichromat and trichromat groups, and across all pedestal conditions (128 threshold values in total), three threshold values met the rejection criteria. All three were for the 64% contrast pedestal level, and therefore these subjects were removed from the dataset (one dichromat and two trichromats); this resulted in the final analysis containing five dichromats and eight trichromats.

Thresholds across pedestal levels, with standard error bars for the estimated threshold, are shown in Figure 3.8 for each subject (grouped by colour vision type). Group averages with standard errors for each pedestal level are shown in Figure 3.9. All subjects (and groups) show the expected 'dip' between 0% and 1% pedestal contrasts, and also show an increase in threshold as a function of pedestal contrast from 1% to 64% pedestal contrasts.

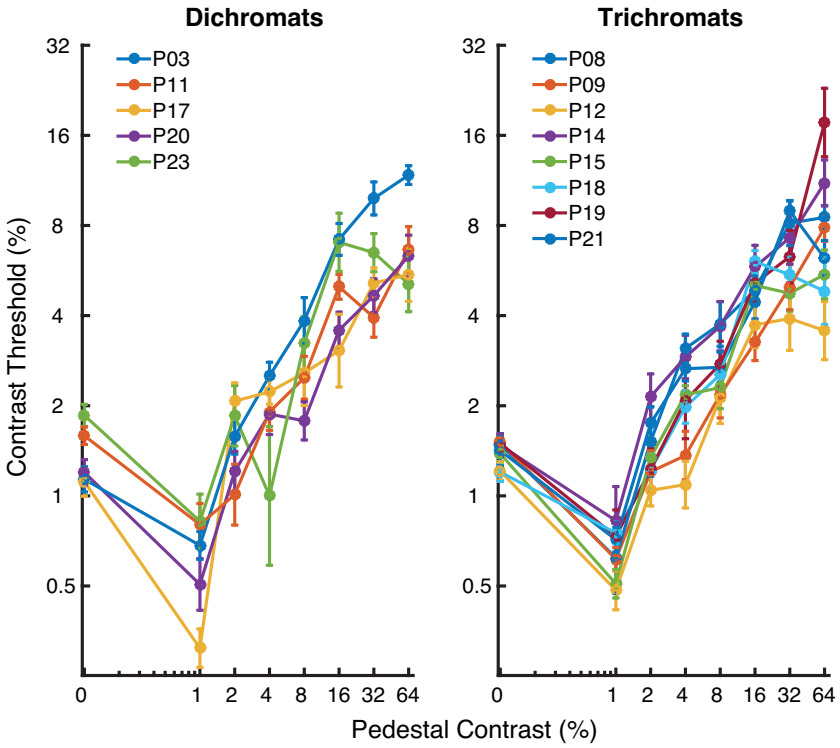

Figure 3.8 Contrast thresholds (%) across pedestal contrast levels (%) for each subject, with standard errors of the threshold estimates. Shown for the dichromatic (left) and trichromatic (right) subjects.

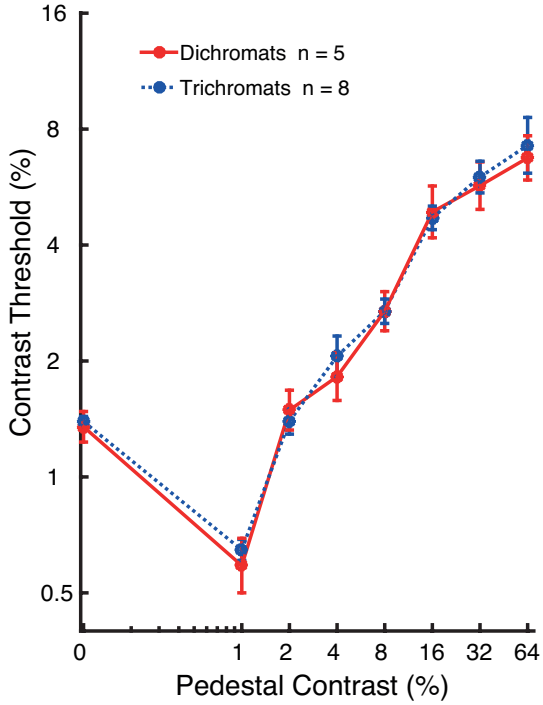

Figure 3.9 Average contrast thresholds (%) across pedestal contrast levels (%) for dichromats (red line) and trichromats (blue dotted line). Error bars represent the standard error of the means.

3.5.3.3 Analysis

To identify whether there was an effect of colour vision group on contrast thresholds, a repeated-measures ANOVA was used with the within-subject factor of pedestal contrast, the between-subject factor of colour vision group and the dependent variable of contrast threshold. Mauchly's test of Sphericity was not violated for the pedestal contrast factor ($\chi^2(27)=32.565$, $p=.260$), therefore sphericity can be assumed. As expected from the standard shape of the TvC functions, a main effect of pedestal contrast was found ($F(7,77)=141.550$, $p<.001$). However, there was no significant between-subject effect of colour vision group ($F(1,11)=0.087$, $p=.774$).

To further test and confirm the rejection of the specific hypothesis that a difference in contrast thresholds would be observed at the highest contrast pedestal levels between dichromatic and trichromatic colour vision groups, an additional independent t-test was carried out between these two colour vision groups for the 64% contrast pedestal level. No significant difference was observed between the groups ($t(11)=-0.294$, $p=.774$).

3.5.4 Discussion of Experiment 1

3.5.4.1 Overview of results

The results from Experiment 1 showed no difference between the colour vision groups across contrast pedestal levels, as tested by a repeated-measures ANOVA, and no difference between dichromats and trichromats for the key contrast pedestal level of interest (64%), as tested by an independent samples t-test. The hypothesis that dichromats would have lower thresholds than

trichromatic individuals, specifically on the 64% contrast pedestal, is therefore rejected.

3.5.4.2 Limitations and Discussion

The design and procedure used in this experiment allowed for good estimations of both the colour vision type of each subject, as well as the anticipated dipper functions for the contrast thresholds across contrast pedestal levels. However, some limitations in the procedure used may have affected the reliability of the threshold estimates, particularly for the highest contrast pedestal – which was the only pedestal level that had thresholds meeting the rejection criteria.

The large maximum number of contrast target levels (20) used in the Bayesian staircase compared to the total number of trials (150), as well as the *range* of contrast target levels (log scaled between 0 and 20) across all contrast pedestals, may have resulted in psychometric fits and threshold estimates that were not wholly representative of the true threshold for an individual on a given contrast pedestal level. The maximum contrast target level used may have reduced the number of relevant/useful target levels for each pedestal level – for lower contrast pedestals a lower maximum would be more appropriate to allow for more target levels around the anticipated threshold level, as would higher minimum and maximum values for the highest contrast pedestal level. Furthermore, a greater number of trials and fewer target levels will generally produce the neatest psychometric functions (García-Pérez & Alcalá-Quintana, 2007). The consequences of these limitations may be particularly evident for the highest contrast pedestal level (64% contrast),

which, as highlighted, was the only pedestal level in which any subjects met the rejection criteria. The maximum contrast level tested for the high contrast pedestal was proportionally low relative to other pedestal levels, when considering that the threshold level is higher. The effect of this may be that because fewer target levels would elicit a ceiling response for the 64% contrast pedestal condition, more variability would be seen in the fit of the psychometric functions when the data was bootstrapped – increasing the standard error of the threshold estimates. The reliability of the estimated thresholds may be improved by adjusting the maximum contrast target levels – setting them independently for each pedestal level – as well as increasing the overall number of trials across fewer target contrast levels.

The number of subjects in each colour vision group (after exclusions) is low – this means that the thresholds represent a very limited sample of the populations. One obstacle in researching colour-deficient observers, is acquiring large samples from the available participant pool – primarily, the University of York student population. Furthermore, as the key focus group in this research is dichromats, there is the additional factor that dichromats are less common than anomalous trichromat colour-deficient individuals, and are therefore likely to be harder to recruit. It would be beneficial to increase the number of dichromatic observers in the experiment to better represent that population, but given the limited resource of dichromatic subjects it may not be possible to achieve a *large* sample for this group. Nevertheless, this issue may be remedied by recruiting an even larger trichromat sample; this would result in a better representation of the range of thresholds across the trichromat population, and make it clearer whether or not this spread

encompasses the dichromat thresholds, i.e. do dichromat thresholds only overlap with a small number of trichromats, or do they truly represent equivalent threshold values between the groups.

3.5.5 Conclusion

The data collected in this experiment support a null hypothesis that there are no differences in the contrast detection thresholds of dichromats compared to trichromats. However, given the limitations in sample sizes and small methodological issues outlined above, a final experiment was carried out to limit the possibility of acquiring a Type II error – of incorrectly supporting the null hypothesis. Experiment 2 modified the existing stimulus design to help strengthen the psychometric fits at each contrast pedestal for observers, and therefore improve the reliability of the threshold estimates. In addition, a larger number of participants were recruited to improve the sample size for all colour vision groups.

3.6 Experiment 2

3.6.1 Introduction

In Experiment 1 no significant differences were observed between the colour vision groups across contrast pedestal levels, including for the key condition of the high contrast (64%) pedestal. However, there were some limitations in the methodology, as well as small sample sizes for both the dichromat and trichromat groups used. In order to validate the findings from Experiment 1, and reduce the likelihood of Type II errors, the experiment was repeated using tighter stimulus parameters and more subjects. Experiment 1 used a large maximum number of target levels, which may have resulted in a poorer fit of

the psychometric functions. In addition, the range of target contrasts used in the staircase was not adjusted to best reflect the likely threshold for a given pedestal. For the higher contrast pedestals this resulted in fewer target levels producing a ceiling response, which may have affected the standard error of the threshold estimates (and resulted in a number of subjects meeting the rejection criteria for this pedestal level). Experiment 2 used fewer target levels in the staircase, and the minimum and maximum values of the target levels for each condition were set to better reflect approximate thresholds.

The aim of Experiment 2 was to re-test the original hypothesis – dichromats were predicted to have lower contrast detection thresholds for the highest contrast pedestal compared to trichromats – to determine whether the hypothesis would still be rejected when more stringent methods and improved sample sizes were used.

3.6.2 Methods

3.6.2.1 Subjects

Fifty-five subjects, matched for age and sex, were recruited for this experiment: 14 male dichromats (mean age = 22.1 ± 4.0 years), 12 male anomalous trichromats (mean age = 22.6 ± 4.6 years), and 29 male trichromats (mean age = 21.6 ± 3.4 years). As with Experiment 1, anomalous trichromat subjects will be shown in the Rayleigh match data, but not included in the group analyses; this data are plotted in Appendices A 2. Three of the dichromats were tested off-site at Newcastle University, and therefore were not able to complete the diagnosis tasks on the colorimeter. Instead, these subjects were diagnosed by performing Rayleigh matches on an Oculus

anomaloscope (Optikgeräte GmbH, Wetzlar), which were carried out by Dr Gabriele Jordan in her laboratory at Newcastle University.

3.6.2.2 Equipment

In addition to the equipment outlined in section 3.4.1, the three subjects tested at Newcastle University performed the experiment using an Apple MacBook Pro (Apple computers, USA) and a Dell P992 CRT monitor, running at 100Hz – the monitor was calibrated with the same Spyder4 display calibrator used to calibrate the monitor in the laboratory at the University of York. The calibration process performed in Psykinematix ensures the visual angle and presentation of the stimuli are comparable between monitors, assuming that accurate information regarding subject viewing distance is provided; Psykinematix uses the specified viewing distance and required visual angle of the stimulus to determine the size of the stimuli presented.

3.6.2.3 Design & Stimulus

The design and stimulus was almost identical to that used in Experiment 1, with several key modifications: the Bayesian staircase was composed of 10 (log distributed) levels, instead of 20, and the total number of trials was increased to 200 per condition, which were spread over four blocks – each block containing 10 practice trials and 50 test trials for each condition. The minimum and maximum values for the target at each condition were adjusted to better reflect the known increase in threshold values with increasing contrast pedestal. For the contrast pedestal conditions the minimum and maximum target levels used are shown in Table 3.1.

Table 3.1 Minimum and maximum contrast target levels used for each contrast pedestal condition in the staircase procedure.

Pedestal Level (%)	Minimum target level (%)	Maximum target level (%)
0	0	6
1	0	6
2	0	6
4	0	6
8	0	10
16	0	15
32	2	25
64	2	30

3.6.3 Results

3.6.3.1 Diagnosis of colour vision deficiency

The colour vision group of each subject was determined using a combination of the Ishihara plates result, Rayleigh matches, and red-to-green matches, as described in the diagnosis criteria in section 3.4.3. Figure 3.10 shows the Rayleigh match results for all subjects except the three dichromats tested at Newcastle University. Dr Gabriele Jordan tested these three subjects on different equipment, and diagnosed their type of colour-vision deficiency.

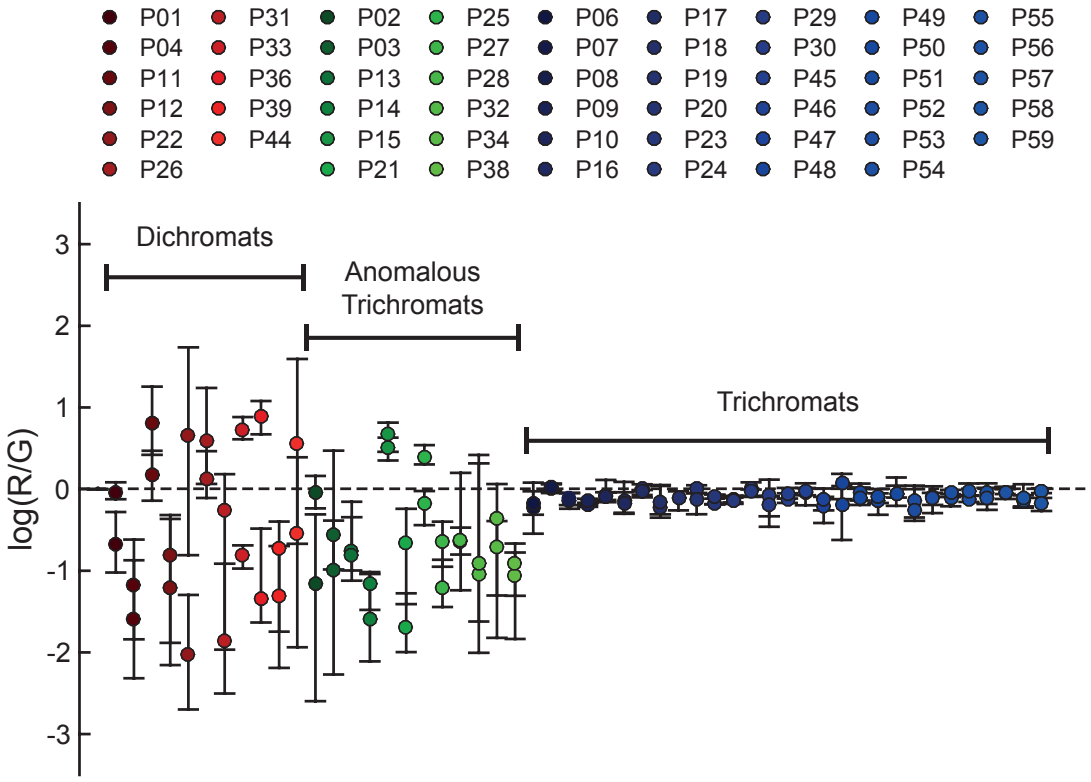

Figure 3.10 Rayleigh match means and matching ranges for subjects in Experiment 2, grouped by colour vision type. Each subject has two data points, one for each eye (shown at the same point on the x axis). Three dichromat subjects that were diagnosed at Newcastle University do not have colorimeter Rayleigh Match data, and are therefore not shown here.

3.6.3.2 Contrast response 'dipper' functions

The same procedure was used from Experiment 1 to fit psychometric functions to the trials for each condition. In brief, the trials from each block were first collated together and log transformed before using the Palamedes Matlab toolbox to fit a logistic psychometric function to the data (using 'PAL_PFML_Fit') and to produce an estimate of the 62% threshold value. Using the 'PAL_PFML_BootstrapParametric' Palamedes function 100 simulations of the data were bootstrapped to produce an estimate of the standard error of the threshold. Rejection criteria of 1.8% contrast (log transformed) for the standard error was used; if the standard error exceeded this value for any of the 'middle' pedestal levels (between 1% and 32% contrast pedestal levels), the threshold estimate was replaced with the subject's colour

vision group mean for that particular pedestal level, whereas if this value was exceeded for either the first (0%) or last (64%) pedestal levels, the entire dataset for that subject would be excluded from the analysis.

Across all dichromatic and trichromatic subjects, and all pedestal conditions (344 threshold values in total), four thresholds met the rejection criteria: one threshold value was replaced with the group average for the pedestal level (from the Dichromat group, at the 16% contrast pedestal), and three subjects were removed from the data set entirely as they met the rejection criteria for the 64% pedestal contrast (one dichromat and two trichromats); this resulted in the final analysis containing 13 dichromats and 27 trichromats.

Thresholds across pedestal levels, with standard error bars for the estimated threshold, are shown in Figure 3.11 for each subject (grouped by colour vision type). In general, most subjects produced the expected 'dip' between 0% and 1% pedestal contrasts, and also showed an increase in threshold as a function of pedestal contrast from 1% to 64% pedestal contrasts. There were some subjects that did not show the dip, which will be discussed. Group averages with standard errors for each pedestal level are shown in Figure 3.12. Data for the anomalous trichromats are shown in Appendices A 2.

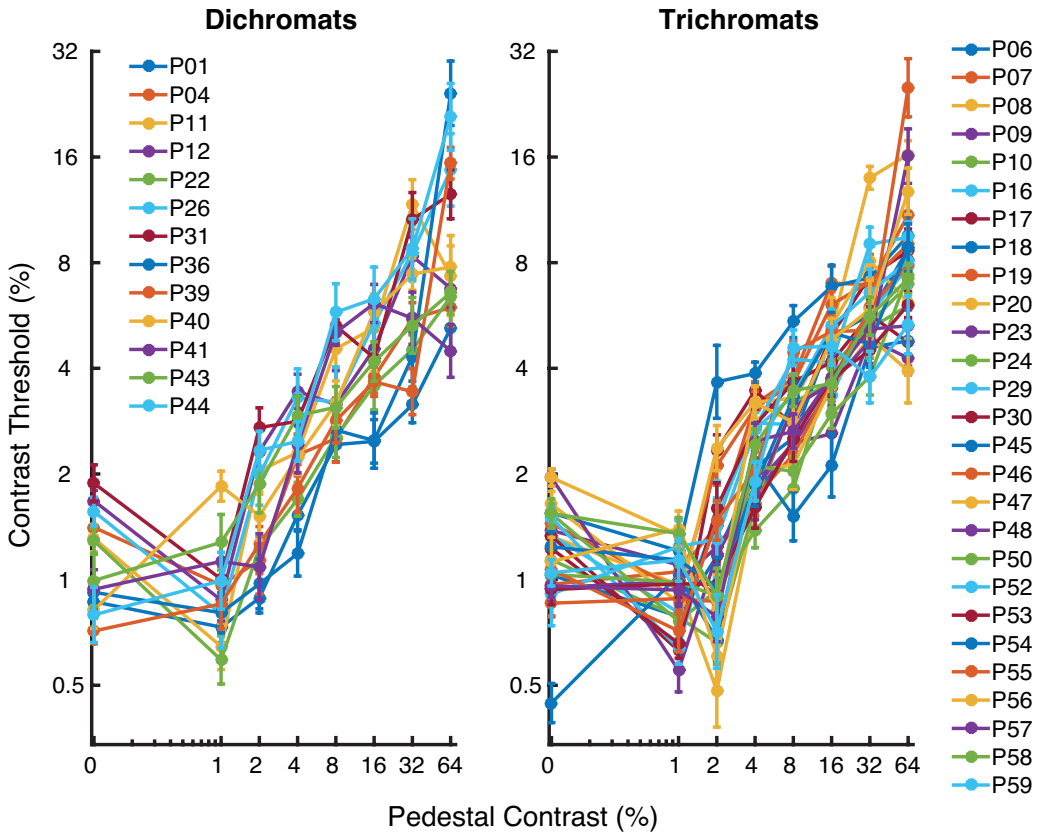

Figure 3.11 Detection thresholds (% contrast) across pedestal contrast levels (%) for each subject, with standard errors of the threshold estimate, shown for the dichromats (left), and trichromats (right).

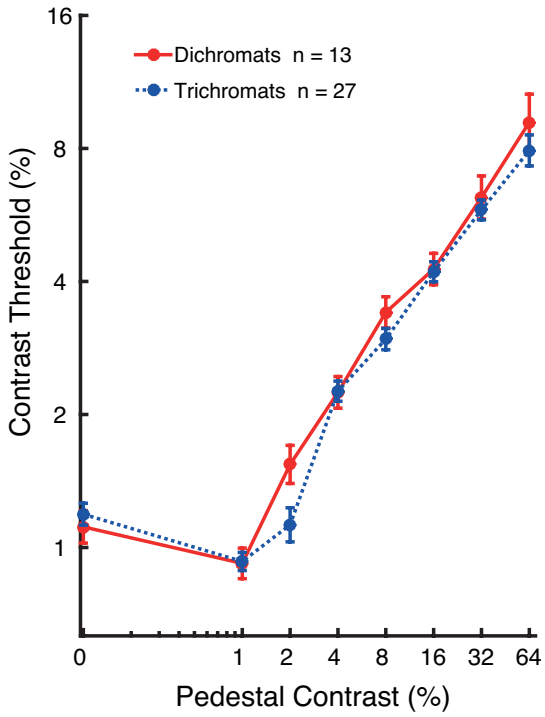

Figure 3.12 Average contrast detection thresholds (%) across pedestal contrast levels (%) for dichromats (red line) and trichromats (blue dotted line). Error bars show the standard error of the means.

3.6.3.3 Analysis

The same statistical analyses were performed as in Experiment 1; a repeated-measures ANOVA was used to test whether there was an effect of colour vision group on contrast thresholds, with the within-subject factor of pedestal contrast, the between-subject factor of colour vision group, and the dependent variable of contrast threshold. Mauchly's test of Sphericity was violated for the pedestal contrast factor ($\chi^2(27)=86.124$, $p<.001$), therefore a Greenhouse-Geisser correction was applied prior to the interpretation of this factor. A main effect of pedestal contrast was found ($F(4.345,165.112)=267.887$, $p<.001$, Greenhouse-Geisser corrected). There was no significant between-subject effect of colour vision group ($F(1,38)=1.159$, $p=.288$).

In keeping with Experiment 1, a final test was performed to test for a difference in contrast thresholds at the highest contrast pedestal level (64%), between the dichromatic and trichromatic colour vision groups. An independent t-test between these two colour vision groups for the 64% contrast pedestal level showed no significant difference between the groups ($t(38)=0.923$, $p=.362$).

3.6.4 Discussion of Experiment 2

3.6.4.1 Overview of Results

No significant between-subject effect was observed between the colour vision groups across the pedestal levels, or specifically at the 64% contrast pedestal level of interest. Therefore the hypothesis that there would be a significant difference between the groups is rejected. In general, subjects showed typical

TvC functions; with a dip in contrast thresholds between 0% and 1% contrast pedestals, and a gradual increase in thresholds between 1% to 64% pedestal levels. However, a number of subjects did not show the anticipated dip, instead showing a steady increase in contrast threshold across pedestal contrasts from the 0% pedestal level.

3.6.4.2 Discussion

The number of dichromatic subjects in this group was substantially smaller than the number of trichromatic subjects. In part, this was by design. In most experimental cases, roughly equal numbers of participants across groups is optimal for comparisons between those population samples, however, the resource of dichromatic participants is limited here, particularly in comparison to available trichromatic subjects, and therefore equal numbers were not possible in this experiment without deliberately limiting the sample sizes for all groups. Instead, a larger group of trichromatic observers – who were easier to recruit than dichromats – was tested to improve the representation of the trichromatic population and produce a spread of data that better reflects individual differences within that population. This tactic strengthened the statistical analysis of the data, by increasing the sample size where it was most possible to do so.

The rejection criterion was met most regularly for the 64% contrast pedestal condition – three of the four values that met the criteria were from this condition (and for Experiment 1, all three values meeting the criteria were from this condition). This bias may reflect increased difficulty in performing the task for the highest (64%) contrast pedestal; this level is arguably the

hardest condition, as demonstrated by the higher contrast detection thresholds. However, proportionally fewer subjects (7%) met the rejection criteria for this pedestal level compared to in Experiment 1 (19%). This indicates that the changes in the number of trials and target levels (and the increase in the maximum target contrast level) may have helped improve the psychometric fits of the data.

A number of subjects did not show a dip between the 0% and 1% contrast pedestal levels. The dip in TvC functions typically occurs when the pedestal level equals the contrast detection threshold, such that individuals with higher contrast detection thresholds will have a dip at a higher contrast pedestal level (Baldwin et al., 2016). In this Experiment, contrast detection thresholds ranged between approximately 0.5% and 2% contrast, and notably, the subjects that did not show the dip tended to have contrast detection thresholds lower than 1%. In order to better identify individual dipper functions, it would have been useful to test several contrast pedestal levels that reflected the contrast detection range, between 0% and 2% (rather than just the 1% level). However, since this component of the TvC function was not of primary concern for the hypothesis, adding further conditions to the low pedestal contrast levels would have been surplus to requirement.

It is possible that another factor may have contributed to the lack of 'dip' for some participants, as well as affecting overall threshold levels: the interleaving of the conditions within each block. The purpose of interleaving the conditions was to avoid any adaptation effects within a condition, which would ultimately aid the detection of the target. However, the weakness of

this method is that the average difficulty of each trial is effectively higher when the trials are interleaved, and short-term adaptation to each trial may affect performance on subsequent trials. For instance, when the presentation of a higher contrast pedestal trial immediately precedes a lower pedestal contrast level, it could have the effect of adding an additional pedestal to the stimuli, and thus increasing the threshold level in line with normal TvC functions (increasing thresholds with increasing pedestal contrasts). The highest contrast pedestal level is therefore unlikely to be affected by this, because all other pedestal levels are lower and are unlikely to cause any interference in the detection of the target. As all trials are randomised within each block, the effect of this should be equal across all subjects, such that all threshold levels may be slightly higher than they would otherwise be if each condition were performed within its own block. The observation that some subjects do not show the anticipated dip may reflect some issues with the method of interleaving. However, it should be noted that the same method of interleaving was employed in Experiment 1, where all subjects showed a dip between the 0% and 1% pedestal levels. These subjects showed a smaller range of contrast detection thresholds than those in Experiment 2, between approximately 1.2% and 1.8%, which may account for the consistent dip seen in these subjects at the 1% pedestal. It seems most probably that the lack of dip for some subjects in Experiment 2 is due to the limited range of pedestal levels tested at low contrast levels, rather than a problem with interleaving affecting the reliability of the data.

3.6.5 Conclusion

The findings of this experiment do not support the hypothesis that dichromats and trichromats differ in their contrast thresholds for high contrast pedestal levels. No differences were observed between the two colour vision groups. Some methodological issues may have impacted on actual threshold values obtained – for instance, the interleaved trials across conditions – however, since the limiting effect of these issues are consistent across all subjects, particularly for the high contrast pedestal level of interest, the overall findings of the experiment are considered to be valid. It is noted that a number of subjects failed to show a 'dip' in their data, which is determined to be due to there not being a large enough range of pedestal levels implemented at the lower contrast range to appropriately capture all dip locations across subjects. There was no hypothesis for any differences between the groups for the 'dip', and, given that between Experiment 1 and Experiment 2 the overall findings were the same (while Experiment 1 did show a dip for all subjects), no further experiments were considered to be necessary to re-test the thresholds at the lower contrast pedestal levels.

3.7 Discussion

3.7.1 Summary of findings

Both Experiment 1 and 2, which had slight methodological and sample size differences, demonstrated no significant effect of colour vision group on contrast thresholds across a range of pedestal levels, and, specifically, no significant difference between thresholds at the high contrast (64%) pedestal condition. These findings do not support the hypothesis that dichromatic

individuals would show an advantage (lower thresholds) at the high contrast pedestal level compared to trichromatic individuals.

The hypothesis was based on predictions about how neuronal populations may be allocated across the opponent pathways present in dichromats compared to trichromats. It was predicted that a reallocation of the 'would-be' L-M tuned neurons in dichromats would be most likely to result in a benefit to contrast discrimination at high contrasts. If any such reallocation does occur in dichromats, the findings of these experiments do not support the prediction that it has any benefit to achromatic contrast discrimination for the parameters used in these experiments.

3.7.2 Rationale for testing contrast detection in the luminance domain

There are a number of possibilities as to how a reallocation of the 'would-be' L-M tuned neurons could affect the remaining pathways. This would depend on which of the characteristic luminance pathway properties were adopted by the neurons, e.g. band-pass spatial frequency tuning or contrast sensitivity. For the experiments described in this Chapter, there were a number of reasons why the focus was on the luminance pathway and on contrast detection.

Firstly, isolating the luminance pathway is a relatively simple process compared to the S-cone isolating pathway, which would depend largely on the ability for naïve participants to carry out difficult isoluminance tasks. Therefore, using only luminance-defined stimuli has the benefit of knowing which particular pathway is being probed in the participants. Secondly, a

number of studies have identified the luminance pathway as a likely candidate for benefiting from the absence of an L-M pathway, and have provided some evidence for a dichromatic advantage in this domain (Sharpe et al., 2006). Finally, focusing on the stimulus dimension of contrast was a deliberate attempt to target a potential candidate for any benefit of neuronal reallocation in dichromats. This dimension also has the advantage that TvC ('dipper') functions have been thoroughly measured in human psychophysical experiments, and therefore it was clear how the data would be expected to look in a 'normal' population of subjects (e.g. Baldwin *et al.*, 2016; Legge & Foley, 1980).

Lutze *et al* (2006) used pulse-pedestal stimuli which were specifically designed to separately measure achromatic processing from the magnocellular and parvocellular pathways. This was done on the assumption that the parvocellular pathway in dichromats should have no chromatic input, and so would only process spatial information, unlike in trichromats, where both spatial and chromatic information is processed. Therefore it was reasonable for the authors to hypothesise that this pathway would be a likely benefactor from the missing chromatic input. Despite this, they found no significant differences between dichromats and trichromats on their tasks. In the rationale for the experiments carried out in this Chapter, it was thought that the contrast levels used by Lutze *et al* were perhaps not high enough to probe the population of neurons that were likely candidates for showing a dichromatic advantage. Yet, in both Experiment 1 and 2, no evidence was found of an improved contrast detection performance by dichromats at high contrast pedestals.

Following the development and running of the experiments described in this Chapter, a recent experiment by Janáky, Borbély, Benedek, Kocsis and Braunitzer (2014) was reported, which sought to re-test the findings by Lutze *et al* (2006). Janáky *et al* increased the number of subjects tested, and used both static and dynamic grating stimuli (diameter 13° visual angle) to measure contrast sensitivity across different spatial frequencies (contrast sensitivity functions (CSFs)). They found that dichromats had significantly higher contrast sensitivities (the reciprocal of contrast thresholds) than trichromats when the spatial frequency exceeded 3.6 cpd for static stimuli, and 1.9 cpd for dynamic stimuli. The authors' argued that probing contrast sensitivity in this way, using sinusoidal gratings instead of a pedestal stimulus, targeted all orientation-selective achromatic neurons, rather than specific magnocellular or parvocellular pathways. Therefore it may be that the dichromatic advantage within the luminance domain lies in the contrast detection of orientation-selective cells, rather than solely in the contrast discrimination ability of cells in the parvocellular pathway.

3.7.1 Limitations of the stimulus

The gratings used in the 4AFC task had a diameter of 3° visual angle, with a spatial frequency of 1 cpd, and the centre of each grating was placed at an eccentricity of 7° from the central fixation point (each in one of four orthogonal directions). Therefore these stimuli necessarily targeted peripheral eccentricities. This was further ensured by using a short stimulus presentation of 200ms, which was not long enough to enable saccades to each of the four locations before the end of the stimulus presentation (Kirchner &

Thorpe, 2006), thus encouraging observers to maintain central fixation throughout. However, the differences between dichromats and trichromats observed by Janáky *et al* (2014) for contrast sensitivity at different spatial frequencies, used a 13° diameter grating which was centred on the fovea (the fixation point was at the centre of the grating). So, even though their stimuli extended peripherally to overlap with the eccentricity of the stimuli used in the Experiments from this Chapter, it is likely that the judgements were primarily made based on the foveal image. Incidentally, it should be noted that the only pedestal condition from Experiments 1 and 2 that is comparable to Janáky *et al*, is the 0% contrast pedestal, which provides the only measure of pure contrast sensitivity. While dichromats showed a trend for lower contrast thresholds than trichromats at the 0% pedestal condition in both experiments, independent t-tests for this pedestal confirms that the difference between dichromats and trichromats is non-significant for both Experiment 1 ($t(11)=-0.346$, $p=.736$) and Experiment 2 ($t(38)=-0.636$, $p=.528$).

The significant differences identified between the dichromats and trichromats by Janáky *et al* (2014) (for their static stimuli), were observed at spatial frequencies of 3.6 cpd and higher. To identify whether the 1 cpd spatial frequency used for peripheral stimuli in the Experiments here, was comparable to a 3.6 cpd foveal stimuli from Janáky *et al*, the cortical magnification factor of retinal images needed to be accounted for. Virsu and Rovamo (1979) reported the magnification (M) factor across eccentricities, which can be used to convert retinal spatial frequency into cortical spatial frequency. Using the M factor that they report for a 7.5° eccentricity ($M=2.31$), the cortical spatial frequency of the stimuli used in the Experiments

here was calculated, by dividing the spatial frequency of the stimulus by the *M* factor (i.e. 1/2.31); this gives a cortical spatial frequency of 0.4329. This value can then be used to determine the equivalent spatial frequency for a foveal stimulus (which is reported to have an *M* factor of 7.75), by multiplying the foveal *M* factor with the cortical spatial frequency calculated for the peripheral stimulus (i.e. 7.75*0.4329); this gives a spatial frequency of 3.355 cpd for a foveal stimulus. This value is slightly lower than the 3.6 cpd spatial frequency reported by Janáky *et al* that was necessary for a difference in contrast sensitivity to be observed between dichromats and trichromats. This may account for the lack of significant difference observed in the Experiments at the 0% pedestal level. In fact, if an estimate of the *M* factor is extracted for the actual centre of the peripheral stimulus at 7° (*M*=~2.4) – using the *M* factor and eccentricity levels that are provided by Virsu and Rovamo – it produces an even lower estimate of the equivalent foveal spatial frequency, of 3.229 cpd. Using a slightly higher spatial frequency for the peripheral stimuli, e.g. 1.2 cpd, would have increased the equivalent foveal spatial frequency; however, it is not clear whether this small change in the spatial frequency of the peripheral stimuli (used in these Experiments) should produce a significant difference between the dichromats and trichromats that is comparable to that found by Janáky *et al* for foveal stimuli.

The spatial frequency of the stimulus, regardless of scaling for cortical magnification, may not be the only limiting factor in identifying differences between dichromats and trichromats. The fact that a peripheral rather than foveal eccentricity was probed may account for the lack of a significant difference between the groups. The over representation of the fovea in visual

processing – the cortical magnification – not only affects the relative sensitivity to spatial frequency, but also represents a change in the ratio of neurons in the magnocellular and parvocellular pathways into the LGN and visual cortex. For instance, a study on the ratio of these pathways in the macaque dLGN, by Azzopardi, Jones and Cowley (1999), demonstrated that the ratio of parvocellular to magnocellular neurons decreases between foveal and peripheral eccentricities. Neuronal tracers were injected into different locations within the striate cortex, to enable a retrograde labelling of the neuronal projections from each pathway as a function of eccentricity. The ratio of parvocellular to magnocellular neurons in the dLGN decreased from between 20:1 and 40:1 in the foveal eccentricities (<1°) to approximately 10:1 at a peripheral eccentricity of 7°. Testing in the periphery may therefore impact on any parvocellular pathway-specific effects in dichromats, as the relative number of these neurons decreases with increasing eccentricity.

However, changes in the relative ratio of neurons in each pathway as a function of eccentricity would not be a confounding factor for testing across different eccentricities if the domain being tested was not specific to just one of the pathways. For instance, Janáky *et al* (2014) concluded that the dichromatic advantages in the luminance domain may be related to orientation-selective achromatic neurons that are found in both the parvocellular and magnocellular pathways.

The use of a 4AFC design, whilst perhaps limiting in that it does not allow foveal testing, does allow for a larger number of trials in a fraction of the time compared to a foveal, 2-interval-forced-choice (2IFC) task. The 4AFC allowed for a large number of pedestal levels to be tested over a manageable time

period for naïve observers. In addition, while a 2IFC method would have allowed for stimuli to be placed at the fovea, the 4AFC method has the increased advantage of producing more reliable psychophysical data for naïve subjects. Jäkel and Wichmann (2006) showed that *experienced* observers show the highest mean contrast sensitivity across a range of spatial frequencies when using a 2AFC or a foveal 2IFC procedure, however, naïve observers show the highest mean sensitivity for 4AFC procedures, and, in fact, their lowest sensitivity is seen for foveal 2IFC tasks. Given that all subjects used in the experiments described in this Chapter were naïve observers, without any prior psychophysical experience, the 4AFC method provided the best measure of their actual psychophysical thresholds.

3.7.2 Implications of data

Protanope and deuteranope dichromats have two cone photoreceptor types in the retina, compared to the trichromats' three. This means that while trichromats have three opponent pathways (luminance, L-M, and S-cone isolating), dichromats have two – they lack the L-M pathway because they are missing either the L (protanope) or M (deuteranope) cone type. There are a number of possibilities as to how the lack of this pathway may affect dichromatic visual processing – in addition to the obvious deficiencies in colour discrimination. One possibility is that the anatomical structure of the dichromatic visual system is affected. If neurons that would have been tuned to the L-M pathway do not develop, one might expect to see a smaller LGN and visual cortex in dichromats compared to trichromats. This has been tested in non-human primates by measuring various aspects of the LGN layers and their projections into visual cortex (FitzGibbon *et al.*, 2015; Goodchild &

Martin, 1998; Solomon, 2002). No differences were observed between the dichromatic and trichromatic individuals on these measures. Given that non-human primates offer a reasonable model of the human visual system, it is likely that the same results would be found with human subjects (if comparable invasive techniques were to be used).

If there are structurally no differences between dichromatic and trichromatic humans, what is an alternative option for the impact of having no L-M pathway? The remaining opponent pathways may repurpose the 'would-be' L-M tuned neurons – effectively increasing the relative number of neurons tuned to these pathways in dichromats compared to trichromats. The effect of increasing the number of neurons on contrast identification performance (i.e. accuracy of correctly identifying a signal in a population of neurons) has been modelled by Chirimuuta and Tolhurst (2005) and Clatworthy *et al* (2003). They showed that performance accuracy increases with the number of neurons in a population, in the same manner that accuracy increases with higher maximum neuronal responses. It has also been shown, by Geisler and Albrecht (1997), that the largest proportions of neurons in cats and macaques optimally responded to lower contrast thresholds, which were associated with lower contrast pedestals levels in a contrast discrimination task. The combination of these studies allows for a relationship to be formed between number of neurons in a population and contrast detection thresholds acquired a different contrast pedestal levels.

If one of the factors affecting threshold level is the size of the population that optimally responds to a given contrast pedestal level, then thresholds may be

improved/lower in individuals with larger populations of neurons. More specifically, if the relative increase in neurons is important, then one could predict that an even distribution of all 'would-be' L-M tuned neurons – onto all neuronal populations responding optimally to different levels of contrast – would have the greatest impact on the smaller neuronal populations. For example, the smaller populations might see a two-fold increase in population size compared to a 10% increase in already-large populations. However, the findings of both Experiment 1 and Experiment 2 indicate that if any such reallocation occurs on these populations, it does not result in a benefit to contrast thresholds in dichromatic individuals under the parameters used here.

As discussed previously, an alternative candidate for showing a dichromatic advantage within the luminance domain, is in contrast sensitivity functions (Janáky et al., 2014). Despite a trend for lower contrast thresholds in dichromats at the 0% contrast pedestal (this pedestal is a measure of contrast sensitivity) in the experiments described here, no significant difference was observed. It is possible that no differences were observed because the peripheral spatial frequency used was equivalent to a scaled foveal spatial frequency that did not show a significant difference between the groups in the Janáky *et al* study (i.e. lower than 3.6 cpd). The case for an advantage in this dimension of luminance processing is suggested by the authors to perhaps be due to a less noisy luminance channel in dichromats than that experienced by trichromats; specifically, within the orientation-selective neurons. The noise reduction in the luminance channel is suggested to be a result of the simpler,

dichromatic cone mosaic, that suffers less noise from chromatic aberration than a trichromatic cone mosaic.

This proposal mirrors the rationale for the hypotheses in this experiment, but applies it to a different dimension – and one in which the authors do in fact find a significant effect of colour-vision type. Their suggestions remain as theoretical as the ones outlined for the present experiments, and rely on more detailed investigations to help determine the legitimacy of the theory. One way of further investigating the potential increase in the contrast sensitivity of dichromats, would be to carry out a hypothesis driven single-cell non-human primate experiment, much like that reported by Geisler and Albrecht (1997), using dichromatic and trichromat primate species (e.g. marmosets). The techniques utilised by Geisler and Albrecht would allow for a comparison of the distribution of neurons tuned to the contrast thresholds associated with different spatial frequencies. It is predicted that dichromatic individuals would have a relative increase in the number of neurons tuned to the contrast thresholds associated with those spatial frequencies that produce significant differences in psychophysical measures of contrast sensitivity, compared to trichromats.

3.8 Conclusion

The experiments outlined in this Chapter aimed to investigate whether there was any evidence of a dichromatic advantage in contrast discrimination tasks, particularly when the task was performed with a high contrast pedestal. It was predicted that dichromats, who lack an opponent L-M pathway, would have more neurons (the 'would-be' L-M tuned neurons) tuned to the

luminance pathway. This 'increase' in neurons was hypothesised to have the greatest impact for small neuronal populations, such as those optimal for discriminating at high contrast pedestals, which would be reflected in contrast detection thresholds at a high contrast pedestal level. The experiments used a 4AFC Bayesian staircase procedure to acquire contrast detection thresholds across eight pedestal levels that were log-sampled between 0% and 64% contrast. No evidence was observed for a significant difference between dichromats and trichromats across contrast pedestals, or, specifically, at the highest contrast pedestal level. Therefore the findings did not support the hypotheses.

Other recent experiments, identified in the literature, indicate that the luminance domain may still benefit from the lack of an L-M pathway, but within the orientation-selective neurons, rather than contrast tuned populations. Future investigations in human participants would be able to behaviourally replicate these findings psychophysically, and more invasive techniques in non-human primates may be able to identify neuronal population size differences between dichromats and trichromats for neurons optimally sensitive to hypothesis-driven features identified within the psychophysical data (i.e. contrast sensitivity across spatial frequencies).

To further the investigation into how visual processing may differ between dichromatic and trichromatic individuals across the opponent channels – in addition to testing possible behavioural advantages – fMRI methods can be utilised to measure neuronal responses to stimuli activating the different channels. One such method, population receptive field (pRF) mapping, would

allow for estimates of pRF sizes across these channels, and may prove to be a valuable tool in further exploring any differences between these two colour-vision groups. However, to date there are no reports of pRF mapping using chromatic stimuli, and so it is imperative to first investigate how pRF sizes would be predicted to differ between opponent channels in trichromatic individuals, before the investigation could be extended to dichromatic visual processing. Chapter 4 reports several experiments measuring chromatic pRF mapping for trichromatic subjects, with a case study example of a single dichromatic subject tested using the same methods.

Chapter 4 pRF Mapping

4.1 Overview

The three pre-cortical colour channels corresponding to the axes of MB-DKL colour space (Derrington et al., 1984; MacLeod & Boynton, 1979) – luminance (L+M+S), red/green (L-M), and yellow/blue (S-(L+M)) – have different spatial frequency sensitivity profiles. This can be determined using psychophysical measurements of contrast sensitivity across different spatial frequency levels; the luminance (L+M+S) pathway has a band-pass resolution, producing a roughly bell-shaped curve of contrast sensitivity as a function of spatial frequency, with a cut-off around 40 cycles per degree (cpd). Conversely, the chromatic pathways (L-M and S-(L+M)) have low-pass spatial resolution, producing a decrease in contrast sensitivity with increasing spatial frequency (Webster et al., 1990) and cut-offs much lower than the achromatic system. These behavioural measures of spatial resolution reflect neuronal-level differences between the pathways, although the limited sampling resolution of the S-cones must also play a part in limiting the spatial acuity of the S-(L+M) system.

At the retinal level, spatial resolution is intrinsically linked to the size of receptive fields. Only small, simple receptive fields are able to support high-resolution vision. However, at the cortical level this need not be true: while it is still generally assumed that small receptive fields are used to code high resolution features, this relationship must break down in higher visual areas which are known to have large receptive field size yet respond to high-spatial

frequency patterns. Even in primary visual cortex, complex cells could, in principle, have large receptive field sizes with many subunits and combine large receptive field sizes with high spatial resolution. Here, the experiments ask whether functional magnetic resonance imaging (fMRI) can inform about the size and spatial frequency tuning of neurons tuned to different opponent colour channels in V1 as well as higher visual areas.

A class of fMRI measurement techniques called 'population receptive field' (pRF) mapping (Dumoulin & Wandell, 2008) has gained widespread use in recent years. pRF mapping is a forward modelling and fitting technique that estimates the average properties (for example, retinotopic position and receptive field size) of neurons within each voxel of visual cortex. The stimulus presented to the subject during the scan must be rich enough to evoke a range of responses in each voxel so that accurate fitting can occur. Traditional pRF mapping uses high contrast black and white stimuli, and therefore the resulting pRF sizes are a pooled measurement of activity in the neuronal populations responding to high contrast achromatic stimuli. The experiments in this Chapter aimed to investigate whether these pRF techniques could be used to measure the neuronal computations underlying the spatial resolutions of the pre-cortical opponent pathways. Specifically, pRF sizes were estimated for voxels in early visual cortex (V1-V4), to identify whether pRF sizes differed systematically with visual area and eccentricity (as has been shown by other groups), and crucially, whether they differed between the pathways (achromatic vs. chromatic). These experiments were based on the assumption that spatial resolution and receptive field size would be highly correlated.

This chapter will describe the pRF method, before discussing what is known about the spatial resolution of the chromatic and luminance pathways and how this can inform predictions for any differences in pRF sizes between these pathways. Two pRF experiments were carried out, which used groups of trichromatic observers and modified versions of the traditional pRF stimulus. A further fMRI experiment and a set of additional behavioural experiments were carried out to measure the spatial sensitivity of the pathways directly, using the same subjects from the second pRF experiment.

Surprisingly, there were no differences in pRF sizes between the achromatic and chromatic pathway conditions. However, the direct measurements of spatial sensitivity, using full-field gratings, did show differences between the pathways. The data indicate that pRF sizes, as measured using fMRI, are not coupled to population-level spatial frequency sensitivity in an obvious manner. Data from a single dichromatic individual are presented and provide a case study example of the same measurements taken from a dichromatic subject.

4.2 Background

4.2.1 Retinotopy and pRF mapping techniques

Retinotopic visual areas in the human cortex can be mapped using functional Magnetic Resonance Imaging (fMRI) and stimuli that systematically move across visual field eccentricities and polar angles. fMRI measures changes in the blood oxygen level-dependent (BOLD) signal in the brain; it is expected

that local changes in oxygenation reflects changes in neural activity, and therefore changes in BOLD signal can be used as an indicator of brain activity as generated by a given stimulus (Wandell, 1995). To map the retinotopic organisation of the visual cortex two primary stimuli are traditionally used; expanding checkerboard rings that move through central to peripheral visual eccentricities, and rotating checkerboard wedges that move across polar angles of the visual field (see Figure 4.1 for examples) (Engel, 1997; Engel et al., 1994).

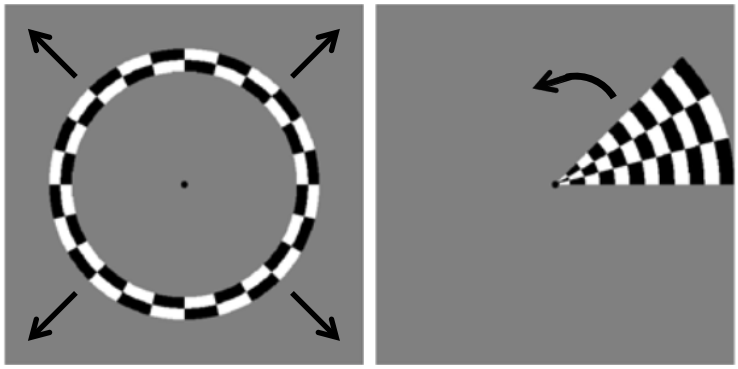

Figure 4.1 Example of expanding ring (left) and rotating wedge (right) stimuli, taken from Dumoulin and Wandell (2008). Arrows indicate the direction of movement.

These stimuli produce a travelling wave of neural activity, which indicate the peak response of neurons (in a voxel) to the stimulus presented at the corresponding time period (after correcting for a lag resulting from the haemodynamic response time). Figure 4.2 shows an example of phase-encoded maps produced by ring and wedge stimuli; boundaries of visual areas are identified using the phase-reversals produced in the polar angle maps.

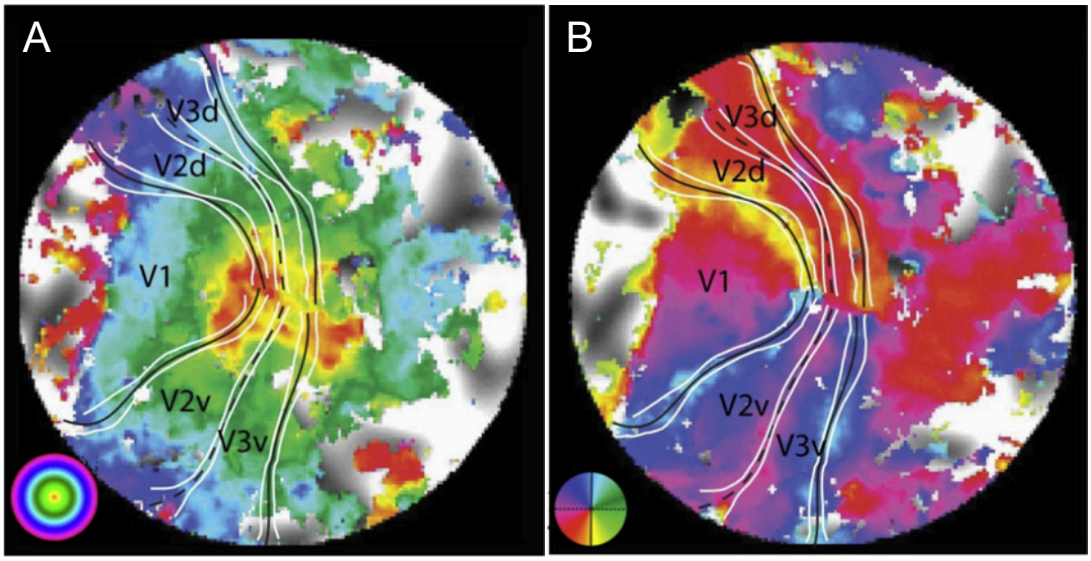

Figure 4.2 Example of (A) eccentricity and (B) polar angle maps for one hemisphere, produced with expanding ring and rotating wedge stimuli, respectively. Taken from Wandell and Winawer (2011).

A more recent technique developed by Dumoulin and Wandell (2008) uses, in addition to rings and wedges, a drifting bar stimulus (Figure 4.3). This method uses a Gaussian model to estimate receptive field sizes of populations of neurons based on the neural activity of each voxel to the various stimuli locations. There are three stages to the model fit, in which the ultimate aim is to produce a best estimate for each voxel of the spread of the Gaussian (sigma) as a measure of the population receptive field size for that voxel; in the first stage the data are smoothed (5-mm full-width at half-maximum Gaussian kernel) and the best fit for every other voxel is estimated from 100,000 sets of fixed pRF parameters (which alter the position and spread of a Gaussian model of the neuronal population). The fit is then optimised for all voxels that have at least 15% of their variance explained by the model by allowing each of the values from the parameter set to vary independently to get the optimum fit for the voxel (using values from the first stage as a starting point). The final fit of the data uses the original non-smoothed voxels and applies the optimised

fits generated in the previous stage. pRF sizes can be visualised on the cortical surface much like the phase and eccentricity maps (see example in Figure 4.4). For any given voxel the pRF information can be correlated with other information held for that voxel, e.g. eccentricity or polar angle tuning.

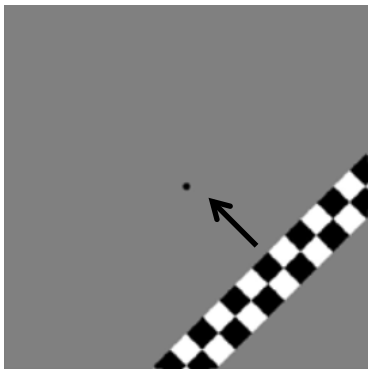

Figure 4.3 Example of bar stimuli used by Dumoulin and Wandell (2008).

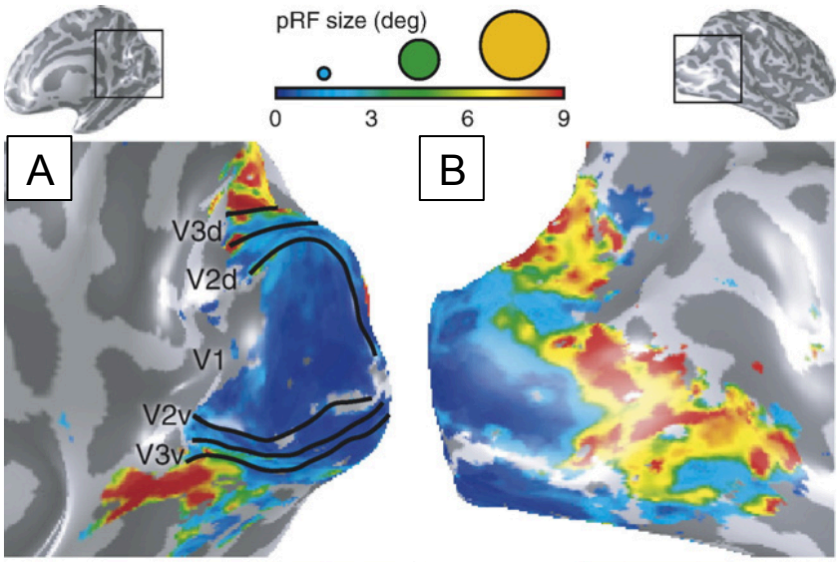

Figure 4.4 pRF size maps shown for medial (A) and lateral (B) view, with boundaries of visual areas indicated in (A). Taken from Dumoulin and Wandell (2008).

pRF models can be run on data generated by a combination of bar, ring and wedge scans. The bar stimuli are typically composed of black and white checkerboards, and move across a circular aperture in eight directions (four different orientations, with two motion directions), or, more accurately, a full

field drifting checkerboard stimuli is exposed through a moving bar aperture. The bars differ from both rings and wedges in that no direction is repeated more than once, so a phase map cannot be produced directly from this stimulus. In the original pRF paper by Dumoulin and Wandell (2008) they also include periods of mean luminance, 'blanks', in the wedge stimuli (presented at a different rate to the number of cycles) to act as a baseline condition. However, bar stimuli can be used on their own in the pRF model, with blanks incorporated into this stimulus (Harvey & Dumoulin, 2011). Both eccentricity and polar angle maps can be calculated from a model that only uses bar stimuli; these are viewed in the same way as data from ring and wedge stimuli, and are used to identify the visual area boundaries.

Variations of the pRF stimuli have been reported in the literature to investigate the effect of altering the composition of the stimulus on the fit of the data and pRF estimates. Alvarez, de Haas, Clark, Rees and Schwarzkopf (2015) looked at a number of different modifications to the stimuli, including logarithmically scaling the bar stimuli with eccentricity to account for known decreases in cortical magnification with increasing eccentricity (Virsu & Rovamo, 1979), and creating a hybrid wedge *and* ring stimulus. All versions of the stimulus produced comparable retinotopic maps and model fits – although slightly more of the variance could be explained with the wedge and ring combination stimuli, i.e. the goodness of fit of the pRF model was greater for this stimulus. The authors also noted that smaller pRF sizes were produced for the logarithmically-scaled bar stimuli. Another study, by Binda, Thomas, Boynton and Fine (2013), compared the use of a multifocal stimulus to a drifting bar stimulus. The multifocal stimulus was composed of 48 arc

apertures that each revealed a section of a contrast-reversing checkerboard; a random sample of the arcs are presented in each block, with the sequence randomised for each block (no neighbouring arcs are ever presented together), see Figure 4.5 for an example. Both stimulus types showed increasing pRF sizes with eccentricity, but the pRF sizes were consistently smaller across eccentricities for the multifocal stimulus condition. A difference in the success of the pRF model fits were also found between the stimulus types; goodness of fit values were higher across voxels for the drifting bar stimulus than the multifocal stimulus.

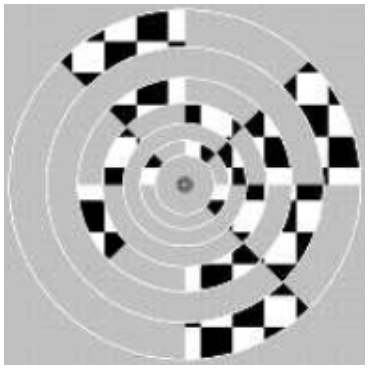

Figure 4.5 Example of the multifocal stimulus used by Binda *et al* (2013).

However, whilst these studies demonstrate that the composition of the pRF stimuli can have effects on both the estimated pRF sizes and the amount of variance explained by the model (goodness of fit), all versions of the stimuli use black and white 100% contrast checkerboards. By virtue of the technique used, neural responses elicited by the stimulus are not only determined by the location of the bars/wedges/rings/arcs, but the actual *content* of these apertures. The pRF estimates produced are necessarily a result of neurons responding to high-contrast achromatic stimuli. This means that current pRF data inherently represents specific populations of neurons that are tuned to

high contrast luminance stimuli (presented at particular spatial and temporal frequencies). The following section describes what is known about the spatial resolution of the chromatic and luminance pathways, and what can be predicted about population receptive field size across visual areas in these different pathways.

4.2.2 Spatial Resolution

Contrast sensitivity functions (CSFs) for the luminance and chromatic pathways have been well studied (Kim et al., 2013; Mullen, 1985; Owsley, Sekuler, & Siemsen, 1983; Webster et al., 1990). These functions plot the reciprocal of contrast detection thresholds (contrast sensitivity) as a function of the spatial frequency of the stimulus. As described in Chapter 3, for luminance stimuli these functions are roughly bell-shaped, with the highest contrast sensitivity found at a spatial frequency of approximately 4 cpd, and decreases in sensitivity either side of this peak. However, CSFs for chromatic stimuli – for both the L-M and S-cone isolating pathways – show a peak contrast sensitivity at very low spatial frequencies (<1 cpd), which decreases with increasing spatial frequency of the stimuli. A comparison of luminance, L-M and S-cone isolating CSFs, taken from the psychophysical data of one observer in a study by Webster *et al* (1990), can be seen in Figure 4.6. Behavioural data of this kind support the principle that the chromatic pathways are spatially low-pass compared to luminance pathways – they respond best to low spatial frequencies.

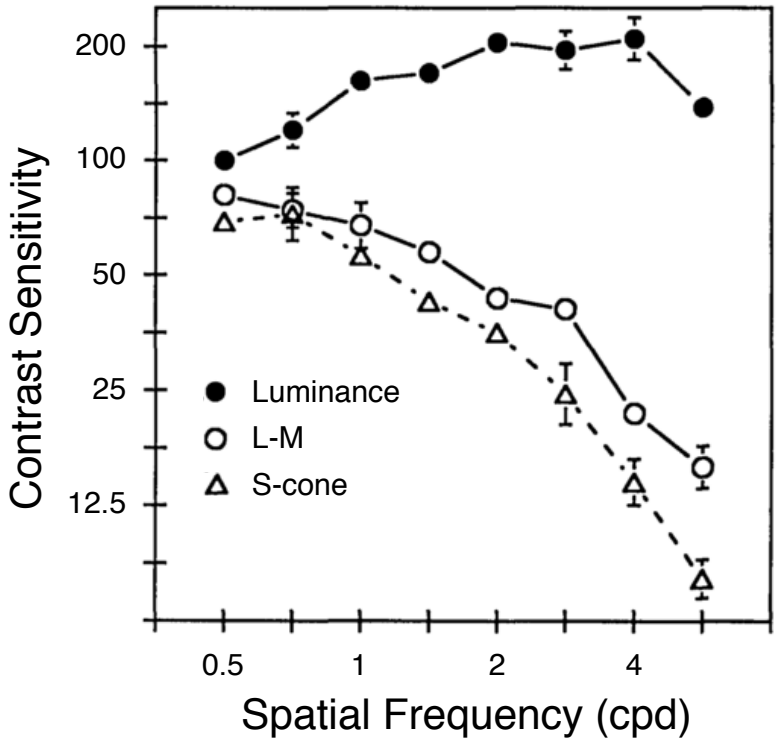

Figure 4.6 Contrast sensitivity plotted as a function of spatial frequency for Luminance (●), L-M (o) and S-cone isolating (Δ) gratings. Measurements for one observer, taken from Webster *et al* (1990)

The low-pass spatial resolution of chromatic pathways has been shown in both human and macaque subjects – a study by Merigan (1989) measured chromatic and achromatic contrast sensitivity in both subject types. Macaques were trained to perform a 2AFC task to identify the location of the stimulus, and were rewarded with fruit juice for correct responses. The same CSF differences between achromatic and chromatic stimuli were observed for both human and macaque subjects – the chromatic stimuli produced the highest contrast sensitivity at the lowest spatial frequency (<0.5 cpd), whereas the highest sensitivity for the luminance stimuli peaked at ~3 cpd.

fMRI studies show that the luminance and chromatic pathways produce distinctive activity in early visual cortex. Vanni, Henriksson, Viikari and

James (2006) measured V1 responses to achromatic and chromatic stimuli and showed differences in BOLD signal strength between the pathways as a function of eccentricity; L-M signals were stronger in the fovea than S-cone signals. Similarly, a study by Mullen, Dumoulin, McMahon, de Zubicaray and Hess (2007) looked for differences in the pathways for different stimulus contrast conditions – either fixed cone contrasts across conditions (e.g. all 6%) or each condition individually set to a multiple of the contrast threshold obtained for that condition. In both contrast conditions differences were observed between the pathways, however responses were better predicted when the cone contrasts were fixed across conditions (especially in V1). Differences in chromatic and achromatic sensitivity were observed across areas V1-V4, and the authors also noted that the S-cone responses were unexpectedly high given the sparse populations of neurons sensitive to the S-cone opponent pathway, which indicates some scaling of the signal amplitudes either in, or before, primary visual cortex.

In addition to these response differences between the pathways, studies have also shown that cortical measures of spatial resolution vary across eccentricities and visual areas, both within and between these pathways.
Henriksson, Nurminen, Hyvärinen and Vanni (2008) used fMRI to show that the mean spatial frequency preferences of neurons (voxels) for *achromatic* stimuli decreased with ascending visual area (from V1 to V3A) and also with eccentricity (in line with cortical magnification). D'Souza, Auer, Frahm, Strasburger and Lee (2016) also used fMRI to measure the effect of eccentricity and found the same decrease in spatial frequency tuning with increased eccentricity within V1 for achromatic stimuli. In addition, the

authors also used chromatic (L-M and S-cone isolating) stimuli, and found the same decrease in spatial frequency tuning with eccentricity. Unlike typical foveal CSF psychophysical data, which show low-pass spatial resolution of the chromatic pathways, responses in foveal V1 demonstrated band-pass responses for all pathways. However, for lower spatial frequency stimuli the luminance condition did still produce smaller responses than the chromatic conditions, showing that innate resolution differences can still be seen in early visual cortex. At a peripheral eccentricity of 9.8°, further differences could be observed between the pathways, with responses to S-cone stimuli decreasing more rapidly with increasing spatial frequencies than either the luminance or L-M conditions. While these observations do not represent all of the differences that are seen psychophysically, they do demonstrate measurable differences in spatial sensitivity between pathways within the visual cortex.

At early stages in visual processing (e.g. ganglion cells, LGN), there is evidence of a relationship between receptive field sizes and spatial frequency tuning. Studies of cat retinal ganglion cells have demonstrated that the optimal spatial frequency preference of cells correlated with the size of receptive field centres – cells tuned to lower spatial frequencies had larger receptive field centres than those tuned to higher spatial frequencies (Cleland, Harding, & Tulunay-Keesey, 1979; Linsenmeier, Frishman, Jakiela, & Enroth-Cugell, 1982). Similarly, Troy (1983) measured dorsal LGN (dLGN) cells in cats, and found the same relationship between spatial frequency tuning and receptive field size (also indicated by centre size of the receptive field).

While cortical measurements of spatial resolution do not correspond directly to the behavioural differences in the pre-cortical pathways, some pathway differences can still be observed, and some aspects of these measurements in the visual cortex appear to be analogous to reported achromatic pRF sizes, namely the effects of visual area and eccentricity. Both spatial frequency tuning (D'Souza et al., 2016; Henriksson et al., 2008) and pRF sizes (Alvarez et al., 2015; Binda et al., 2013; Dumoulin & Wandell, 2008; Harvey & Dumoulin, 2011) have been shown to change as a function of eccentricity and visual area. If pRF sizes are coupled with spatial resolution, then differences between chromatic and luminance pathways within the visual cortex should be equally reflected in *both* pRF and spatial resolution measures.

As discussed, there is some indication that measures of spatial resolution in the cortex do not mirror exactly the resolutions obtained from behavioural data (D'Souza et al., 2016). However, regardless of the coherence between behavioural and cortical measures of spatial resolution, it would still be possible to assess whether measures of pRF sizes are coupled with the *cortical* representations of spatial resolution, which have been shown to differ between achromatic and chromatic pathways.

4.2.3 Opponent pathways in dichromats and trichromats

Literature outlined in Chapter 3 postulated about the possible differences between dichromatic and trichromatic opponent pathways. In brief, dichromats that lack either L or M cones also lack an L-M opponent pathway. But anatomical studies of non-human primates have shown that dichromatic and trichromatic individuals do not show any structural size or distribution

differences across the magnocellular, parvocellular or koniocellular pathways (FitzGibbon et al., 2015; Goodchild & Martin, 1998; Solomon, 2002). Consequently, it is possible that the remaining luminance and/or S-cone isolating pathways in dichromats gain in some way from those 'would-be' L-M selective neurons.

The experiments carried out in Chapter 3 showed that any potential increases in relative population sizes within the luminance pathway do not benefit contrast detection thresholds across different contrast pedestal levels. However, a study by Janáky *et al* (2014) demonstrated that there may be a benefit associated with contrast sensitivities across spatial frequencies – their behavioural data indicated greater contrast sensitivities across mid-level spatial frequencies (from 3.6 cpd). But despite this difference in sensitivity, the data did not indicate differences in spatial resolution (the spatial frequency corresponding to the peak sensitivity was the same for both dichromats and trichromats). If differences in spatial resolution are unlikely between dichromats and trichromats, it is possible that no differences in pRF mapping exist between these groups.

At present it is unclear how *relative* differences in neuronal population sizes affect pRF sizes, however, some assumptions can be made based on the data previously discussed regarding eccentricity. A number of studies have reported changes in spatial frequency tuning, receptive field (RF) sizes and pRF sizes, with increasing eccentricity (D'Souza et al., 2016; Dumoulin & Wandell, 2008; Henriksson et al., 2008; Troy, 1983). Further to this, the overrepresentation of the fovea in the cortex means that a disproportionate

number of neurons are allocated to foveal eccentricities relative to peripheral eccentricities. It could be inferred that spatial frequency tuning, RF sizes and pRF sizes, are affected by the size of the neuronal populations across eccentricities. If larger neuronal populations are associated with smaller pRF sizes, then smaller pRF sizes may be predicted for either the luminance or S-cone pathways in dichromats (if dichromats have proportionately more neurons within these pathways than trichromats).

4.3 Aims and hypothesis

The experiments described in this chapter were designed to identify cortical pRF maps of the pre-cortical chromatic and achromatic channels. The aim was to identify whether innate spatial resolution differences between the pathways were correlated with fMRI measurements of cortical pRF sizes.

The literature demonstrates that behavioural measurements of spatial resolution are not perfectly mirrored by cortical neurons. However, some differences in spatial frequency tuning have been observed between the pathways as a function of eccentricity, and within both the chromatic and achromatic pathways it has been shown that tuning changes occur as a function of both eccentricity and visual area; pRF sizes have also been shown to vary in this manner. Therefore, it was hypothesised that pRF sizes, measured for visual areas V1-V4, would be coupled with cortical measurements of spatial resolution (reported as a spatial sensitivity index) of the chromatic and achromatic pathways. Specifically, it was hypothesised that the chromatic pathway conditions would produce larger pRF sizes than the luminance pathway condition as a function of eccentricity, with the largest

pRF sizes shown for the S-cone isolating condition. This hypothesis is in line with single-cell studies that showed low-pass spatial tuning was associated with larger receptive field centres (Cleland et al., 1979; Linsenmeier et al., 1982; Troy, 1983), and with an fMRI study that found S-cone responses to high spatial frequencies decreased more rapidly than luminance and L-M responses between foveal and peripheral eccentricities (D'Souza et al., 2016). This hypothesis maintains an underlying assumption that pRF sizes are coupled with spatial resolution, but makes fewer assumptions regarding *how* spatial resolution is represented in the cortex compared to behavioural measurements.

A single dichromatic individual was also tested in this experiment. Not only does the data provide a case-study for pRF sizes across pathways in dichromats, but it also allows for a measure of how much luminance noise is produced by the L-M stimulus condition (if properly isoluminant, this stimulus should be invisible to the dichromat). It is hypothesised that for the L-M condition the pRF model will not be able to fit the data from the dichromatic subject. It is also hypothesised that there will be a trend for smaller pRF sizes in the dichromat compared to the trichromats, in line with the prediction that the larger neuronal populations suggested for the dichromatic luminance pathway will result in smaller pRF sizes.

To directly test the hypothesis that pRF sizes are coupled with cortical measures of spatial resolution, the same pRF subjects carried out an fMRI experiment to produce measures of spatial sensitivity (in response to different spatial frequency gratings across conditions). A spatial sensitivity index was

calculated using the relative fMRI responses (beta values) to the different spatial frequency stimuli, presented for each pathway condition. It was hypothesised that the same differences between the pathway conditions would be shown for both the pRF sizes and the spatial sensitivity measures.

4.4 Methodology for pRF Experiments

4.4.1 MRI structural scans

Prior to the fMRI sessions, all subjects carried out structural scans in a GE 3 Tesla HDx Excite MRI scanner, using an 8-channel surface coil. All subjects had at least one T1-weighted anatomical scan, with several subjects also having T2-weighted scans; T1- and T2-weighted scans produce differences in the image contrast of the brain tissue. These scans were used to reconstruct a structural image of each subject's brain using FSL (http://fsl.fmrib.ox.ac.uk/fsl/fslwiki/) (Smith et al., 2004) and Freesurfer (http://surfer.nmr.mgh.harvard.edu/) (Dale, Fischl, & Sereno, 1999; Reuter, Schmansky, Rosas, & Fischl, 2012) software – the functional scans from each session were then aligned to these structural anatomies, as described below in Data Processing.

In cases where there was more than one T1 or T2 scan, the repeated scans within each scan type were first aligned to each other using the FSL 'flirt' function (Jenkinson, Bannister, Brady, & Smith, 2002), and then an average was produced using 'fslmaths' to add the aligned scans together. Cortical reconstruction and segmentation was then carried out using the Freesurfer 'recon' function. Once complete, the segmentation was manually checked

using the Freesurfer program 'Freeview' to ensure the correct directions had been applied (i.e. anterior/posterior, superior/inferior, left/right) and to check for any 'handles' or 'holes' – where voxels of white matter have been classified as grey matter, and vice versa. In order for the anatomy files to be used within mrVista (see below), they were converted with 'mri_convert' into a mrVista compatible 'nifti' format.

4.4.2 fMRI protocol

The fMRI scans were carried out using the same GE 3 Tesla HDx Excite MRI scanner, with a 16-channel surface coil situated at the occipital pole. The subject's head was positioned in the coil mount and surrounded by foam padding and a forehead strap to ensure the head was stable and that the subject was comfortable. Scan slices were aligned to adequately cover the region containing and surrounding the calcarine sulcus (the anatomical region containing the primary visual cortex). A total of 39 slices were taken within an FOV of 192 x 192 mm^2, with $2mm^3$ isotropic voxels (TR=3000ms, TE=30ms, flip angle=90, acquisition/reconstruction matrix=96x96). Four dummy TRs (12 seconds) were included at the beginning of each scan to allow for the stabilisation of the magnetic field prior to stimulus presentation. In addition to the functional scans, an axial proton density (PD) scan was acquired at the beginning of each session – this scan was used to align the fMRI data to the structural scan of the full brain.

4.4.3 Data processing

All the data processing was done using various modules (prefixed with 'mr', e.g. mrVista) from the VISTASOFT package (Vista Lab, Stanford University), which uses the commercial software package Matlab (The MathWorks Inc.,

Natick, MA, USA). fMRI scan data was imported and motion corrected between and within scans from each session using mrInit. The scans were then aligned to the anatomical structural scan using the Nestares alignment function within mrVista, following a manual initial alignment. Alignments were manually checked for accuracy, and any necessary adjustments were made. A final point-to-point alignment stage was then performed by selecting corresponding points on the reference and prescribed slices across multiple slices (a minimum of 50 points were used in total) – these selected points were used to perform the final alignment with the fine-alignment function in mrVista.

mrVista pRF modelling was used to extract the desired retinotopic and pRF information. For each condition the scans were first averaged together to produce a single scan. The parameters of the pRF model were then set, to provide information on the aperture size and duration (i.e. to tell the model where the bar was throughout the scan), and a two-gamma haemodynamic response function (HRF) was selected (which accounts for both positive and negative BOLD responses). The pRF model was also applied to an average of all scans (i.e. across all chromatic and luminance conditions), and the resulting retinotopic polar angle and eccentricity maps from this average were used for drawing the visual area ROIs (the same ROIs were then used to extract pRF information across each condition). The final pRF estimates by default only include voxels that have at least 10% of the variance explained by the model fit.

To increase the processing speed of the pRF modelling, the model was run on a restricted area of the cortex; an ROI was drawn in a Flat map view of the cortex (which was built from unfolds centred approximately on the calcarine sulcus in each hemisphere), the boundaries of the ROI comfortably exceeded the predicted locations of visual areas V1-V4, based on the anatomic identifiers for key visual areas. The pRF models were then run only within this 'extended visual areas' ROI for each condition.

4.4.4 Experiment and stimulus design

The stimuli used in these experiments were designed and presented using *Psykinematix* software (KyberVision, Montreal, Canada, psykinematix.com).

Retinotopic experiments require subjects to maintain central fixation throughout in order to produce accurate retinotopic (and in this case pRF) maps of the visual cortex. To help the subjects maintain central fixation an attention task was used in which the subjects were required to press a response button each time the fixation cross changed between '+' and 'x' symbols; the time between symbol changes was randomised so that the subject could not predict when the next change would occur.

To ensure the chromatic stimuli were isoluminant for each subject, minimum motion isoluminance tasks were carried out while inside the scanner, so that the stimuli could be specifically tailored for each subject's isoluminant point. Subjects fixated centrally while adjusting the colour of a drifting grating that was placed in their lower left periphery (see Figure 4.7); the grating had a 2° radius, centred at an eccentricity of 7° from the fixation point, with a drift rate

of ~1 degree per second. The point at which the drifting motion appears to stop, or is minimised, is considered to reflect the isoluminant point of the stimulus (Anstis & Cavanagh, 1983). The colour direction of the grating was determined within the Psykinematix software using LMS values in MacLeod-Boynton colour space (MacLeod & Boynton, 1979), and assuming 2° cone fundamentals from Stockman and Sharpe (2000). Three repeats of the adjustment were made initially, followed by further repeats if the range of values varied by more than 0.2 (mean values are given below). Subjects practised these minimum motion tasks outside the scanner in the laboratory (on a calibrated CRT monitor) prior to performing them in the scanner.

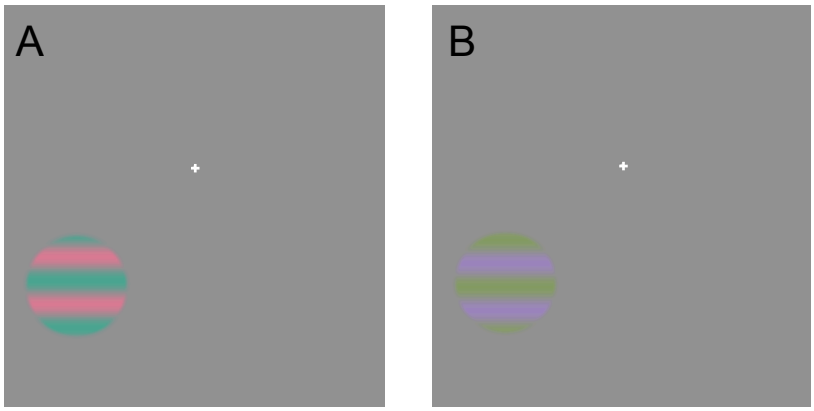

Figure 4.7 Example of minimum motion isoluminant stimuli for (A) L-M and (B) S-cone isolating conditions

For the L-M stimulus the ratio of L:M was adjusted in the minimum motion task by altering 'RGtheta' in the formulas shown in Table 4.1 for setting the L, M, and S values. These values can vary markedly between subjects, but tend to centre on RGtheta values of approximately 2, giving [L, M, S] values of approximately [-0.4, 0.9, 0]. For the S-cone isolating stimulus the values assigned to L, M, and S can be determined by adjusting YBtheta in the

formula shown in Table 4.1. The range of YBtheta values are generally small between subjects, and centre around 1.6, which equates to [L M S] values of approximately [0, 0, 1].

Table 4.1 Formulas used to adjust the L, M, and S values when creating the chromatic stimuli in the minimum motion isoluminance tasks for L-M and S-cone isolating conditions

Condition	L	M	S
L-M	cos(RGtheta)	sin(RGtheta)	0
S-cone isolating	cos(YBtheta)/sqrt(2)	cos(YBtheta)/sqrt(2)	sin(YBtheta)

The delivery system used for the visual stimulus in the scanner was an Epson EB-G5900 projector with a long throw lens, which projects the stimulus onto a custom-made acrylic screen. The participant viewed the screen with a mirror set-up in the scanner. The screen was calibrated for the gamma (using the Spyder4 display calibrator) and geometry within the Psykinematix calibration tools. Colour calibration measurements were made using the Jaz (Ocean Optics) photospectrometer, and the corresponding spectra were imported and used in the Psykinematix colour calibration. The benefit of using the photospectrometer for this measure was that the spectra could be recorded from the position of the participant, i.e. viewing the stimulus from the mirror, to produce the most accurate calibration for the colour.

Only the bar stimulus was used in the pRF experiments; this was primarily due to time constraints within the scanner, which meant running multiple scans of ring, wedge, and bar stimuli for each of the three conditions was not feasible. There were eight directions in which the bar moved (in both motion directions for horizontal, vertical, and each of the diagonals), and the bar was contained within a circular aperture with a 10° radius. The total time for each

directional sweep was 48 seconds. Four periods of mean luminance were included to provide a baseline condition within each scan, these periods always occurred in the second half of diagonal bar sweeps and lasted 24 seconds (see Figure 4.8). Subjects carried out a maximum of four scans of each condition over two or three sessions.

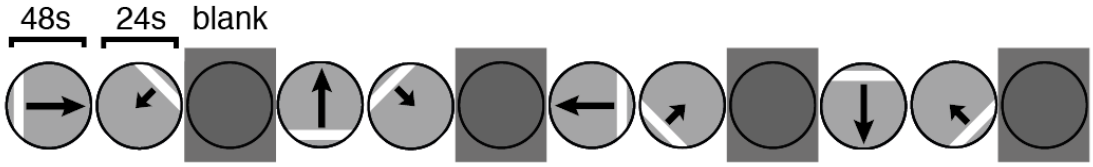

Figure 4.8 Schematic of the bar movement throughout a single scan. The 'blank' dark grey sections represent the mean-luminance periods (24 seconds). Larger arrows indicate that the bar swept across the full length of the direction (48 seconds), smaller arrows indicate that the bar swept across half of the direction (24 seconds).

The departmental Ethics Committee at The University of York, and the York Neuroimaging Centre Ethics Committee, both granted approval for the experiments presented in this Chapter.

4.5 Experiment 1: Chromatic pRF mapping

4.5.1 Introduction

A modified version of the Dumoulin and Wandell (2008) drifting bar stimulus was used for the first experiment. The modification allowed for three different conditions to be tested – Luminance, L-M and S-cone isolating. The checkerboards were replaced with a 1/f (pink noise) carrier for all conditions, and therefore the primary aim of this first experiment was to identify whether the retinotopic and pRF maps produced for the luminance condition were comparable to those presented by Dumoulin and Wandell. The pRF maps for the chromatic and luminance conditions were then compared to test the hypothesis there would be significant differences in pRF size between the

conditions; specifically, that the chromatic conditions would produce larger pRF sizes than the luminance condition.

4.5.2 Methods

4.5.2.1 Subjects

There were six trichromatic subjects (3 female) with a mean age of 27.3 years (±8.6 years). Four of the subjects were experienced in taking part in fMRI experiments (including retinotopy scans), and had very good fixation ability. All subjects were screened with Ishihara plates and confirmed colour-normal.

4.5.2.2 Experiment and stimulus design

In Experiment 1, the bar width was 2.5°, moving in 16 steps across the 20° diameter (each step lasting 3 seconds). Each of the three conditions (Luminance, L-M and S-cone isolating) had the traditional checkerboard replaced with a 1/f pink noise carrier, which randomly updated with each contrast reversal at a frequency of 2Hz (see Figure 4.9).

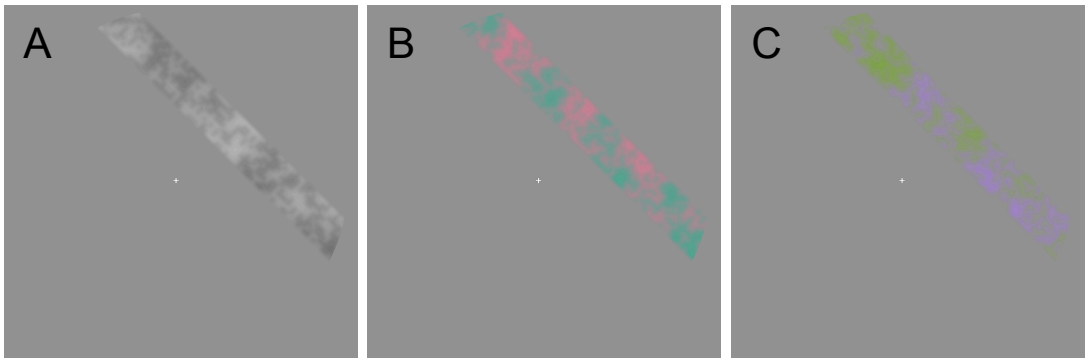

Figure 4.9 Example of the stimuli used in Experiment 1 for each condition: (A) Luminance, (B) L-M, and (C) S-cone isolating.

Pink noise was used so that, in theory, neurons responsive to a range of spatial frequencies for each particular pathway could respond to the stimulus. It was

also important to remove the hard-edged checkerboard stimulus, which may inadvertently stimulate luminance-tuned neurons during a chromatic stimulus presentation. The root-mean-squared (RMS) contrast values of each condition were arbitrarily selected such that the conditions appeared to have perceptually comparable contrast levels: Luminance=30%, L-M=5%, S-cone isolating=30%.

For this experiment, three subjects completed all four scans for each condition, whereas the other three subjects had fewer than four scans on one of the conditions. Specifically, for the L-M condition one subject completed two scans, and another completed three scans, and for the S-cone isolating condition one subject completed 2 scans. The discrepancies in the number of scans completed was due to scan time limitations, primarily from delays at the beginning of the scanning session reducing the number of possible scans that could be performed in that session.

In the minimum motion isoluminance task in the scanner, RGtheta values varied between 1.1 and 2.24 between subjects, e.g. between [L, M, S] values of [0.45, 0.89, 0] and [-0.62, 0.78, 0], with three of the subjects selecting values of 1.1 and the remaining three subjects setting values of 2, 2.01 and 2.24. These values were consistently set by each subject, and represent an unexpected spread of RGtheta values – values would be expected to fall around 2 to give LMS values of roughly [-0.4, 0.9, 0]. Given that these subjects made the settings consistently within the scanner, it was important that these values were used in producing the L-M stimulus. However, to assess whether the 'low RGtheta subjects' were selecting non-isoluminant

RGtheta values, the pRF data from each group of subjects (separated by the values selected) are also considered separately in the results.

The typical range of YBtheta values taken in the laboratory were extremely consistent between subjects, ranging between 1.55 and 1.6, i.e. between LMS values of [0.01, 0.01, 1.00] and [-0.02, -0.02, 1.00]. Therefore, owing to time constraints within the scanner, and the high levels of consistent and comparable values set by subjects outside the scanner on the S-cone isolating isoluminance task, for this experiment the [L, M, S] values for the S-cone isolating condition were set to [0, 0, 1] for all subjects; in the scanner only the L-M isoluminance task was carried out.

4.5.3 Results

4.5.3.1 Retinotopic maps and ROIs

For each subject the visual areas were identified using the polar angle and eccentricity maps produced by the pRF model that was run on the average of all scans across all conditions. Flat maps of the brain (created before the pRF models were run) were used to better view the polar angle and eccentricity maps. Boundaries of the visual areas were determined using the phase reversals from the polar angle map, as described in section 4.2.1, and the calcarine sulcus was used to orientate to the location of the primary visual cortex (V1) – the eccentricity maps determined the extent of the visual areas activated by the stimulus; see Figure 4.10 for an example of the visual boundaries for one subject. Visual areas from each hemisphere were combined to create the ROIs for visual areas V1-V4 (i.e. V1 left and V1 right were combined into a V1 ROI).

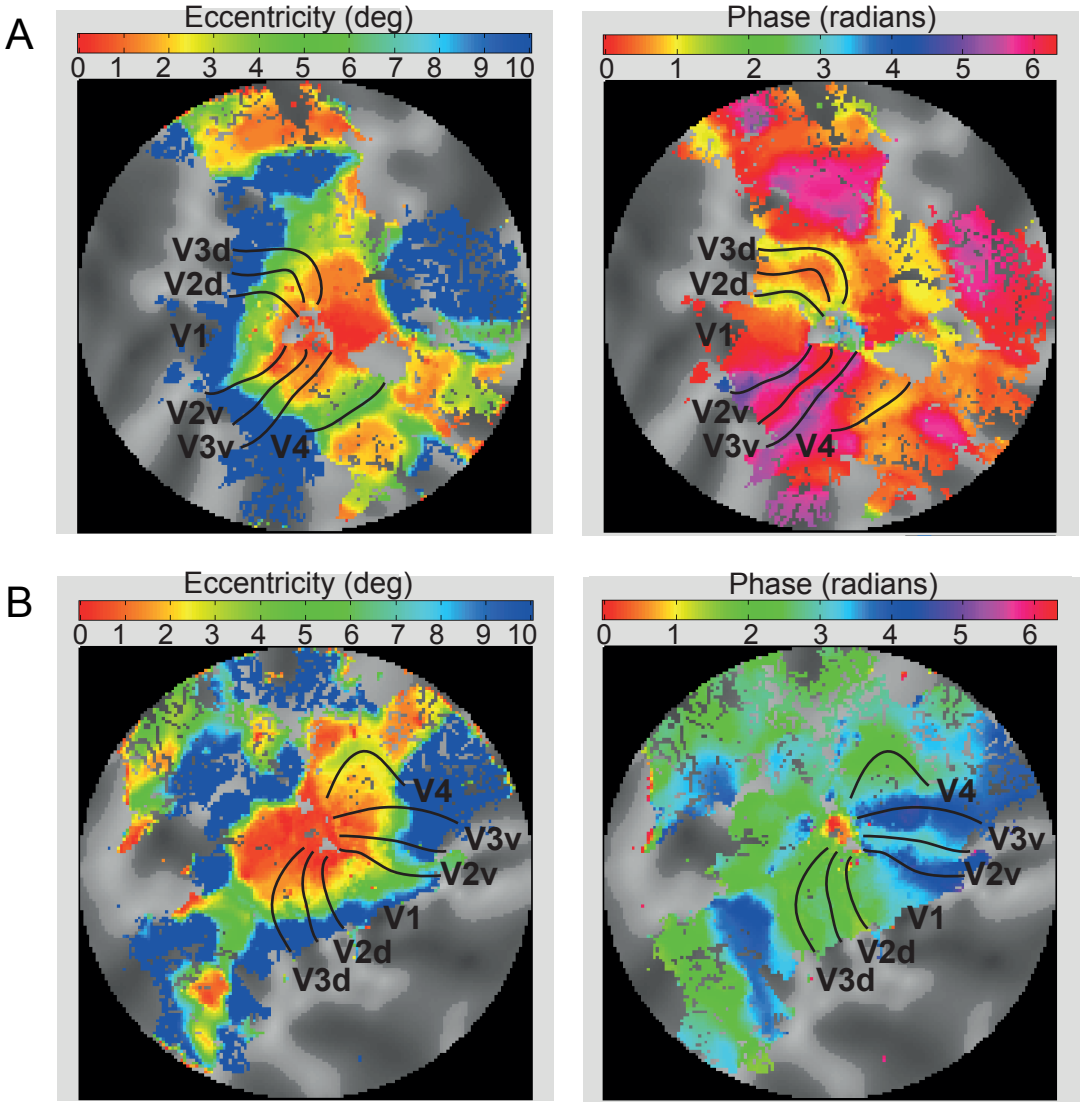

Figure 4.10 Example of eccentricity (left) and polar angle (right) maps produced by the pRF model for one subject, shown for (A) left and (B) right hemispheres. Boundaries of the visual areas are shown in black.

4.5.3.2 Size of visual areas

The surface area of the ROIs for each visual area and each subject were extracted with the 'measureFlatROIAreaMesh' function from the Flat view in mrVista. Average sizes of each visual area with standard deviations are shown in Table 4.2, with total surface area for all visual areas, total brain surface area (taken from the files produced by the Freesurfer 'recon'), and estimates of the proportion of cortical surface area that each visual area occupies (given as a

percentage). The surface area of visual areas decreases with ascending visual area hierarchy.

Table 4.2 Mean surface area of visual areas (combined left and right hemispheres) with standard deviations (stDev). Also shown as a percentage of the total brain surface area with standard deviations.

Visual Area	Mean size in mm^2 (stDev)	Percentage of total brain surface area (stDev)
V1	2967 (544)	1.89 (0.35)
V2	2725 (321)	1.73 (0.20)
V3	2330 (259)	1.48 (0.16)
V4	1059 (447)	0.67 (0.28)
Total Visual Areas	9080 (745)	5.78 (0.47)
Total Brain	157121 (9373)	

4.5.3.3 pRF size versus eccentricity

Mean pRF sizes across subjects were plotted against eccentricity for each visual area and each condition (Figure 4.11). For all conditions pRF size scaled with both eccentricity and ascending visual area. The data were extracted for each subject and condition and entered into a repeated-measures ANOVA to look for the effects of eccentricity, visual area and condition factors on the dependent variable of pRF size. Mauchly's test of Sphericity was not violated for the factors of condition ($\chi^2(2)=0.336$, $p=.845$) or visual area ($\chi^2(5)=3.369$, $p=.653$) (and could not be calculated for the eccentricity factor as the number of levels exceeded the degrees of freedom), and therefore sphericity could be assumed in the interpretation of the data (i.e. all possible group pairings show roughly equal variance in the differences between the pairings). There was a significant effect of visual area ($F(3,15)=291.880$, $p<.001$), and eccentricity ($F(18,90)=177.022$, $p<.001$), but no effect of condition ($F(2,10)=1.051$, $p=.385$), on pRF sizes. There was also

no interaction of condition with visual area ($F(6,30)=0.804$, $p=.575$). However, there were significant interactions between condition and eccentricity ($F(36,180)=3.754$, $p<.001$), between visual area and eccentricity ($F(54,270)=17.607$, $p<.001$), and a three-way interaction between condition, visual area and eccentricity ($F(108,540)=1.385$, $p=.011$).

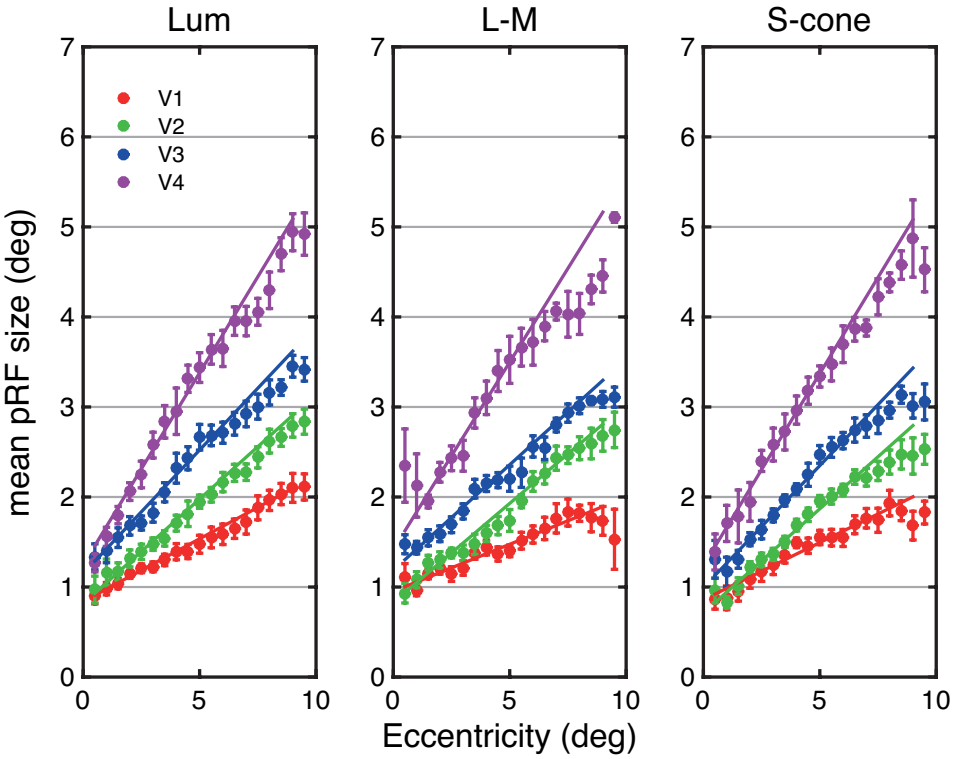

Figure 4.11 Mean pRF sizes plotted against eccentricity for each visual area, and each condition (from left to right: Luminance, L-M, S-cone isolating)

To further investigate these interactions, the pRF data were averaged into foveal (<2°) and peripheral (between 8°and 10°) eccentricity groups, and the same analysis was re-run on the data. The data are plotted in Figure 4.12; mean pRF sizes are plotted against visual areas for each eccentricity, and different bars are shown for each condition.

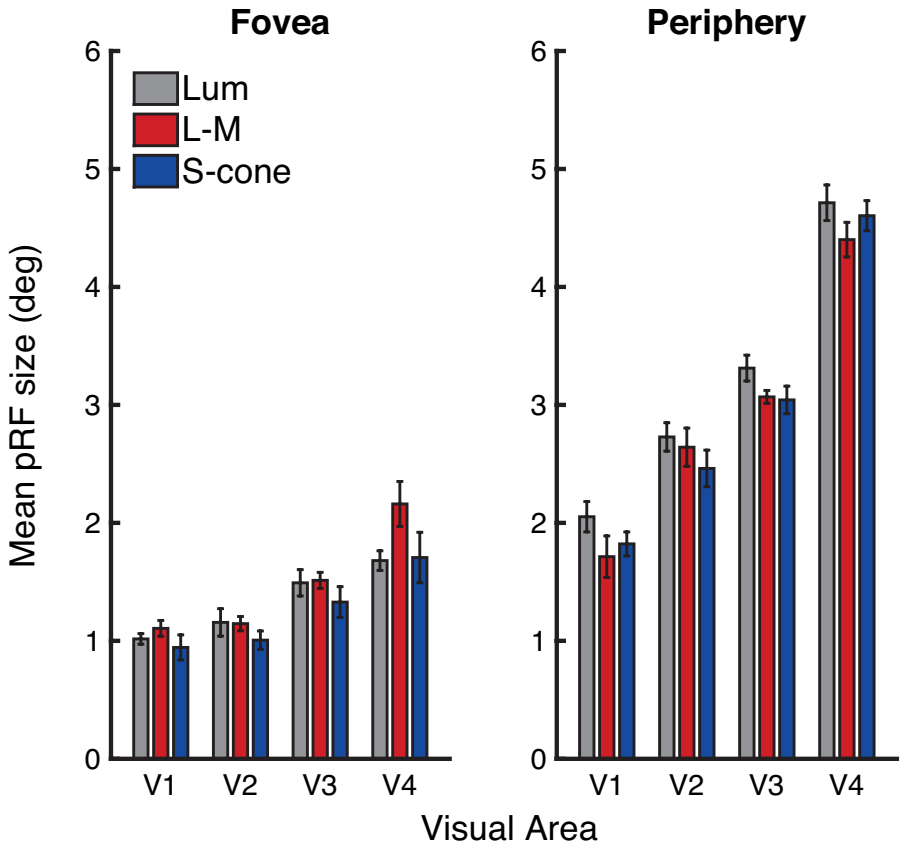

Figure 4.12 Average pRF sizes for foveal (left) and peripheral (right) eccentricities. Mean pRF sizes across subjects (with standard error bars) are shown for each condition (see legend) and clustered by visual area.

Mauchly's test of Sphericity was not violated for the condition ($\chi^2(2)=0.779$, $p=.677$), or visual area factors ($\chi^2(5)=8.472$, $p=.144$), and as there were only two levels in the eccentricity factor, sphericity can be assumed for all of these factors. As with the first analysis, significant effects were observed for the factors of eccentricity ($F(1,5)=449.892$, $p<.001$), and visual area ($F(3,15)=201.788$, $p<.001$), and no significant effect of condition was observed ($F(2,10)=2.465$, $p=.135$). There were also significant interactions between eccentricity and visual area ($F(3,15)=62.174$, $p<.001$), and condition and eccentricity ($F(2,10)=8.349$, $p=.007$), and no significant interaction between condition and visual area ($F(6,30)=0.528$, $p=.783$). However, the three-way interaction between all factors fell above the significance criteria in this analysis ($F(6,30)=2.217$, $p=.069$).

A final analysis of the data investigated whether there were any differences in pRF sizes for the L-M condition between subjects that set different theta values for the L-M isoluminance values, i.e. those that set low (~1.1) theta values compared to those that set higher (~2) theta values. A repeated-measures ANOVA was carried out for just the L-M condition. The eccentricity groups (foveal and peripheral) and visual areas were set as within-subject factors, and the 'theta group' as the between-subject factor. Mauchly's test of Sphericity was not violated for the visual areas factor ($\chi^2(5)=7.630$, $p=.202$), or the interaction between visual area and eccentricity ($\chi^2(5)=2.557$, $p=.781$). In agreement with the data previously reported, there were significant effects of eccentricity ($F(1,4)=196.953$, $p<.001$), and visual area ($F(3,12)=78.318$, $p<.001$). However, there was no significant between-subject effect of theta group ($F(1,4)=2.400$, $p=.196$).

4.5.3.4 Variance Explained

The amount of variance explained, calculated within the pRF model, can be used to compare how well the model was able to fit the data across conditions. It is also a useful measure of how well the pink noise carrier replaces the black and white checkerboard in the luminance condition. The amount of variance explained (%) by the voxels that were included in final pRF estimate (i.e. all that explained at least 10% variance) was averaged across visual areas for each subject within each condition, and then paired t-tests were carried out between each of the conditions (significance criteria were Bonferroni-corrected to account for the multiple comparisons). The data are shown in Figure 4.13. There was a trend for more variance to be explained in the

luminance condition, however, there were no significant differences between the values for any of the conditions (Luminance vs. L-M: $t(5)=1.146$, $p=.304$; Luminance vs. S-cone: $t(5)=2.082$, $p=.092$; L-M vs. S-cone: $t(5)=0.199$, $p=.850$). Therefore, the accuracy of the model-fits across conditions was comparable.

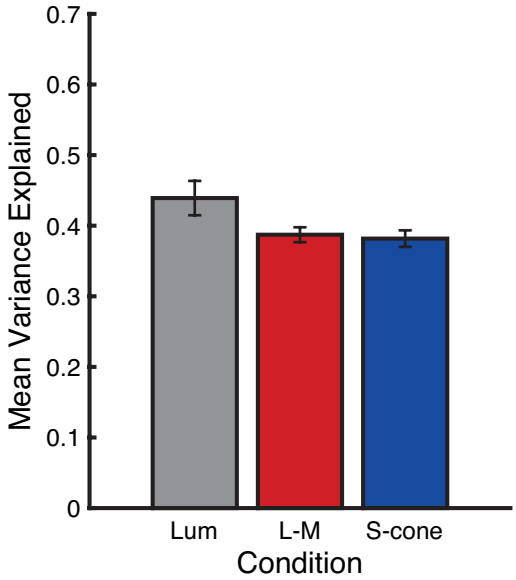

Figure 4.13 Mean variance explained (%) across subjects (with standard error bars) for each condition.

4.5.4 Discussion of Experiment 1

4.5.4.1 Summary of Results

For all conditions, pRF size scaled with eccentricity and with ascending visual area (V1-V4), which is in line with luminance pRF data produced by other groups (Alvarez et al., 2015; Binda et al., 2013; Dumoulin & Wandell, 2008). However, the hypothesis that there would be a significant difference in pRF sizes between the chromatic and luminance conditions was not clearly supported here; there was no significant effect of condition on pRF sizes, but there were some significant interactions between condition, visual area, and eccentricity. There were no trends in the data that indicated the S-cone

condition had larger pRF sizes than the other conditions, which was hypothesised.

4.5.4.2 Consequences of modifying the bar content

The luminance condition can be used to estimate how pRF sizes are affected by the content of the bars – there are a number of papers that report pRF data from luminance stimuli that can be used as a comparison to the data in this experiment. Here, the bars contained a lower contrast and a 1/f pink noise carrier, instead of the traditional 100% contrast black and white checkerboards. As described, the data correspond well to that reported by other groups in relation to the increase in pRF sizes with eccentricity and visual area (Alvarez et al., 2015; Binda et al., 2013; Dumoulin & Wandell, 2008). However, average pRF sizes reported here for the foveal eccentricities (~1° for V1) are larger than the averages shown elsewhere (~0.5° for V1) (Alvarez et al., 2015; Dumoulin & Wandell, 2008). The pRF sizes at more peripheral locations were in closer agreement with some of conditions reported by Alvarez *et al*, despite still being slightly larger than those reported by Dumoulin and Wandell. One possibility is that the bar width used only allowed for a coarse, conservative estimate of pRF sizes, particularly at foveal regions. This possibility is supported by Alvarez *et al*, who found that when the bar width is adjusted to account for cortical magnification across eccentricities (i.e. the width logarithmically increases across eccentricity), smaller pRF sizes are found across both visual areas and eccentricities.

4.5.4.3 Chromatic versus luminance pRF sizes

pRF sizes increased with both eccentricity and visual area for all chromatic and luminance conditions. The analyses showed no effect of condition on pRF sizes, and therefore these findings do not support the hypothesis.

It could be argued that any inaccuracies in the isoluminance values for the chromatic conditions could have resulted in activation of neuronal populations tuned to both luminance *and* the chromatic pathway, for each chromatic condition, i.e. pRF sizes for the chromatic conditions may actually be representing pRFs from a combination of luminance *and* chromatic pathways. However, within the L-M isoluminance values there was a distinctive group split between individuals who selected (the anticipated) isoluminant levels ('high theta') and those that did not ('low theta'). There was found to be no significant effect of the theta group on the pRF sizes. If the low theta group truly had erroneous and non-isoluminant stimuli in the L-M condition, whereas the high theta group did not, a difference in pRF sizes would be expected between these groups if there were a difference in actual pRF sizes between these pathways. Therefore these data support the general lack of effect of condition on pRF sizes.

In this experiment the LMS values for the S-cone isolating condition were fixed across all subjects due to there being very little variance in typical isoluminance values set between subjects outside of the scanner. However, for the second experiment (described below), it was appropriate to confirm

isoluminance of this channel, and increase confidence in the findings, by having the isoluminance values set individually for each subject.

The L-M isoluminance task was found to be more difficult for all the subjects when within the scanner performing the task – it was harder to find the point of minimum motion in the stimulus, and subjects often adjusted the RGtheta value to ~1.1 (i.e. L=0.45 and M=0.89) in the scanner, despite producing the expected value of ~2 (i.e. L=-0.4 and M=0.9) in the practice task outside the scanner. This effect may be due to the actual difficulty of the task combined with the unusual viewing conditions when within the scanner (compared to in the lab). For the second experiment subjects were given more training on the task in the laboratory to acquire accurate and consistent RGtheta values, prior to entering the scanner. The aim of this was to eliminate any potential inaccuracies in the settings made which are a result of different viewing conditions and limited training. Both the projector used in the scanner, and the CRT monitor used in the lab, were calibrated, and therefore should produce comparable stimuli using the same parameters. Although it should be noted that the projector screen is somewhat limited in its clarity compared to viewing the stimulus directly on a CRT monitor, so whilst calibration of the colour and gamma can be controlled, the precise quality of the image cannot be as accurately controlled.

The contrast levels in this experiment were arbitrarily set to be perceptually equivalent across conditions, however it is possible that if contrast levels were too high for the chromatic conditions this may also contribute to incidental activation of luminance pathways; this issue can be rectified by using a

multiplication of contrast detection thresholds (i.e. 3x threshold) to set the contrast levels of the stimulus in each condition.

4.5.5 Conclusion

The ultimate aim of this experiment was to investigate the coupling of pRF size with spatial resolution, as measured by analysing pRF sizes between luminance and chromatic pathways. However, it was also important to establish whether the modifications made to the content of the bars (1/f pink noise instead of 100% contrast black and white checkerboards) affected the pRF estimates produced for the luminance condition, in comparison to data reported by other groups. The same pattern of pRF data was found for the luminance condition as anticipated based on previous reports (Alvarez et al., 2015; Binda et al., 2013; Dumoulin & Wandell, 2008); pRF sizes increased with increasing eccentricity as well as with ascending visual areas. The pRF sizes at more peripheral locations were generally in agreement with corresponding data from Alvarez *et al* (2015), despite being slightly larger than those reported by Dumoulin and Wandell (2008). However, foveal pRF sizes were larger than either of those reported by these two groups. It is possible that this difference may be a result of the bar width, which was perhaps too large to accommodate the cortical magnification of the fovea. To account for this, Experiment 2 used a narrower bar width in order to allow the model to better estimate pRF sizes nearer foveal eccentricities. Any potential improvement in the estimates of the pRF sizes at this eccentricity may help to further establish whether any differences in the pRF sizes can be observed between the chromatic and luminance conditions.

4.6 Experiment 2: pRF sizes and spatial resolution

4.6.1 Introduction

Experiment 1 found no overall effect of condition (luminance/L-M/S-cone) on pRF sizes, despite some significant interactions between condition, visual area, and eccentricity. The expected relationship was found between pRF sizes and both eccentricity and visual areas; however, slightly larger than anticipated pRF sizes were observed in the foveal measurements for the luminance condition, compared to previous reports of achromatic pRF sizes.

Experiment 2 aimed to modify the methodology to help minimise any potential over-estimations of pRF sizes in the fovea (which may have disguised any clear pRF size differences between the conditions) and eliminate any luminance noise infiltration into the chromatic conditions. This was achieved using a narrower bar width for the stimuli, and more thorough training for the minimum motion isoluminance tasks for both chromatic conditions prior to testing in the scanner. In addition, the contrast levels of the stimuli were altered based on contrast detection thresholds obtained from three of the subjects in Experiment 2 (prior to scanning).

To directly test the hypothesis that pRF sizes are coupled with cortical measurements of spatial resolution, the same subjects carried out fMRI scans for three full-field spatial frequency grating conditions (0.5, 2 and 8 cpd) which were matched to the key parameters used in the pRF stimuli. Responses across spatial frequencies were used to produce a spatial sensitivity index within foveal and peripheral eccentricities for each visual area and

condition. If pRF size and spatial resolution were coupled, the same pattern of responses would be expected for both the pRF sizes and spatial sensitivity index values across conditions. A behavioural psychophysics experiment was also performed to gather contrast detection information across the same spatial frequency levels and conditions, using two eccentricity positions. These data were used to identify whether the expected behavioural data could be observed in the subjects, and whether responses in visual areas V1-V4 corresponded to the behavioural data. Based on the studies discussed in the Background sections, it was hypothesised that the behavioural measurements would show low-pass spatial resolution for the chromatic conditions, and band-pass resolution for the luminance condition. It was further hypothesised, based on the work by D'Souza *et al* (2016), that this same difference between pathways would not be clearly demonstrated in the cortical measurements across eccentricities: specifically, whilst a difference between the luminance and chromatic conditions was hypothesised for foveal eccentricities, the actual spatial sensitivity values for the chromatic conditions were hypothesised to not show *low* spatial sensitivity, but just *lower* values than the luminance condition. For the peripheral eccentricities the S-cone condition was hypothesised to show lower spatial sensitivity than the other conditions, i.e. there would be some effect of condition on cortical measures of spatial sensitivity, which would differ across eccentricities.

A dichromatic individual was also tested on these same experiments to be used as a case-study example of a dichromat response. The responses from this participant were used to determine the level of luminance noise that may be experienced for trichromatic subjects; the L-M stimuli should be invisible

to the dichromat if it is truly isoluminant, and therefore any fit of the pRF model can only be due to luminance-based responses.

4.6.2 Methods

4.6.2.1 Subjects

For this experiment six trichromatic subjects were recruited (2 female) with a mean age of 28.7 years (±8.1 years), four of these subjects had also taken part in Experiment 1 of this study. For the spatial frequency experiments (carried out after the pRF experiment), one of the subjects was unable to take part, therefore the means presented for that data are based on the remaining five subjects. One dichromatic (deuteranope) male subject (age 32) was also used in this experiment. This subject has previously been involved in scientific experiments at other Universities that measured his colour vision deficiency as well as his cone mosaic – the subject reported that his mosaic is non-patchy. All trichromatic subjects were confirmed as colour-normal with Ishihara plates, and the dichromat diagnosis was confirmed using Ishihara plates, Rayleigh matches and the red-to-green match described in Chapter 3.

4.6.2.2 pRF experiment and stimulus design

The bar width was set to 0.5°, and a continuous drifting motion of the bar was introduced (instead of 16 steps) such that the bar crossed the full 20° diameter of the aperture in 48 seconds (moving ~0.42° per second). The same fixation task was used as in Experiment 1 to help subjects maintain central fixation.

Due to the reduced width of the bar, it was not feasible to use 1/f pink noise within the bars, as it often resulted in the bar appearing to contain two large

blocks of colour/contrast at any given time or large gaps within the bar. Therefore a white noise carrier was used instead for the stimuli in this experiment; see an example of a pink noise carrier compared to a white noise carrier for the L-M stimuli in Figure 4.14.

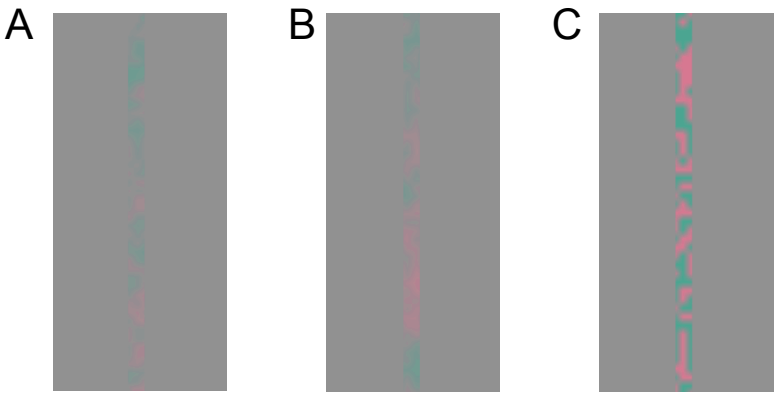

Figure 4.14 Example of how the narrow bar stimulus would look with a 1/f pink noise carrier (A and B) compared to a white noise carrier (C) for the L-M condition.

The contrast levels of the stimuli were set using values that were approximately 3x the RMS contrast threshold levels. Three of the trichromatic subjects performed a contrast detection task in the laboratory using a 4AFC method, with circular (2° diameter) white noise stimuli placed at 7° eccentricity from the central fixation mark, for each of the three conditions: luminance, L-M and S-cone isolating. Average contrast detection thresholds were calculated across subjects and multiplied by three to determine the contrast to be used; contrasts were rounded to the nearest whole percentage resulting in the following RMS contrast values for each condition (see Figure 4.15): Luminance=5%, L-M=4%, S-cone isolating=15%.

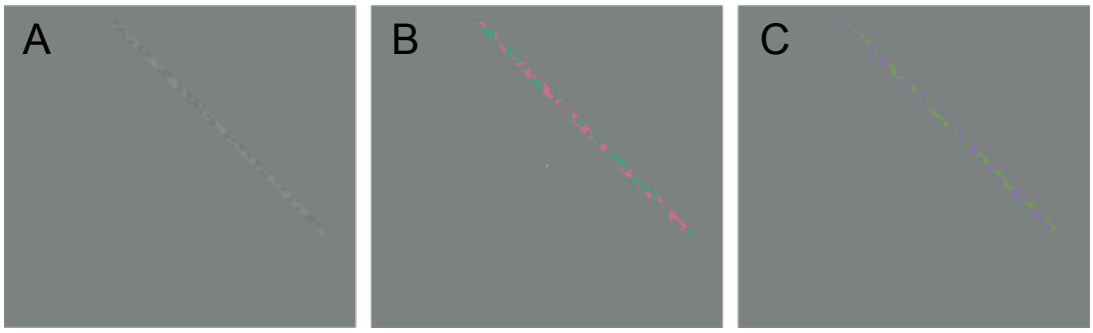

Figure 4.15 Example of the stimuli used in Experiment 2 for each condition: (A) Luminance, (B) L-M, and (C) S-cone isolating.

For this experiment the minimum motion isoluminance task was performed for both chromatic conditions. For the S-cone isolating task all subjects performed extremely consistently between repeats of the task, and between subjects the range of values differed by a maximum of 0.06 (mean YBtheta=1.57). As with Experiment 1, RGtheta values were more difficult for subjects to obtain within the scanner, however, training improved the consistency in settings across subjects, and the mean RGtheta value across subjects was 1.94, with the range of values differing by a maximum of 0.19. The values set by the dichromat were 1.02 for RGtheta, and 1.62 for YBtheta. For RGtheta, the stimulus was invisible to the participant at this value – both in the periphery, where the task was performed, and when the subject was directed to look towards the location of the grating to place it in the fovea.

4.6.2.3 Spatial frequency experiment and stimulus design

The stimuli used in the fMRI experiment were full-field sinusoidal gratings of different spatial frequencies (0.5, 2 and 8 cpd), which had a randomised orientation that was updated with each contrast reversal (at 2Hz). The stimuli for each condition matched the pRF stimulus in contrast, isoluminance values

used (set for the pRF stimuli with the minimum motion task), total eccentricity (20° diameter), and temporal frequency (2Hz) (see example in Figure 4.16). Subjects fixated centrally throughout, using the same fixation task from the pRF experiments.

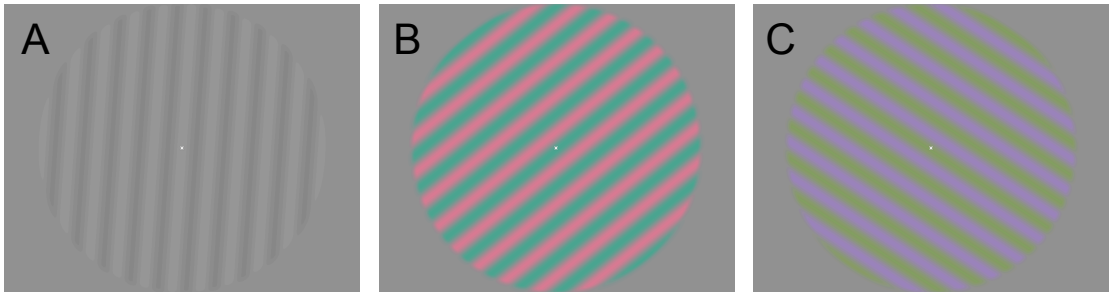

Figure 4.16 Example stimuli for the (A) luminance, (B) L-M, and (C) S-cone isolating conditions, at a spatial frequency of 0.5 cpd.

An event-related design was used to present the stimuli from each event condition; there were a total of 10 events (3 spatial frequencies for 3 conditions, plus one blank condition). Each event was presented for 3 seconds (1 TR) with a randomised inter-stimulus interval of between 3-6.5 seconds. Within each scan each event was presented four times, with all events presented in a randomised order. A total of four scans were completed for each subject, which resulted in 16 trials for each event condition.

The stimuli in the behavioural contrast detection task used the same spatial frequencies as the fMRI experiment, and measured contrast detection thresholds for each condition at each of the spatial frequencies. The task was carried out at two eccentricity positions – 2° and 8° (from fixation to the centre of the gratings). A 2AFC method was used with a Bayesian staircase procedure; the participants had to select which of two locations contained a

grating target (presented for 100ms). There were 10 log-distributed contrast levels tested for each condition. The minimum contrast level tested for all conditions was 0%, and the maximum contrast level used varied across the conditions, as shown in Table 4.3. The stimulus gratings had a 2° diameter, and the two possible stimulus locations were outlined with thin white circles to remove spatial uncertainty (see Figure 4.17).

Table 4.3 Maximum contrast levels (%) set for the contrast detection tasks for each eccentricity and spatial frequency (cpd) condition.

	2° eccentricity			8° eccentricity		
Condition	0.5 cpd	2 cpd	8 cpd	0.5 cpd	2 cpd	8 cpd
Luminance	5	5	10	5	5	15
L-M	5	5	5	5	5	5
S-cone	10	10	15	15	20	20

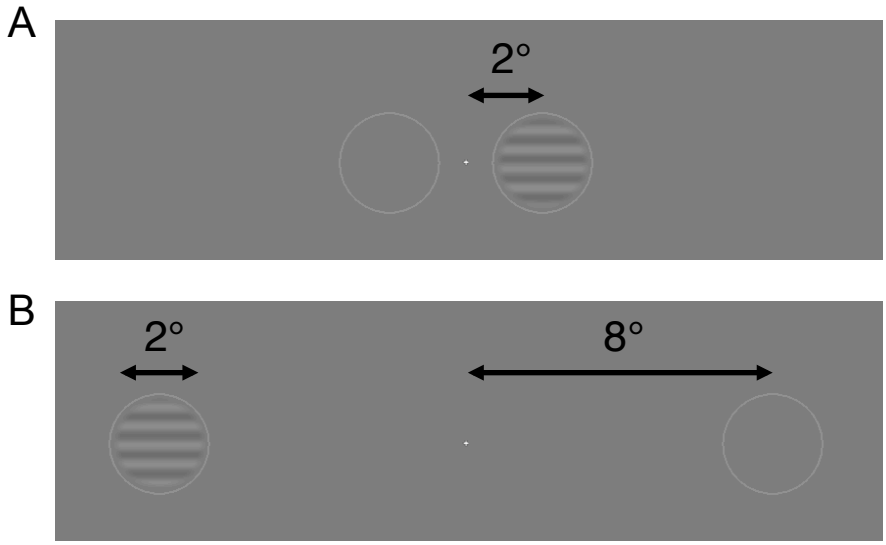

Figure 4.17 Example trials from the (A) 2° and (B) 8° eccentricity conditions for the luminance 2 cpd condition.

A total of 200 trials were carried out for each eccentricity and spatial frequency condition, spread over four blocks for each chromatic condition (luminance, L-M, and S-cone isolating), i.e. in total 12 blocks were carried out.

Within each block an additional 10 practice trials were included for each condition, which were not included in the analysis. All trials for each condition were performed successively, but the actual order that the conditions were presented in was randomised for each block.

For each of the chromatic conditions, minimum motion tasks were carried out first to set the isoluminance levels for each eccentricity – the stimuli used in the minimum motion tasks were the same as those previously described, but set at the two eccentricities used in this experiment with the same grating diameter, and positioned horizontally in line with the fixation point.

4.6.3 Results

4.6.3.1 Retinotopic maps and ROIs

Retinotopic maps were produced for each trichromat subject based on a pRF model run on the average of all scans from all conditions, and for the dichromat subject the average was for all scans from the luminance and S-cone conditions. The ROIs for each visual area were defined using the polar angle and eccentricity maps outputted by the pRF model. Figure 4.18 shows retinotopic maps for one trichromatic subject, and Figure 4.19 shows retinotopic maps for the dichromatic subject. The edge of the 'extended visual areas' ROI used for the trichromat (the region that the pRF models were run in) can be seen as the rounded boundary on the phase maps. If the visual areas appeared too close to the edge of the 'extended visual areas' ROI, the ROI was re-drawn over a larger area and the pRF models re-run for all conditions. For the dichromatic subject, the 'extended visual areas' ROI was drawn to the edges of the flat maps in each hemisphere.

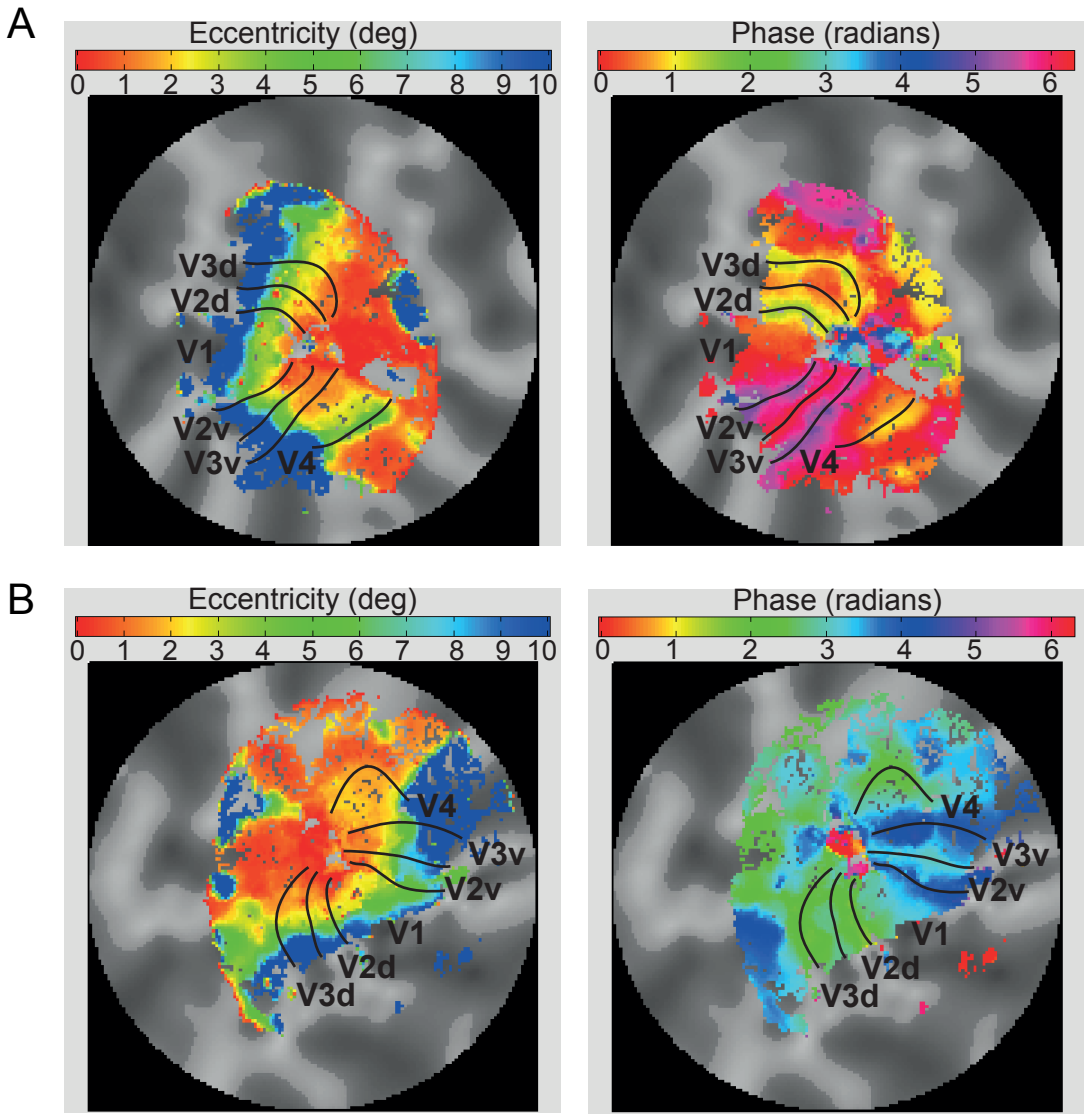

Figure 4.18 Example of retinotopic maps for one trichromatic subject, showing eccentricity (left) and polar angle (right) phase maps, which were used to identify the visual area ROIs in the left (A) and right (B) hemispheres. The boundaries of the visual areas are overlaid on the maps in black. Note that the maps are restricted by the 'extended visual areas' ROI – the pRF model was only applied to this area to improve the processing speed of the model.

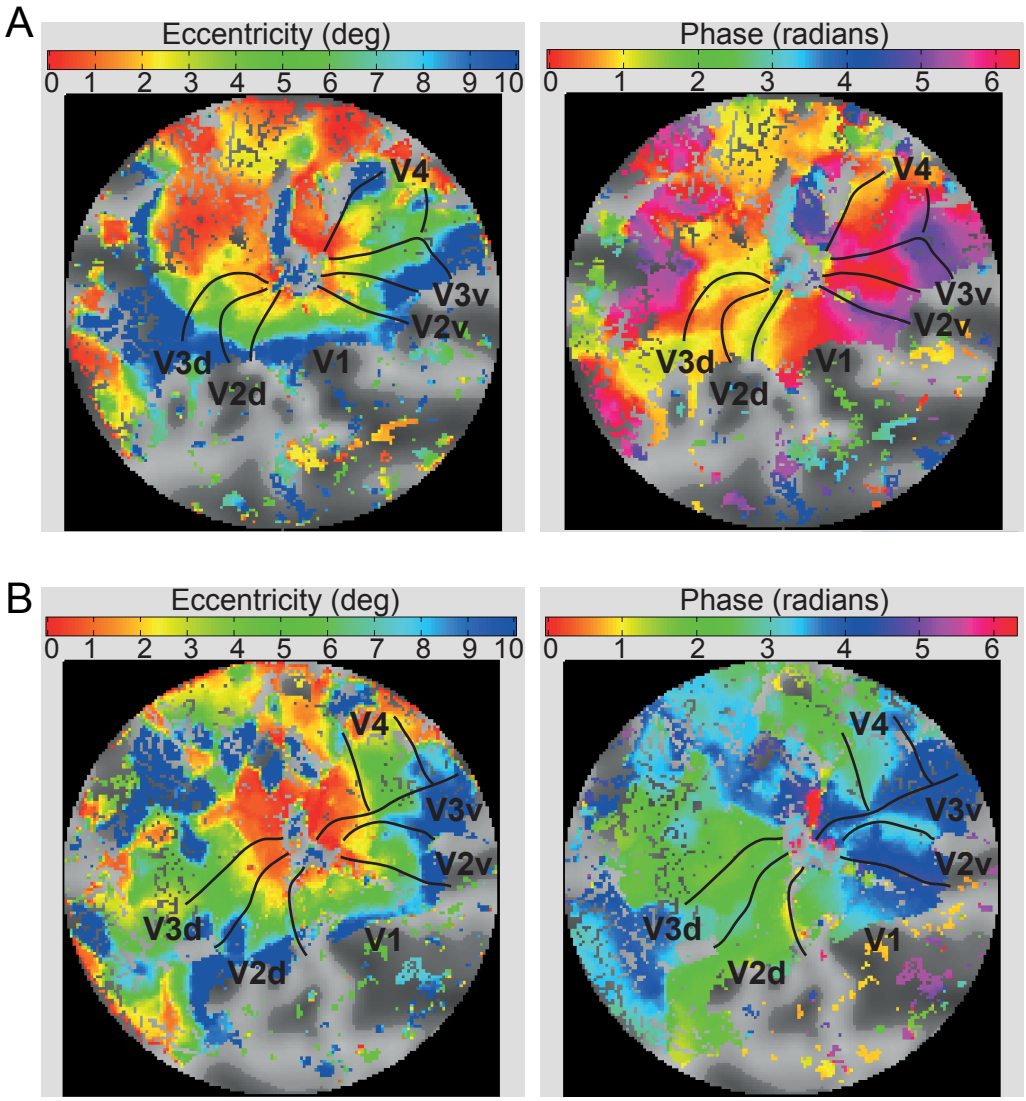

Figure 4.19 Retinotopic maps for the dichromatic subject. Eccentricity (left) and polar angle (right) phase maps were used to identify the visual area ROIs in the left (A) and right (B) hemispheres. The boundaries of the visual areas are overlaid on the maps in black.

4.6.3.2 Size of visual areas

The surface area of each ROI was calculated in mrVista from the Flat maps (using 'measureFlatROIAreaMesh'). ROIs were then combined across dorsal and ventral areas (where applicable) and across each hemisphere to give total surface areas for each visual area, for each subject. The average surface areas across subjects and the standard deviation are shown in Table 4.4, with total surface area for all visual areas, total brain surface area (taken from the

Freesurfer cortical reconstruction files), and mean proportion of cortical surface area that each visual area occupies (given as a percentage). Trichromatic means are shown separately from the dichromatic subject. Despite the dichromat showing a larger total surface area for the visual areas, when these values are shown as a proportion of the total brain area, the values are comparable between the trichromats and dichromats – the dichromat shows a slightly smaller V4 compared to the trichromats, however as there is only one dichromatic subject it is unclear whether this is likely to be a significant size difference between the groups.

Table 4.4 Surface area of visual areas (combined left and right hemispheres); mean with standard deviations (stDev) shown for the trichromats (n=6), and individual dichromat values shown separately. Percentage of total brain surface area occupied by each visual area is calculated from the trichromatic group average for the trichromats, and the dichromatic values are calculated from this subject alone.

	Surface area of each visual area (mm^2)		Percentage of total brain surface area occupied by each visual area	
Visual Area	Trichromats mean (stDev)	Dichromat	Trichromats mean (stDev)	Dichromat
V1	2718 (285)	3029	1.71 (0.18)	1.65
V2	2684 (331)	3185	1.69 (0.21)	1.74
V3	2254 (182)	2620	1.42 (0.11)	1.43
V4	1116 (189)	1047	0.70 (0.12)	0.57
Total Visual Areas	8772 (690)	9881	5.51 (0.43)	5.40
Total Brain	159286 (11025)	183125		

4.6.3.3 pRF size versus eccentricity

Data were plotted in the same manner as the data from Experiment 1, with separate plots for the trichromatic and dichromatic subjects for comparison. The statistical analyses are performed only for the trichromatic subjects;

however, it can be seen for both trichromats (Figure 4.20) and the dichromat (Figure 4.21) that pRF sizes scaled with both eccentricity and visual area.

A repeated-measures ANOVA was carried out to assess the effects of eccentricity, visual area and condition factors on the dependent variable of pRF size. Mauchly's test of Sphericity was not violated for either factors of condition ($\chi^2(2)=4.886$, $p=.087$) or visual area ($\chi^2(5)=7.120$, $p=.226$), and therefore sphericity could be assumed in the interpretation of the data. There was a significant effect of visual area ($F(3,15)=219.371$, $p<.001$), and eccentricity ($F(18,90)=429.780$, $p<.001$), but no effect of condition ($F(2,10)=3.412$, $p=.074$), on pRF sizes. However, as in Experiment 1, there was an interaction of condition with both visual area ($F(6,30)=3.585$, $p=.008$) and eccentricity ($F(36,180)=2.239$, $p<.001$), as well as the expected interaction between visual area and eccentricity (based on the independent scaling of pRF size with both eccentricity and visual area) ($F(54,270)=28.146$, $p<.001$). For this experiment there was no significant three-way interaction between condition, visual area and eccentricity ($F(108,540)=1.066$, $p=.322$).

As there is only data for a single dichromatic subject, there is far more variability in the data points (less linearity). However, for both luminance and S-cone conditions the same increase in pRF sizes can be seen across eccentricities and ascending visual areas. For the L-M condition, the model has been able to fit some data, although not for foveal eccentricities, and with very large standard deviations (further discussion on this is given in the following sections).

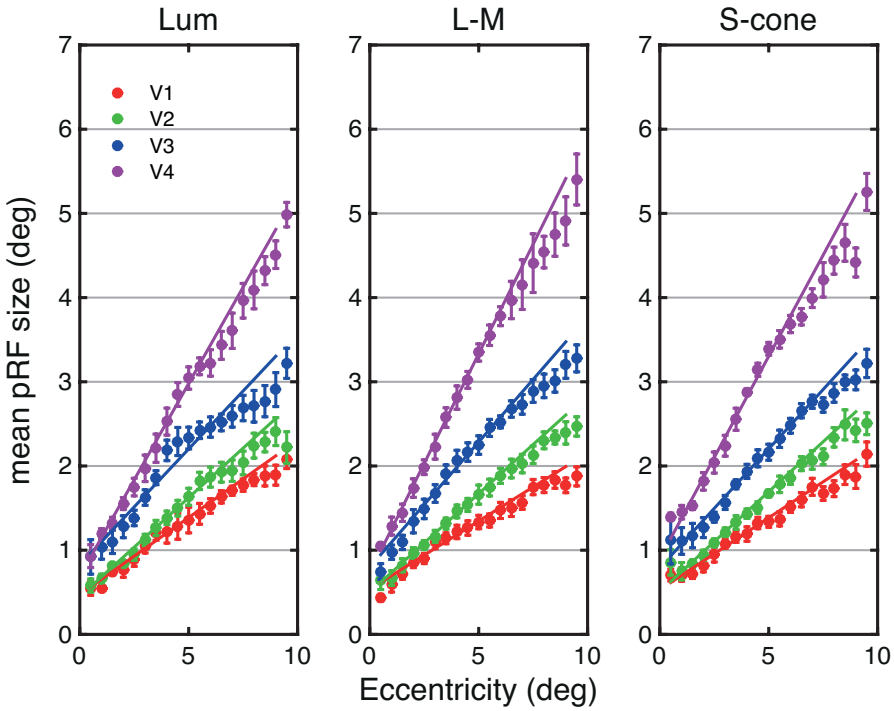

Figure 4.20 Trichromats data: pRF sizes plotted as a function of eccentricity for each visual area (V1-V4, shown on the legend) and each condition. Data are the mean values across trichromatic subjects, with standard error bars.

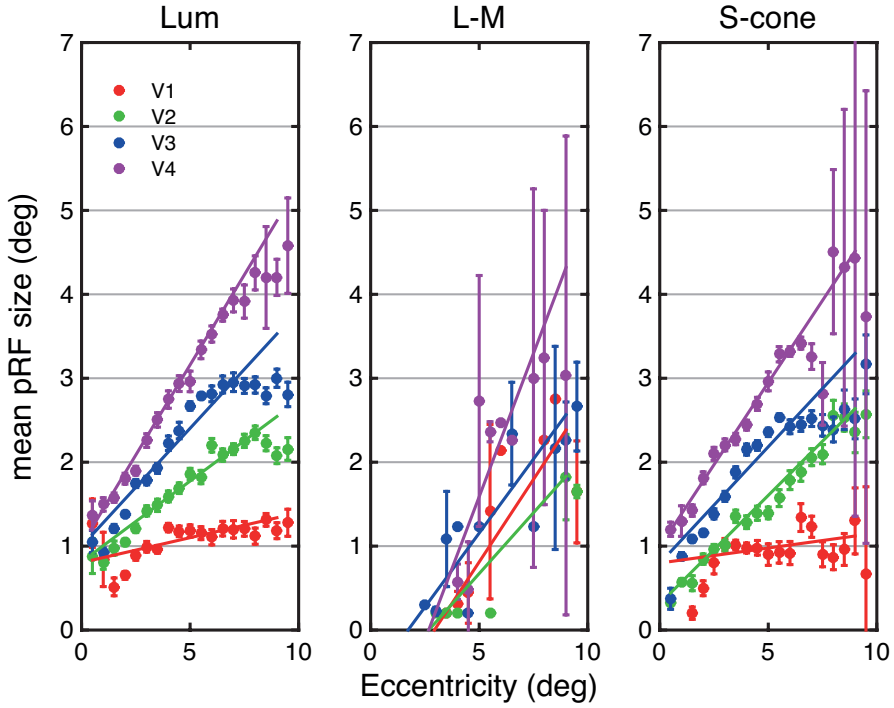

Figure 4.21 Dichromat subject data: pRF sizes for each visual area (V1-V4, see legend) are shown for each condition. Error bars represent the standard error of the mean for all voxels grouped at each eccentricity level, for the single dichromatic subject.

The pRF data were then split into two eccentricity groups for each visual area and condition for the trichromatic (Figure 4.22) and dichromatic (Figure 4.23) subjects – foveal (<2°) and peripheral (between 8° and 10°). The same repeated-measures ANOVA test was then carried out for the trichromatic data. Mauchly's test of Sphericity was not violated for the condition factor ($\chi^2(2)=5.528$, $p=.063$), or interactions between eccentricity and condition ($\chi^2(2)=3.657$, $p=.161$) and eccentricity and visual area ($\chi^2(5)=4.848$, $p=.448$), and as there were only two levels in the eccentricity factor, sphericity can be assumed for all of these factors. However, the test was violated for the visual areas factor ($\chi^2(5)=15.695$, $p=.010$) – suggesting unequal variance in the differences between each of the test pairings – and therefore a Greenhouse-Geisser correction was applied prior to the interpretation of the visual area factor and associated interactions where Mauchly's test could not be run (i.e. three-way interaction and the interaction with condition).

Significant effects were observed for the factors of eccentricity ($F(1,5)=2458.257$, $p<.001$), and visual area ($F(1.574,7.871)=107.981$, $p<.001$, Greenhouse-Geisser corrected). The interaction between visual area and eccentricity also remained significant ($F(3,15)=85.102$, $p<.001$). However, no significant effects were observed for the condition factor ($F(2,10)=2.37$, $p=.144$), or for any of the interactions with condition: condition and visual area ($F(2.580,12.899)=1.253$, $p=.327$, Greenhouse-Geisser corrected); condition and eccentricity ($F(2,10)=1.905$, $p=.199$); and the three-way interaction between all factors ($F(1.765,8.825)=1.675$, $p=.241$, Greenhouse-Geisser corrected).

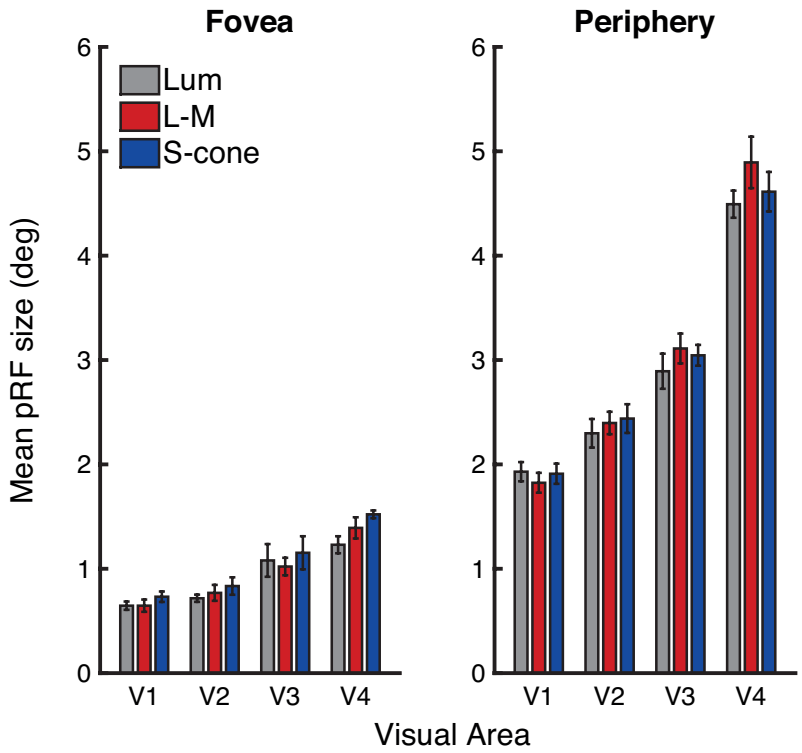

Figure 4.22 Trichromats data: Mean pRF sizes for trichromatic subjects, for each condition, with bars grouped by visual area. Plots are split by eccentricity: foveal (left) and peripheral (right). Error bars show the standard error of the mean.

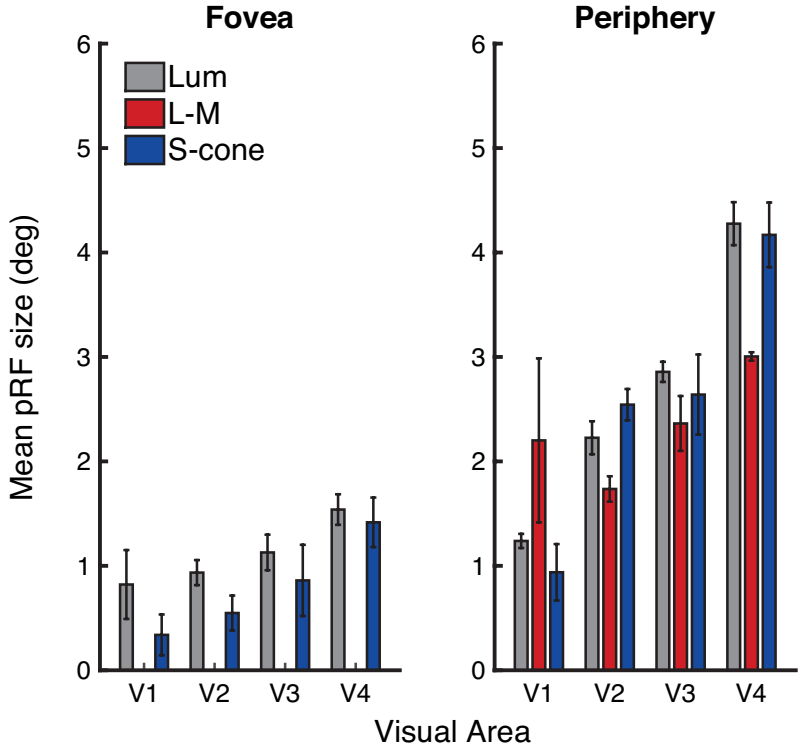

Figure 4.23 Dichromat data: Mean pRF sizes averaged across foveal and peripheral regions for each visual area and condition. Error bars show the standard error of the means. There were no foveal pRF sizes produced by the model for the L-M condition.

4.6.3.4 Variance Explained

The variance explained (%) by the model in each of the voxels that are included in the final pRF estimate (i.e. all that explained at least 10% variance) were averaged for each condition across visual areas for each subject and are shown in Figure 4.24 for the trichromat group and the dichromat subject.

Paired t-tests were carried out between each of the conditions for the trichromats and the dichromat separately; a Bonferroni corrected significance criterion of .0167 was used instead of .05. Comparisons made for the trichromat data are based on subject means across visual areas, whereas the dichromat data compares the values from each visual area between conditions. No significant differences were observed between the luminance and S-cone conditions for either the trichromats ($t(5)=-1.401$, $p=.220$) or the dichromat ($t(3)=-0.828$, $p=.469$). For the trichromats, the amount of variance explained in the L-M condition was significantly greater than the luminance ($t(5)=7.184$, $p=.001$) and S-cone ($t(5)=7.616$, $p=.001$) conditions. For the dichromat, the amount of variance explained in the L-M condition for each visual area was significantly lower than the luminance ($t(3)=-6.589$, $p=.007$) and S-cone ($t(3)=-8.287$, $p=.004$) conditions.

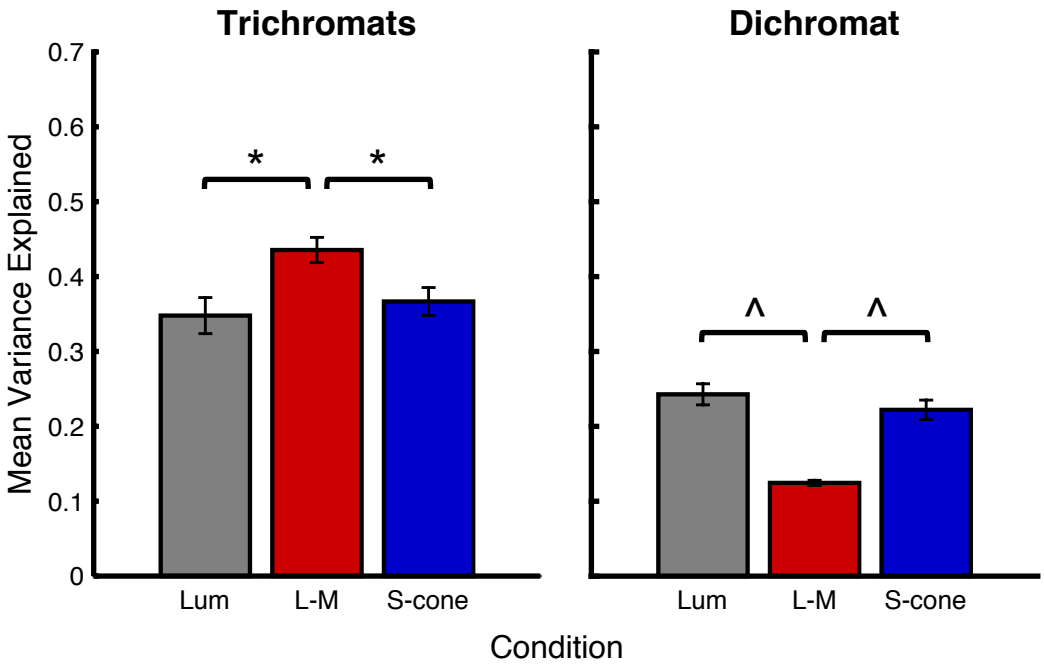

Figure 4.24 Mean variance explained across voxels in all visual areas for each condition. Shown for the trichromat group (left) and the dichromat subject (right). Significant results of paired t-tests are indicated: ^p<.05, *p<.01 (Bonferroni corrected). Results for trichromats are comparing subject means across visual areas in each condition. Results for the dichromat are comparing mean values for each visual area in each condition.

However, it should be noted that whilst the mean variance explained by the L-M condition in the dichromat appears relatively high for a condition that should be invisible to the subject, all voxels included in the average are ones that explained at least 10% of the variance – therefore *all* means would be over this value if the model could be fit to even one voxel for each condition. What is perhaps more relevant here is the total number of voxels that met this 10% variance criteria. Table 4.5 shows the total number of voxels across all visual areas (V1-V4) that met the 10% variance explained criteria for each condition – for the trichromats these are given as the mean across subjects with the standard deviation in parentheses. The relative proportion of voxels activated for each condition in each colour vision group are given in square

brackets as a percentage (note that these are not necessarily unique voxels in each condition).

Table 4.5 Total number of voxels across visual areas that explain at least 10% of the variance in the pRF model, for each condition. The mean values (with standard deviations) are provided for the trichromats. The relative proportion of voxels that met the 10% criteria for each condition is given in square brackets [%] – these are calculated within each group across conditions.

	Total number of voxels (across visual areas) that have >10% variance explained by the pRF model for each condition [Percentage of voxels for each condition out of group total]	
Condition	Trichromats Mean (std)	Dichromat
Luminance	7791 (1733) [31.3%]	8855 [54.4%]
L-M	8738 (1343) [35.1%]	198 [1.2%]
S-cone	8352 (1532) [33.6%]	7217 [44.4%]

4.6.3.5 Spatial frequency tuning – Behavioural experiment

The behavioural contrast detection thresholds were extracted using the same methods outlined in Chapter 3. For each condition all trials were combined from across the blocks. To ensure that the psychometric functions would be appropriately fitted in line with the log sampling of the target contrast levels, the levels were log transformed ($\log_{10}$(Contrast)) before using the Palamedes 'PAL_PFML_Fit' function to fit a logistic psychometric function to the data. As this was a 2AFC task, the probability correct level was 50%, and the level used for the threshold was 75% correct. Bootstrapping of 100 simulations of the data was done to estimate the standard error of the outputted threshold, this was done using the Palamedes 'PAL_PFML_BootstrapParametric' function, which required the same parameters as the PAL_PFML_Fit function, as well as the output from the fit of the data.

Five of the six trichromatic subjects that were used in the pRF experiment were tested in the spatial frequency tasks. The mean contrast detection

thresholds for each condition across these subjects are plotted as a function of spatial frequency in Figure 4.25, with separate plots shown for the 2° and 8° eccentricity conditions. These data show the anticipated low pass spatial resolution of the chromatic channels at both eccentricities, i.e. lower contrast thresholds at the lower spatial frequency. The band-pass resolution of the luminance channels is also demonstrated, with the lowest contrast thresholds shown for the middle spatial frequency level. The same data for the dichromat subject is shown in Figure 4.26 – note the absence of the L-M condition, which cannot be carried out by the dichromat because the isoluminant stimuli is not visible. The same low-pass resolution of the S-cone channel and the band-pass resolution of the luminance channel are shown for the dichromat.

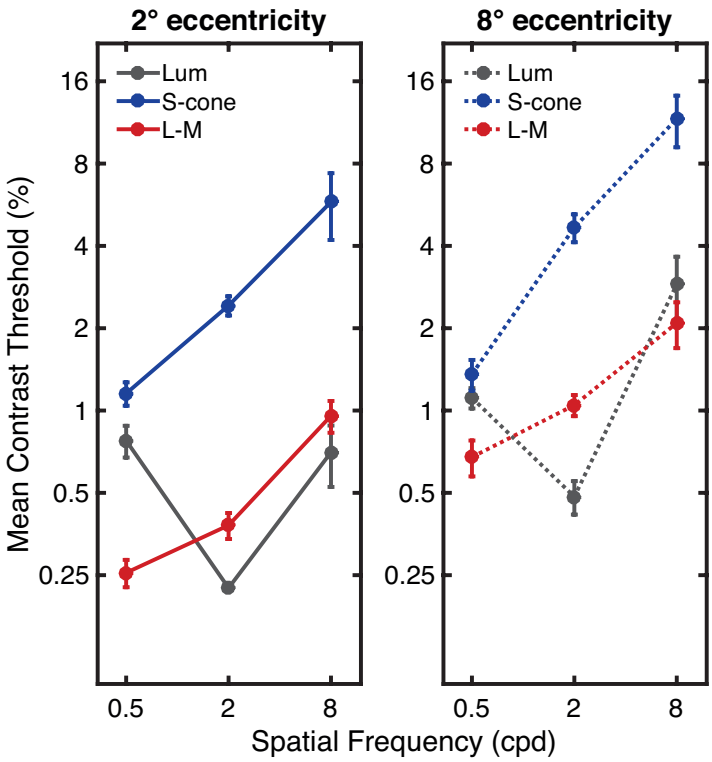

Figure 4.25 Trichromats data: Average contrast detection thresholds across trichromatic subjects for each condition (Luminance, S-cone, L-M) across spatial frequencies (both axes are log scaled). Each plot shows data from two eccentricities: 2° (left) and 8° visual angle (right). Error bars show the standard errors of the means.

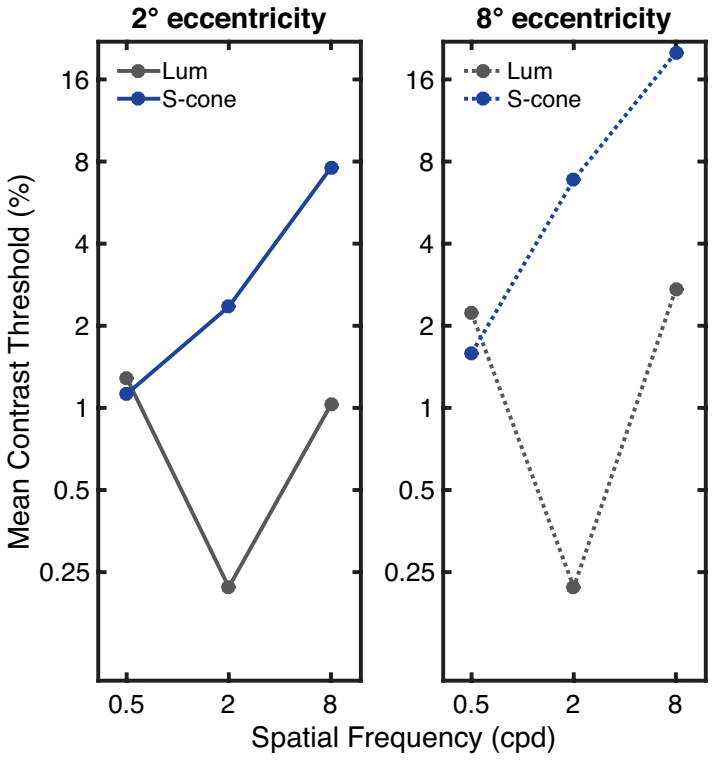

Figure 4.26 Dichromat data: Contrast detection thresholds for the dichromatic subject for each condition (Luminance, S-cone, L-M) across spatial frequencies (both axes are log scaled). Each plot shows data from the two eccentricities: 2° (left) and 8° visual angle (right).

4.6.3.6 Spatial frequency tuning – fMRI experiment

For each subject, all the scans from the spatial frequency experiment were processed using the same mrInit and alignment procedures that were described in the Methodology section to align the PD structural scan from the fMRI session to the detailed structural scans for that subject. The events in each scan were coded and paired with the onset times for each occurrence of the events; this information is inputted into a General Linear Model (GLM) analysis. The GLM uses all the trials for each event (with the blank condition event as the base level) to explain the BOLD time series from the fMRI scans, and determine how much each event contributes to the time series – this produces weighted beta values, which indicate the weighted level of activity to each of the events in the scans. The haemodynamic response function (HRF) used in the model was SPM's difference-of-gammas, which accounts for both positive and negative BOLD in the time course and therefore produces better estimates of activity for events in the GLM. The beta weights were extracted for each subject for each event, and group averages were produced for the same ROIs that were created and used in the pRF experiment. Data are plotted in Figure 4.27 for the mean trichromat data and Figure 4.28 for the dichromat data; averages are shown for each visual area and for foveal and peripheral regions of each visual area.

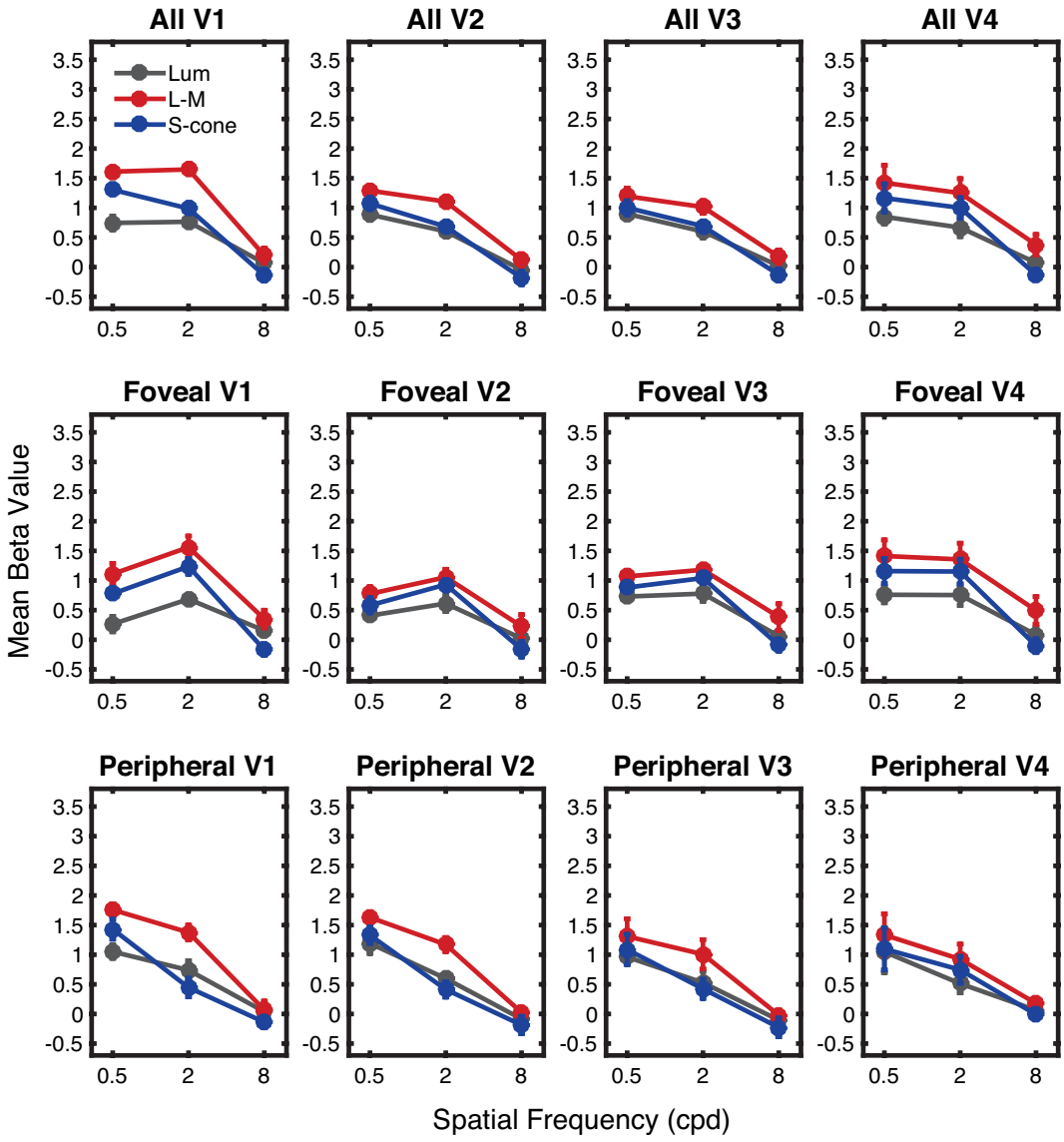

Figure 4.27 Trichromats Data: Mean beta values plotted as a function of spatial frequency for each condition. Each column shows the data from within visual areas V1-V4. Top, middle and bottom rows show averages across entire visual areas, foveal ROIs, and peripheral ROIs, respectively.

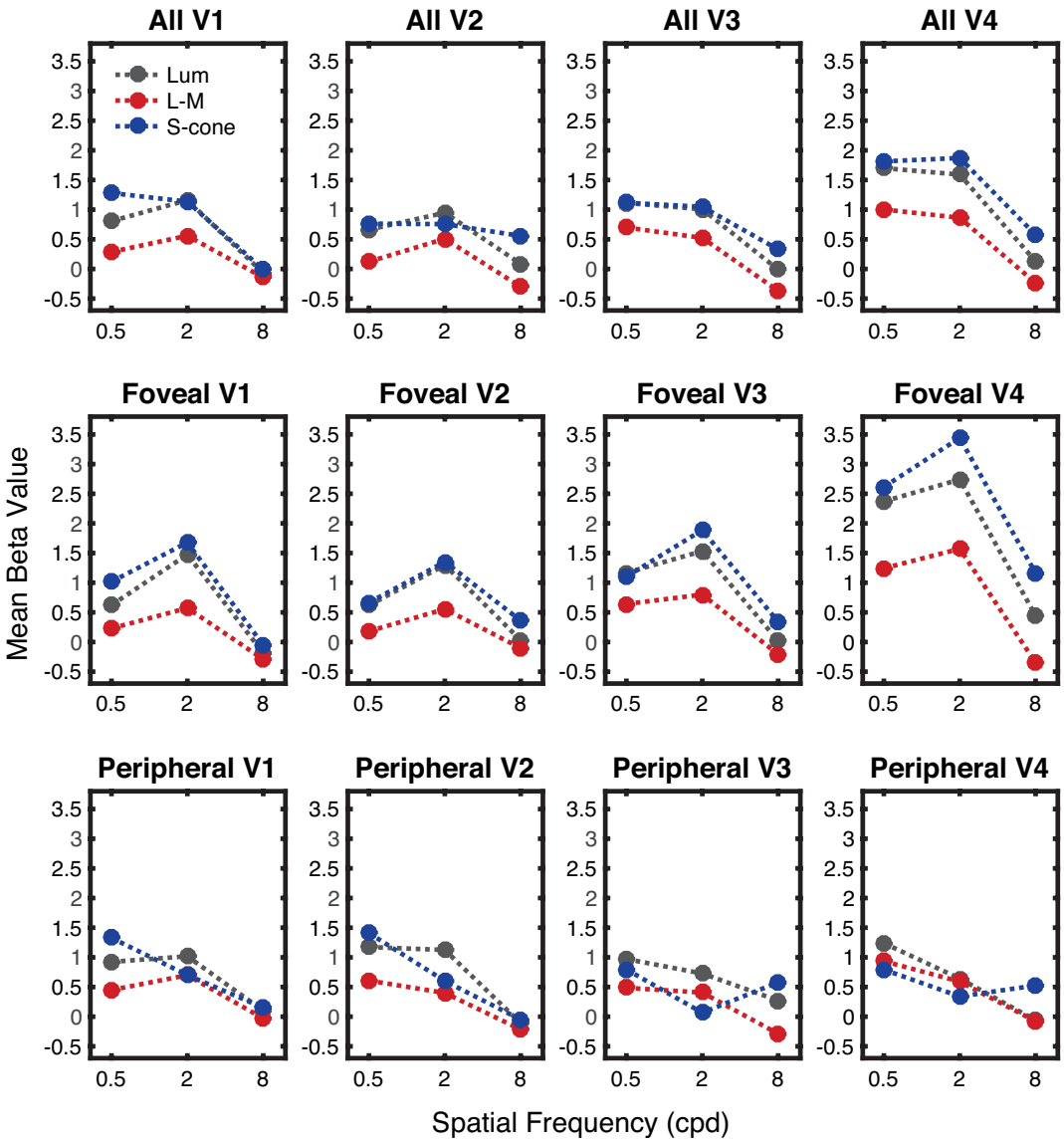

Figure 4.28 Dichromat Data: Mean beta values plotted as a function of spatial frequency for each condition. Each column shows the data from within visual areas V1-V4. Top, middle and bottom rows show averages across entire visual areas, foveal ROIs, and peripheral ROIs, respectively.

For the trichromatic subjects, the average beta values across foveal regions of each visual area show that all conditions produce a band-pass-type response to the spatial frequency stimuli, whereas in peripheral regions all produce low-pass-type responses. The dichromatic subject generally shows the same pattern of responses, however, there is a clearer difference between the luminance and S-cone conditions within V1 – the luminance condition shows a band-pass-type response across *both* foveal and peripheral regions. The L-

M condition has notably lower responses than the other conditions, and likely reflects activity from similar voxels that the pRF model could fit (although here the voxels are not reduced based on the amount of variance explained, unlike the pRF data).

For both the trichromats and the dichromat the responses to the 8 cpd spatial frequency are particularly low – possibly due to limitations in the stimulus display in the scanner, as will be discussed later. Therefore, to produce a more reliable estimate of 'spatial resolution', a spatial sensitivity index was calculated using only the 0.5 and 2 cpd conditions. To do this, the beta values were first normalised to the peak response out of these two spatial frequencies, within each condition and each eccentricity (for each subject), and then the difference between the 2 cpd and 0.5 cpd beta values was calculated for each condition in each visual area. Low, negative values indicate lower spatial frequency sensitivity, whereas higher, non-negative values indicate higher spatial frequency sensitivity. In line with the pRF data figures, these spatial sensitivity indices were plotted across visual areas for each eccentricity region – mean values for the trichromats are shown in Figure 4.29 and the dichromat data are shown in Figure 4.30. For foveal V1 in the trichromats (Figure 4.29), the luminance condition showed higher spatial sensitivity than the chromatic conditions, whereas in peripheral V1 the S-cone condition showed much lower spatial sensitivity than either the luminance or L-M conditions. This same pattern is shown for the dichromat (Figure 4.30) – the L-M data are not shown for this subject, as they do not actually represent an L-M pathway.

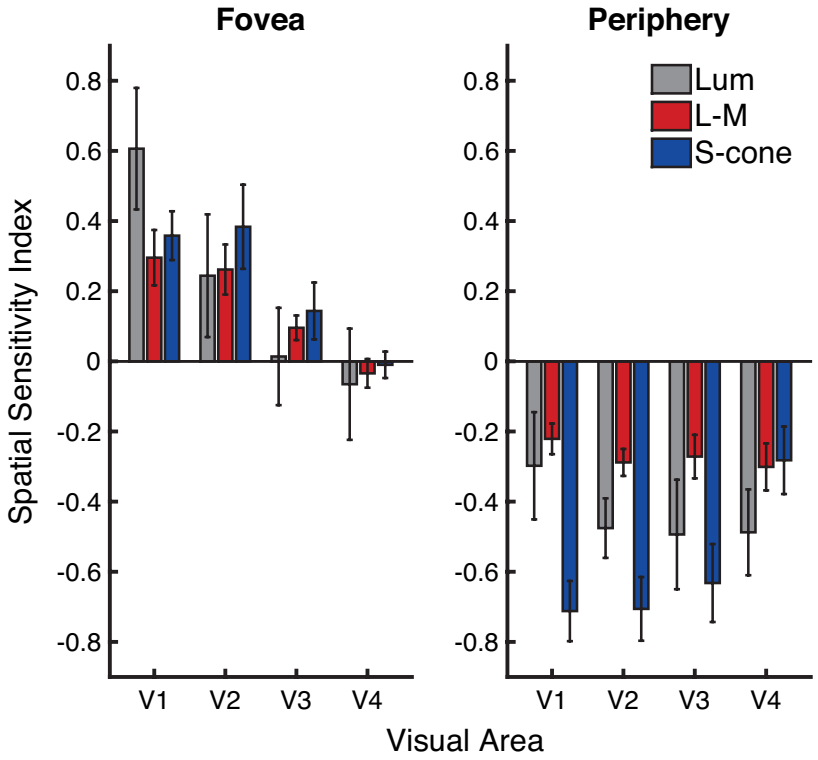

Figure 4.29 Trichromats Data: Mean spatial sensitivity index across trichromatic subjects, with error bars showing the standard error of the means. Values for each condition are shown across visual areas for foveal (left) and peripheral (right) eccentricity ROIs.

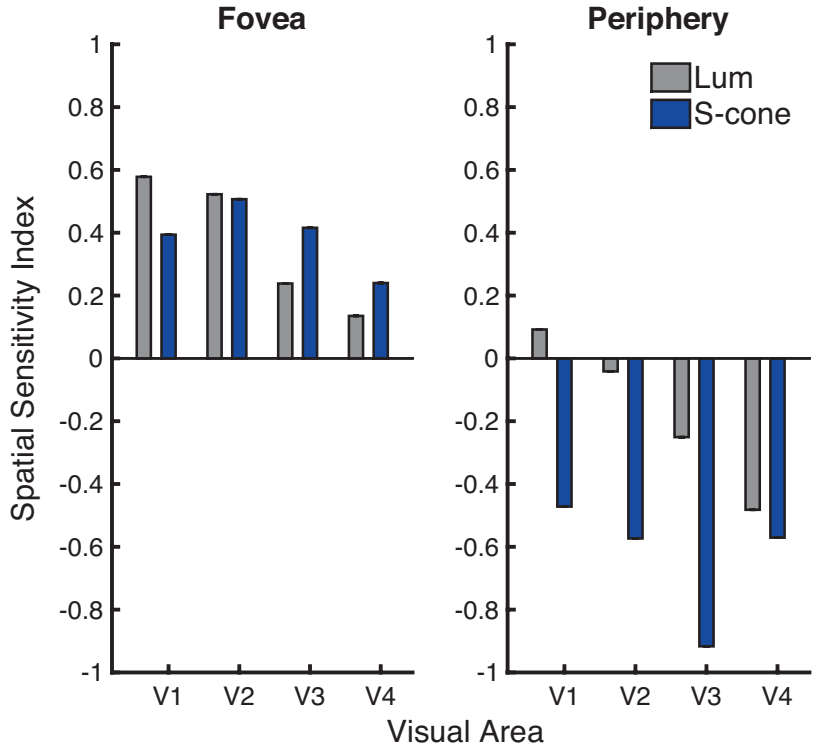

Figure 4.30 Dichromat Data: spatial sensitivity indices for the dichromat subject. Values for the luminance and S-cone conditions are shown across visual areas for foveal (left) and peripheral (right) eccentricity ROIs.

A repeated-measures ANOVA was carried out on the trichromat data using factors of visual area, eccentricity and condition, to determine any effect on the spatial sensitivity index values. Mauchly's test of Sphericity was not violated for most of the conditions or interactions (visual area ($\chi^2(5)=2.652$, $p=.767$), condition ($\chi^2(2)=2.966$, $p=.227$), eccentricity*condition ($\chi^2(2)=2.168$, $p=.338$)), with the exception of the interaction between eccentricity and visual area ($\chi^2(5)=12.243$, $p=.042$), therefore a Greenhouse-Geisser correction was applied to the results of this interaction. There was a significant effect of eccentricity ($F(1,4)=78.636$, $p=.001$), and visual area ($F(3,12)=11.110$, $p=.001$), but no significant effect of condition ($F(2,8)=0.655$, $p=.545$). However, all interactions were shown to be significant: eccentricity and visual area ($F(1.682,6.726)=8.375$, $p=.017$, Greenhouse-Geisser corrected), eccentricity and condition ($F(2,8)=4.682$, $p=.045$), condition and visual area ($F(6,24)=6.330$, $p<.001$), and between all factors ($F(6,24)=3.805$, $p=.008$). These significant interactions with condition support the visual observations made above for the differences in the data.

4.6.3.7 pRF sizes and spatial frequency tuning in V1

To provide a clear, final, comparison between the pRF sizes and spatial frequency tuning measures across the conditions, the data are re-plotted here just for visual area V1 to show to the differences between conditions across foveal and peripheral eccentricities (Figure 4.31). Mean pRF sizes for each condition overlap within both the foveal and peripheral eccentricities. Conversely, for the spatial sensitivity index values the luminance condition is shown to differ from both the chromatic conditions in the fovea, whereas in

the periphery the S-cone condition differs from the luminance and L-M conditions. Paired t-tests were carried out between the conditions within the peripheral eccentricity, and within the foveal eccentricity (i.e. six comparisons, reducing the significance criteria with Bonferroni correction to .008 instead of .05).

For the spatial sensitivity index values, the differences between the conditions in the fovea were not significant between any of the condition pairs, despite the trend for higher spatial sensitivities for the luminance condition (luminance and S-cone ($t(4)=1.155$, $p=.312$), luminance and L-M ($t(4)=1.535$, $p=.199$), and S-cone and L-M ($t(4)=0.986$, $p=.380$). There was also no significant difference between the L-M and luminance conditions in the periphery ($t(4)=0.642$, $p=.556$). However, in the periphery the S-cone condition did significantly differ from both the L-M condition ($t(4)=-8.002$, $p=.001$), and the luminance condition ($t(4)=-5.793$, $p=.004$). For the pRF sizes, there were no significant differences between any of the condition pairs at either the fovea or periphery.

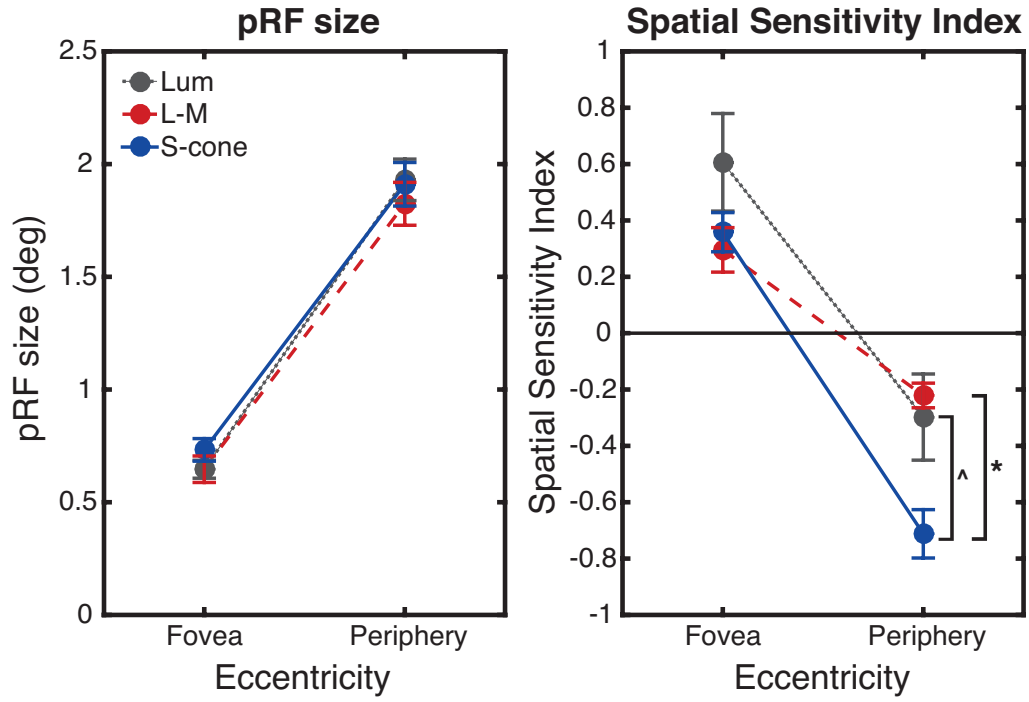

Figure 4.31 Data from V1: Mean pRF sizes (degrees) and spatial sensitivity index values are plotted as a function of eccentricity on the left and right, respectively. Data are shown for each condition, from visual area V1. Significant results of paired t-tests between the peripheral spatial sensitivity indices are indicated: ^p<.05 *p<.01 (Bonferroni corrected), see text for details.

4.6.4 Discussion of Experiment 2

4.6.4.1 Summary of the Data

Experiment 2 demonstrated a significant effect of visual area and eccentricity on pRF sizes; pRF sizes scaled with increasing eccentricity and ascending visual areas. There was no effect of condition (luminance, L-M and S-cone) on pRF sizes, and no significant interactions between condition and either visual area or eccentricity.

Behavioural spatial frequency data showed typical low-pass spatial resolution in the chromatic channels, and band-pass resolution for the luminance channel, for both 2° and 8° stimulus eccentricities – the actual thresholds changed across the two eccentricities, but the shape of the functions remained

the same. The fMRI estimates of 'spatial resolution' – which were calculated as spatial sensitivity index values from the difference between normalised responses (beta values) to the 2 cpd and 0.5 cpd spatial frequency stimuli – showed a change from high to low spatial sensitivity between foveal and peripheral eccentricities for all conditions. At face value, these findings appear to mirror the increase in pRF sizes with eccentricity (with smaller pRF sizes associated with high spatial sensitivity, and larger pRF sizes associated with low spatial sensitivity). However, the spatial sensitivity index values for the foveal and peripheral eccentricities were not equal for all conditions (unlike the pRF sizes), as demonstrated clearly for visual area V1 in Figure 4.31; significant differences were observed between the S-cone isolating condition and the L-M and luminance conditions for the peripheral eccentricity.

These data do not support the hypothesis that there would be a significant effect of condition on pRF sizes, which indicates that *cortical* pRF sizes are not coupled with spatial resolution differences for the chromatic and luminance pathways (which can be observed behaviourally). This is supported by the measurements of cortical spatial sensitivity for the same conditions, which did show a significant effect of condition on the spatial sensitivity index values; the S-cone condition had a significantly lower spatial sensitivity than either the luminance or the L-M condition for the peripheral eccentricity. This finding supports the hypothesis that the S-cone condition would show lower spatial sensitivity than either of the other conditions in the periphery. It was also hypothesised that the luminance condition would be less sensitive to low spatial frequencies in the fovea than the chromatic

conditions; there was a trend that supported this hypothesis, with the luminance condition showing a higher spatial sensitivity in the fovea than the chromatic conditions, however, the differences between the conditions were not significant.

4.6.4.2 Effect of narrower bars on pRF sizes

All conditions in Experiment 2 showed an average decrease in pRF size within the fovea compared to Experiment 1. The most likely explanation for this difference between the two experiments is the use of narrower bars, which may have allowed for smaller pRF estimates to be produced. These data are in line with pRF size differences demonstrated by Alvarez *et al* (2015) in their comparison of size invariant bars and logarithmically scaled bars – in the log-scaled stimulus the bars were narrower closer to the fovea, and produced smaller pRF sizes than the size invariant bars. The narrow bars in Experiment 2 may have therefore reduced any error in the foveal pRF estimates, strengthening the non-significant effect of condition on the pRF sizes – increased error in these estimates in Experiment 1 may account for the significant interactions that were found with condition for that experiment.

4.6.4.3 Behavioural and fMRI measures of spatial resolution

Behavioural contrast detection thresholds obtained across three spatial frequency stimuli for chromatic and luminance stimuli indicated low-pass spatial resolution of the chromatic pathways and band-pass resolution of the luminance pathway, for stimuli presented at both 2° and 8° eccentricities. These resolutions are in line with other behavioural studies of these pathways (e.g. Webster *et al* (1990)).

However, the spatial frequency experiments carried out in this chapter only used a small number of spatial frequency levels. This has the consequence that detailed contrast sensitivity functions and spatial frequency tuning curves cannot be obtained to give accurate measures spatial resolution. Therefore, for the fMRI experiment, the difference between normalised beta values for the 2 cpd and 0.5 cpd frequencies were used as a spatial sensitivity index. High, non-negative values indicated higher spatial sensitivity (2cpd>0.5cpd), whereas low, negative values indicated lower spatial sensitivity (2cpd<0.5cpd). However, this index does not help determine if the *actual* spatial frequency tuning is *between* the 0.5 and 2 cpd levels, or if it lies outside (or on) either of these values; so the index is primarily used to represent potential shifts in sensitivity, which can then be compared between conditions. Measuring intermediate levels of spatial frequency would have helped to clarify the peak of the spatial frequency tuning curves across conditions and eccentricities. However, for the purposes of this study (and owing to scan time constraints), the spatial sensitivity index is a useful indicator of any shift between eccentricities, or differences between conditions, even if the actual peak in spatial frequency tuning cannot be determined.

In contrast to the behavioural data, the fMRI measures of spatial sensitivity showed higher spatial sensitivity across *all* conditions within foveal eccentricities (<2°) and lower spatial sensitivity across *all* conditions for peripheral eccentricities (8-10°). This shift to lower spatial sensitivity with increasing eccentricity is consistent with other studies of cortical spatial frequency tuning in both achromatic and chromatic pathways (D'Souza et al.,

2016; Henriksson et al., 2008). There was a trend for higher spatial sensitivity in the luminance condition compared to the chromatic conditions within the fovea in V1, which is consistent with the behavioural measures of spatial resolution, however this difference was not significant. Within peripheral V1, the S-cone condition showed significantly lower spatial sensitivity values than the other conditions (i.e. responses to 0.5 cpd were higher than responses to 2 cpd). These findings reflect those of D'Souza *et al* (2016) – the authors showed S-cone responses decrease more rapidly at higher spatial frequencies as a function of eccentricity, compared to luminance and L-M conditions.

4.6.4.4 pRF sizes and spatial resolution

To better enable a comparison of pRF sizes and spatial sensitivity index values within each of the conditions – to test the hypothesis that pRF sizes would be coupled with spatial resolution – values from V1 in the fovea and periphery were plotted side by side for each measure (Figure 4.31). If pRF sizes were coupled with cortical measures of spatial sensitivity, the change across eccentricities and conditions should be equivalent between the two. Both pRF sizes and spatial resolution changed in a relatable manner between foveal and peripheral eccentricities – pRF sizes increased, and spatial sensitivity decreased. This relationship is in line with the findings of single-cell studies that showed low-pass spatial tuning was associated with larger receptive field centres (Cleland et al., 1979; Linsenmeier et al., 1982; Troy, 1983).

However, the change between eccentricities was not equivalent across conditions in each measure; there was no effect of condition on pRF sizes

while there was a significant effect on spatial resolution. pRF sizes did not differ between conditions across eccentricities, whereas for the spatial sensitivity index the S-cone condition differed significantly from the other two conditions in the periphery. The stimuli used for these experiments were matched in contrast, isoluminance values, and temporal frequency between the same conditions in each experiment. Therefore they, as closely as possible, targeted the same populations of neurons. Further to this, the same ROIs that were defined by and used in the pRF data were used in the spatial frequency data, i.e. the V1 comparison plot represents data from within the same voxels.

4.6.4.5 Limitations of the chromatic stimuli

The dichromat subject tested in these experiments not only provided an insight into how pRF sizes and measures of spatial resolution would compare in a colour-deficient observer, but this subject also acted as a control to indicate the degree of luminance noise that was present in the L-M chromatic condition. When carrying out the isoluminant minimum motion task for the L-M condition, the dichromat was unable to see the stimulus when it reached isoluminance. Therefore, if there were no luminance noise at any point in the pRF stimulus presentation, the pRF model would not have been able to produce any estimates of pRF size based on the data produced. It was shown that for a number of voxels the pRF model could explain at least 10% of the variance in the fMRI response (this was the criterion for including pRF size estimates in the analysis). However, no voxels in the fovea (<2°) met this criterion, and across all visual areas only 198 voxels produced pRF size estimates meeting this criterion for the L-M condition (compared to 8738 in

the trichromats for this condition, and a mean of 8036 across the other conditions for the dichromat). This indicates a very small level of luminance noise in the stimulus, which, if there were significant pRF size differences between the chromatic and luminance pathways, would be unlikely to affect the mean pRF sizes to the extent of showing no differences between the conditions.

Compared to Experiment 1, the trichromatic subjects were able to produce more reliable isoluminance settings for the L-M condition, and also gave consistent isoluminance settings for the S-cone stimulus. The level of luminance noise experienced by the trichromatic subjects for the chromatic conditions may therefore only be equivalent to the level of noise experienced by the dichromat in the L-M condition. As stated above, it seems unlikely that that degree of noise could have any overwhelming bias on the pRF sizes produced for these conditions.

To best minimise any luminance noise for chromatic stimuli in future experiments, it would be beneficial to carry out the minimum motion isoluminance task at various eccentricities. This would enable the stimulus to be altered as a function of eccentricity in the pRF experiment, and account for the effects of macular pigment on the isoluminance values in the fovea.

4.6.4.6 Dichromat case study

As discussed above, the dichromatic subject was a useful control for measuring luminance noise within the L-M condition in the pRF mapping, but further to that they gave an insight into pRF sizes and spatial sensitivity

differences between trichromats and dichromats. In general, the dichromat showed similar patterns of data as the trichromatic subjects, for both the pRF sizes and spatial sensitivity indices.

For a qualitative comparison between the trichromats and the dichromat for foveal and peripheral measures of pRF sizes and spatial sensitivity, the values are shown in Table 4.6 (pRF sizes) and Table 4.7 (spatial sensitivity) – however it is noted that differences between the colour vision groups cannot be tested statistically owing to the sample size of the single dichromat; therefore these measurements are provided primarily as a record of the actual values recorded in the dichromat compared to the means of the trichromats.

Table 4.6 Mean pRF sizes (with standard error) for each visual area in each condition, for foveal and peripheral eccentricities in Trichromats and the Dichromat. For the trichromats the means are across subjects for each visual area in each eccentricity group, with standard error of the means. Only the visual area mean is given for the Dichromat subject.

		Mean pRF size (standard error)			
		Fovea		Periphery	
Condition	Visual Area	Trichromats	Dichromat	Trichromats	Dichromat
Luminance	V1	0.65 (0.04)	0.82	1.93 (0.09)	1.24
	V2	0.72 (0.03)	0.94	2.30 (0.14)	2.23
	V3	1.08 (0.16)	1.13	2.89 (0.17)	2.86
	V4	1.23 (0.08)	1.54	4.49 (0.13)	4.28
L-M	V1	0.65 (0.06)	-	1.82 (0.10)	2.20
	V2	0.77 (0.08)	-	2.40 (0.11)	1.74
	V3	1.02 (0.08)	-	3.11 (0.14)	2.36
	V4	1.39 (0.10)	-	4.89 (0.25)	3.00
S-cone Isolating	V1	0.73 (0.05)	0.34	1.91 (0.10)	0.94
	V2	0.83 (0.08)	0.55	2.44 (0.14)	2.54
	V3	1.15 (0.16)	0.86	3.05 (0.10)	2.64
	V4	1.52 (0.04)	1.42	4.61 (0.19)	4.17

In general, the dichromat showed smaller pRF sizes for both the foveal and peripheral measures of the S-cone condition across visual areas. There are no

consistent qualitative differences between the groups for the luminance condition.

For the spatial sensitivity index, the dichromat showed higher spatial sensitivity in the fovea for both the S-cone and luminance condition across visual areas V2-V4 (whereas minimal differences were seen in V1). For the peripheral measures, the dichromat showed high spatial sensitivity for the luminance condition in V1 with a gradual decrease in spatial sensitivity with ascending visual area (trichromats show low spatial sensitivity across all visual areas).

Table 4.7 Mean spatial sensitivity index (with standard error) for each visual area in each condition, for foveal and peripheral eccentricities in Trichromats and the Dichromat. For the trichromats the means are across subjects for each visual, for the dichromat the mean value at each visual area is given (excluding the L-M condition).

		Mean Spatial Sensitivity Index (standard error)			
		Fovea		Periphery	
Condition	Visual Area	Trichromats	Dichromat	Trichromats	Dichromat
Luminance	V1	0.61 (0.17)	0.58	-0.30 (0.15)	0.09
	V2	0.24 (0.17)	0.52	-0.48 (0.08)	-0.04
	V3	0.01 (0.14)	0.24	-0.49 (0.16)	-0.25
	V4	-0.07 (0.16)	0.14	-0.49 (0.12)	-0.48
L-M	V1	0.30 (0.08)	-	-0.22 (0.04)	-
	V2	0.26 (0.07)	-	-0.29 (0.04)	-
	V3	0.10 (0.04)	-	-0.27 (0.06)	-
	V4	-0.03 (0.04)	-	-0.30 (0.07)	-
S-cone Isolating	V1	0.36 (0.07)	0.39	-0.71 (0.09)	-0.47
	V2	0.38 (0.12)	0.51	-0.71 (0.09)	-0.57
	V3	0.14 (0.08)	0.42	-0.63 (0.11)	-0.92
	V4	-0.01 (0.04)	0.24	-0.28 (0.10)	-0.57

As stated, it is not possible to draw conclusions regarding pRF size and spatial sensitivity differences between trichromats and dichromats from this data, without acquiring a larger sample of dichromatic individuals. However, this is the first dataset collected from a dichromatic subject on a chromatic pRF

mapping experiment, and it provides an invaluable control for the amount of potential luminance noise experienced by the trichromats in the chromatic conditions (as discussed in the previous section).

4.6.5 Conclusion

It was hypothesised that if cortical measures of spatial resolution (i.e. the spatial sensitivity index) were coupled with pRF sizes then there would be a significant increase in pRF sizes in the S-cone isolating condition compared to the luminance condition. This hypothesis was not supported by the data; there was no significant effect of condition on pRF sizes. Measurements of spatial sensitivity that were acquired from full-field spatial frequency stimuli, showed some similarities to the pRF data with regards to changing values across eccentricities, however, significant differences between conditions *were* found for the spatial frequency data.

When tested behaviourally, outside the scanner, the same subjects showed the anticipated resolutions for chromatic and luminance stimuli at both 2° and 8° eccentricities, i.e. low-pass spatial resolution for the chromatic stimuli and band-pass resolution for the luminance stimuli. However, in line with other studies measuring cortical spatial frequency tuning of both the chromatic and achromatic pathways (D'Souza et al., 2016), the fMRI measures of spatial sensitivity showed that all conditions had higher spatial sensitivity in the fovea, which decreased in the periphery. The S-cone pathway showed significantly lower spatial sensitivity in the periphery than the other conditions.

Data from a dichromatic subject indicated that the non significant effect of condition on pRF sizes is not simply due to over activating the luminance pathway with the chromatic stimuli – for the L-M condition, in the dichromat, very few voxels (1.2% of the all voxels across the three conditions) were fit by the pRF model (with more than 10% of the variance explained). Further to this, a comparison between pRF sizes and spatial sensitivity across the conditions in V1, showed that while no differences in pRF sizes were seen between the conditions, differences in spatial sensitivity were observed. These data suggest that differences between the pathways are detectable in the visual cortex, but that pRF sizes are not closely related to the spatial sensitivity differences between the pathways.

4.7 Further Discussion

A limiting factor in trying to couple behavioural psychophysical measurements with fMRI responses is the resolution of the technique. Identifying relationships between the responses produced in fMRI and those produced in a behavioural task, requires that the activity from crucial neuronal populations can be detected from averages across voxels (which could contain hundreds of thousands of neurons (Carlo & Stevens, 2013)), as well as from averages across ROIs. Further to this, behavioural responses are the product of a multitude of mechanisms (occurring at various points in both cortical and pre-cortical visual processing), and they are affected by a number of observer factors, not least the observer's attention to the task and stimulus (Pestilli, Ling, & Carrasco, 2009; Somers, Dale, Seiffert, & Tootell, 1999; Williford & Maunsell, 2006); Moran and Desimone (1985) were the first to show that the response of a neuron to a stimulus within its receptive field

varied dependent on whether the stimulus was being attended to (non-attended stimuli caused a decrease in neuronal response, whereas attended stimuli caused an increase, relative to normal passive viewing of the same stimulus).

Of primary importance for the experiments described here, was whether or not differences in the achromatic and chromatic pathways were detectable in early visual cortex. Specifically, whether differences in spatial sensitivity could be detected between the pathways. A number of studies have shown that these pathways are still distinguishable in early visual cortex (D'Souza et al., 2016; Mullen et al., 2007; Vanni et al., 2006), and the findings from the fMRI spatial frequency experiment reported here also show differences between the pathways. The fact that the same subjects did not show differences between the pathways for pRF sizes can therefore not be explained by the pathways not showing any cortical response differences to spatial stimuli.

It was shown here that measuring cortical responses to spatial frequency stimuli produced estimates of spatial sensitivity that did not directly reflect all behavioural observations. However, it remains possible to investigate whether the *cortical* measures of spatial sensitivity are coupled with pRF sizes, as both of these measures are determined by the same level of fMRI resolution, and using stimuli that share the same key parameters (e.g. contrast, isoluminance settings, temporal frequency); each measure would contain the same degree of information blurring and averaging as each other, over the same voxels. Therefore, the comparisons between the fMRI

measures of pRF sizes and spatial sensitivity are appropriate here, and provide an insight into how these two measures are related in regards to the fMRI signals they produce.

The studies by Henriksson *et al* (2008) and D'Souza *et al* (2016), described earlier, demonstrated that changes in spatial frequency tuning (to lower spatial frequencies) occurred in both achromatic and chromatic pathways as a function of eccentricity, with D'Souza *et al* also showing that responses to higher spatial frequencies decreased more rapidly with increasing eccentricity in the S-cone pathway compared to either the luminance or L-M pathways. The findings of the Experiments described in this Chapter are consistent with these studies; spatial sensitivity decreased with increasing eccentricity, and the S-cone spatial sensitivity was significantly lower than both luminance and L-M sensitivities at peripheral eccentricities in V1 – lower spatial sensitivity in the S-cone condition represents relatively lower responses to the higher (2 cpd) spatial frequency. The fact that there were no significant effects of condition (or interactions with condition) for the pRF sizes in the same set of subjects (using the same key stimulus parameters), suggests that differences observed between achromatic and chromatic pathways for spatial frequency tuning are not a product of – or directly related to – pRF sizes in the cortex.

4.8 Conclusions

The ultimate purpose of these experiments was to identify whether innate spatial resolution differences between the pre-cortical pathways could be identified in early visual cortex and whether pRF sizes were systematically

coupled with these pathway differences. fMRI pRF techniques were utilised to measure the pRF sizes in the achromatic and chromatic pathways.

The experiments carried out in this Chapter provide the first account of pRF mapping of the chromatic pathways using fMRI. It was found that pRF sizes do not differ between the pathways, and all conditions showed an increase in pRF sizes with both eccentricity and ascending visual area. Data from a dichromatic subject indicated that potential luminance noise in the chromatic conditions is likely to be very low, with only a very small number of voxels able to produce any estimate of pRF size in the L-M condition. This indicates that in the trichromats, the overwhelming majority of activity produced by the chromatic stimuli should reflect chromatic rather than luminance pathway activation.

Measures of spatial resolution collected behaviourally in the same subjects show the anticipated band-pass resolution of the luminance pathway, and low-pass resolution of the L-M and S-cone pathways. In agreement with other studies, it was found that fMRI measures of spatial resolution (reported here as a spatial sensitivity index) do not directly reflect the behavioural data, but do still show some significant differences between the conditions.

While cortical measures of spatial sensitivity and pRF sizes showed some similarities (they both change as a function of eccentricity), there was a disparity in how they vary between conditions; pRF sizes do not differ with condition, whereas spatial sensitivities do. The findings of these experiments

suggest that spatial resolution differences of the pre-cortical pathways are not coupled with cortical pRF sizes.

Chapter 5 Cone isolation using an LED system

5.1 Overview

Multi-channel LED stimuli have been used by a number of groups to isolate and record behavioural responses from single cone types or channels using the technique of 'silent substitution'. Multi-channel LED stimuli have some advantages over other display types, such as LCD monitors, as they have superior bit-depth, spectral purity, and temporal resolution. This enables more precise control over the stimuli, and consequently more reliable isolation of targeted cones. In principle, this should enable the isolation of an additional fourth cone type carried by some women (tetrachromats), which has a peak sensitivity in between the (already close) peaks of the L and M cones. As described in Chapter 1, tetrachromats are carriers for anomalous trichromacy, and have the capacity to express all three normal cone types, as well as the additional anomalous cone type, in the retina.

The aim of this Chapter was to develop and test a multi-channel LED system that would be capable of differentiating tetrachromatic from trichromatic individuals. The method of silent substitution and cone isolation are described, with discussion of other studies that have used such a system. The system that has been produced here is then described, along with the fundamentals of the programming scripts used to create and present the stimuli. Two experiments that track the development of the system are presented. The first experiment tests the principles of a system that accounts for three cone types (L, M, and S), which is tested on trichromatic and

dichromatic subjects. The second experiment shows a slightly modified system that can account for four photoreceptor types (L, L-prime, M and S cones). Modelling is used to demonstrate how well this stimulus might be able to isolate the 'L-prime' cone in a tetrachromatic individual. For a stimulus that accounts for four cone types, it is determined that accurate selection of the cone fundamentals for an observer (specifically, the location of the cone peaks) would be essential to successfully isolate the L-prime cone.

5.2 Background

5.2.1 Silent substitution and cone isolation

The method of silent substitution (Estévez & Spekreijse, 1982) concerns the process of eliciting a steady response from one (or more) specified cone types (e.g. L, M or S) – unwanted cone types are 'silenced'. As described below, silent substitution can be achieved by computing a transform matrix that governs the mapping of stimulus primaries (LEDs are used here) to cone activations, and then inverting this matrix to create a transform from an arbitrary cone space to a set of primary amplitudes. Modulations along single axes in the cone space can then be converted to modulations of the display primaries. A condition of this matrix inversion procedure is that the system must have at least as many primaries as there are individual photoreceptor classes.

Silent substitution allows for the measurement of various properties of individual cone types (such as contrast sensitivity as a function of temporal frequency), while assuming no input from the other, silenced, cones. Changes

in the stimulus that are detectable/perceptible by the isolated cone can be recorded behaviourally (e.g. using psychophysical tasks (Cao, Nicandro, & Barrionuevo, 2015)) and physiologically (e.g. with electroretinography (ERG) (Kremers & Pangeni, 2012)).

Creating a stimulus that uses the silent substitution and cone isolation method requires information on the spectral sensitivities of the cones present in the observer (e.g. L, M, and S), as well as the spectra of the primaries (e.g. the RGB guns in a monitor, or the LEDs in a multi-channel system). With this information, it is possible to calculate the output of each of the primaries (i.e. their relative brightness) necessary to simultaneously silence and isolate specific cones. First, the relation between the cone spectra and the primary spectra are determined by a matrix multiplication between the two spectra matrices (stimulus emission spectra x cone absorption spectra); the linear transformation matrix produced by this is a 'Primary to Cone' transform – this transform matrix can be multiplied by known primary output values to calculate how each cone type responds to that stimulus. Conversely, the inverse of the transformation matrix – the 'Cone to Primary' transform – can determine the output levels of the primaries needed for a specified cone response by multiplying the inverse transform matrix by the cone activations desired (e.g. for an S-cone isolating stimulus the inverse matrix is multiplied by [L, M, S] activation levels of [0, 0, 1]) (Estévez & Spekreijse, 1982). The output values for each primary can then be used to create a temporally modulated stimulus, which silences and/or isolates cones (as required and specified in the formula), and can be scaled to produce varying degrees of cone contrast.

For LED stimuli, the modulation of the LEDs is typically controlled using a Pulse Width Modulation (PWM) technique. PWM controls the brightness/dimming of each LED by rapidly adjusting the number of on and off periods across a single presentation (typically measured in ms) – the higher the percentage of 'on' periods, the brighter the LED (this percentage is the 'duty cycle'); many modern experiments make use of microcontrollers (e.g. Arduino) to control this modulation (Cao et al., 2015). Arduino programming enables a simple implementation of this technique – the duty cycle required for each LED is computed automatically, providing the on-board PWM hardware is initialised and used. The bit depth achievable using PWM on the Arduino Due (12 bits/channel) is sufficient to allow 4096 different amplitudes on each channel, and these values can modulate at a rate of 200Hz.

5.2.2 Use of multi-channel LED systems

Shapiro, Pokorny and Smith (1996) highlighted an important fact about the silent substitution method: in order to invert the cone activation matrix, the number of primaries (e.g. LEDs) needs to be equal or greater than the number of photoreceptors to be silenced/isolated. For instance, the four-primary system they proposed would enable isolation of rods while all three cone types (L, M, and S) were silenced. Therefore, an LED system with at least four (ideally more) primaries, rather than a three-primary RGB monitor, is necessary for producing a stimulus that could silence/isolate more than three photoreceptors, such as isolating the 4^{th} cone in a tetrachromatic subject (assuming experiments are run under photopic conditions to silence rods).

A number of studies have used multi-channel LED systems to isolate responses from cone photoreceptors as well as other cells (i.e. rods, retinal ganglion cells, penumbral cones). Kremers and Pangeni (2012) used a four-primary multi-channel LED system to perform a 'triple silent substitution' technique; their method accounted for the three cone types (L, M, and S) as well as rods, so any three of these photoreceptors could be simultaneously silenced while the fourth was isolated. The four LEDs used had peak spectral outputs ranging between 469nm to 638nm, with a half-bandwidth (at half-height of maximal output) ranging between ±8-19nm. The authors determined that these narrow bandwidths of the LEDs allowed for a good range of contrasts to be achieved for each photoreceptor. ERGs were recorded for each isolation condition (as well as opponent L-M and L+M conditions) across a range of temporal frequencies (between 2-60Hz) at fixed contrasts (L=19%, M=18%, S=71%, rods=33%, L+M=42%, L-M=9%). They were able to show differences in phase and amplitude responses between the conditions. For instance, they demonstrated that the L- and M-cone isolating stimuli produced low-pass temporal sensitivity patterns below 12Hz, and then show a second peak in responses at higher frequencies, in line with luminance pathway responses.

Cao *et al* (2015) aimed to isolate responses from the photopigment melanopsin, which is found in photosensitive retinal ganglion cells. In addition to accounting for the four photoreceptor types (L, M, and S cones, and rods), like Kremers and Pangeni (2012), they also required the spectral sensitivity function for melanopsin, giving a total of five 'sensors'. As previously described, an equal or greater number of primaries are necessary

for adequate silent substitution and isolation to occur; therefore a five-primary LED system was utilised by Cao *et al.* The peak spectral outputs of the LEDs ranged between 456nm and 632nm, with half-bandwidths between ±10-17nm. Contrast sensitivity was measured as a function of temporal frequency for melanopsin, S-cone and L+M (luminance) conditions, using a Yes/No staircase procedure. They were able to show differences in the temporal contrast sensitivity functions for each condition using the silent substitution method. S-cones showed a low-pass temporal resolution, while L+M (luminance) showed band-pass responses, and the melanopsin condition produced peak responses at low temporal frequencies with a gradual reduction in response up to the maximum available frequency that could be tested (see Chapter 6 for a discussion of these melanopsin findings).

The numbers of primaries used in these studies are equal to the number of sensors of interest (i.e. photoreceptors/photopigments). However, a study by Spitschan, Aguirre and Brainard (2015), which aimed to isolate responses from penumbral cones – cones that lie under (and are therefore shadowed by) blood vessels – used a total of 56 LEDs to produce the stimuli, using the same principles of silent substitution. This technique accounted for eight sensors (rods, melanopsin, and normal and penumbral L, M, and S cones). The increase in sensors does have an impact on the cone contrasts available; the maximum contrasts were smaller than those reported by Kremers and Pangeni (2012). For both the normal and penumbral variations of each cone, a maximum of 3-5% was available for L and M cones, and 20% for S cones, compared to 19%, 18% and 71% for L, M, and S cones, respectively, in the Kremers and Pangeni stimuli. A reduction in the maximum contrast that can

be produced for a given cone isolation may have some implications, for example, measuring ERG responses across a range of contrast levels. However, if the maximum contrast comfortably exceeds detection thresholds, this limitation does not affect measurements of contrast sensitivity in the specified photoreceptors.

Spitschan *et al* (2015) also produced estimates of the amount of 'contrast splatter' in their stimulus, which is a measure of the amount of contrast on the 'silenced' cones. To do this they calculated the effect of having discrepancies in the peak spectral sensitivities of the cones that are specified in the stimulus compared to those actually present in the observer, as well as effects of age (lens density). They found that contrast splatter did not exceed 1.23% (combined splatter across silenced cones) for any observer across any condition. In studies such as this, contrast splatter effectively adds a small amount of noise into the measurements (taken either behaviourally or physiologically). However, for the experiments that will be described in this Chapter, contrast splatter may present problems in distinguishing between the responses of trichromatic and tetrachromatic observers, as will be discussed shortly.

5.2.3 Tetrachromat photoreceptors

Tetrachromatic women are carriers for anomalous trichromacy; one of their X chromosomes carries genes for healthy L and M cones, while the other carries genes for one healthy cone type (e.g. a healthy M cone) and one anomalous cone type (e.g. an 'L-prime' cone with a shifted spectral sensitivity). As described in Chapter 1, a process of random X chromosome inactivation

determines which genes are expressed in any given cell, resulting in these women being able to express up to four cone types in the retina – the L, L-prime, and M cones, which are determined by this process, plus the S cone, which is determined by chromosome 7. The actual proportion of L, L-prime and M cones within the retina would be expected to vary greatly between tetrachromats, much in the same way that the proportion of L and M cones varies widely between trichromats (Carroll et al., 2002).

Jordan *et al* (2010) demonstrated that for a tetrachromat to produce behavioural responses that differ from a trichromat, it may be necessary (although not necessarily sufficient) for the peak spectral sensitivity of the fourth, L-prime, cone to be mid-way between the L and M cones. They found that an individual with well-spaced cone sensitivities produced the clearest demonstration of tetrachromacy; the peak sensitivity of the L-prime was positioned a roughly equal distance from the L and M cone peaks (as determined by a genetic analysis). However, they also showed that other women with this same spacing did not produce the same tetrachromatic responses, i.e. they were non-behavioural tetrachromats.

Utilising a method of silent substitution and cone isolation may enable the identification and further investigation of behavioural tetrachromats, however, the close proximity of the L, L-prime and M cone peaks may affect the available cone contrasts that can be produced by such a stimulus.

5.3 Aims and Hypotheses

The aim of this Chapter was to produce a portable, MRI-safe, multi-channel LED stimulus that would be capable of identifying tetrachromatic women using the method of silent substitution and cone isolation, as well as allowing the system to be easily transported outside of the lab. Such a stimulus would enable properties of the isolated cones to be measured behaviourally, in line with other studies that have employed these techniques (e.g. measuring temporal contrast sensitivity), as well as enabling functional MRI experiments to be carried out with the same stimuli.

While the method of silent substitution has been well used elsewhere, it has not been reported for use in this context. One of the challenges here is establishing a system that would allow the isolation of a fourth cone that corresponds very closely to the cones either side of it (in terms of peak spectral sensitivity). Further to this, if this device were to be used to *identify* tetrachromatic women, the stimulus needs to not only account for photoreceptors/sensors that *are* present in a trichromat (L, M, and S) but also one that is *not* present (the L-prime). Theoretically, a temporally modulated stimulus designed to isolate a cone that does not exist in a trichromatic observer should be invisible, i.e. contrast thresholds would be unattainable when attempting to isolate the L-prime in a trichromat. However, if the contrast 'splatter' on the silenced L and M cones is high while trying to isolate a non-existent L-prime, a detectable flicker may be produced.

Two experiments are described here. Experiment 1 describes the first version of a multi-channel LED system designed to test that the underlying principles of silent substitution can be successfully implemented – this experiment used a four-primary system, and measured RMS contrast detection thresholds (at 2Hz temporal frequency) of the opponent pathways (L-M, L+M+S, and S-cone isolating) in trichromatic and dichromatic observers. It was hypothesised that dichromatic subjects would not be able to detect the L-M stimulus, and that trichromatic subjects would show threshold differences between the chromatic and luminance pathway conditions, in line with known contrast resolution differences. A small subset of trichromats was also tested at several temporal frequencies to better determine whether the expected temporal contrast sensitivity functions are produced in each condition. It was hypothesised that a low-pass temporal resolution would be observed for the chromatic conditions, and a band-pass resolution would be seen for the luminance condition.

The second experiment used a five-primary system, and the equipment was upgraded to include an integrating sphere, to better merge the output of the LEDs. A single trichromatic subject was tested on the same conditions from Experiment 1 (L-M, L+M+S, and S-cone isolating), across the same range of temporal frequencies and also assuming the three normal cone types. It was hypothesised that temporal contrast sensitivity functions would reflect those identified elsewhere for opponent pathways (low-pass chromatic pathways, and band-pass luminance pathways). Stimuli were also produced that accounted for four cone types (L, L-prime, M, and S). It was hypothesised that the cone contrast available for an L-prime cone would be lower than for

either L or M cone isolating stimuli, but would be above estimated contrast detection thresholds. Modelling was carried out to determine the impact of inaccuracies in the cone spectra used to produce the stimuli, on the ability to isolate the L-prime cone. The size of discrepancy between the observer's actual cone sensitivity peaks, and those used to create the stimuli, was simulated to indicate what level of shift would produce a perceptible amount of contrast splatter on the L and M cones.

5.4 Methods

5.4.1 Equipment

The LED system used was a Prizmatix multi-channel light source (Prizmatix Ltd, Israel). This is a fibre-coupled system, which has separate outputs for each LED. The LED outputs are connected to branches of a fibre-optic cable; each branch is combined and merged down a 15m length of fibre-optic cable. Input to the LED system was via an Arduino microcontroller (BAC cables connected the Prizmatix box to the Arduino, which was wired to connect each LED input to a specified pin on the Arduino board). The Arduino was, in turn, connected via serial connection to an Apple Mac computer used to run the Arduino script (which controlled the LEDs) and Matlab (which created the stimulus values that were sent to the Arduino script).

In Experiment 1 an Arduino Mega board was used; this was upgraded to an Arduino Due in Experiment 2 – which improved the bit depth capabilities (from 8bit (256 levels) to 12bit (4096 levels)), allowing more control over the LEDs.

Owing to a technical fault, one of the five available LEDs on the Prizmatix system was unavailable for Experiment 1 (so only four LEDs could be used). This issue was resolved prior to Experiment 2, where all five LEDs were used.

To improve the merging of the LEDs, and to help reduce the overall brightness of the stimulus, Experiment 1 used three light shaping diffusers and 2 neutral density filters, positioned at approximately 1" intervals from the end of the fibre optic cable. The end of the fibre-optic cable was approximately 4mm in diameter, so this process also helped increase the overall available stimulus size by dispersing the light. In Experiment 2, an integrating sphere was acquired to produce a perfectly merged stimulus; the end of the fibre-optic cable was connected to the integrating sphere, and a single neutral density filter was placed over the exit point of the integrating sphere (approximately 1.5cm diameter). This filter served two functions, firstly, it prevented anything from entering the sphere and affecting the inner surface and integration of the light, and secondly, it provided a final diffusion of the light to control the brightness of the stimuli. In both cases an artificial aperture was used to control the final diameter of the stimulus, which allowed the visual angle of the stimulus to be set as desired (the distance of the subject was fixed with the use of a chin rest). All calibrations of the LEDs occurred from the observer viewpoint, i.e. after light had passed through diffusers/integrating sphere, to ensure stimuli were determined based on the end-point of the stimulus.

5.4.2 Design and creation of the stimulus

For all the experiments in this Chapter, the stimuli were created using the same basic principles of the silent substitution and cone isolation method described previously. This method determined the LED output values necessary to silence specific cones while other cones/opponent pathways were isolated; the final stimulus produced was a temporally modulated stimulus, which contained a visible flicker (at a specified frequency) when the contrast was above detection threshold. A 2-interval-forced-choice (2IFC) task was used to determine the contrast thresholds. One interval contained the target stimulus, modulated against a constant background light level, while the other interval contained only the background – both intervals had a small amount of noise added to the modulation amplitudes so that each interval onset showed some perceptual change relative to the background, this avoided the subject making judgements based on changes in the stimulus that were not specific to the target (the stimulus would briefly flash off in between each interval, but would then return to the background level between trials to maintain consistent adaptation to the background).

For each experiment, a transformation matrix was calculated between a set of cone fundamentals and the measured spectra of the LED primaries used (both resampled to a matching wavelength range); a schematic of the matrix multiplication used for the 'Primary to Cone' transform is shown below in Equation 1, and is referred to as the 'LED2Cone' matrix. L, M, and S refer to the cone type, and LED1 to nLED refers to the LED number. Cone sensitivities and LED intensity values for a specified range of wavelengths are

used in the multiplication – in the equation, λ_{min} is the value at the shortest wavelength, and λ_{max} is the value at the longest wavelength. The inverse of this transform matrix, i.e. 'Cone2LED', was calculated using the pseudo-inverse function ('pinv') in Matlab; the pseudo-inverse, rather than inverse, was used to allow unequal numbers of LEDs and cones. When the numbers of LEDs and cones are equal, 'pinv' and 'inv' functions generate the same result, but with more LEDs than cones, the solution is undetermined (many combinations of LEDs can produce the same set of cone modulations). In this case, 'pinv' provides a solution that minimises the output power summed over all primaries.

$$LED2Cone = \begin{pmatrix} L_{\lambda min} & \cdots & \cdots & L_{\lambda max} \\ M_{\lambda min} & \cdots & \cdots & M_{\lambda max} \\ S_{\lambda min} & \cdots & \cdots & S_{\lambda max} \end{pmatrix} \times \begin{pmatrix} LED1_{\lambda min} & \cdots & nLED_{\lambda min} \\ \vdots & \vdots & \vdots \\ \vdots & \vdots & \vdots \\ LED1_{\lambda max} & \cdots & nLED_{\lambda max} \end{pmatrix}$$

Equation 1 Equation for calculating the LED-to-Cone matrix.

The spectra of the LEDs were measured using a fibre-optic photospectrometer ("Jaz", Ocean Optics, FL) – itself calibrated to a NIST-traceable standard. Measurements were taken after the light had passed through the delivery display (specific details of the delivery display are provided in each experiment), with the LEDs turned on at maximum output individually for each measurement. The Stockman and Sharpe (2000) L, M, and S cone fundamentals were used as standard sensor primaries (downloaded from www.cvrl.org). These spectra were downloaded in 0.1nm step format, and then resampled to fit wavelengths from 390nm to 720nm in 1nm steps. This same sampling was also used for the LED spectra, as the wavelength range

and step size must be identical in each matrix in order to do the matrix multiplication.

The transform matrix, 'Cone2LED', was used to compute the LED values needed for the specified cone isolation/silencing, by multiplying the transform by a vector that specified the activity of each cone, e.g. an L cone isolation, with M and S cones silenced, would be specified with [L, M, S] values of [1, 0, 0]. This vector was first scaled to account for the background LED output (set at half the intensity available for each LED), and then the resulting LED values were scaled to achieve the desired contrast – checks were put in place to determine maximum contrasts available, to ensure the contrast level never exceeded that value in the 2IFC tasks. All calculations associated with the generation of these values - and trials for the 2IFC tasks - were performed within Matlab; once the necessary LED values were generated for the current condition trial this information was sent via a USB serial connection to an Arduino, which produced the sine-wave modulation for the LEDs.

The departmental Ethics Committee at The University of York granted approval for these experiments.

5.5 Experiment 1: Developing the LED equipment

5.5.1 Introduction and hypotheses

This Experiment aimed to test the principles of the silent substitution method on the newly acquired equipment, by accounting for only L, M, and S cones. This experiment used a four-primary system, and measured contrast detection

thresholds of the opponent pathways (L-M, L+M+S, and S-cone isolating) in trichromatic and dichromatic observers. It was hypothesised that dichromatic subjects would not be able to detect the L-M stimulus (and would therefore not be able to produce reliable thresholds), and that trichromatic subjects would show threshold differences between the chromatic and luminance pathway conditions, in line with known contrast resolution differences. A 2Hz temporal frequency stimulus was used, and at this frequency the sensitivity of the chromatic channels would still be high (but decreasing from the peak), while that of the luminance channel would still be low (but increasing towards the peak), therefore luminance sensitivity would be predicted to be lower than the chromatic sensitivity.

Two trichromats were also tested at five log-sampled temporal frequencies (2, 4, 8, 16 and 32Hz) to better determine whether the expected temporal contrast sensitivity functions are produced in each condition. It was hypothesised that low-pass temporal sensitivity profiles would be observed for the chromatic conditions, and a band-pass response would be seen for the luminance condition.

5.5.2 Method

5.5.2.1 Subjects

A total of 15 subjects were used in this Experiment: four male dichromats with a mean age 21.75 (± 2.22) years, and 11 trichromats (8 female, 3 male) with a mean age of 21.09 (± 2.02) years. Colour vision type was determined using Ishihara plates, Rayleigh matches, and a red-to-green colour match, using the same testing procedure and classification criteria as described in Chapter 3.

5.5.2.2 *Equipment Calibration*

The calibration of the four LEDs used in this experiment, as described in the Methods section, identified the maximal spectral output ± the half-bandwidth (at half-height) for each LED: LED1=414.70 ± 7.72nm, LED2=461.90 ± 12.38nm, LED3=531.70 ± 20.32nm, LED4=636.60 ± 6.98nm. The spectra of each of the LEDs are plotted in Figure 5.1. The Stockman and Sharpe (2000) cone fundamentals that were used are plotted in Figure 5.2. The calibration occurred at the point of the observer, i.e. after the light had passed through the stimulus display.

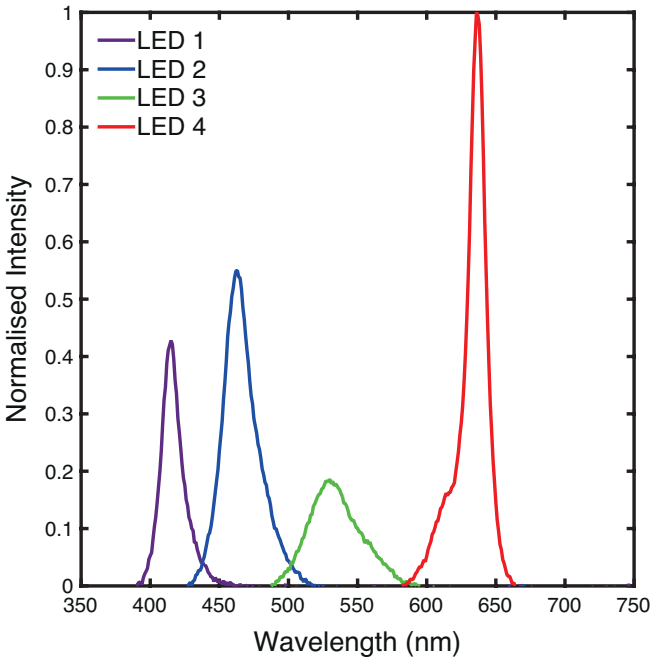

Figure 5.1 Spectral distributions of the LEDs used in Experiment 1, with normalised intensity values.

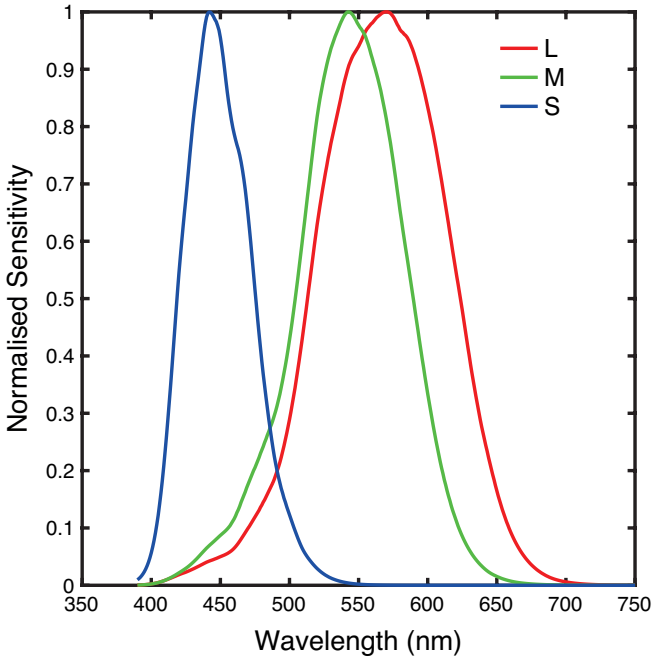

Figure 5.2 L, M, and S cone fundamentals, from Stockman and Sharpe (2000) (downloaded from www.cvrl.org), plotted with normalised sensitivity values.

5.5.2.3 Design

A 2IFC procedure was used to present the stimuli, with each interval lasting 1 second, and the inter-stimulus-interval (ISI) lasting 0.5 seconds. The start of each interval was cued by an audible beep. Feedback was given to the subject responses in the form of a high-pitched tone for correct responses, and a low-pitched tone for incorrect responses. This experiment was self-paced, so the next trial began once a response had been given. A flicker detection task was used to determine the contrast thresholds for subjects across each condition. Subjects pressed '1' or '2' on a keypad to indicate which interval (the first or second) contained the target; subjects were told to guess if they could not detect the target in either interval. The target flickered at 2Hz for the majority of the subjects, with the exception of the two trichromats who were presented with the stimulus at various spatial frequencies (2, 4, 8, 16 and 32Hz). The conditions tested were luminance (L+M+S), L-M, and S-cone isolating, using

the following [L, M, S] directions in the stimulus: luminance=[1, 1, 1], L-M=[0.5, -1, 0], S-cone=[0, 0, 1]. The maximum contrast level tested for each condition was capped at 5% for L-M, 20% for luminance and 45% for S-cone isolating.

The contrast levels used for the trials were selected from a log-sampled range using the Quest toolbox (distributed as part of Psychtoolbox for Matlab), the functions in this toolbox select contrast levels based on previous responses to estimate observer threshold levels (set at 82% for this Experiment). Three runs of each condition were carried out. Within each, 50 trials were carried out using the Quest toolbox to test across a range of contrast levels and produce an estimate of the observer's threshold. The three threshold estimates produced were then averaged together and used as the contrast detection threshold value for that condition. An exclusion criterion was put in place to exclude any threshold estimate from the three repeats that differed greatly from the other estimates (e.g. due to poor attention for that particular block); the standard deviation was calculated from the three values, and if any of the threshold estimates were more than one and a half standard deviations away from the median value, that value was not included in the final average.

Subjects were positioned at a fixed distance from the stimuli with a chin rest, which could be adjusted in height so that the stimulus was best aligned with the subjects' eyes. The aperture size and the subject's viewing distance resulted in a circular stimulus that subtended 1.2° visual angle.

The presentation of each stimulus interval contained a small amount of temporal noise, which was randomly added to the sine wave (for each LED modulation) within the Arduino script. This noise added a subtle 'white noise' type flicker to both intervals, which did not disguise the clear modulation of the target (when the contrast was at a detectable level).

5.5.2.4 Procedure

All subjects were first tested on the colour vision tasks (Ishihara plates, Rayleigh matches and red-to-green colour matches). Only subjects that met the criteria for trichromacy or dichromacy were used in the experiment – for the purpose of this study only trichromats and dichromats (not anomalous trichromats) were needed to test the success of the stimulus design. These diagnostic criteria are set out in detail in Chapter 3, but in brief, trichromats made no more than 2 errors on the Ishihara plates, were unable to make a match on the red-to-green colour match, and produced Rayleigh matches with small match ranges and mid-points consistent with a larger database of subjects. Dichromats made at least 6 errors on the Ishihara plates, had large Rayleigh match ranges, with abnormal mid-points, and were able to match the stimuli in the red-to-green task.

All testing took place in a dark lab, with subjects dark-adapting for approximately 5 minutes before the first task was carried out. Subjects carried out one run of each condition in a randomised order before moving on to the next run. One run of a condition took a maximum of four minutes to complete, and subjects were encouraged to take breaks between each run as required. For the two trichromats that carried out additional conditions at

different temporal frequencies, the runs were carried out over two sessions (at least one run of each condition was carried out within each session).

5.5.3 Results

5.5.3.1 Contrast Sensitivity and Thresholds

The contrast detection thresholds were converted into contrast sensitivity values (1/threshold) for each subject. Threshold values that exceeded the maximum contrast level for that condition indicated that an accurate threshold could not be obtained – in these cases the threshold values were set to the maximum contrast value tested for that condition; once converted into contrast sensitivity, these are the lowest contrast sensitivity values. Temporal contrast sensitivity functions are plotted in Figure 5.3 for the two trichromats (T1 and T2) that carried out the task across multiple temporal frequencies – the mean values across temporal frequencies for the two subjects are shown with the dotted yellow line. For both subjects the L-M condition shows a low-pass temporal resolution, and the luminance condition shows a band-pass resolution. However, for the S-cone condition one subject shows the predicted low-pass resolution, while the other shows a more band-pass response.

The averaged data for all the trichromats (including T1 and T2) and dichromats at the 2Hz temporal frequency are also plotted on Figure 5.3. The groups showed the same mean contrast sensitivity for the S-cone condition (mean sensitivity = 0.12), and the dichromats show poor sensitivity in the L-M condition, as predicted; three of the dichromats did not produce thresholds, so the values were arbitrarily set to the maximum contrast level tested, and

one dichromat was able to produce a threshold, but the sensitivity (sensitivity=0.52) was poorer than all other trichromat values. The dichromats also showed poorer contrast sensitivity than the trichromats for the luminance condition at 2Hz. However, an independent t-test between the two groups shows that the difference in sensitivity values was not significant ($t(13)=1.574$, $p=.140$). For this condition, one dichromat and two trichromats had their threshold values set to the maximum contrast level (as thresholds were not obtained for these subjects); even with these subjects removed, the t-test continued to show a non-significant difference ($t(10)=1.664$, $p=.127$).

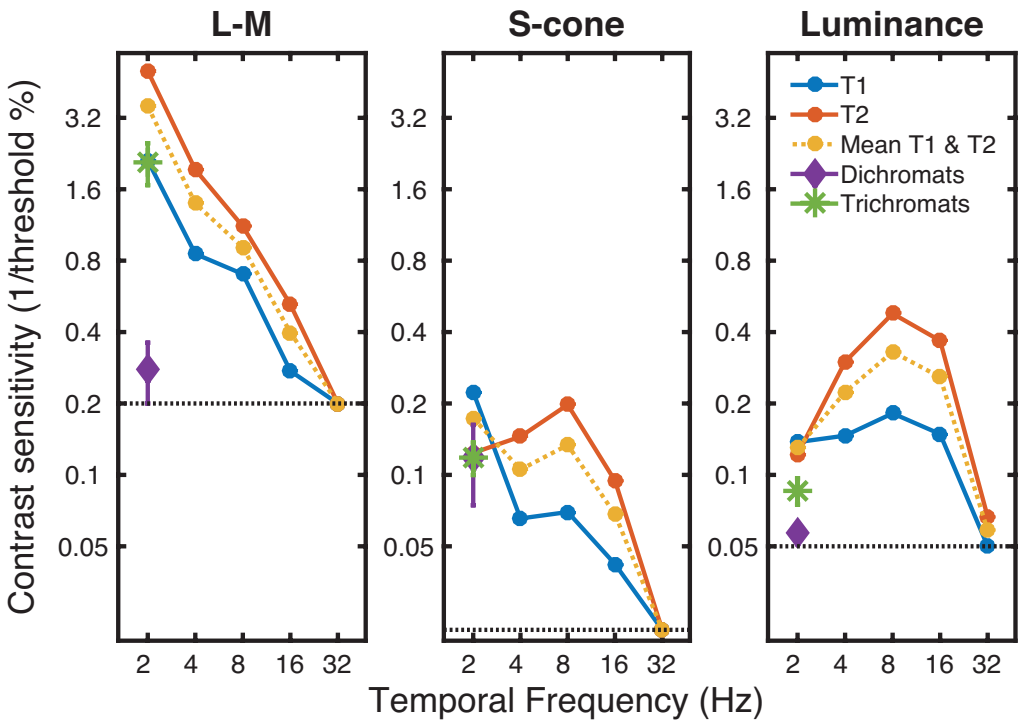

Figure 5.3 Data plotted in contrast sensitivity (1/threshold %) as a function of temporal frequency, for each condition: L-M (left), S-cone (middle), and Luminance (right). Black dotted lines indicate the maximum contrast level tested for each condition (the default value if no threshold could be obtained). Mean contrast sensitivities are plotted with standard error bars for the trichromats (green asterisk) and dichromats (purple diamond) for the 2Hz frequency.

5.5.4 Discussion

5.5.4.1 Overview of Results

The contrast sensitivity measurements taken for the trichromatic and dichromatic subjects showed no differences in the mean values for the S-cone condition, and no significant differences for the luminance condition – despite a trend for poorer contrast sensitivity values for the dichromats. In addition, three of the four dichromats were unable to produce thresholds for the L-M condition. These data support the hypotheses, and demonstrate that the stimulus is able to successfully target the L, M, and S cones (and their integrations into opponent pathway stimuli). Further to this, the temporal contrast sensitivity functions acquired for two trichromats supported the hypothesis that the L-M condition would show low-pass temporal resolution, and the luminance condition would show band-pass temporal resolution. However, the data were mixed for the S-cone condition, with one subject showing low-pass resolution and the other a more band-pass resolution, perhaps indicating that the stimulus was not fully optimised.

5.5.4.2 Limitations

In general, the data gathered from the various stimulus conditions demonstrated good evidence of cone isolation and silent substitution, however, there were some exceptions. One of the two trichromatic subjects did not produce low-pass temporal resolution responses for the S-cone isolating condition, indicating some luminance activation in the stimulus for this subject, and one of the four dichromats was able to produce a threshold

for the L-M task – although it is noted that the contrast sensitivity value fell below all of the trichromatic subject values.

One possibility is that the LEDs were not perfectly merged – despite travelling down several meters of fibre-optic cable and passing through three diffuser screens. This could, potentially, have resulted in some inhomogeneity across the stimulus field, which would, in turn, have generated stimuli that were not properly 'silenced'.

Another possibility is that the cone fundamentals used were not perfectly matched to the peak spectral sensitivities of all the subjects. There is some variation in the exact peak of photoreceptor sensitivities between individuals (within the ranges of normal trichromatic colour vision), which is also affected by differences in pre-receptoral filters (lens and macular pigment density) (Stockman & Sharpe, 2000). The further away the peak is from the actual cone peaks for an individual, the worse the silent substitution/cone isolation of those cones would be.

5.5.5 Conclusion

This experiment produced a good demonstration of the silent substitution method, with temporal contrast sensitivity functions that were, for the most part, in line with predictions. Similarly, the differences (and similarities) between trichromatic and dichromatic subjects across the conditions also indicated that opponent pathways were successfully targeted. However, there may be some limitations in the stimulus design that could account for some anomalies in the data. In order to allow a 4^{th} (L-prime) cone to be isolated

with this stimulus, it is important to minimise these anomalies. Therefore, an integrating sphere is used in Experiment 2 to ensure the LED stimuli is perfectly merged and homogenised.

5.6 Experiment 2: Accounting for a 4th cone

5.6.1 Introduction and hypotheses

In this experiment five LED primaries were used. A single subject carried out the same conditions as in Experiment 1, with the same set of L, M, and S cone fundamentals specified. In line with the hypotheses and data from Experiment 1, the S-cone isolating and L-M conditions were predicted to show low-pass temporal resolutions, and the luminance condition was predicted to show a band-pass resolution.

Stimuli were then generated using four cone fundamentals (L, L-prime, M and S); the L-prime spectrum was interpolated as the mid point between the L and M fundamentals. It was hypothesised that when accounting for four cones the maximum cone contrasts available in cone isolation cases would be much lower (on the L, L-prime, and M cones) than when accounting for just the normal L, M, and S cones. In addition, the available contrast for the L-prime was expected to be lower than either the L or M cones, given the close proximity of these cone spectra at each side of the L-prime. To predict how successful the isolation of an L-prime cone could be, the amount of contrast 'splatter' on the silenced cones was estimated. Further estimates of cone contrast levels were then made to model the effect of an observer possessing different cone fundamentals from those that were used to create the stimuli.

These estimates were used to predict the necessary accuracy in the observer's cone fundamentals for successful isolation of the L-prime.

5.6.2 Methods

5.6.2.1 Subjects

One female subject was used in this experiment (28 years). This subject was confirmed to be trichromatic using the Ishihara plates and Rayleigh matches, and is an experienced psychophysical observer.

5.6.2.2 Equipment

As described in the Chapter Methods sections, an integrating sphere was used in this experiment instead of the light shaping diffusers, to produce a perfectly merged LED stimulus. The calibration of the five LEDs used in this experiment occurred from the point of the observer (after passing through the integrating sphere), and identified the maximal spectral output ± the half-bandwidth (at half-height) for each LED: LED1=414.70 ± 7.93nm, LED2=463.80 ± 12.43nm, LED3=503.80 ± 15.70nm, LED4=531.00 ± 20.77nm, LED5=638.30 ± 6.90nm. The spectra of each of the LEDs are plotted in Figure 5.4.

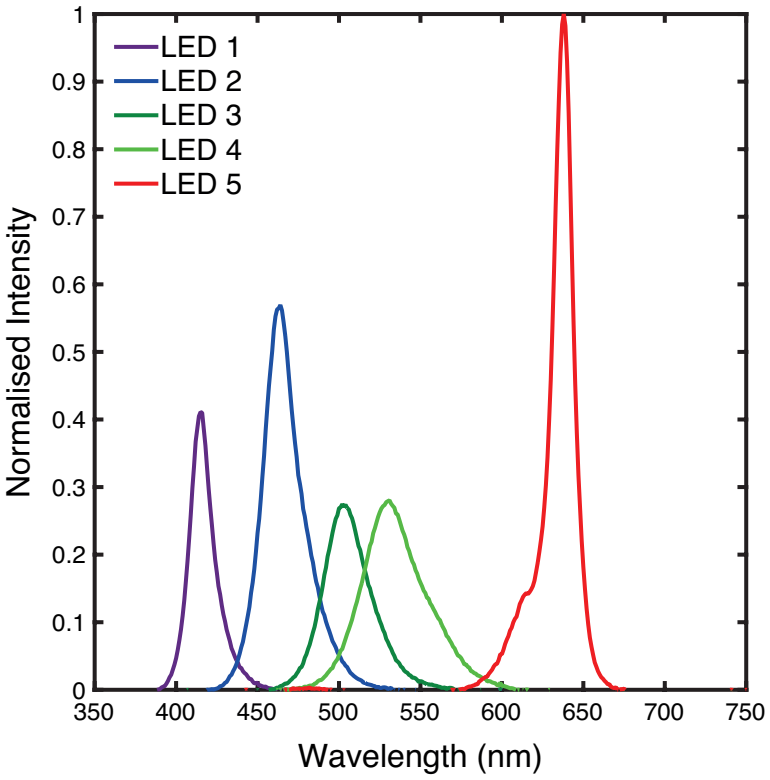

Figure 5.4 Spectral distributions of the LEDs used in Experiment 2, with normalised intensity values.

5.6.2.3 Design

All of the tasks in this experiment were performed in a similar manner to those in Experiment 1; a 2IFC task was used, with auditory beeps to signal the onset of each interval and feedback for the responses. The visual angle of the stimulus was approximately 0.8°, and the Quest Bayesian staircase procedure was used to produce threshold estimates; the test contrast for a subsequent trial is calculated from previous trial contrasts and responses. The conditions were each carried out four times so that average threshold values could be calculated.

There were five temporal frequency conditions (2, 4, 8, 16, and 32Hz) for the following conditions: S-cone, L-M, and L+M+S (luminance). As in Experiment 1, for these conditions the stimulus was created by

silencing/isolating across *three* cones (L, M, and S), using the following [L, M, S] directions in the stimulus: luminance=[1, 1, 1], L-M=[0.5, -1, 0], S-cone=[0, 0, 1].

5.6.2.4 Procedure

Four repeats of each condition were performed. The subject carried out each condition repeat within a block, i.e. five temporal frequencies for each of the three conditions. Conditions were presented in a randomised order in each block. Each condition lasted approximately 3.5 minutes; breaks were taken between conditions as required, and a longer break was taken between each repeat block.

5.6.3 Results

The average contrast detection threshold for each condition was calculated and converted into contrast sensitivity (1/threshold); the contrast sensitivity data are plotted in Figure 5.5.

For the luminance condition the peak contrast sensitivity was at 8Hz and sensitivity decreased at higher and lower frequencies, which supports the hypothesis for this condition. For both the L-M and S-cone conditions the highest sensitivity was at the lowest temporal frequency (2Hz), as predicted, however, the decrease in sensitivity with increasing frequency was extremely gradual in both cases. It was particularly surprising that there was still relatively high sensitivity at the 16Hz level. However, it is reassuring that neither of these chromatic conditions could produce a thresholds at 32Hz (the values for this level are arbitrarily plotted at the maximum contrast level tested in the Figure as no threshold could be obtained).

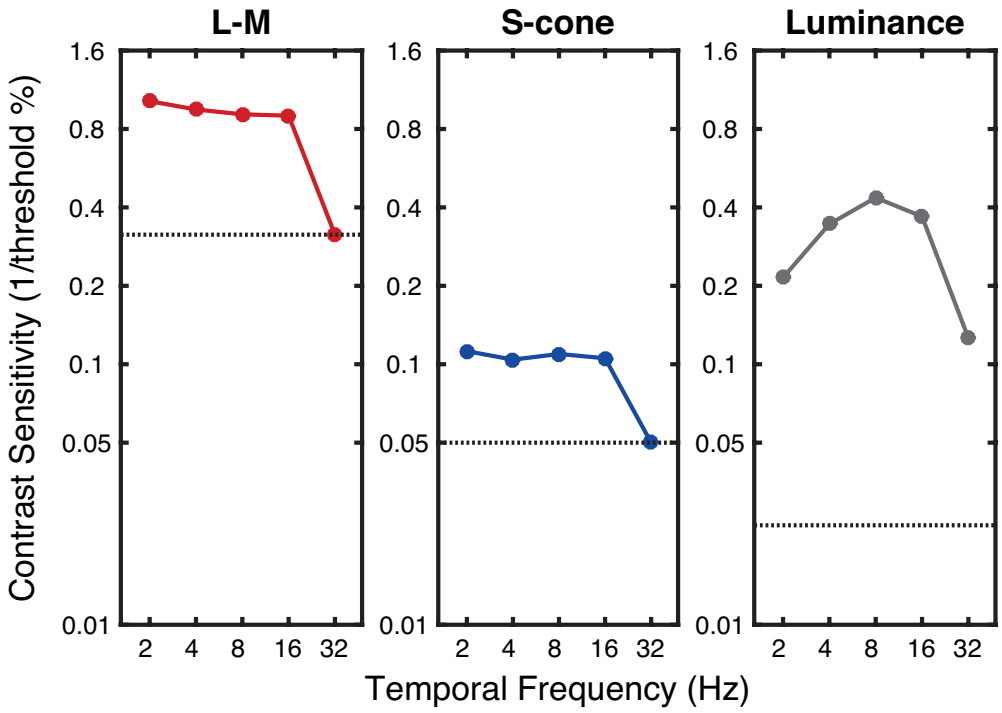

Figure 5.5 Data from the single subject plotted in contrast sensitivity (1/threshold %) as a function of temporal frequency (Hz) for three conditions: L-M (left), S-cone isolating (middle), and luminance L+M+S (right). Black dotted lines indicate the maximum contrast level tested for each condition – this is the default value if no threshold could be obtained, and therefore points lying on the line represent conditions that could not be perceived by the observer.

5.6.4 Modelling the L-prime cone

To produce a stimulus that would account for four cones (L, L-prime, M, and S), a spectrum for the L-prime cone had to be created. It was assumed that the wavelength corresponding to the L-prime peak sensitivity (λ_{max}) was in between the L and M λ_{max} values, and so an interpolation between the L and M spectra was carried out to produce the L-prime spectrum. The Stockman and Sharpe (2000) cone fundamentals were used, and are plotted in Figure 5.6, with the L-prime curve shown by the dotted orange line.

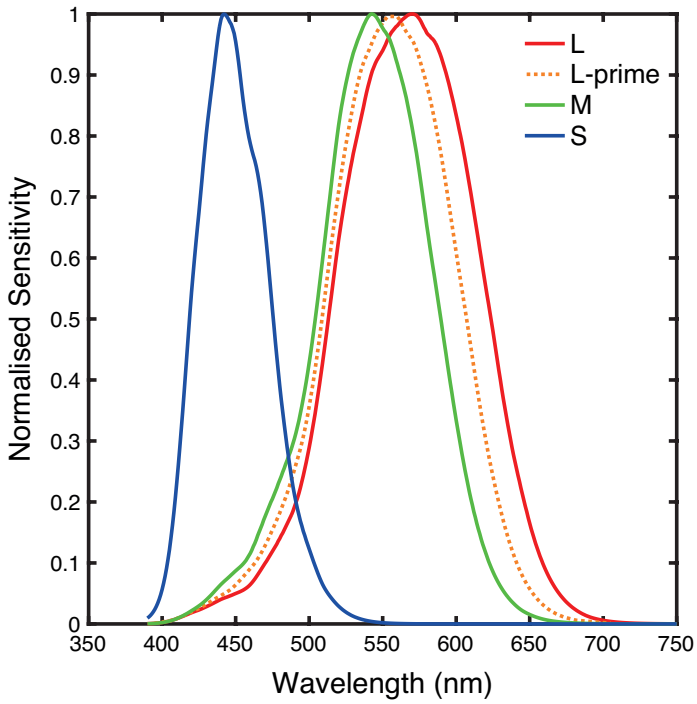

Figure 5.6 Spectral sensitivities for L, L-prime, M and S cones, plotted with normalised sensitivity values. The L, M, and S cone fundamentals are from Stockman and Sharpe (2000) (downloaded from www.cvrl.org), and the L-prime spectra is interpolated from the L and M spectra, with a peak at 556.5nm. The cone peaks for the L, M, and S cones are 570nm, 543nm and 442nm, respectively.

LED modulations were calculated for the four cone isolation conditions using the same procedure as for the three cone spectra stimulus – the only change was to the number of cone spectra used in the calculations. The modulations for the maximum available cone contrast in each condition are shown in Figure 5.7B; modulations are shown as a percentage of the maximum range of LED intensity around a background LED modulation (the zero line), the background LED intensity spectrum is shown in Figure 5.7A.

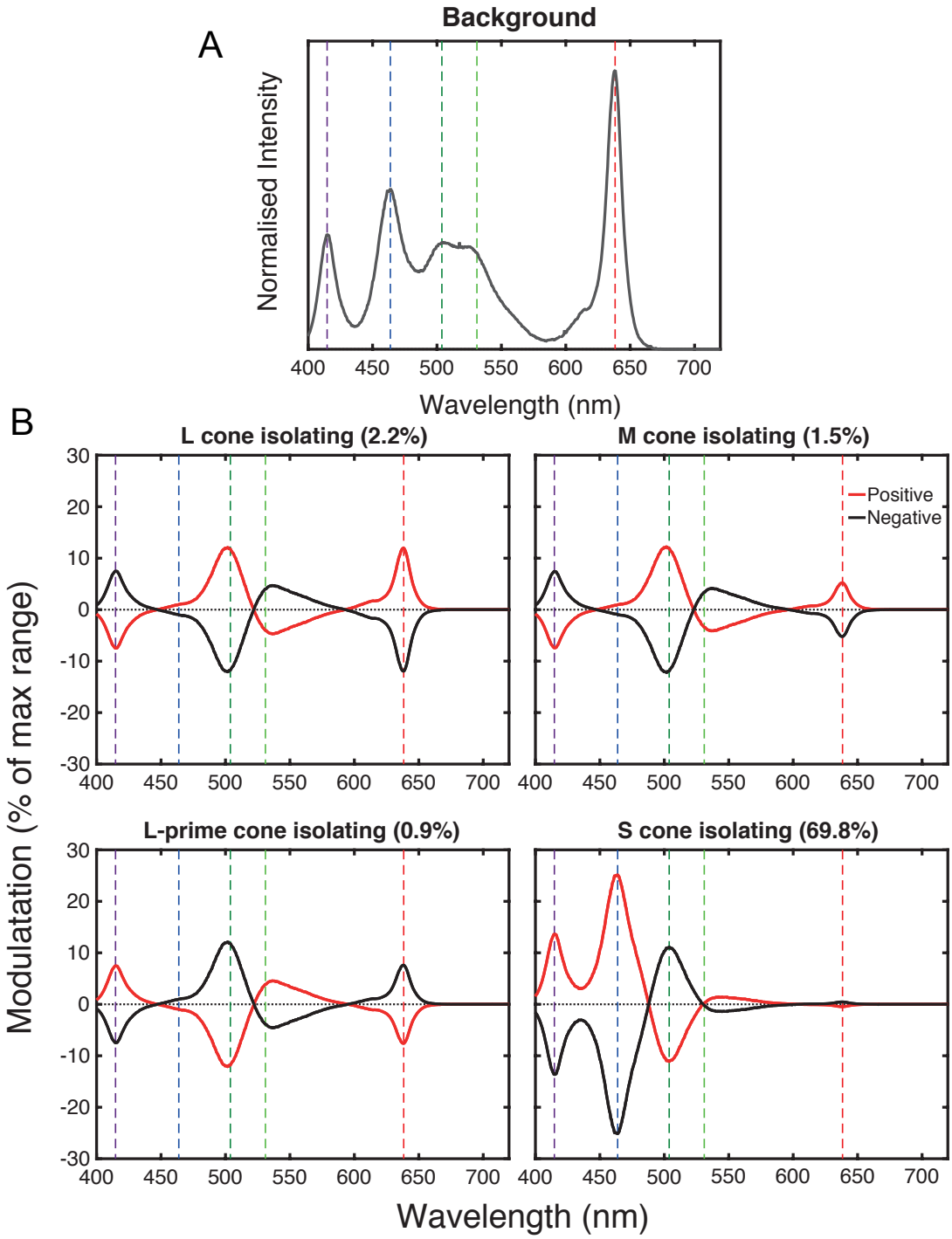

Figure 5.7 LED stimulus modulations, for (A) the background LED level (plotted as normalised intensity), and (B) for the cone isolating conditions, which modulate around the background (the zero line). LED intensities modulate between the positive (red) and negative (black) modulations (plotted as a % of the maximum range). Vertical dashed lines indicate the wavelength peaks of each of the LEDs.

As hypothesised, the maximum cone contrast available for the L-prime (0.9%) was lower than for either the L (2.2%) or M (1.5%) cones. Further to this, each of these maximum contrasts is relatively low because of the close proximity of

these three cone spectra. It can be assumed that successful isolation of any of these cones would be reliant on accurate silencing of the remaining cones. Any error in the assumed λ_{max} of the silenced cones could produce a degree of contrast 'splatter' on these cones, and ultimately affect how successful the cone isolation is. For instance, a trichromatic subject should not be able to perceive an L-prime stimulus, however, if the amount of contrast splatter on the silenced L or M cones reaches perceptible levels, the L-prime stimulus will be visible. Here, estimates of contrast splatter were produced for different levels of shift in the λ_{max} for each cone. The ability to isolate the L-prime cone is of primary interest, and so all modelling described below is focused on this condition.

First, cone excitations were calculated for the L-prime isolating condition (at its maximum available contrast of 0.9%), using cone spectra that matched those used to generate the stimulus; these will be referred to as the 'original' cone excitations. For each cone the excitation value was calculated by multiplying the cone spectra by the LED modulation and summing the output; the difference between the excitation value produced for the final stimulus (i.e. background + stimulus modulation) and the value produced for the background alone was used to reflect the actual cone excitation level relative to the steady background (see Equation 2).

$$Excitation_C = \Sigma\left(Spectra_C \times Mod_{FinalStim}\right) - \Sigma\left(Spectra_C \times Mod_{Background}\right)$$

Equation 2 Calculation for producing cone excitation values ($Excitation_C$), from the cone spectra ($Spectra_C$) and the LED modulations of the background ($Mod_{Background}$) and the final stimulus containing background plus stimulus modulation ($Mod_{FinalStim}$).

The cone excitations were transformed into cone contrasts by normalising all values against the isolated cone excitation value, i.e. the original L-prime excitation, and then multiplying each normalised value by the known cone contrast level (0.9).

In a situation where the observer's cone spectra match those used to produce the stimulus, this process calculates that the amount of contrast on the silenced cones is negligible: L=-0.008, M=-0.010, and S=0.000. Therefore, the maximum 0.9% contrast on the L-prime is possible without producing a perceptible response from the silenced cones.

To measure the effect of shifted λ_{max} values on these estimates of cone contrast (the contrast 'splatter'), the same process as above is repeated but instead of using the original cone spectra, a shifted spectrum is used (with the shift ranging between ±2nm). For this, the entire column of cone sensitivity values was adjusted relative to the corresponding wavelengths by the specified amount, e.g. 1nm, by adding or removing rows from the start/end of the column (depending on whether the shift was positive or negative relative to the original λ_{max}). This method of adjustment was used because it ensures that the shape of the fundamentals remains the same between those used to create the stimulus and those in the observer simulation, with only the λ_{max} shifting. An alternative method would be to use a Matlab function that can create cone spectra from a specified peak (e.g. 'StockmanSharpeNomogram'). However, this would create an additional adjustment variable – other than the cone peak – of spectra shape, which may result in an over-estimation of

contrast splatter. Given the purposes of this modelling, more conservative estimates produced with the adjustment method are the most appropriate.

Figure 5.8 plots the difference between the original cone contrast value and the contrast value produced for each λ_{max} shift, for the L-prime isolating condition – shown for shifts of each cone. If shifting the λ_{max} of the M cone had no effect on the contrast of the cone, the difference across the shifts would be zero, and therefore the cone would remain silenced. Since the original contrasts from the silenced cones were practically zero, the difference values for these cones (L, M, and S) can be considered as the amount of contrast on the cones for each λ_{max} shift. Conversely, the values shown for the L-prime demonstrates a *change* in cone contrast from the original (0.9%) contrast. The difference values are absolute changes, and so represent both positive and negative shifts from the original contrasts.

In general, it is shown that larger disparities in the observer's λ_{max} (compared to those used to produce the stimulus) produce larger amounts of contrast splatter on the cones that should be silenced. The S cones appear to be most sensitive to contrast splatter when there is a disparity in λ_{max}. This is somewhat surprising given its spectral distance from the isolated cone, however it is also noted that the amount of contrast required to produce a perceptible stimulus on the S cone (typically at least 5%) is larger than the estimated contrast splatter shown in the range of S cone shifts here (<1.7%).

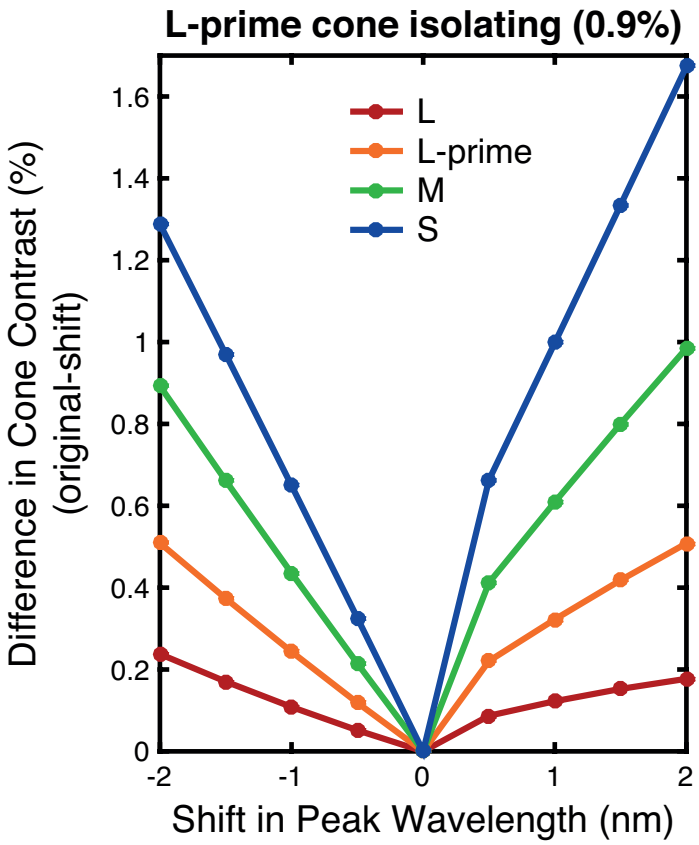

Figure 5.8 Difference between the original cone contrast value and shifted λ_{max} contrast value for each cone at each shift step from the original. The cone contrasts were calculated for the L-prime isolating condition.

Spitschan *et al* (2015) estimated contrast splatter in a similar way to the method described above (with additional considerations for lens density) and assumed a standard deviation in the λ_{max} variance of 1.5, 0.9, and 0.8nm for the L, M, and S cones, respectively – they used these shift values to estimate the combined maximum contrast splatter across silenced cones. If those standard deviation values are implemented here, the maximum absolute contrast on each of the silenced cones is: L=0.18%, M=0.56%, and S=0.86%. Contrast detection thresholds for L and M cone isolating stimuli have been reported at levels between 0.33-0.87% for L cones, and 0.41-1.00% for M cones, across different spatial frequency conditions (Wuerger & Morgan,

1999). The maximum amount of contrast splatter predicted for the M cones at a shift of 0.9nm (0.56%) exceeds the minimum contrast detection threshold (0.41%) for an M-cone isolating stimulus. Therefore the L-prime isolating stimulus would likely be visible to a trichromatic observer whose M cone λ_{max} differed from the 'stimulus-creating' λ_{max} value by at least 0.9nm. Based on the lowest contrast detection thresholds presented above (0.33% for L cones, and 0.41% for M cones), from Wuerger and Morgan, the *minimum* necessary disparity in the λ_{max} of each cone to produce a cone contrast at detection threshold is 2.58nm for L cones, and 0.52nm for M cones.

5.6.5 Discussion

5.6.5.1 Overview of Results

The experimental task demonstrated distinctions between the chromatic (S-cone, and L-M) and luminance (L+M+S) conditions, with the luminance condition producing a clear band-pass sensitivity function across temporal frequencies. The sensitivity functions produced for the chromatic conditions did not show the expected steep decrease in sensitivity with increasing temporal frequency – as is typically shown in low-pass sensitivity functions. However, the peak sensitivity was at the lowest temporal frequency for both conditions, as expected.

A stimulus was created that accounted for *four* cone types (L, L-prime, M, and S), to allow the isolation of one cone type while the other three were silenced. As hypothesised, the maximum available cone contrast for an L-prime condition (0.9%) was lower than for either the L (2.2%) or M (1.5%) cone isolating conditions. The resulting LED modulations for the L-prime isolating

stimulus were used to model how successfully this cone could be isolated in tetrachromatic and trichromatic individuals – the temporal flicker of this stimulus would not be visible to a trichromat. The effect of cone λ_{max} values differing between the observer and the cone spectra that were specified for the stimulus were simulated. It was shown that a discrepancy of only 0.52nm in the M cone λ_{max} would be enough to produce a perceptible level of contrast on this cone during L-prime isolation.

5.6.5.2 Implications

Stimulus presentation via the integrating sphere should undoubtedly produce a more efficient merging of the LEDs than multiple light shaping diffusers, and so in this respect alone the stimulus was improved from Experiment 1. Therefore, the unexpected shape of the sensitivity functions for the chromatic conditions are unlikely to be a product of the stimulus display system. Instead, the higher than expected sensitivities for middle temporal frequencies could be the product of some inadvertent stimulation in the luminance pathway (which is most sensitive at these frequencies). For both conditions, the luminance pathway could be activated by contrast splatter on the silenced cones. This ultimately ties into the same problem modelled for the L-prime stimulus, regarding accuracy of the cone spectra used relative to the observer's actual cone sensitivities. In the case of the L-M condition, there is the additional possibility that the direction in cone space assigned to each of the cones may not produce an isoluminant stimulus for the observer (the direction was fixed at L=0.5, M=-1). This could be resolved by introducing an adjustment task; the observer would adjust the L:M ratio of a stimulus presented at the maximum available contrast for an L-M stimulus, with a high

temporal frequency (e.g. 20Hz). Theoretically, a stimulus at a high temporal frequency is only visible for the luminance pathways, and so the observer would carry out the adjustment until the flicker was no longer visible.

The modelling that was carried out estimated how much contrast splatter could be expected on silenced cones for a stimulus designed to isolate the L-prime cone. When accuracy was assumed between the observer's cone spectra and those used to create the stimulus, there was minimal contrast splatter on the L and M cones (<0.01%) when the L-prime was isolated at the maximum cone contrast available (0.9%). However, when the difference increases between the cone λ_{max} values of the stimulus and those of the simulated observer, the amount of contrast splatter also increases. It was found that a shift of 0.52nm for the M cone λ_{max}, and 2.58nm for the L cone λ_{max} would be enough to produce a perceptible contrast on these cones, when they should be silenced.

5.6.6 Conclusion

The stimulus display system presented here has the capability to produce an L-prime isolating stimulus with enough cone contrast to be perceptible (0.9%) – assuming roughly equivalent contrast sensitivity in an L-prime cone relative to L and M cones. However, there are caveats to this; because of the close proximity between the L, L-prime and M cone spectra, successful isolation of the L-prime cone is dependent on accuracies in the cone spectra used, i.e. the peak sensitivities of the cones (λ_{max}). For the M cone in particular, a difference of only 0.52nm in the observer's λ_{max} compared to that used in the

stimulus is enough to produce a visible amount of cone contrast on this cone (when it should be silenced).

5.7 Discussion

5.7.1 Stimulus size

The stimulus used here had a small visual angle (0.8° in Experiment 2, and 1.2° in Experiment 1). The advantage of using a stimulus of this size is that this region of the retina (central fovea) is not obscured by blood vessels and does not contain any rods. Therefore the stimulus does not need to control for penumbral cones (described in the Spitschan *et al* (2015) study) and the rods. Incidentally, a larger number of LEDs (nine) would be necessary if four penumbral cones types and the rods needed to be accounted for in addition to the four cones already used here (L, L-prime, M, and S).

5.7.2 Control of the LED modulations

An assumption was made regarding the linearity of LED intensity with amplitude, which is crucial for the calculated and anticipated stimulus to be produced by the modulation of the LEDs. As described previously, the Arduino microcontroller uses a pulse-width modulation (PWM) method to control the brightness of the LEDs. This method determines the LED intensity by adjusting the percentage of time that the LED is turned on within a given (brief) time period – this is the duty cycle. A 100% duty cycle means the LEDs are always on and at 100% intensity, similarly, a duty cycle of 50% means the LEDs are on for only 50% of the time, and therefore the LED is 50% less bright. This principle was checked in the LEDs used here by taking measurements of the LED spectra at different duty cycle levels. Figure 5.9

shows the normalised intensity values of each LED plotted as a function of duty cycle (%). The relationship shown for each LED is highly linear; small errors in the intensity measurements, which cause some deviation from linearity, are expected to be a product of measurement noise and the bit depth used in these calibration experiments (8bits).

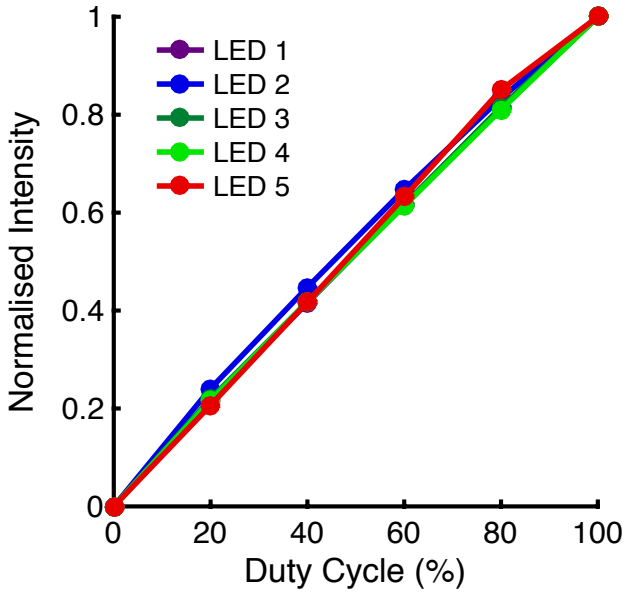

Figure 5.9 Normalised intensity as a function of duty cycle (%) for each LED.

5.7.3 Isolating the L-prime cone

Trichromats should not be able to detect an L-prime isolating stimulus when all cone λ_{max} values are correctly determined. This principle could be utilised to acquire the correct λ_{max} values; an adjustment of the values used for the L and M cones could be made until the L-prime stimulus is no longer visible. As the M cone appears most susceptible to contrast splatter (a smaller shift is needed than for the L cones before contrast splatter is high enough to be visible), it would be logical to begin an adjustment task with this cone. Such a task would require the L-prime to be isolated at a fixed contrast, e.g. the maximum available of 0.9%, while the M cone λ_{max} value is adjusted. When

the flicker of the stimulus is minimised the same process could then be done with the L cone, while the M cone is fixed at the new λ_{max} value.

One potential practical issue with the proposed method is that the L-prime λ_{max} was defined here as the mid point between the L and M cone λ_{max} values. For this to remain the case in this adjustment task, the L-prime would also have to be recalculated with each change in either the L or M cones.

5.7.4 Advantage of the LED system

The system developed here merges the LEDs via a fibre-optic cable and integrating sphere, and is fully portable. The advantage of such a setup is not only that it allows easy transportation of the device, but also enables this stimulus to be placed into an MRI environment. A second fibre-optic cable can be connected to the current output port of the integrating sphere, and as fibre-optic cables are MRI safe, this is the only part of the system that would need to be fed into the MRI scan room to be presented to the observer.

This particular advantage was in mind during the development of the system, as one of the ultimate aims of this system was to further investigate the visual processing pathways of tetrachromatic women. An example of the next steps for the application of this stimulus into fMRI is outlined in Chapter 6.

5.8 Conclusions

This Chapter described the development of a multi-channel LED optical display system that is capable of eliciting responses from a single, specified cone. The method of silent substitution was used, which maintains a steady

level of activation in 'silenced' cones, while the specified cone is 'isolated' and generates a response. Here it was shown that the maximum available cone contrast for an L-prime isolating stimulus (0.9%) would be high enough to be detectable by a tetrachromatic individual. However, it was also demonstrated that in order to produce a successfully isolated cone, while other cones remain silenced, it is paramount for the cone spectra used in the stimulus to match the observer's cone fundamentals very closely. A disparity of 0.52nm in the M cone λ_{max} would be capable of producing a perceptible level of cone contrast splatter.

Therefore, in both trichromats and tetrachromats, accuracy in predicted λ_{max} values appears to be crucial in ensuring that contrast splatter stays below perceptible levels. The consequence of ineffective L-prime isolation would be most apparent in trichromats, as it would be the difference between a perceptible and an invisible stimulus.

Chapter 6 General Discussion and Conclusions

6.1 Overview of the thesis

The aim of this thesis was to investigate pre-cortical factors that affect human colour perception. Three main factors and questions were considered: the effects of slow adaptation to changes in the external environmental on unique hue settings; how dichromacy impacts spatial visual processing within achromatic channels; and how the three pre-cortical pathways are represented in early visual cortex.

The experiments described make novel contributions to the field in their findings and/or in the methods used.

First, it was shown that unique yellow settings shift to shorter wavelengths between winter and summer. This is the first time that changes in this percept have been shown to occur following a non-artificial change in the chromatic environment. Previously, evidence of this shift in unique yellow had only been shown with adaptation to extreme artificial changes in the chromatic environment (Belmore & Shevell, 2008, 2011; Neitz et al., 2002). These findings support the hypothesis that a slow normalisation mechanism, governed by changes in the average chromatic environment, adjusts the gain of the L and M cones into an opponent unique hue system.

Secondly, achromatic contrast discrimination thresholds were measured across different contrast pedestal levels for colour-normal trichromats and

colour-deficient dichromats. The aim was to identify whether dichromats show any advantages in achromatic processing as a result of possessing fewer pre-cortical pathways than trichromats (functionally, rather than anatomically). No differences were observed between the groups; both performed equally well at each contrast pedestal level tested. These findings suggest that, for this particular measure, the dichromats' luminance pathway does not benefit from recruiting neurons that would otherwise be allocated to the opponent L-M pathway.

Finally, fMRI-based population receptive field (pRF) mapping was used to measure pRF sizes in both the achromatic and chromatic channels. These experiments asked whether differences in the spatial resolution of these pre-cortical pathways would be reflected in the average receptive field sizes of chromatically-tuned neurons in visual cortex. This is the first time pRF sizes have been measured for chromatic pathways. Surprisingly, it was shown that pRF sizes do not vary between the pathways. Separate fMRI measures of spatial frequency sensitivity were made with the same set of subjects to confirm that differences between the pathways *could* be detected in early visual cortex. These data indicate that spatial frequency tuning in early visual cortex may be decoupled from neuronal receptive field sizes.

Further to these main experiments, an additional chapter described the development of a multi-channel, MRI-safe, LED system, which was designed to produce cone-isolating stimuli using the method of silent substitution. The ultimate aim was to design a stimulus that would be capable of isolating a 4th type of photoreceptor – the 'L-prime' cone that is expressed along with the L,

M, and S cones in tetrachromatic women. There are currently no reports of such a system being used for this purpose; however, the methods have been applied elsewhere for similar endeavours (e.g. measuring responses from melanopsin-containing ganglion cells, and penumbral cones). It was demonstrated that the system was capable of silent substitution and cone isolation using L, M, and S cones. Modelling was then carried out to estimate how accurately the system would be able to isolate the L-prime cone. It was shown that the accuracy of the cone fundamentals used for an observer (i.e. the wavelengths at the peak sensitivities of the L and M cones) would be critical to enable the isolation of the L-prime, which has a spectral sensitivity between those of the L and M cones. Work is continuing to refine this system for experimental use.

6.2 Other peripheral factors

There are many other peripheral factors affecting human colour perception that have not been explored in this thesis. Almost all stages in the early visual system can affect colour vision in some way: some stages can act as filters to the input received by photoreceptors (e.g. the lens or macular pigment); others are fundamental parts of the colour transduction pathways that produce substantial deficiencies when they are absent (e.g. lack of functional cone photoreceptors in rod monochromats); and there are even features that contribute in ways that are still not fully understood (e.g. the photosensitive melanopsin-containing retinal ganglion cells). The effects of each of these are discussed here briefly.

6.2.1 Prereceptoral filters

Macular pigment is concentrated within the central retina, and is composed of two yellow-coloured carotenoids (lutein and zeaxanthin) that strongly absorb light between 400 and 500nm (Broekmans et al., 2002). Not only is macular pigment concentrated centrally and rapidly decreases outside the fovea, but the density of this pigment is also shown to vary markedly between individuals (Davies & Morland, 2004; Trieschmann et al., 2008). The absorption properties of this pigment mean that less light in the absorption range reaches the photoreceptors in individuals with a high macular pigment density. This principle allows estimates of macular pigment optical density (MPOD) to be made psychophysically; a colour-matching task can be used – much like the Rayleigh match – where the observer is required to adjust the energy of *three* primaries (typically in long, middle, and short wavelength ranges) to produce a match to a single monochromatic short-wavelength reference light (Ruddock, 1963). Because macular pigment absorbs short wavelength light, observers with a high density of macular pigment will need to set the energy of the short wavelength primary to a *higher* value than observers with lower macular pigment density; this results in an equivalent intensity of light reaching the photoreceptors (after passing through the macular pigment) between the observers, and for a match to be made in the task (Davies & Morland, 2004; Welbourne et al., 2013).

A study of MPOD and wavelength settings of unique green has found that the measures are positively correlated; observers with high densities of macular pigment made longer wavelengths settings for unique green (Welbourne et al.,

2013). For a monochromatic light to mimic an internal representation of 'unique green', the activation of the cones needs to be equivalent between the monochromatic light and the internal representation, which is based on a broadband input. Therefore, the authors conclude that for an individual with a high density of macular pigment to mimic the same cone excitations elicited by a broadband 'green' stimulus, they would have to select a longer wavelength of light to produce lower activation of the S cones (which they experience from a broadband stimulus because of high absorption by the macular pigment).

The lens of the human eye absorbs harmful ultraviolet (UV) light, as well as, to a lesser degree, short wavelengths of light in the visible spectrum, and with minimal absorption across longer wavelengths. With age, the optical density of the lens increases, producing a visible yellow colour and causing an increase in the absorption of the lens (Pokorny, Smith, & Lutze, 1987). Mimicking this effect of aging in young observers shows a impact on colour naming in blue/green stimuli (Hardy, Frederick, Kay, & Werner, 2005); stimuli are altered so that the relative cone activation in the young observers reflects that of older observers. However, no such differences are observed between younger and older observers on non-altered stimuli, which was predicted to show the equivalent difference as that observed within the young observers for altered and non-altered stimuli. Similarly, it has been shown that a number of percepts remain stable throughout the life span, such as the perception of white, unique yellow and unique blue (Schefrin & Werner, 1990; Werner & Schefrin, 1993). Studies such as these suggest that a *gradual* yellowing of the lens produces a slow normalisation to the 'filtered' environment, and

therefore the actual perception of the colours measured in these studies remains stable.

6.2.2 Photoreceptor disorders

A rare recessive genetic disorder, rod monochromacy, affects the functioning of all cone photoreceptors (L, M, and S cones); these individuals only have functioning rod photoreceptors (which are not present in central fovea), and as a result have no colour vision and poor visual acuity (Sharpe et al., 1999). In most cases, the actual cones are present in the retina, but their mutations render them inactive. Given the well-documented cortical magnification of the retina in the cortex – with an overrepresentation of the fovea – Baseler *et al* (2002) investigated whether any reorganisation of the cortical retinotopic maps occurred in individuals with rod monochromacy, as a result of having no input from the fovea into the cortex. They found that areas of the cortex that typically represent the rod-free foveal regions in colour-normal subjects are actually activated in rod monochromats. During development, certain aspects of V1 structure are established prior to the functioning of photoreceptors, and therefore develop regardless of any genetic abnormalities in the cones (Weliky & Katz, 1999). However, the findings by Baseler *et al* demonstrate that the functional organisation within these visual areas is plastic, and reorganisation in response to retinal input can and does occur.

6.2.3 Melanopsin

The discovery of an additional photosensitive protein in the retina – melanopsin – was made only within the last 20 years (Provencio et al., 2000; Provencio, Jiang, De Grip, Hayes, & Rollag, 1998). Hattar, Liao, Takao, Berson and Yau (2002) demonstrated that melanopsin can be found in some

retinal ganglion cells – 'melanopsin-containing retinal ganglion cells' – and researchers have since been investigating the contribution of this hitherto unknown photoreceptor type to human vision. A number of studies have labelled melanopsin the 'circadian photoreceptor'; suggesting that because melanopsin-containing retinal ganglion cells project into the suprachiasmatic nucleus (SCN) – which is involved in circadian rhythms – that these photosensitive cells provide the information on daylight/darkness required by the circadian mechanisms for maintaining biological rhythms (Hannibal & Fahrenkrug, 2002; Hannibal, Hindersson, Knudsen, Georg, & Fahrenkrug, 2002; Kavakli & Sancar, 2002).

There is also evidence that the melanopsin-containing retinal ganglion cells project into the LGN (Allen et al., 2014) and that changes in melanopsin contrast can be detected as a change in brightness in human psychophysical tasks (Brown et al., 2012). The study by Cao *et al* (2015), described previously in Chapter 5, used the method of silent substitution to isolate responses from these melanopsin-containing retinal ganglion cells (which they refer to as intrinsically photosensitive retinal ganglion cells – ipRGCs). Isolation of these cells produced a perceptible stimulus that had a distinctive temporal contrast sensitivity function in comparison to L+M or S-cone isolating pathways – with a peak sensitivity shown at high (>10Hz) temporal frequencies.

However, it is also possible that melanopsin modulates a response from the other visual pathways, rather than producing its own distinct response. This is addressed in a recent study by Spitschan, Datta, Stern, Brainard and Aguirre (2016), which suggests that responses interpreted as being

melanopsin-invoked may actually be caused by inadvertent activity in penumbral cones. They used a silent substitution method to control activity in cones, rods and melanopsin, and measured fMRI activity to temporally modulated cone/melanopsin isolating stimuli. They found that activity elicited by a melanopsin stimulus did not exceed the responses generated in a control modulation – which simulated the effect of stimulus imperfections and accidental stimulation of penumbral cones.

Whilst there is general agreement that melanopsin is implicated in the circadian system, the possibility that it produces a perceptible input in its own right (independent of rod and cone input) is still very much under investigation.

6.3 Future Directions

6.3.1 Dichromat advantage

The experiments described here found no differences between the achromatic contrast discrimination thresholds of dichromatic and trichromatic observers. In some ways this is puzzling: the dichromatic visual system presumably has spare capacity to process achromatic information. Therefore, performance improvements might have been expected, particularly in tasks where performance might be constrained by signal to noise issues (for example, at the high end of the contrast discrimination range).

However, there are many other routes to explore in the hypothesis that dichromats benefit in some way from not having an L-M pathway. For

instance, the work by Janáky *et al* (2014) found that dichromats *did* show improved contrast sensitivity in the luminance pathway compared to trichromats, but this specifically occurred at higher spatial frequencies in static stimulus conditions – conditions that presumably biased the stimulus towards the parvocellular pathway, which should be the pathway affected most in dichromats. Aside from attempting to replicate these findings, the advantage could be further probed by using tasks with more ecological relevance. As identified in Chapter 1, a number of non-human primate studies have shown that dichromats have advantages in foraging and camouflage-breaking compared to trichromats (Melin et al., 2007; Saito et al., 2005), and in humans it has also been shown that dichromats may have advantages in detecting camouflaged stimuli (Morgan et al., 1992). However, it is noted that there are also studies showing no difference in foraging ability between dichromatic and trichromatic primates (Caine et al., 2003; Hiramatsu et al., 2008), and a human study demonstrates that *trichromats* show advantages in detecting fruit, particularly if they are at a large distance (12m) from the target (Bompas et al., 2013).

To apply the findings of Janáky *et al* (2014), further investigate the potential camouflage advantage, and to better probe the parvocellular pathway, it may be interesting to devise a number of camouflage stimuli that vary in a spatial frequency dependent manner. For example, detecting targets from surrounds with anisotropic 'tiger-stripe' type patterning, which could be altered to reflect a range of spatial frequency differences between stimuli – an example is shown in Figure 6.1 for two spatial frequency conditions, as well as for two luminance-based conditions (luminance only, or with chromatic noise). If

dichromats have increased sensitivity or acuity at higher spatial frequencies, they may show a better performance than trichromats on tasks that require discriminating targets composed of higher spatial frequencies.

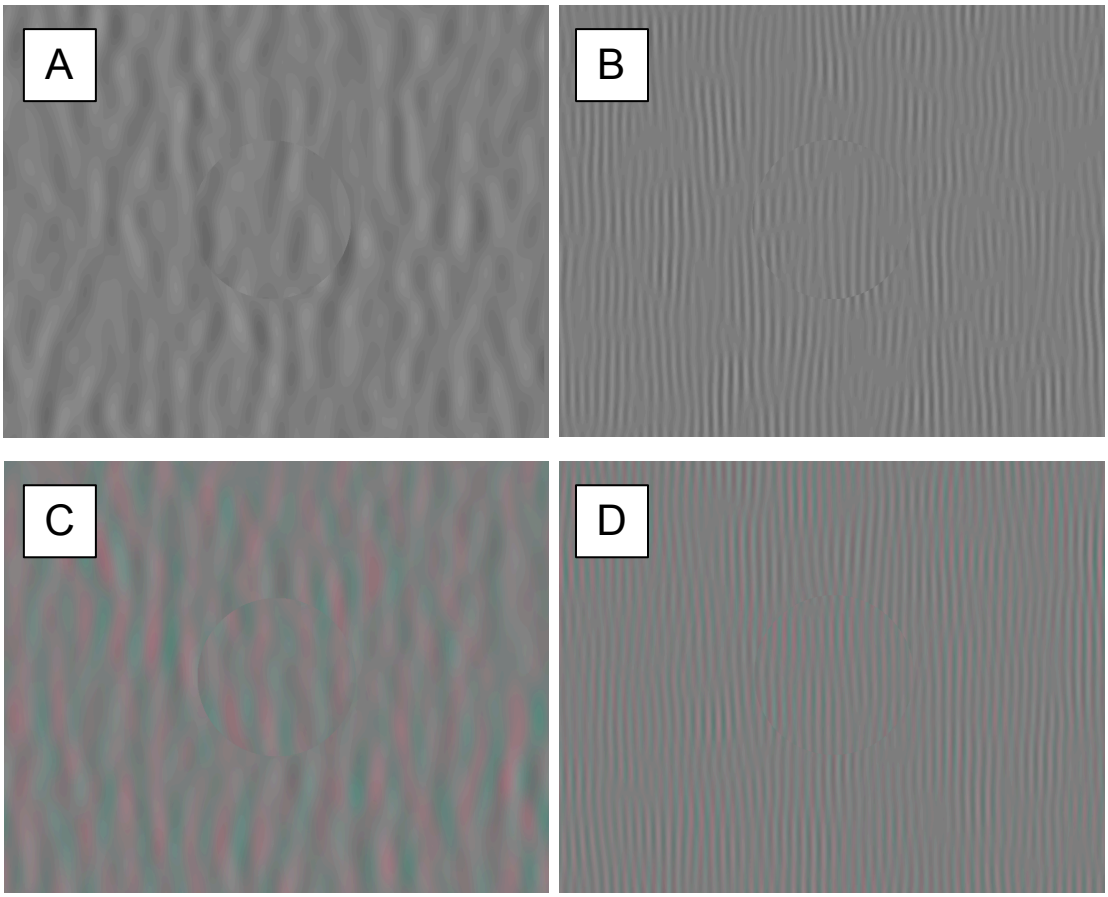

Figure 6.1 Example of camouflage 'tiger-stripe' stimuli for low (A and C) and high (B and D) spatial frequency conditions. Examples are shown for a luminance only stimulus (A and B), and for a condition with both luminance and chromatic components (C and D). Circular targets are overlaid in the centre of each image, containing the same pattern-type as the surround.

6.3.2 Population receptive fields

The dichromat case study used in the pRF experiments showed a trend for smaller pRF sizes in the S-cone channel for both the foveal and peripheral eccentricities, compared to trichromats. This trend could be investigated further in the context of cortical magnification. Cortical magnification produces an overrepresentation of the fovea in the cortex, with retinotopic areas decreasing in size with eccentricity (Virsu & Rovamo, 1979; Wandell &

Winawer, 2011). At the same time, pRF sizes are shown to increase with eccentricity (Alvarez et al., 2015; Dumoulin & Wandell, 2008; Harvey & Dumoulin, 2011), and therefore this increase in pRF sizes correlates with the decrease in cortical area sizes for increasing eccentricities. It would be useful to measure cortical magnification in dichromats to identify whether the trend in pRF sizes found here corresponds to any fundamental differences in cortical magnification. A cohort of dichromatic subjects would need to be recruited to carry out the same pRF experiment as the one described in Chapter 4, which would allow a between-group comparison of pRF sizes across both the luminance and S-cone pathway conditions. Measurements of foveal and peripheral region sizes within visual areas – relative to the total size of the visual area – would enable a comparison of cortical magnification between dichromats and trichromats.

6.3.3 Tetrachromacy and multi-primary stimuli

The development of an MRI-safe multi-channel LED system for producing cone isolating stimuli has the obvious future use of testing tetrachromats – both psychophysically and in an MRI scanner. This would allow an assessment of how stimuli that isolate a putative fourth cone photoreceptor drive visual cortex.

Once all necessary adjustments of cone fundamentals have been made for individual observers (as discussed in Chapter 5), it should be possible to identify clear temporal contrast sensitivity functions (tCSFs) for each of the four cone types in a tetrachromat, but only for the L, M, and S cone types in a

trichromat – with the L-prime stimulus appearing invisible to the trichromats at all contrast levels.

The next stage in this research would be to measure the cortical responses to each of these conditions in trichromats and tetrachromats – including both 'behavioural' and 'non-behavioural' tetrachromats. From the exit point of the integrating sphere, a fibre-optic cable can be attached and fed into the MRI scan room via a waveguide from the scanner control room – fibre-optic cables are scanner-friendly and are small enough to be passed through the scanner bore and positioned at a close viewing distance to the observer. This would allow the same stimulus to be presented to the observer both inside and outside the scanner, using exactly the same stimulus set-up; the additional fibre-optic cable would also be attached during behavioural testing outside the scanner to ensure continuity in the stimulus. An fMRI experiment, using an event-related design to measure responses to the different cone-isolating stimuli of fixed contrast (perhaps at the different temporal frequencies to complement the behavioural data), would enable responses to be measured from the LGN through to early visual cortex – assuming good alignment of the scan slices to encompass both. It would be particularly interesting to identify whether any responses to the L-prime stimuli would be detected in the non-behavioural tetrachromats, i.e. is input from the L-prime received at any stage in visual processing (either in the LGN and/or visual cortex) but just does not lead to a conscious percept?

Current methods of assessing tetrachromatic women would not be useful in the scanner environment; Jordan *et al* (2010) use a number of behavioural

tasks in order to build up a picture of the behavioural capabilities of tetrachromatic women (who are genetically confirmed as carriers for the anomalous photoreceptor). The tasks include 3AFC versions of Rayleigh matches (identifying the odd one out), and multidimensional scaling (which involves judging the similarities of many pairs of stimuli). Whilst these may be good diagnostic tools, they are not easily transferred into an fMRI stimulus. A multi-channel LED system for carrying out silent substitution and cone isolation would provide valuable information on the manner in which tetrachromatic individuals process this unusual colour channel.

6.4 Conclusions

This thesis explored the fundamental importance of peripheral factors in mediating and transmitting the inputs that produce the perception of colour. The pre-cortical pathways, differences in cone photoreceptor types, and the effect of the environment were all considered. For the first time, natural seasonal changes in the environment were shown to affect measurements of unique yellow, and a novel use of pRF mapping in fMRI revealed that the pre-cortical pathways do not produce differences in mean pRF sizes within the early visual cortex. Possible future directions were discussed to further the investigation into how the number of cone types in the retina (e.g. in dichromacy and tetrachromacy) affect perception within each of the pre-cortical pathways and how they are represented in visual cortex.

Appendices

A 1 Results from Chapter 3 Experiment 1, showing the anomalous trichromat data alongside the dichromat and trichromat data. Contrast threshold (%) is plotted as a function of the pedestal contrast (%) for (A) individual subjects (showing the standard error of the thresholds), and (B) averages across each group (showing standard error of the means).

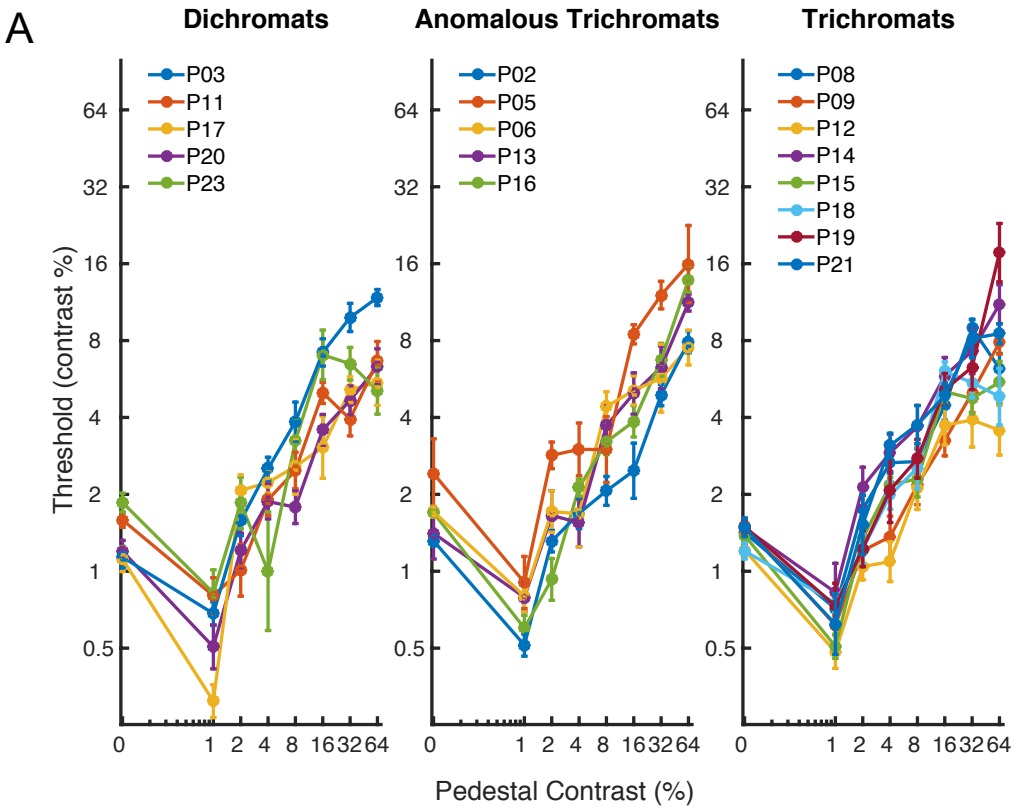

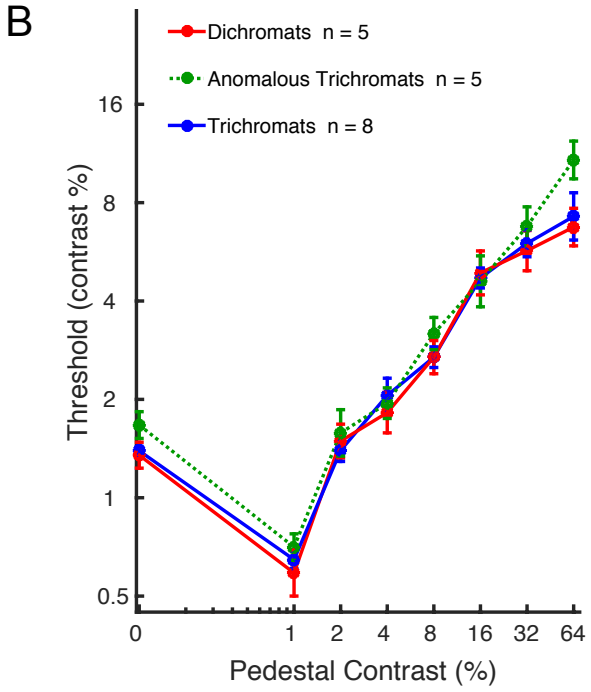

A 2 Results from Chapter 3 Experiment 2, showing the anomalous trichromat data alongside the dichromat and trichromat data. Contrast threshold (%) is plotted as a function of the pedestal contrast (%) for (A) individual subjects (showing the standard error of the thresholds), and (B) averages across each group (showing standard error of the means).

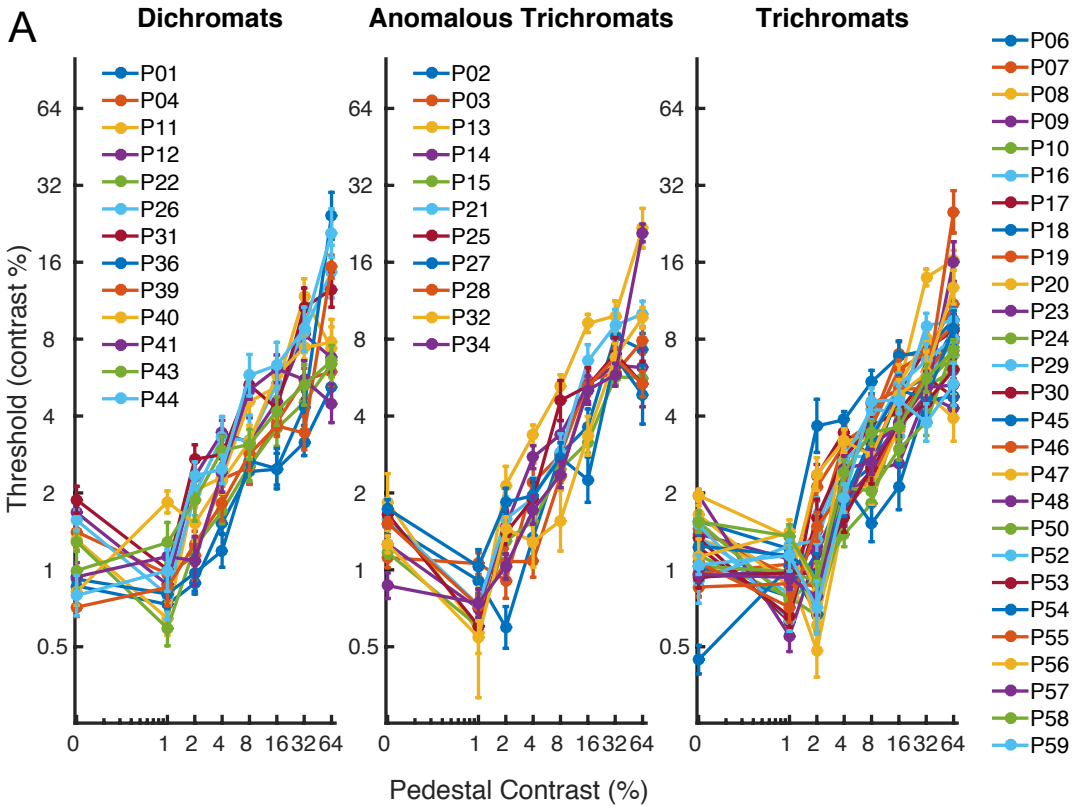

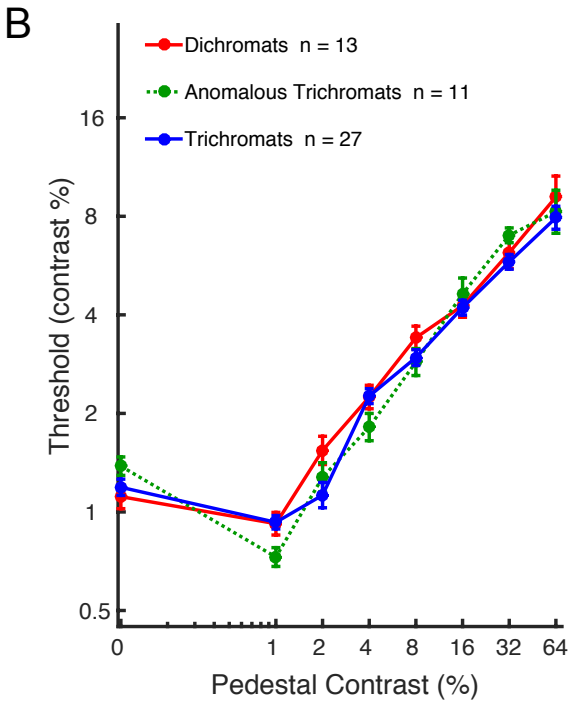

References

Allen, A. E., Storchi, R., Martial, F. P., Petersen, R. S., Montemurro, M. A., Brown, T. M., & Lucas, R. J. (2014). Melanopsin-driven light adaptation in mouse vision. *Current Biology*, *24*(21), 2481–2490. doi:10.1016/j.cub.2014.09.015

Alvarez, I., de Haas, B., Clark, C. A., Rees, G., & Schwarzkopf, D. S. (2015). Comparing different stimulus configurations for population receptive field mapping in human fMRI. *Frontiers in Human Neuroscience*, *9*, 1–16. doi:10.3389/fnhum.2015.00096

Andrews, T. J., Halpern, S. D., & Purves, D. (1997). Correlated size variations in human visual cortex, lateral geniculate nucleus, and optic tract. *The Journal of Neuroscience*, *17*(8), 2859–2868.

Anstis, S. M., & Cavanagh, P. (1983). A minimum motion technique for judging equiluminance. In J. D. Mollon & L. T. Sharpe (Eds.), *Colour vision: Psychophysics and physiology* (pp. 156–166). London: Academic Press.

Azzopardi, P., Jones, K. E., & Cowey, A. (1999). Uneven mapping of magnocellular and parvocellular projections from the lateral geniculate nucleus to the striate cortex in the macaque monkey. *Vision Research*, *39*(13), 2179–2189. doi:10.1016/S0042-6989(98)00319-8

Baker, D. H. (2013). What is the primary cause of individual differences in contrast sensitivity? *PloS One*, *8*(7), e69536. doi:10.1371/journal.pone.0069536

Baldwin, A. S., Baker, D. H., & Hess, R. F. (2016). What Do Contrast Threshold Equivalent Noise Studies Actually Measure? Noise vs.

Nonlinearity in Different Masking Paradigms. *PloS One*, *11*(3), e0150942. doi:10.1371/journal.pone.0150942

Baseler, H. A., Brewer, A. A., Sharpe, L. T., Morland, A. B., Jägle, H., & Wandell, B. A. (2002). Reorganization of human cortical maps caused by inherited photoreceptor abnormalities. *Nature Neuroscience*, *5*(4), 364–370. doi:10.1038/nn817

Belmore, S. C., & Shevell, S. K. (2008). Very-long-term chromatic adaptation: test of gain theory and a new method. *Visual Neuroscience*, *25*(3), 411–414. doi:10.1017/S0952523808080450

Belmore, S. C., & Shevell, S. K. (2011). Very-long-term and short-term chromatic adaptation: are their influences cumulative? *Vision Research*, *51*(3), 362–366. doi:10.1016/j.visres.2010.11.011

Berendschot, T. T. J. M., van de Kraats, J., & van Norren, D. (1996). Foveal cone mosaic and visual pigment density in dichromats. *The Journal of Physiology*, *492*(1), 307–314.

Binda, P., Thomas, J. M., Boynton, G. M., & Fine, I. (2013). Minimizing biases in estimating the reorganization of human visual areas with BOLD retinotopic mapping. *Journal of Vision*, *13*(7), 1–16. doi:10.1167/13.7.13

Boettner, E. A., & Wolter, J. R. (1962). Transmission of the Ocular Media. *Investigative Ophthalmology & Visual Science*, *1*(6), 776–783.

Bompas, A., Kendall, G., & Sumner, P. (2013). Spotting fruit versus picking fruit as the selective advantage of human colour vision. *I-Perception*, *4*(2), 84–94. doi:10.1068/i0564

Bowker, D. E., Davis, R. E., Myrick, D. L., Stacy, K., & Jones, W. T. (1985). *Spectral reflectances of natural targets for use in remote sensing studies. NASA reference publication 1139*. Hampton, Virginia: NASA,

Scientific and Technical Information Branch.

Boynton, G. M., Demb, J. B., Glover, G. H., & Heeger, D. J. (1999). Neuronal basis of contrast discrimination. *Vision Research*, *39*(2), 257–269. doi:10.1016/S0042-6989(98)00113-8

Broekmans, W. M. R., Berendschot, T. T. J. M., Klöpping-Ketelaars, I. A. A., de Vries, A. J., Goldbohm, R. A., Tijburg, L. B. M., … van Poppel, G. (2002). Macular pigment density in relation to serum and adipose tissue concentrations of lutein and serum concentrations of zeaxanthin. *The American Journal of Clinical Nutrition*, *76*(3), 595–603.

Brown, T. M., Tsujimura, S.-I., Allen, A. E., Wynne, J., Bedford, R., Vickery, G., … Lucas, R. J. (2012). Melanopsin-based brightness discrimination in mice and humans. *Current Biology*, *22*(12), 1134–1141. doi:10.1016/j.cub.2012.04.039

Buchsbaum, G. (1980). A spatial processor model for object colour perception. *Journal of the Franklin Institute*, *310*(1), 1–26. doi:10.1016/0016-0032(80)90058-7

Caine, N. G., Surridge, A. K., & Mundy, N. I. (2003). Dichromatic and trichromatic Callithrix Geoffroyi differ in relative foraging ability for red-green color-camouflaged and non-camouflaged food. *International Journal of Primatology*, *24*(6), 1163–1175. doi:10.1023/B:IJOP.0000005985.18112.25

Callaway, E. M. (2005). Structure and function of parallel pathways in the primate early visual system. *The Journal of Physiology*, *566*(1), 13–19. doi:10.1113/jphysiol.2005.088047

Cao, D., Nicandro, N., & Barrionuevo, P. A. (2015). A five-primary photostimulator suitable for studying intrinsically photosensitive retinal

ganglion cell functions in humans. *Journal of Vision*, *15*(1), 1–13. doi:10.1167/15.1.27

Carlo, C. N., & Stevens, C. F. (2013). Structural uniformity of neocortex, revisited. *PNAS*, *110*(4), 1488–1493. doi:10.1073/pnas.1221398110

Carroll, J., Neitz, J., & Neitz, M. (2002). Estimates of L:M cone ratio from ERG flicker photometry and genetics. *Journal of Vision*, *2*(8), 531–542. doi:10:1167/2.8.1

Carroll, J., Neitz, M., Hofer, H., Neitz, J., & Williams, D. R. (2004). Functional photoreceptor loss revealed with adaptive optics: an alternate cause of color blindness. *Proceedings of the National Academy of Sciences of the United States of America*, *101*(22), 8461–8466. doi:10.1073/pnas.0401440101

Chirimuuta, M., & Tolhurst, D. J. (2005). Does a Bayesian model of V1 contrast coding offer a neurophysiological account of human contrast discrimination? *Vision Research*, *45*(23), 2943–2959. doi:10.1016/j.visres.2005.06.022

Clatworthy, P. L., Chirimuuta, M., Lauritzen, J. S., & Tolhurst, D. J. (2003). Coding of the contrasts in natural images by populations of neurons in primary visual cortex (V1). *Vision Research*, *43*(18), 1983–2001. doi:10.1016/S0042-6989(03)00277-3

Cleland, B., Harding, T., & Tulunay-Keesey, U. (1979). Visual resolution and receptive field size: examination of two kinds of cat retinal ganglion cell. *Science*, *205*(4410), 1015–1017. doi:10.1126/science.472720

Cobb, S. R. (1975). The Unique Green phenomenon and colour vision. *Clinical Genetics*, *7*(4), 274–279.

D'Souza, D. V, Auer, T., Frahm, J., Strasburger, H., & Lee, B. B. (2016).

Dependence of chromatic responses in V1 on visual field eccentricity and spatial frequency: an fMRI study. *Journal of the Optical Society of America. A*, *33*(3), A53–A64. doi:10.1364/JOSAA.33.000A53

Dacey, D. M. (2000). Parallel Pathways for Pectral Coding in Primate Retina. *Annual Review of Neuroscience*, *23*, 743–775.

Dacey, D. M., & Lee, B. (1994). The "blue-on" opponent pathway in primate retina originates from a distinct bistratified ganglion cell type. *Nature*, *367*, 731–735. doi:10.1038/367731a0

Dale, A. M., Fischl, B., & Sereno, M. I. (1999). Cortical Surface-Based Analysis. *NeuroImage*, *9*(2), 179–194. doi:10.1006/nimg.1998.0395

Davies, N. P., & Morland, A. B. (2004). Macular pigments: their characteristics and putative role. *Progress in Retinal and Eye Research*, *23*(5), 533–559. doi:10.1016/j.preteyeres.2004.05.004

de Vries, H. (1948). The fundamental response curves of normal and abnormal dichromatic and trichromatic eyes. *Physica*, *14*(6), 367–380. doi:10.1016/0031-8914(48)90021-4

Derrington, A. M., Krauskopf, J., & Lennie, P. (1984). Chromatic mechanisms in lateral geniculate nucleus of macaque. *The Journal of Physiology*, *357*, 241–265.

Derrington, A. M., & Lennie, P. (1984). Spatial and temporal contrast sensitivities of neurones in lateral geniculate nucleus of macaque. *The Journal of Physiology*, *357*, 219–240.

Dimmick, F. L., & Hubbard, M. R. (1939). The spectral location of psychologically unique yellow, green, and blue. *American Journal of Psychology*, *52*(2), 242–254.

Dumoulin, S. O., & Wandell, B. A. (2008). Population receptive field estimates

in human visual cortex. *NeuroImage*, *39*(2), 647–660. doi:10.1016/j.neuroimage.2007.09.034

Engel, S. A. (1997). Retinotopic organization in human visual cortex and the spatial precision of functional MRI. *Cerebral Cortex*, *7*(2), 181–192. doi:10.1093/cercor/7.2.181

Engel, S. A., Rumelhart, D. E., Wandell, B. A., Lee, A. T., Glover, G. H., Chichilnisky, E. J., & Shadlen, M. N. (1994). fMRI of human visual cortex. *Nature*, *369*, 525. doi:10.1038/369525a0

Enroth-Cugell, C., & Robson, J. G. (1966). The contrast sensitivity of retinal ganglion cells of the cat. *The Journal of Physiology*, *187*(3), 517–552. doi:10.1113/jphysiol.1966.sp008107

Estévez, O., & Spekreijse, H. (1982). The "silent substitution" method in visual research. *Vision Research*, *22*(6), 681–691.

FitzGibbon, T., Erikoz, B., Grunert, U., & Martin, P. R. (2015). Analysis of the lateral geniculate nucleus in dichromatic and trichromatic marmosets. *Journal of Comparative Neurology*, *523*(13), 1948–1966. doi:10.1002/cne.23772

García-Pérez, M. A., & Alcalá-Quintana, R. (2007). Bayesian adaptive estimation of arbitrary points on a psychometric function. *The British Journal of Mathematical and Statistical Psychology*, *60*(1), 147–174. doi:10.1348/000711006X104596

Geisler, W. S., & Albrecht, D. G. (1997). Visual cortex neurons in monkeys and cats: detection, discrimination, and identification. *Visual Neuroscience*, *14*(5), 897–919. doi:10.1017/S0952523800011627

Goodchild, A. K., & Martin, P. R. (1998). The distribution of calcium-binding proteins in the lateral geniculate nucleus and visual cortex of a New

World monkey, the marmoset, Callithrix jacchus. *Visual Neuroscience*, *15*, 625–642.

Granzier, J. J. M., Smeets, J. B. J., & Brenner, E. (2006). A direct test of the "Grey World Hypothesis"; A comparison of different matching methods. In *Colour in Graphics, Imaging, and Vision* (pp. 131–136). Society for Imaging Science and Technology.

Hannibal, J., & Fahrenkrug, J. (2002). Melanopsin: a novel photopigment involved in the photoentrainment of the brain's biological clock? *Annals of Medicine*, *34*(5), 401–407. doi:10.1080/078538902320772151

Hannibal, J., Hindersson, P., Knudsen, S., Georg, B., & Fahrenkrug, J. (2002). The photopigment melanopsin is exclusively present in pituitary adenylate cyclase-activating polypeptide-containing retinal ganglion cells of the retinohypothalamic tract. *Journal of Neuroscience*, *22*, 1–7.

Hardy, J. L., Frederick, C. M., Kay, P., & Werner, J. S. (2005). Color naming, lens aging, and grue: what the optics of the aging eye can teach us about color language. *Psychological Science*, *16*(4), 321–327. doi:10.1111/j.0956-7976.2005.01534.x

Harvey, B. M., & Dumoulin, S. O. (2011). The relationship between cortical magnification factor and population receptive field size in human visual cortex: constancies in cortical architecture. *The Journal of Neuroscience*, *31*(38), 13604–13612. doi:10.1523/jneurosci.2572-11.2011

Hattar, S., Liao, H. W., Takao, M., Berson, D. M., & Yau, K. W. (2002). Melanopsin-containing retinal ganglion cells: architecture, projections, and intrinsic photosensitivity. *Science*, *295*(5557), 1065–1070. doi:10.1126/science.1069609

Henriksson, L., Nurminen, L., Hyvärinen, A., & Vanni, S. (2008). Spatial

frequency tuning in human retinotopic visual areas. *Journal of Vision*, *8*(10), 1–13. doi:10.1167/8.10.5

Hiramatsu, C., Melin, A. D., Aureli, F., Schaffner, C. M., Vorobyev, M., Matsumoto, Y., & Kawamura, S. (2008). Importance of achromatic contrast in short-range fruit foraging of primates. *PloS One*, *3*(10), e3356. doi:10.1371/journal.pone.0003356

Hofer, H., Carroll, J., Neitz, J., Neitz, M., & Williams, D. R. (2005). Organization of the human trichromatic cone mosaic. *The Journal of Neuroscience*, *25*(42), 9669–9679. doi:10.1523/jneurosci.2414-05.2005

Hubel, D. H., & Wiesel, T. N. (1962). Receptive fields, binocular interaction and functional architecture in the cat's visual cortex. *The Journal of Physiology*, *160*, 106–154.

Hurvich, L. M., Jameson, D., & Cohen, J. D. (1968). The experimental determination of unique green in the spectrum. *Perception & Psychophysics*, *4*(2), 65–68. doi:10.3758/BF03209508

Jacobs, G. H. (2007). New world monkeys and color. *International Journal of Primatology*, *28*(4), 729–759. doi:10.1007/s10764-007-9168-y

Jägle, H., de Luca, E., Serey, L., Bach, M., & Sharpe, L. T. (2006). Visual acuity and X-linked color blindness. *Graefe's Archive for Clinical and Experimental Ophthalmology*, *244*(4), 447–453. doi:10.1007/s00417-005-0086-4

Jäkel, F., & Wichmann, F. A. (2006). Spatial four-alternative forced-choice method is the preferred psychophysical method for naïve observers. *Journal of Vision*, *6*(11), 1307–1322. doi:10.1167/6.11.13

Jameson, D., & Hurvich, L. . (1968). Opponent-Response Functions Related to Measured Cone Photopigments. *Journal of the Optical Society of*

America, *58*(3), 429–430.

Jameson, D., & Hurvich, L. M. (1955). Some quantitative aspects of an opponent-colors theory. I. Chromatic responses and spectral saturation. *Journal of the Optical Society of America*, *45*(7), 546–552. doi:10.1364/JOSA.45.000546

Janáky, M., Borbély, J., Benedek, G., Kocsis, B. P., & Braunitzer, G. (2014). Achromatic luminance contrast sensitivity in X-linked color-deficient observers: An addition to the debate. *Visual Neuroscience*, *31*, 99–103. doi:10.1017/S0952523813000400

Jenkinson, M., Bannister, P., Brady, M., & Smith, S. (2002). Improved optimization for the robust and accurate linear registration and motion correction of brain images. *NeuroImage*, *17*(2), 825–841. doi:10.1016/S1053-8119(02)91132-8

Jordan, G., Deeb, S. S., Bosten, J. M., & Mollon, J. D. (2010). The dimensionality of color vision in carriers of anomalous trichromacy. *Journal of Vision*, *10*(8), 1–19. doi:10.1167/10.8.12

Jordan, G., & Mollon, J. D. (1993). The Nagel anomaloscope and seasonal variation of colour vision. *Nature*, *363*, 546–549. doi:10.1038/363546a0

Jordan, G., & Mollon, J. D. (1995). Rayleigh matches and unique green. *Vision Research*, *35*(5), 613–620.

Kavakli, I. H., & Sancar, A. (2002). Circadian photoreception in humans and mice. *Molecular Interventions*, *2*(8), 484–492. doi:10.1124/mi.2.8.484

Kim, K. J., Mantiuk, R., & Lee, K. H. (2013). Measurements of achromatic and chromatic contrast sensitivity functions for an extended range of adaptation luminance. In *SPIE 8651, Human Vision and Electronic Imaging XVIII* (p. 86511A). International Society for Optics and

Photonics. doi:10.1117/12.2002178

Kirchner, H., & Thorpe, S. J. (2006). Ultra-rapid object detection with saccadic eye movements: visual processing speed revisited. *Vision Research*, *46*(11), 1762–1776. doi:10.1016/j.visres.2005.10.002

Kremers, J., & Pangeni, G. (2012). Electroretinographic responses to photoreceptor specific sine wave modulation. *Journal of the Optical Society of America A*, *29*(2), 306–313.

Kuehni, R. G. (2004). Variability in unique hue selection: A surprising phenomenon. *Color Research & Application*, *29*(2), 158–162. doi:10.1002/col.10237

Lee, B., Martin, P. R., & Valberg, A. (1988). The physiological basis of heterochromatic flicker photometry demonstrated in the ganglion cells of the macaque retina. *The Journal of Physiology*, *404*, 323–347.

Legge, G. E., & Foley, J. M. (1980). Contrast masking in human vision. *Journal of the Optical Society of America*, *70*(12), 1458–1471. doi:10.1364/JOSA.70.001458

Lennie, P. (2003). The physiology of color vision. In S. K. Shevell (Ed.), *The Science of Color* (2nd ed., pp. 218–242). Elsevier.

Lennie, P., Krauskopf, J., & Sclar, G. (1990). Chromatic mechanisms in striate cortex of macaque. *The Journal of Neuroscience : The Official Journal of the Society for Neuroscience*, *10*(2), 649–669.

Leventhal, A. G., Thompson, K. G., Liu, D., Zhou, Y., & Ault, S. J. (1995). Concomitant sensitivity to orientation, direction, and color of cells in layers 2, 3, and 4 of monkey striate cortex. *Journal of Neuroscience*, *15*(3), 1808–1818.

Linsenmeier, R. A., Frishman, L. J., Jakiela, H. G., & Enroth-Cugell, C. (1982).

Receptive field properties of x and y cells in the cat retina derived from contrast sensitivity measurements. *Vision Research*, *22*(9), 1173–1183. doi:10.1016/0042-6989(82)90082-7

Lutze, M., Pokorny, J., & Smith, V. C. (2006). Achromatic parvocellular contrast gain in normal and color defective observers: Implications for the evolution of color vision. *Visual Neuroscience*, *23*(3-4), 611–6. doi:10.1017/S0952523806233078

Lyon, M. F. (1961). Gene action in the X-chromosome of the mouse (Mus musculus L.). *Nature*, *190*, 372–373. doi:10.1038/190372a0

Lyon, M. F. (2002). X-chromosome inactivation and human genetic disease. *Acta Paediatrica*, *91*(439), 107–112. doi:10.1111/j.1651-2227.2002.tb03120.x

MacLeod, D. I. A., & Boynton, R. M. (1979). Chromaticity diagram showing cone excitation by stimuli of equal luminance. *Journal of the Optical Society of America*, *69*(8), 1183–1186. doi:10.1364/JOSA.69.001183

May, K. A., & Solomon, J. A. (2015). Connecting psychophysical performance to neuronal response properties II: Contrast decoding and detection. *Journal of Vision*, *15*(6), 1–21. doi:10.1167/15.6.9

Melin, A., Fedigan, L., Hiramatsu, C., Sendall, C., & Kawamura, S. (2007). Effects of colour vision phenotype on insect capture by a free-ranging population of white-faced capuchins,Cebus capucinus. *Animal Behaviour*, *73*(1), 205–214. doi:10.1016/j.anbehav.2006.07.003

Merigan, W. H. (1989). Chromatic and achromatic vision of macaques: role of the P pathway. *The Journal of Neuroscience*, *9*(3), 776–783.

Moran, J., & Desimone, R. (1985). Selective attention gates visual processing in the extrastriate cortex. *Science*, *229*, 782–784.

doi:10.1126/science.4023713

Morgan, M. J., Adam, A., & Mollon, J. D. (1992). Dichromats detect colour-camouflaged objects that are not detected by trichromats. *Proceedings: Biological Sciences*, *248*(1323), 291–295. doi:10.1098/rspb.1992.0074

Mullen, K. T. (1985). The contrast sensitivity of human colour vision to red-green and blue-yellow chromatic gratings. *The Journal of Physiology*, *359*, 381–400.

Mullen, K. T., Dumoulin, S. O., McMahon, K. L., de Zubicaray, G. I., & Hess, R. F. (2007). Selectivity of human retinotopic visual cortex to S-cone-opponent, L/M-cone-opponent and achromatic stimulation. *The European Journal of Neuroscience*, *25*(2), 491–502. doi:10.1111/j.1460-9568.2007.05302.x

Nachmias, J., & Sansbury, R. V. (1974). Letter: Grating contrast: discrimination may be better than detection. *Vision Research*, *14*(10), 1039–1042.

Neitz, J., Carroll, J., Yamauchi, Y., Neitz, M., & Williams, D. R. (2002). Color perception is mediated by a plastic neural mechanism that is adjustable in adults. *Neuron*, *35*(4), 783–792.

Neitz, J., & Neitz, M. (2011). The genetics of normal and defective color vision. *Vision Research*, *51*(7), 633–651. doi:10.1016/j.visres.2010.12.002

Owsley, C., Sekuler, R., & Siemsen, D. (1983). Contrast sensitivity throughout adulthood. *Vision Research*, *23*(7), 689–699.

Packer, O., & Williams, D. R. (2003). Light, the Retinal Image, and Photoreceptors. In S. K. Shevell (Ed.), *The Science of Color* (2nd ed., pp. 41–97). Elsevier.

Pestilli, F., Ling, S., & Carrasco, M. (2009). A population-coding model of

attention's influence on contrast response: Estimating neural effects from psychophysical data. *Vision Research*, *49*(10), 1144–1153. doi:10.1016/j.visres.2008.09.018

Pokorny, J., Smith, V. C., & Lutze, M. (1987). Aging of the human lens. *Applied Optics*, *26*(8), 1437–1440. doi:10.1364/AO.26.001437

Prins, N., & Kingdom, F. A. A. (2009). Palamedes: Matlab routines for analyzing psychophysical data. http://www.palamedestoolbox.org.

Provencio, I., Jiang, G., De Grip, W. J., Hayes, W. P., & Rollag, M. D. (1998). Melanopsin: An opsin in melanophores, brain, and eye. *Proceedings of the National Academy of Sciences*, *95*(1), 340–345. doi:10.1073/pnas.95.1.340

Provencio, I., Rodriguez, I., Jiang, G., Hayes, W., Moreira, E., & Rollag, M. (2000). A novel human opsin in the inner retina. *Journal of Neuroscience*, *20*(2), 600–605.

Purves, D., Augustine, G. J., Fitzpatrick, D., Katz, L. C., LaMantia, A. S., McNamara, J., & Williams, S. M. (2001). Functional Specialization of the Rod and Cone Systems. In *Neuroscience* (2nd ed.). Sunderland (MA): Sinauer Associates.

Regan, B. C., Reffin, J. P., & Mollon, J. D. (1994). Luminance noise and the rapid determination of discrimination ellipses in colour deficiency. *Vision Research*, *34*(10), 1279–1299. doi:10.1016/0042-6989(94)90203-8

Reuter, M., Schmansky, N. J., Rosas, H. D., & Fischl, B. (2012). Within-subject template estimation for unbiased longitudinal image analysis. *NeuroImage*, *61*(4), 1402–1418. doi:10.1016/j.neuroimage.2012.02.084

Rinner, O., & Gegenfurtner, K. R. (2000). Time course of chromatic adaptation for color appearance and discrimination. *Vision Research*,

40(14), 1813–1826. doi:10.1016/S0042-6989(00)00050-X

Roorda, A., & Williams, D. R. (1999). The arrangement of the three cone classes in the living human eye. *Nature*, *397*(6719), 520–522. doi:10.1038/17383

Rubin, M. L. (1961). Spectral Hue Loci of Normal and Anomalous Trichromats. *American Journal of Ophthalmology*, *52*(2), 166–172.

Ruddock, K. H. (1963). Evidence for Macular Pigmentation from Colour Matching Data. *Vision Research*, *3*(61), 417–429.

Saito, A., Mikami, A., Kawamura, S., Ueno, Y., Hiramatsu, C., Widayati, K. A., … Hasegawa, T. (2005). Advantage of dichromats over trichromats in discrimination of color-camouflaged stimuli in nonhuman primates. *American Journal of Primatology*, *67*(4), 425–436. doi:10.1002/ajp.20197

Schade, O. H. (1956). Optical and Photoelectric Analog of the Eye. *Journal of the Optical Society of America*, *46*(9), 721–739. doi:10.1364/JOSA.46.000721

Schefrin, B. E., & Werner, J. S. (1990). Loci of spectral unique hues throughout the life span. *Journal of the Optical Society of America. A*, *7*(2), 305–311.

Schmidt, B. P., Neitz, M., & Neitz, J. (2014). Neurobiological hypothesis of color appearance and hue perception. *Journal of the Optical Society of America. A*, *31*(4), 195–207.

Schmidt, B. P., Touch, P., Neitz, M., & Neitz, J. (2014). The relative number of L and M cones shapes color experience. In *OSA Fall Vision Meeting* (Vol. 14, p. 29). Journal of Vision. doi:10.1167/14.15.29

Schmidt, B. P., Touch, P., Neitz, M., & Neitz, J. (2016). Circuitry to explain

how the relative number of L and M cones shapes color experience. *Journal of Vision*, *16*(8), 1–17. doi:10.1167/16.8.18

Shapiro, A. G., Pokorny, J., & Smith, V. C. (1996). Cone – rod receptor spaces with illustrations and light-emitting-diode spectra, *13*(12), 2319–2328.

Sharpe, L. T., de Luca, E., Hansen, T., Jägle, H., & Gegenfurtner, K. R. (2006). Advantages and disadvantages of human dichromacy. *Journal of Vision*, *6*(3), 213–223. doi:10.1167/6.3.3

Sharpe, L. T., Stockman, A., Jägle, H., & Nathans, J. (1999). Opsin genes, cone photopigments, color vision, and color blindness. In K. R. Gegenfurtner & L. T. Sharpe (Eds.), *Color vision: From Genes to Perception* (pp. 3–51). Cambridge: Cambridge University Press.

Shevell, S. K., He, J. ., Kainz, P., Neitz, J., & Neitz, M. (1998). Relating color discrimination to photopigment genes in deutan observers. *Vision Research*, *38*(21), 3371–3376. doi:10.1016/S0042-6989(97)00434-3

Simons, D., Lleras, A., Martinez-Conde, S., Slichter, D., Caddigan, E., & Nevarez, G. (2006). Induced visual fading of complex images. *Journal of Vision*, *6*(10), 1093–1101. doi:10.1167/6.10.9

Smith, S. M., Jenkinson, M., Woolrich, M. W., Beckmann, C. F., Behrens, T. E. J., Johansen-Berg, H., … Matthews, P. M. (2004). Advances in functional and structural MR image analysis and implementation as FSL. *NeuroImage*, *23*, S208–S219. doi:10.1016/j.neuroimage.2004.07.051

Solomon, S. G. (2002). Striate cortex in dichromatic and trichromatic marmosets: neurochemical compartmentalization and geniculate input. *The Journal of Comparative Neurology*, *450*(4), 366–381. doi:10.1002/cne.10327

Solomon, S. G., & Lennie, P. (2007). The machinery of colour vision. *Nature*

Reviews Neuroscience, *8*(4), 276–286. doi:10.1038/nrn2094

Somers, D. C., Dale, A. M., Seiffert, A. E., & Tootell, R. B. H. (1999). Functional MRI reveals spatially specific attentional modulation in human primary visual cortex. *Proceedings of the National Academy of Sciences*, *96*(4), 1663–1668. doi:10.1073/pnas.96.4.1663

Spitschan, M., Aguirre, G. K., & Brainard, D. H. (2015). Selective stimulation of penumbral cones reveals perception in the shadow of retinal blood vessels. *PloS One*, *10*(4), e0124328. doi:10.1371/journal.pone.0124328

Spitschan, M., Datta, R., Stern, A. M., Brainard, D. H., & Aguirre, G. K. (2016). Human visual cortex responses to rapid cone and melanopsin-directed flicker. *The Journal of Neuroscience : The Official Journal of the Society for Neuroscience*, *36*(5), 1471–1482. doi:10.1523/jneurosci.1932-15.2016

Stockman, A., & Sharpe, L. T. (2000). The spectral sensitivities of the middle- and long-wavelength-sensitive cones derived from measurements in observers of known genotype. *Vision Research*, *40*(13), 1711–1737. doi:10.1016/S0042-6989(00)00021-3

Tailby, C., Solomon, S. G., & Lennie, P. (2008). Functional asymmetries in visual pathways carrying S-cone signals in macaque. *The Journal of Neuroscience*, *28*(15), 4078–4087. doi:10.1523/jneurosci.5338-07.2008

Thomas, P. B. M., & Mollon, J. D. (2004). Modelling the Rayleigh match. *Visual Neuroscience*, *21*(3), 477–482.

Trieschmann, M., van Kuijk, F. J. G. M., Alexander, R., Hermans, P., Luthert, P., Bird, a C., & Pauleikhoff, D. (2008). Macular pigment in the human retina: histological evaluation of localization and distribution. *Eye*, *22*, 132–137. doi:10.1038/sj.eye.6702780

Troxler, D. (1804). Über das Verschwinden gegebener Gegenstände innerhalb

unseres Gesichtskreises. *Ophthalmologische Bibliothek*, *2*(2), 1–53.

Troy, J. B. (1983). Spatial contrast sensitivities of X and Y type neurones in the cat's dorsal lateral geniculate nucleus. *The Journal of Physiology*, *344*(1), 399 –417. doi:10.1113/jphysiol.1983.sp014948

van Essen, D. C. (2004). Organization of visual areas in macaque and human cerebral cortex. In L. Chalupa & J. S. Werner (Eds.), *The Visual Neurosciences* (pp. 507–521). MIT Press.

Vanni, S., Henriksson, L., Viikari, M., & James, A. C. (2006). Retinotopic distribution of chromatic responses in human primary visual cortex. *The European Journal of Neuroscience*, *24*(6), 1821–1831. doi:10.1111/j.1460-9568.2006.05070.x

Virsu, V., & Rovamo, J. (1979). Visual resolution, contrast sensitivity, and the cortical magnification factor. *Experimental Brain Research*, *37*(3), 475–494. doi:10.1007/BF00236818

Wallis, S. A., Baker, D. H., Meese, T. S., & Georgeson, M. A. (2013). The slope of the psychometric function and non-stationarity of thresholds in spatiotemporal contrast vision. *Vision Research*, *76*, 1–10. doi:10.1016/j.visres.2012.09.019

Wandell, B. A. (1995). *Foundations of Vision*. Sinauer Associates.

Wandell, B. A., & Winawer, J. (2011). Imaging retinotopic maps in the human brain. *Vision Research*, *51*(7), 718–737. doi:10.1016/j.visres.2010.08.004

Webster, M. A., De Valois, K. K., & Switkes, E. (1990). Orientation and spatial-frequency discrimination for luminance and chromatic gratings. *Journal of the Optical Society of America. A*, *7*(6), 1034–1049. doi:10.1364/JOSAA.7.001034

Webster, M. A., Mizokami, Y., & Webster, S. M. (2007). Seasonal variations in

the color statistics of natural images. *Network: Computation in Neural Systems*, *18*(3), 213–233. doi:10.1080/09548980701654405

Webster, M. A., & Mollon, J. D. (1997). Adaptation and the color statistics of natural images. *Vision Research*, *37*(23), 3283–3298. doi:10.1016/S0042-6989(97)00125-9

Welbourne, L. E., Thompson, P. G., Wade, A. R., & Morland, A. B. (2013). The distribution of unique green wavelengths and its relationship to macular pigment density. *Journal of Vision*, *13*(8), 1–10.

Weliky, M., & Katz, L. C. (1999). Correlational structure of spontaneous neuronal activity in the developing lateral geniculate nucleus in vivo. *Science*, *285*(5427), 599–604.

Werner, J. S., & Schefrin, B. E. (1993). Loci of achromatic points throughout the life span. *Journal of the Optical Society of America A*, *10*(7), 1509–1516. doi:10.1364/JOSAA.10.001509

Werner, J. S., & Wooten, B. R. (1979). Opponent chromatic mechanisms: Relation to photopigments and hue naming. *Journal of the Optical Society of America*, *69*(3), 422–434. doi:10.1364/JOSA.69.000422

Wickens, T. D. (2001). *Elementary Signal Detection Theory*. Oxford University Press.

Williford, T., & Maunsell, J. H. R. (2006). Effects of spatial attention on contrast response functions in macaque area V4. *Journal of Neurophysiology*, *96*(1), 40–54. doi:10.1152/jn.01207.2005

Wright, W. D. (1928). A trichromatic colorimeter with spectral primaries. *Transactions of the Optical Society*, *29*(5), 225–242.

Wright, W. D. (1939). A colorimetric equipment for research on vision. *Journal of Scientific Instruments*, *16*, 10–19.

Wuerger, S. M., Atkinson, P., & Cropper, S. (2005). The cone inputs to the unique-hue mechanisms. *Vision Research*, *45*(25), 3210–3223. doi:10.1016/j.visres.2005.06.016

Wuerger, S. M., & Morgan, M. J. (1999). Input of long- and middle-wavelength-sensitive cones to orientation discrimination. *Journal of the Optical Society of America A*, *16*(3), 436–442. doi:10.1364/JOSAA.16.000436